1-1-2009

Optical diagnostics and therapeutics in peripheral nerve surgery.

Francis P. Henry
Royal College of Surgeons in Ireland

TITLE

Optical Diagnostics and Therapeutics in Peripheral Nerve Surgery

Presentation of a thesis by

Francis Patrick Henry MB Bch BAO LRCP& SI MRCS

For the degree of Doctor of Medicine (MD) by research.

The Royal College of Surgeons in Ireland, 2009

Work carried out in The Plastic Surgery Research Laboratory and The Wellman Center for Photomedicine,

Massachusetts General Hospital, Harvard Medical School, Boston, MA.

Supervisor (RCSI): Professor A.D.K. Hill

Supervisor (USA): Dr J. M. Winograd

Declaration

I declare that this thesis, which I submit to RCSI for examination in consideration of the award of a higher degree M.D. is my own personal effort. Where any of the content presented is the result of input or data from a related collaborative research programme this is duly acknowledged in the text such that it is possible to ascertain how much of the work is my own. I have not already obtained a degree in RCSI or elsewhere on the basis of this work. Furthermore, I took reasonable care to ensure that the work is original, and, to the best of my knowledge, does not breach copyright law, and has not been taken from other sources except where such work has been cited and acknowledged within the text.

Signed 

Student Number 96207

Date 15/11/2009

Acknowledgements

Were it not for the patience, help and expertise of a number of people, this thesis would have never been completed.

The principle investigators involved in each facet of these projects at the Wellman Center for Photomedicine, Massachusetts General Hospital provided the inspiration, much needed guidance, expertise and supervision required for this thesis. These included Johannes F. deBoer, Charles P. Lin, Robert W. Redmond and in particular my direct supervisors Jonathon M. Winograd and Irene E. Kochevar. In addition, the daily support of Mark A. Randolph as lab director of the Plastic Surgery Research Laboratory, Massachusetts General Hospital was invaluable to the smooth running of all projects and in creating a very cordial work environment as both friend and mentor.

My colleagues at the Wellman Center for Photomedicine and The Plastic Surgery Research Laboratory, Massachusetts General Hospital, in particular Hyle B. Park and Daniel Côté whose help and patience as I tried to grasp the fundamentals of biomedical optics proved invaluable. Professor Arnold D. K. Hill who supervised my work and writing from back home, Namita Goyal and in particular Andrew Rohr for providing a supportive environment beyond the confines of the lab which has continued since my return from Boston and for whom editing, advice and encouragement has amazingly become routine.

The Medical Free Electron Program, Department of Defence and The Plastic Surgery Educational Foundation granted the resources that enabled me to complete these projects as well as stipend support through the Bullock Wellman Fellowship award, Harvard Medical School.

I am, as always, indebted to my parents, for their constant love, help, encouragement and guidance through everything I do and this thesis is testament to their support and efforts throughout my life.

Thank you to all.

Index

4. Results & Discussion - Optical Microscopy & Diagnostics

5. Optical Therapeutics in Peripheral Nerve Surgery

Appendix 1

Improving electrophysiologic and histologic outcomes by photochemically sealing amnion to the peripheral nerve repair site.

Henry FP, Goyal NA, David WS, Wes D, Bujold KE, Randolph MA, Winograd JM, Kochevar IE, Redmond RW.

Surgery. 2009 Mar;145(3):313-21. Epub 2009 Jan 25. PMID: 19231584

Appendix 2

Real-time in vivo assessment of the nerve microenvironment with coherent anti-Stokes Raman scattering microscopy.

Henry FP, Côté D, Randolph MA, Rust EA, Redmond RW, Kochevar IE, Lin CP, Winograd JM

Plast Reconstr Surg. 2009 Feb;123(2 Suppl):123S-30S. PMID: 19182671

Summary

Despite advances in clinical practice Sunderland's grades of nerve injury as described in 1951 remain a clinical measurement often aided by non specific diagnostic tools such as neurophysiological testing or indeed verified experimentally by destructive histological techniques. Furthermore regarding grade 5 injuries or nerve transection, microsurgical repair with sutures has remained the gold standard clinically despite a relatively poor outcome when the regenerative capability of the neural microenvironment is considered.

The objectives of this thesis are to apply novel optical technologies across the spectrum of nerve injuries as described by Sunderland. This includes evaluation of two optical diagnostic microscopes as well as a light activated neurorrhaphy addressing a grade 5 injury.

We hypothesize that Optical microscopy may have a role in analyzing injury to, and the recovery of, the peripheral nerve *in vivo*. Utilising Coherent Anti-stokes Raman Scattering (CARS) Microscopy to categorize peripheral nerve damage *in vivo*, and to monitor the recovery process of a damaged nerve and a Multifunctional Optical Coherence Tomography (OCT) system to assess quantitative and qualitative changes in optical density and polarisation of nerve tissue following injury. Regarding grade 5 injury we hypothesis that isolation of the nerve repair site using photochemical tissue bonding (PTB) in combination with human amniotic membrane can improve both functional and histological recovery.

Optical Diagnostics: A demyelinating crush injury was reproduced in the sciatic nerves of Sprague Dawley rats. Animals were randomised into groups and optical microscopy was undertaken at day one and weekly up to four weeks following

injury. Functional analysis was undertaken weekly and histomorphometry was completed following imaging. The uninjured nerve was used as a control.

All animals demonstrated loss of sciatic nerve function following injury. Recovery was documented with functional data approaching normal at three and four weeks. Demyelination was confirmed using CARS Microscopy in nerves up to two weeks post injury, remyelination was observed in the three week group and beyond. Imaging of normal nerve revealed structured myelin bundles. These results were consistent with histology.

OCT imaging revealed a quantifiable change in birefringence of the nerve (as measured by phase retardation graphs) following a simple crush injury. Histological markers of axonal myelination such as myelin thickness and g-ratio (axon diameter / fiber diameter) were then calculated and directly compared to the slope of the graph obtained from imaging (Birefringence). Scatter plot analysis of the complete data set showed a statistically significant relationship with both myelin thickness and g-ratio when compared to imaging results.

Optical Therapeutics: Photochemical tissue bonding (PTB) is a sutureless tissue repair process that seals the repair site allowing prompt restoration of the normal endoneural environment and healing. In PTB, a photoactive dye is applied to tissue surfaces that are then placed in contact and irradiated with green light. This technique utilises visible light at a power that does not thermally damage the tissue. The light activates the dye leading to immediate formation of covalent crosslinks between proteins on both surfaces, thereby forming a water tight seal.

New Zealand White Rabbits (n = 24) underwent transection of the right common peroneal nerve. Standard neurorrhaphy (SN) was performed using 10/0 nylon sutures. The repair site was then wrapped in a cuff of human amniotic membrane (HAM), which was either secured with sutures (SN & HAM) or sealed using PTB (SN & HAM/PTB). Standard neurorrhaphy alone was assessed as a control group. Functional recovery was recorded at 30 day intervals post-operatively by electrophysiological assessment. At 120 days animals were sacrificed and nerves harvested for histomorphometry.

Nerves treated with amnion wraps, sealed with PTB demonstrated a statistically significant improvement across both functional and histological parameters. Functional recovery, as measured by repeated electrophysiological studies over time, revealed a 26.2% improvement over standard neurorrhaphy alone ($p<0.05$). Nerves treated with PTB sealed amnion wraps had significantly ($p <0.001$) greater axon fibre diameters as well as myelin thickness and G-ratio distal to the repair site compared to standard neurorrhaphy alone.

In conclusion, both CARS Microscopy and OCT have the ability to image the peripheral nerve revealing structural (CARS) as well as quantitative and qualitative changes (OCT) in composition which may be used to grade injury and regeneration over time and isolation of the peripheral nerve repair site using a photochemically sealed amnion wrap improves electrophysiological and histological recovery when compared to that of standard suture neurorrhaphy.

1. Introduction

1.1. The Peripheral Nervous System

In the fourth century Aristotle believed that the nerves were controlled by and originated in the heart. While it had been known since the time of Hippocrates in the 5th century BC that the brain controlled the muscles it was six centuries before Aristotle was contradicted by Galen who concluded that the brain was the most important organ in the body and source of the peripheral nerve. This confusion as to the identity and source of the peripheral nerve is evidenced by the origin of the word nerve, meaning tendon or sinew, and remains an indication of the centuries of confusion regarding their true nature.

"By means of nerves, the pathways of the senses are distributed like the roots and fibres of a tree" - Alexandro Benedetti, 1497

Benedetti, albeit providing an accurate assessment of neural function still subscribed to the ideal of 'spiritis', where it had been though that the nerve was a conduit of sorts in which the spirit, or source of vitality, travelled down to enact their will. This mixture of medieval and ancient beliefs with the then modern scientific findings due to dissection remained prominent throughout the scientific community until the 18th century when scientists made the link between the nervous system and electrical impulses (Ochs 2004).

The peripheral nervous system is the extension of the central nervous system that connects via a network of plexus and branches out to the end organs of the body. Divided into somatic and autonomic, its primary function remains that of transmitting each and every impulse from the brain and conversely from the end organs centrally. While similar in nature and structure the clinical manifestations of the somatic nervous system remain more acute in the surgical setting. Injury or trauma to either motor or sensory nerves serves a deficit that is easily apparent to the patient and the examining clinician.

The sequelae of injury to the nervous system both central and peripheral encompass a significant burden on the healthcare systems of the western world. Estimated in the United States as costing an annual $7 billion this is further defined as involving in excess of 50,000 nerve repair procedures (Evans 2001). In isolating limb trauma the most recent data analysis suggested that peripheral nerve injury was a consequence in 1.64% of cases (Taylor, Braza et al. 2008). Considering this database of 16 million where only 220,593 episodes of limb trauma were recorded this figure is admittedly low. These figures, while published data, admit to probable underestimation of the actual number given the many facets of both long term disability and multiple classification of nerve injury which exist in compiling census statistics. The consensus remains that injury to the peripheral nervous system whether via trauma or chronic disease remains a significant drain on resources in modern healthcare throughout the world.

This thesis aims to address two particular facets of the modern approach to peripheral nerve surgery, both diagnostically and therapeutically. The application of

optical based techniques to evaluate the internal microenvironment of the peripheral nerve would aid the clinician in a manner previously unachieved. Providing microscopic information with an *in vivo* non-destructive technique would allow for a more accurate assessment of injury and regeneration, thus providing information regarding diagnosis and prognosis following initial insult. The second approach concerns definitive surgical repair following nerve transection, augmented with an optical technique. This is of particular importance in a field in which the gold standard has stagnated since the introduction of microsurgery and still provides results which fall below preoperative function. Utilising these optical techniques in this manner would add to the current body of knowledge in the field of peripheral nerve surgery and indeed following the encouraging results discussed in the following chapters, would provide promise for their translation across to clinical practice.

1.2. Anatomy and Physiology of the Peripheral Nerve

Understanding the basic anatomy of the nervous system remains key to any surgical or scientific approach in the field. The basic unit of the nerve is the axon which when combined with its associated support structure may be termed a nerve fibre. These fibres include the axon with associated Schwann cell, the number of which depends on the type of nerve. These fibres travel through the nerves bundled in fascicles which may be arranged in various patterns, from monofascicular to oligo and polyfascicular nerves depending on the number comprising the entire nerve, examples of which are shown in figure 1.1. Peripheral nerves consist of motor, sensory and sympathetic nerve fibres surrounded by connective tissues which were

described by Ranvier (Ranvier 1878) and Key and Retzius (Key and Retzius 1876). The latter suggested anatomical divisions based on fascicular position and the perifascicular, lamellated sheath and intrafascicular connective tissue (described by Ranvier) became termed epineurium, perineurium and endoneurium, respectively and this description from 1876 remains in universal use today.

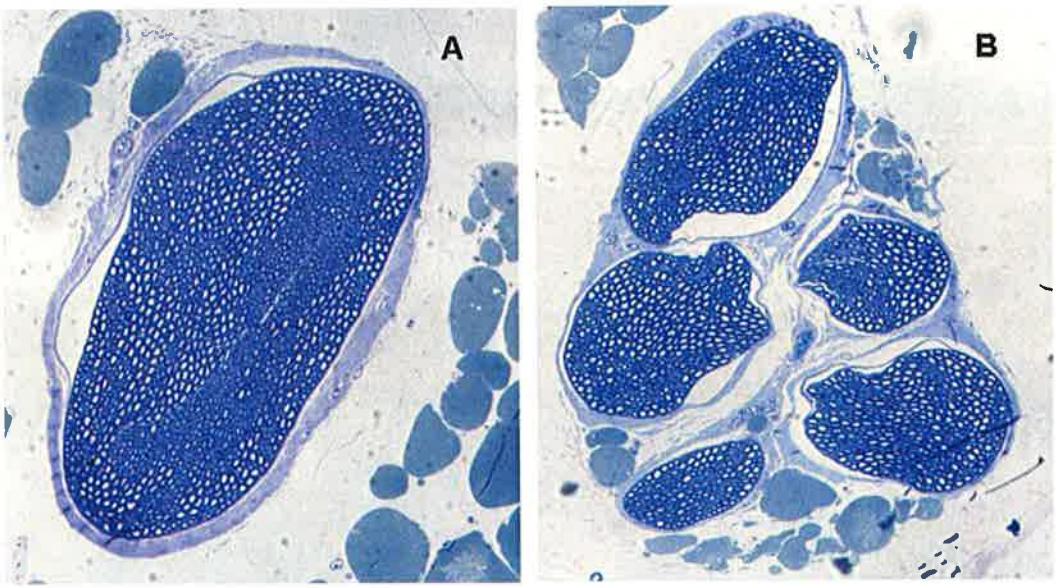

Figure 1.1 – Examples of A) Monofascicular nerve and B) Polyfascicular nerve, 40X, Toluidine Blue.

The gelatinous endoneurium is found within the fascicle between each nerve fibre whereas the perineurium, a thick connective tissue layer, surrounds each fascicle and this is encased anatomically by the external epineurium. The internal epineurium is a term that is commonly used to describe the connective tissue between the fascicles and in total accounts for up to 50% of the nerve cross section volume. A final anatomical layer which has recently gained wide accepted is the mesoneurium which

provides the mode of entry of the segmental blood supply and allows gliding of the nerve within anatomical planes (Sunderland 1978; Mackinnon and Dellon 1988).

From a functional standpoint, the ventral horn of the spinal cord contains the lower motor neuron cell bodies and from here their axons travel through the ventral spinal root to join the spinal nerve exiting the vertebral foramen. Presynaptic sympathetic fibres are also found in the ventral horn and send fibres to the sympathetic ganglia (found adjacent from T1 – T7). In contrast the sensory cell bodies are found in the dorsal root ganglia and send axons distally from their synapse in the spinal cord to receive stimuli from the sensory end organs (Mackinnon and Dellon 1988). These three distinct neural pathways may travel peripherally as a single entity, being often found, albeit as separate fascicles, in the same mixed nerve.

Axons exist as either myelinated or unmyelinated entities in a ratio of 4:1 respectively. The smaller myelinated axon typically possesses a series of Schwann cells along its length, each with its cell membrane wrapped concentrically around the axon. Between each cell an interspace exists which remains unmyelinated and is known as the node of Ranvier (Ranvier 1878). The internodal space, the space between each consecutive node of Ranvier correlates with axon diameter and may be up to a distance of 1.8mm. Larger unmyelinated fibres are often found groups with a single Schwann cell enveloping many axons. The Schwann cell is a unique cell, possessing a double basement membrane whose number is determined at development and does not increase during growth (Winograd and MacKinnon 2006). Named from the German physiologist Theodore Schwann, this variety of glial cell functions not only as the source of the myelin sheath but also, in unmyelinated

axons, are essential for axonal support and neuronal survival. Conduction of an electrical impulse down the axon is propagated as a depolarising wave along the entire length of the nerve by means of voltage gated ion channels. Typical conduction speeds in an unmyelinated axon reach 2 – 2.5 m/sec with the larger axon diameter allowing for faster conduction. The presence of the myelin sheath allows for faster conduction at smaller axon diameters by means of saltatory conduction. In these myelinated axons, depolarisation at one node of Ranvier triggers depolarisation at the next node without involvement of the insulated segment of the axon. This allows conduction speeds of up to 3 – 150 m/sec and therefore a more efficient functioning of the nervous system.

The physiology of the peripheral nerve depends on the unique relationship of the blood supply with the neural tissue. As with other tissues found in the nervous system, a specialised barrier exists in histological continuity with the blood brain barrier that protects the central nervous system. The blood nerve barrier helps maintain the stabilised environment for the nerve fibres within the fascicle by limiting invasion of proteins and maintaining homeostasis. The anatomical blood supply of the nerve may be classified much like that of a muscle, as defined by Breidenback and Terzis, into one of three patterns; segmental with no dominant pedicle, one dominant pedicle that runs longitudinally with the nerve or multiple dominant pedicles along the nerve length (Breidenbach and Terzis 1986). The vessels are coiled to allow for gliding and enter the vaso nervorum from the mesoneurium, into the epineurial space. In the epineurium and perineurium the vessels run longitudinally in a plexus formation and branch into a fine network of

capillaries in the endoneurium (Lundborg 1979). Venous drainage parallels that of the arterial supply (Del Pinal and Taylor 1990).

The Blood nerve barrier comprises of the anatomical blood supply as described and its relationship to the nerve fibres. Specifically, the spinal nerves carry with them the pia arachnoid layer of the meninges which is in histological continuity with the innermost layers of the perineurium and the endothelial cells of the epineurium (Shanthaveerappa and Bourne 1966). Tight junctions are present in these cells and they remain impermeable to many substances present in the vascular system and are of particular importance in the presence of sepsis given that then nerves themselves do not possess an intrinsic lymphatic system (Larson, Rodin et al. 1966; Shanthaveerappa and Bourne 1966; Olsson and Reese 1971). Disruption of this system occurs following nerve injury, results in a loss of neural homeostasis and the resulting endoneurial oedema secondary to leaking capillaries within the perineurium is thought to be a predominant mechanism behind neuropraxia (Mackinnon and Dellon 1988). Immunogenic protection of the nerve by the blood nerve barrier is also thought to play a critical role in the reaction of the nerve to injury. Invasion of inflammatory cells across the barrier and their reaction with previously shielded antigens in the perineurial space further compounds inflammation and injury with eventual scar formation. This phenomenon is supported by recent evidence suggesting a beneficial role for immunosuppression in improving neural regeneration (Sobol, Lowe et al. 2003; Snyder, Fox et al. 2006).

Additional considerations regarding the physiology of the peripheral nerve involves the complex system of axoplasmic transport. This is the means by which

neurotransmitters and structural proteins are manufactured in the cell body and transported down the axon with the reverse being true of anterograde transport of recycled vesicles and neurotransmitters. Initially described by Weiss in the 1940's (Weiss 1944) it has been subsequently shown by means of labelled amino acids (Droz and Leblond 1963) that both slow and fast systems operate in an anterograde manner with fast systems operating in the retrograde system (Smith and Kornblith 1982). Major structural proteins such as actin and tubulin are believed to be transported in the slow anterograde, ATPase independent system with fast transport of neurotransmitters, enzymes and glycoproteins being ATPase dependent (Lasek, Shelanski et al. 1981). This process occurs with remarkable efficiency and transports with speeds in the fast systems of the anterograde and retrograde streams of 410 and 240 mm/day respectively (Lubinska and Niemierko 1971; Droz, Rambourg et al. 1975; Thoenen and Stockel 1975; Ochs 1977). Additionally, it has also been demonstrated to play an integral role in the function of the Schwann cell and retrograde transport of neurotrophic factors following injury to the peripheral nerve (Stockel, Paravicini et al. 1974).

1.3. The Response of the Peripheral Nerve to Injury

Injury to the peripheral nerve, whether traumatic or degenerative triggers a complex sequence of events which while extensively studied is still not completely understood. The ability of the nerve to regenerate is well recognised, however successful recovery requires optimisation of several permissive states in the neural microenvironment. These states may be summarised according to changes which occur in the cell body, the proximal nerve segment, the distal nerve segment and the

target organ. Detailed analysis of this complex and intricate system is beyond the scope of this thesis; the following consists of the more salient features and their impact on reconstructive efforts following injury.

1.3.1. The Cell Body

As the main support structure for the production and turnover of neurotransmitters, the cell body plays a key role in the response of the nerve following injury and its relationship with the axon is depicted in figure 1.2 below. Its fate following injury lies with one of two possible pathways; 1) transition to a cell which promotes regeneration and projection of new axons or 2) apoptotic cell death (Ducker, Kempe et al. 1969). Certain environments predispose to cell death, sensory neurons more so than motor neurons, developing neurons and more proximal nerve injuries (Arvidsson, Ygge et al. 1986; Schmalbruch 1988; Ygge 1989). The presence of neurotrophic factors secreted by macrophages, glial cells and the distal target organs have been shown to be transported in a retrograde fashion to the cell body decreasing the risk of apoptosis and this is evidenced by the increased regeneration seen in lesions in continuity rather than physiologically isolated nerve transactions (Fu and Gordon 1997). Conversely, through repair or approximation via an impermeable conduit, neurotrophic factors can remain influential in supporting the cell body and increasing likelihood of survival.

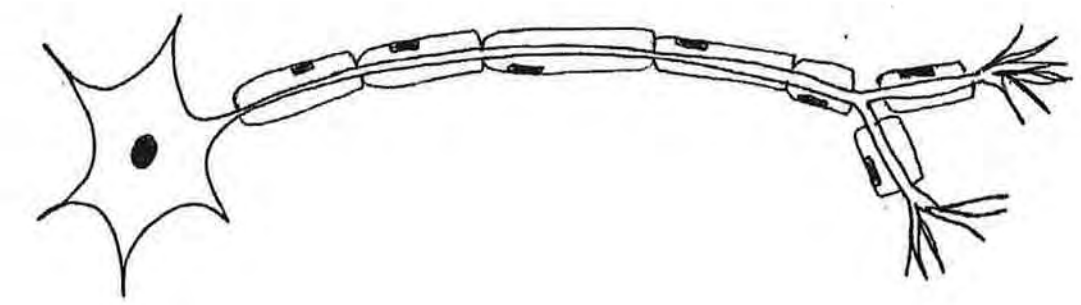

Figure 1.2 – Basic representation of a cell body and associated myelinated axon

Neuronal survival results in a process of chromatolysis that can be characterised by several distinct histological changes to the cell body. These include neuronal nuclear eccentricity, nucleolar swelling and discolouration of Nissl bodies (Nissl 1892; Kreutzberg 1995). These changes represent the response of the cell body to the increased metabolic demands of the regenerating axon with down-regulation of neurotransmitters and proteins and up-regulation of neuropeptides and the structural proteins required for axonal regeneration (actin and tubulin). Metabolic changes include an increase in RNA, lipid and protein synthesis as well as increased production of Glucose-6-phosphate dehydrogenase and hydrolytic enzyme (Fu and Gordon 1997). Expression of cytokines following axotomy is also increased, particularly that of Interleukin 1, 2, and 6 as well as transforming growth factor-ß. These act on macrophages either locally in the cell body, or at the axotomy site promoting axonal regeneration and recovery of neural function (Kiefer, Lindholm et al. 1993; Murphy, Grondin et al. 1995).

1.3.2. The Regenerating unit: Proximal stump

The proximal stump is the nerve end that remains in continuity with the cell body following axotomy. In the event that the cell body undergoes chromatolysis rather than apoptosis the proximal stump becomes the main regenerating unit of the nerve. Initial changes involve degeneration of the axon body following injury. This degeneration occurs in a retrograde fashion back to the previous node of Ranvier or further, a distance which may be up to 3mm in length (Cajal 1928). As early as 5 hours following injury the distal surviving portion of the axon loses its electron dense undercoat and the plasma membrane protrudes as regenerating sprouts. Initially containing sparse vesicles, these sprouts mature and form growth cones which eventually appear as well developed axons with an abundance of vesicles and mitochondria. Each node of Ranvier may produce up to 100 of such sprouts and with the supportive presence of a distal neural microenvironment this number is reduced to approximately 5 with a further reduction to one axon per node of Ranvier occurring over time (Mackinnon, Dellon et al. 1991; Fu and Gordon 1997). Axonal sprouting may occur in the absence of stimulation from the cell body although further regeneration will not occur without the necessary growth factors provided via axonal transport. Successful reinnervation may be due either to an intact epineurium or surgical repair of the nerve ends. In the absence of such a supportive environment distally the initial sprouts will continue to grow following stimulation from the cell body, this disorganised growth results in neuroma formation that clinically may present as a painful mass at the site of the nerve injury. This phenomenon may occur, although to a lesser degree, with poor approximation of the nerve ends and

increasingly results in inefficient axonal regeneration (Cajal 1928; Sunderland 1978; Fu and Gordon 1997).

Following a short latency period (up to 3 days) the rate of axonal regeneration accelerates to a constant rate of 1 to 3 mm per day (Seddon, Medawar et al. 1943; Winograd and MacKinnon 2006). Growth is achieved though the basal lamina tubes in the proximal segment with an inherent ability to cross a small amount of connective tissue to the appropriate basal lamina tube of the distal segment. Further regeneration to reinnervate the distal target organ becomes wholly dependant of the presence of a receptive distal environment.

1.3.3. The Distal Stump Environment

Once the distal axon is separated form the cell body a process of Wallerian degeneration occurs. This process describes the degeneration and ultimate disappearance of the axon in preparation for reinnervation from the proximal segment. The removal of the axon not only provides a clear acellular pathway or tube for regeneration but also removes the myelin sheath which has been shown to directly inhibit axonal regeneration (Jacobs and Fehlings 2003). Phagocytosis of the axonal remnants is initiated by the Schwann Cells in the first few days following injury. Subsequently this process is accelerated by infiltration to the site via the compromised blood nerve barrier of exogenous macrophages (Reichert, Saada et al. 1994). The release of growth factors and cytokines by the macrophages further stimulate the Schwann cell and fibroblast proliferation. This results in a proliferation

of cells which switch to a nonmyelinated state and fill the endoneurial sheath in longitudinal columns known as Bünger (Fu and Gordon 1997).

During this state of proliferation the Schwann becomes the key facilitator of regeneration through the distal segment and dramatic changes occur in the growth factor profile. Whether in intact distal stumps or within grafts it is the Schwann cell which has been shown to support axonal outgrowth, achieved through contact guidance as well as growth factor stimulation and the production of extracellular mileau. It is thought that the failure of regeneration through an artificial or acellular conduit is limited only by the ability of the Schwann cell to migrate within the confines of its structure (Hall 1997).

Response of the Schwann cell to axotomy is not limited to proliferation alone. The switch from a myelinated to nonmyelinated state signals the cessation of the production and maintenance of myelin as well as an upregulation of the production of essential stimulants such as nerve growth factor, neurotrophin 4/5, brain derived neurotrophic factor, epidermal growth factor, insulin-like growth factors 1 and 2, and glia-derived neurotrophic factor (Winograd and MacKinnon 2006). Production of extracellular matrix proteins is unregulated, in particular that of laminin and tenascin, the latter usually only expressed at the node of Ranvier, is expressed throughout the distal segment following Wallerian degeneration (Winograd and MacKinnon 2006). Growth of the regeneration axon along the bands of Schwann cells is mediated by cell adhesion molecules which facilitate the adhesion of the axons to the Schwann cells, basal lamina and each other. Adhesion molecules such as glycoprotein L1, neural cell adhesion molecule (NCAM) and N-cadherin can be

altered to facilitate selection of motor or sensory regeneration (Brushart 1993; Fu and Gordon 1997).

In 1911, Ramón y Cajal provided definitive histological evidence of neural regeneration from the proximal stump to the distal nerve segment in a selective manner (Cajal 1928). This work has been further extended using Y chambers, confirming that when presented with a variety of options the regenerating axons will preferentially grow towards nervous tissue rather than the alternatives (Lundborg, Dahlin et al. 1986; Mackinnon, Dellon et al. 1986). Motor nerves have also been shown in the same manner to grow preferentially towards motor rather than sensory nerves as well as demonstrating anatomical specificity (Brushart, Tarlov et al. 1983; Brushart 1993). While the validity of these hypotheses has been challenged (Fu and Gordon 1997), the phenomenon by which it may occur has been described as that of neurotropism. This guidance of regeneration through diffusible or spatially fixed factors is in contrast to the concept of neurotrophism in which the immediate microenvironment is thought to provide a structural guidance for regeneration. It has been widely accepted that a combination of both phenomena result in efficient regeneration from the proximal nerve, through to the distal stump. Despite this, and even with all mechanisms working in favour of reinnervation of the target organs, there is evidence from retrograde labelling of cat tibial nerves following neurorrhaphy that up to 51% of nerve fibres form inappropriate connections following surgical repair (Shinohara, Naora et al. 1990; Watchmaker and Mackinnon 1996), thus highlighting the inadequacies of the current gold standard technique of suture neurorrhaphy.

1.3.4. The Target Organ

The response of the end organs to injury of the peripheral nerve is key to a complete understanding of the process of efficient functional regeneration. The ability of the regenerating nerve to reinnervate largely depends on the condition in which it finds its target organ, usually following lengthy periods without stimulation.

The end organs of sensory nerve fibres are not as dependant on time restraints as their motor counterparts. Organs such as Messner corpuscles, free nerve endings, Ruffini ending and Merkel cells have the ability to regenerate to varying degrees and while the quality of renervation and recovery may be enhanced by a more rapid return of neural stimulation, it is not prevented by a slower one (Mackel, Kunesch et al. 1983; Watchmaker and Mackinnon 1996). Pacinian corpuscles, innervated by a single axon, undergo complete fibrosis and do not reinnervate (Krishnamurti, Kanagasuntheram et al. 1973).

In motor nerves, regenerating axons are guided through the distal segment of the nerve by the Schwann cell toward the neuromuscular junction. After axotomy the neuromuscular junction remains present for over a year following injury and undergoes little change. Acetylcholine receptors are found diffusely throughout denervated fibres in contrast to a central position in innervated fibres (Gorio, Nunzi et al. 1982). Upon contact with the neuromuscular junction the axon forms connections to the muscle fibre and those adjacent by collateral sprouting. Maturation over time results in pruning to reduce the distribution to one dominant

axon and end plate for each muscle fibre (Mackinnon and Dellon 1988; Watchmaker and Mackinnon 1996).

In contrast, motor responses to nerve injury result in a number of histological changes to the muscle itself. The fibres atrophy with a reduction in their cross sectional area of up to 90% (Sunderland and Ray 1950). This is accompanied by movement of the nucleus to a central position gives the myocyte a target cell appearance. Should denervation continue for a period of 3 months or more, deposition of connective tissue along the epimysium signifies the onset of tissue fibrosis which may reach advanced stages by 11 months (Aird and Naffziger 1953). At this stage, even with effective reinnervation, the presence of fibrosis in the tissue limits the efficacy of muscular contraction following neural stimulation. Despite the absence of definitive timeframes it is widely believed that should distal atrophy and fibrosis be allowed to continue for a period of 12 to 18 months post injury, the prospects of meaning functional recovery are greatly reduced (Watchmaker and Mackinnon 1996; Winograd and MacKinnon 2006). This remains of utmost consideration clinically, particularly in the case of more proximal nerve lesions and highlights the case for more advanced diagnostic and prognostic evaluators in the field of neural injury as well as more efficient neurorrhaphy techniques as evaluated further in this thesis.

1.4. Clinical Classification of Peripheral Nerve Injury

In 1941, Henry Cohen proposed a clinical classification of nerve injury, detailing a spectrum of neural trauma ranging from minor contusion to complete transaction.

Largely overlooked at the time, it was two years later in 1943 when a clinical series of 650 cases of nerve injuries were analysed by Seddon (Seddon 1943) and this classification scheme applied, that it became known as Seddon's classification of nerve injury (Neuropraxia, Axonotmesis and Neurotmesis). This triple classification was criticised as being over simplifying and lead to work by Sir Sydney Sunderland in 1951, which expanded on the classification and described a five point scale of neural injury (Sunderland 1951). This scheme remains in use today and is largely unchanged apart from a sixth degree of injury proposed by Susan E. Mackinnon in 1989, which detailed a mixed nerve injury comprising of a combination of the previous five degrees (Mackinnon 1989). The evolution of one classification system into the other allows for them to be discussed together and below is a brief outline of their characteristics.

First-Degree Injury (Neuropraxia)

Neuropraxia has the distinguishing feature over all other types of nerve injury in that Wallerian degeneration does not occur. In practice a conduction block is seen, generally as a result of a compressive injury and histologically, focal demyelination with preservation of axon continuity may be noted with recovery of symptoms in days to weeks following injury (Seddon, Medawar et al. 1943; Sunderland 1951).

Second-Degree Injury (Axonotmesis)

Classified by the presence of axonal disruption with subsequent Wallerian degeneration, Second-degree injury maintains the integrity of the adnexal axonal support structures and is therefore associated with a positive clinical outcome. The intact endoneurial sheaths and basal laminae of the Schwann cells allows for

regeneration to occur uninterrupted along the axons own path. Recovery may extend beyond a period of 3 months depending on the injury placement however clinical improvement encourages such a diagnosis. While nerve conduction studies may add information initially, they cannot reliably diagnose or predict recovery of a second-degree injury in the early stages following insult. As further discussion of more severe injuries will show, a significant amount of time may lapse before clinical differentiation of the degree of nerve lesion in-continuity may be elicited. This time can be of utmost importance given the response of the end target organs to denervation as previously described above (Seddon, Medawar et al. 1943; Sunderland 1951; Mackinnon and Dellon 1988).

Third-Degree Injury (Axonotmesis)

As in second-degree injury, third-degree injury also involves axonotmesis. Sunderland differentiated this injury based on the disruption not only to the axon with Wallerian degeneration, but also to the contents of the endoneurial sheath, the basal laminae and all other structures within the perineurium. While grossly intact fascicles are observed the lack of the perineurial sheath is significant in that axons are not guided across and mismatch of fibres from proximal to distal segments may occur. Failure of the axons to progress, along with scar formation within the endoneurial sheaths are variables which determine the extent of regeneration. The clinical recovery or precise diagnosis of this injury is impossible to determine until reinnervation of the target end organs has been achieved with limited success or simply failed (Seddon, Medawar et al. 1943; Sunderland 1951; Mackinnon and Dellon 1988).

Fourth-Degree Injury (Neurotmesis with Anatomic Continuity)

The most significant neural injury in the intact nerve is that of the fourth-degree injury. Macroscopically indistinguishable from any of the previous injuries (the epineurium is intact), all subepineurial layers are disrupted and undergo complete degeneration with subsequent scar formation. As a result of this injury no neural regeneration occurs. The inability of diagnostics, either clinical or electrically, to differentiate this lesion from the others in the early stages usually results in delayed intervention in the form of surgical excision and nerve grafting (Seddon, Medawar et al. 1943; Sunderland 1951). Unlike third-degree injuries where surgical intervention may not provide an improvement in clinical outcome, intervention in this case is a necessity in order to appreciate any return of function (Mackinnon and Dellon 1988). Therefore an avoidance of the lengthy period of observation required would hasten time to surgery, decrease the mal-effects of end organ denervation and subsequently provide an improved clinical outcome.

Fifth-Degree Injury (Neurotmesis without Anatomic Continuity)

Complete anatomical division or transection of all layers of the nerve is defined as a fifth-degree injury. Direct visualisation on surgical exploration allows for definitive management with microsurgical repair, without which no recovery is possible. Of note however, is that a failed or inadequate repair of the nerve ends may result in a fourth-degree injury following which, a second surgical procedure will be necessary to achieve any functional recovery (Seddon 1943; Sunderland 1951; Mackinnon and Dellon 1988).

Sixth-Degree Injury (Neuroma-in-Continuity)

In proposing the sixth-degree nerve injury, Mackinnon addressed a mixed trauma in which the nerve undergoes a combination of all five previously described patterns of injury. Arguably the most challenging of all lesions clinically, the management involves precise identification of the injury on a fascicular level, fascicle by fascicle and tailoring a surgical approach, if any, to each fascicle independently. While time will differentiate more favourable lesions, the critical management call involves a timely identification of the more severely injured bundles in order to optimise functional outcome (Mackinnon 1989).

1.5. Current Techniques in Evaluation of the Peripheral Nerve

1.5.1. History and Clinical Examination

History and Physical examination of the patient remain the most valuable tools available in assessing the patient following peripheral nerve injury. An in depth history of mechanism of injury, history of symptoms and premorbid conditions will paint a very astute picture as to the nature of the injury. Examination is paramount from the site of trauma (open or closed) to a generalised physical examination outlining any areas of concern prior to establishing a diagnosis and pursuing a treatment. This leads to a focused clinical examination of the nerve in question. Motor nerves yield information when the target muscle or muscle group is examined. Attention must also be given to the uninjured side to elicit any premorbid condition that may otherwise give a false impression of injury.

In the case of the sensory nerve, and following a description from the patient of the sensory abnormality, further information may be elicited by using clinical investigations, the more common of which are summarised below.

Non specific examination techniques include Tinel's test in which the nerve is tapped gently and should axonal injury be present paraesthesia can be evoked along the sensory distribution of the nerve. More specific quantifiable examinations include two-point discrimination which can be performed using a discometer. The ability of the blinded patient to discriminate between two blunt points on the discometer is measured in millimeters. This test can be undertaken in a dynamic (moving along the nerve distribution) or static manner (Hunter 2002). Touch Test Sensory Evaluation may also be undertaken using a Semmes-Weinstein Monofilament (figure 1.3) and is seen as a more sensitive and standardised approach to assessment of sensation clinically. These monofilaments are placed over the affected region and the size of the filament is increased until the subject can detect the pressure of the filament. Each filament is standardized to a specific size which corresponds to a target force. Results range from that of normal sensation to no response, and a score of 0 – 6 can be assigned to the variables between (Hunter 2002).

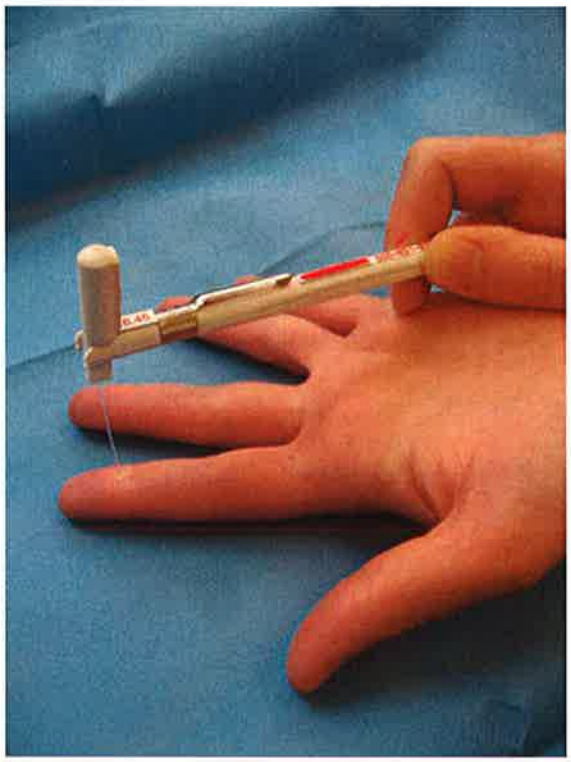

Figure 1.3 – Touch Test Sensory evaluation using a Semmes-Weinstein Monofilament being used to investigate sensation over the distribution of the median nerve of the hand.

Mixed motor and sensory nerve functional assessments include The Moberg Picking-up test which is used to test hand function, specifically fine motor control, dexterity and sensibility. The test consists of two parts: 1) Placing objects into a cup and 2) Placing objects into a cup while blindfolded. During both parts the subject is asked to place the objects into the cup as quickly as possible, first with the uninjured hand then with the injured hand. The time from when the first object is picked up until the last object is placed in the cup is recorded for each test. The test results are the total aggregate time (in seconds) for each part of the test. The materials used are

standardised to a wing nut, large and small coin, washer, screw, safety pin, large and small nut, paper clip, nail, cup and key (Hunter 2002).

As with all neurological investigations, the true value of these few described lies not with a single examination, but that of serial data over time.

1.5.2. Electrical Studies

Nerve conduction studies and electromyography may be used in conjunction with history and physical exam in determining and monitoring the initial injury and recovery of the peripheral nerve. While imaging techniques have evolved regarding the diagnosis across a spectrum of specialities, analysis of the peripheral nerve microenvironment is beyond the scope of the methods in use and indirect observation by means of electrical stimulation of the nerve or target organ remains the only useful technique available. While not without their limitations they remain the only clinical investigation in common use today in this field and can aid in the diagnosis and are used, albeit with caution, as a prognostic indicator following nerve injury.

Nerve Conduction studies

Nerve conduction studies, in which part of the nerve is stimulated electrically with needle or cutaneous electrodes and transcutaneous electrodes are used to record responses are useful in both preoperative diagnostics, monitoring regeneration and in intraoperative studies, particularity in the case of difficult lesions. Results are analysed in graphical form as shown in figure 1.4 below. While an efficient and

skilled operator can complement the clinical analysis of the case, they in no way can be used as an alternate to clinical examination and history and are dependant on the expertise of the operator.

Motor axons are directly assessed by their compound muscle action potential (CMAP), generated by the nerve at the muscle resulting in a large amplitude response to stimulation. Sensory axons may be assessed by recording along the nerve at two points in either an antegrade (orthodromic) or retrograde (antidromic) fashion. The sensory nerve action potential (SNAP) is more difficult to assess and interpret given the smaller fibre size and low amplitude responses to stimulation. Amplitude, the height of the action potential expressed in milivolts, provides an assessment of the number of conducting axons and while normal values are difficult to predict, the best rule of thumb is an amplitude drop of more than 50% when compared to the normal side indicates neural pathology. Thereafter, monitoring over time would reveal whether or not recovery was taking place. Other measurements recorded such as latency and conduction velocities indicate the speed of nerve conduction in milliseconds and meters per second respectively. Unlike amplitude they do not reflect the number of axons and are limited in representing only the fastest conducting fibres present (MacKinnon and Novak 2005).

Pitfalls involved in interpreting nerve conduction studies include the ability of the transected or injured nerve to evoke a response up to six weeks following degeneration, giving a false negative result and therefore, up to six weeks following injury electrical studies may be deemed unreliable. Additionally, when used as an tool to monitor regeneration, stimulation beyond the level of injury may provide

some evidence of recovery over time but will only evaluate myelinated axons and is not a sensitive investigation in determining extent of regeneration. In situations in which more than one level of injury exists or in the case of systemic polyneuropathies, nerve conduction studies are even less reliable. Subtle connective tissue changes in the nerve microenvironment which would distinguish a second-degree from a third-degree injury cannot be evaluated with electrical studies.

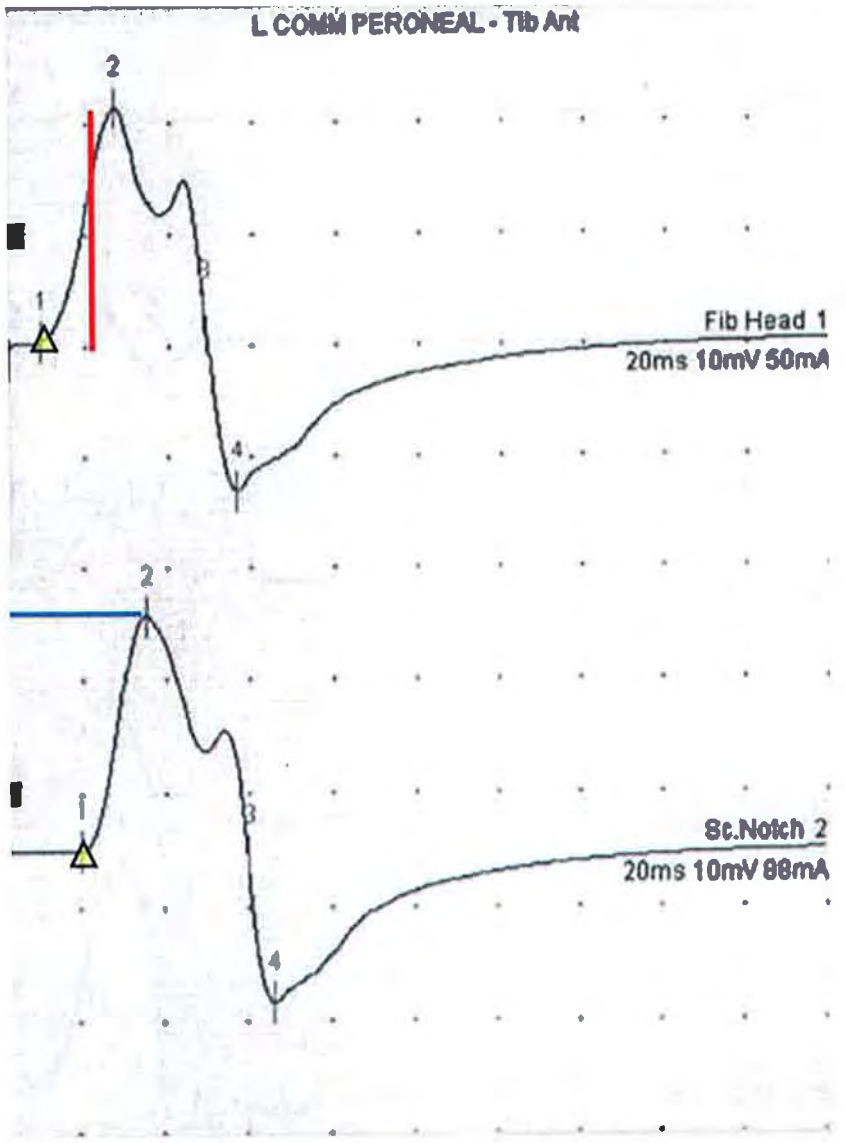

Figure 1.4 – Graphical result of a nerve conduction study performed on the left common peroneal nerve of the rabbit (uninjured). The top study is representative of stimulation at the fibular head with the bottom study showing stimulation at the sciatic notch. The red line represents the amplitude, the blue line represents nerve latency and the distance between both triangles is calculated as the nerve conduction velocity.

Electromyography

In evaluating the target organ alone, motor nerve injury can be assessed by muscle response to needle insertion, at rest alone and then followed by an activation response on voluntary contraction. Insertional activity in the normal muscle consists of a number of spikes following needle placement. Abnormalities include electrical silence in chronic denervation or sharp waves in the early stages of denervation. In the rest phase, electrical silence denotes a normal muscle unit. The presence of fibrillation potentials and spontaneous activity may be indicative of neural injury and can be the earliest signs of muscle denervation. Voluntary Motor Unit Potentials (MUPs) are numerous on normal contraction and single MUPs are not discernable. In nerve injuries both incomplete and low amplitude MUPs are seen as well as reduced recruitment. With reinnervation the amplitude of the MUPs will slowly increase and remodel to that of a normal range (MacKinnon and Novak 2005).

Muscle reinnervation however, may never result in full functional recovery given the response of the muscle to denervation. Thus, EMG studies may provide an overly optimistic result and as with nerve conduction studies, are best interpreted with caution and in conjunction with a thorough history and physical examination.

1.6. Hypothesis & Aims of this Thesis

The broad aims of this thesis are to address deficiencies in the surgical management of peripheral nerve injuries, both diagnostically and therapeutically utilising novel optical based techniques.

The hypothesis that optical microscopy may have a role in analysing injury to, and the recovery of, the peripheral nerve *in vivo* is explored using Coherent Anti-stokes Raman Scattering (CARS) Microscopy to categorise peripheral nerve damage *in vivo*, and to monitor the recovery process of a damaged nerve as well as a Multifunctional Optical Coherence Tomography (OCT) system to assess quantitative and qualitative changes in optical density and polarisation of nerve tissue following injury.

Regarding complete nerve transection the hypothesis that isolation of the nerve repair site using an optical technique can improve both functional and histological recovery is explored using a photochemical tissue bonding (PTB) technique in combination with human amniotic membrane.

Optical Diagnostics

The concept and practice of the lengthy period of observation required to clinically assess, diagnose, and differentiate, between second, third and fourth-degree nerve injuries can lead to deleterious effects on functional outcome given the response of the target organ to denervation. Of relevance especially in the case of a fourth-degree injury, it remains impossible by visualisation (due to an intact epineurium) or electrical studies (due to lack of conduction throughout the early period) to decipher whether surgical intervention be undertaken. The ability to image and assess the microenvironment of the nerve following injury during the very early stage of recovery would aid in the more rapid assessment of the degree of injury and avoid lengthy periods of denervation should surgery be required. This degree of *in vivo*,

non-destructive high-resolution imaging is not in practice either experimentally or clinically to date.

The first section of this thesis examines the ability of two novel optical microscopes to image the nerve in such a manner, providing real time information regarding the microenvironment of the normal, injured and regenerating peripheral nerve.

Optical Therapeutics

The second section of this thesis concerns the operative management of fourth and fifth-degree injuries. Microsurgical suture repair remains the current gold standard in clinical practice, but obvious deficiencies remain with this technique given that surgical repair of peripheral nerves does not result in complete functional recovery with functional outcomes of between 30% and 70% reported (Nicholson and Seddon 1957). While the environment of sensory and motor axons will support axonal regeneration, it is often compromised by intraneural scarring which can be exacerbated following microsurgical repair and serves as a mechanical barrier to regenerating axons, converting a 'repaired' fifth-degree injury to a fourth-degree injury (Mackinnon 1989). Augmentation of the microsurgical repair technique to improve regeneration both electrically and histologically as well as decreasing inefficient axonal outgrowth would add greatly to this field. This concept is evaluated using an optical photochemical sealing technique in combination with a modified amnion wrap around the suture neurorrhaphy site in a large animal model. Photochemical tissue bonding (PTB) is a sutureless tissue repair process that seals the repair site without trauma or foreign body reaction, thus allowing prompt restoration of the normal endoneurial environment and subsequent regeneration. The

augmented histological and electrical outcomes following repair using this optical technique are discussed further in the latter section of this thesis.

The broad aim of this section is to evaluate the efficacy of photochemical tissue bonding with an amnion nerve wrap in the repair of the peripheral nerve of a large animal model using neurophysiological assessments as a functional outcome along with histological analysis.

2. Optical Microscopy & Diagnostics of the Peripheral Nerve

2.1. Optical Microscopy

2.1.1. Evolution of the Microscope; A Brief History

To observe beyond our limited human vision is a goal which has been chased by generations. Human perception is restricted in many ways; while we can see, hear, taste, smell and touch, these abilities are relatively feeble. We can only see a tiny amount of the light around us and this vision is limited to readily understandable scales. The human eye, while a unique organ with a large dynamic range is limited to a resolving power of .02 degrees under ideal conditions (Potmesil and Chakravarty 1981; Liang and Williams 1997). Thankfully, human curiosity and ingenuity know no bounds and when we find ourselves limited, we innovate. This has historically pushed pioneers to see beyond biological limitations and explore our world using a basic understanding of the eye as a template.

The very first record of an optical magnification device appeared in 424 BC with the mention of a "burning glass" - a concave piece of glass used to start fires in Aristophane's play "The Clouds" (Dover 1989). Physical evidence predates the written word with high quality lenses known as Visby lenses having been discovered dating back to the Vikings in the 11^{th} century (Schmidt, Wilms et al. 1999). The quality of these rock crystal lenses are comparable to modern optics and are theorised to have been used for telescopes. Lens-making continued in the Roman Empire (Rawson 1988) and through the dark ages by the work of Arabic craftsmen

(Rashed 1990) and by the 13th century, the very first eyeglasses had been produced (Bardell 1981). Despite this body of historical evidence, the invention of the first "true" microscope is attributed to a father-son team, Hans and Zacharias Janssen, in the 1590's (Gottschal, Harder et al. 1991).

Work continued slowly in the field and with continued improvements in lens quality and craftsmanship the first single lens microscope was created by Nathaniel Highmore sixty years later. Observing the formation of the heart and blood vessels in a chick embryo (Figure 2.1 below), Highmore became the first recorded person to visualise a living specimen on the microscopic scale (Bardell 2005).

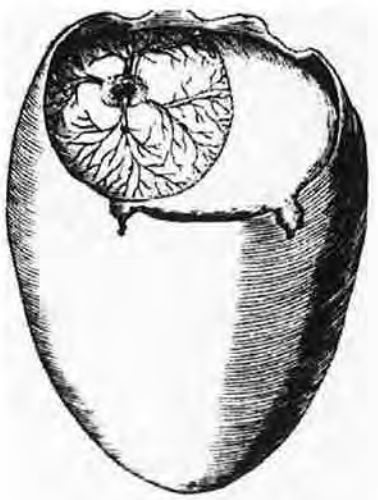

Figure 2.1 - Original Illustration of a developing chick embryo by Nathaniel Highmore (Highmore 1965).

Poor lens quality due to aberrations limited the magnification of these early microscopes (Amos 2000) and consequently their use as a observational tool, yet fuelled by curiosity, advancements continued over time.

In the mid-seventeenth century, Robert Hooke developed, amongst other things, far more advanced compound microscopes. These microscopes were built by combining two or three individual lenses (Bardell) and included a system for sample illumination. Hooke reported and illustrated many of his observations in his work *Micrographia (Hooke 1665)*, including a unique observation on the structure of cork:

> . . . I could exceedingly plainly perceive it to be all perforated and porous, much like a Honey-comb, but that the pores of it were not regular. . . . these pores, or cells, . . . were indeed the first microscopical pores I ever saw, and perhaps, that were ever seen, for I had not met with any Writer or Person, that had made any mention of them before this. . .

Through his observations and recordings, Hooke, coined the word for the basic unit of life - the cell - although it may not have occurred to him at the time that whole organisms may be composed of such units (Darden 1978) (Figure 2.2). Hooke's compound microscopes, however, were still limited to low magnifications due to inherent lens aberrations.

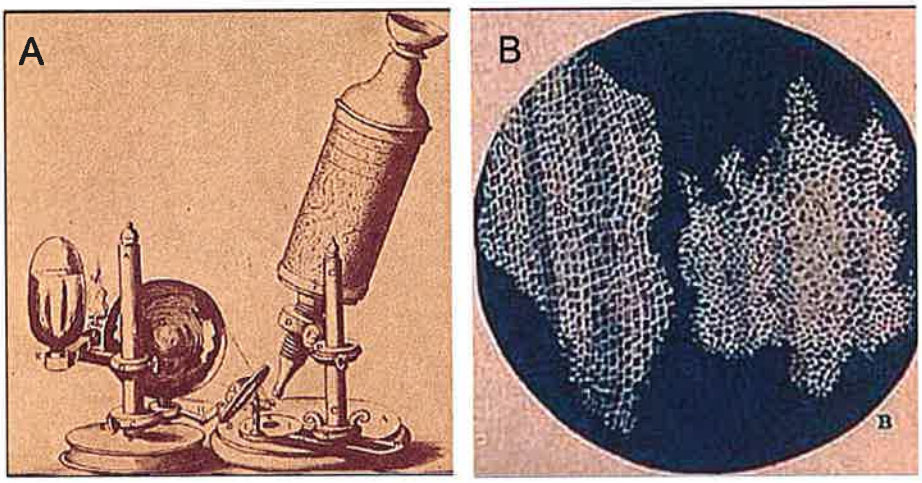

Figure 2.2 - A) Robert Hooke's Microscope and illumination system and B) Hooke's observation of 'cells' in cork slices in Micrographia (Hooke 1665).

Near the end of the seventeenth century, a young Dutch apprentice in a dry goods shop (Waggoner) overcame these restrictions. Now known as the "Father of Microscopy", Antoni van Leeuwenhoek was a contemporary of Hooke who observed drapers in his shop using magnifying glasses to examine cloth. Intrigued by their craftsmanship, he set out to improve on existing lens-making techniques. Over the course of a decade Van Leeuwenhoek's lens grinding and polishing skills allowed him to build low-aberration optics with very short focal lengths. By the mid 1790's, Antoni van Leeuwenhoek had completed 247 microscopes with magnifications ranging up to 270X (Waggoner). An example on one such microscope is shown in Figure 2.3.

Figure 2.3 - An example of a microscope as designed by Antoni van Leeuwenhoek. The sample is placed on the pin and brought into focus using the screw. This image is of a replica built by Al Shinn (Shinn).

Over the course of his lifetime, Van Leeuwenhoek's curiosity and persistence led him to examine nearly any sample he could obtain. His subject matter ranged from his environment; lake water in his hometown of Delft (from which he observed numerous micro-organisms) to more personal specimens; his discovery of parasitic protozoa came from a sample of his own faeces. He also described five different types of bacteria present in his mouth (Waggoner). Through his achievements, Van Leeuwenhoek demonstrated that the combination of curiosity and technological ability can lead to amazing advancements and discoveries and while not the first person to build a microscope, his perseverance, talent and practical applications have resulted in his being known as 'The father of Microscopy'.

Over time lens quality continued to improve, the compound microscope became the standard for high magnification imaging and the development of the achromatic lens in 1729 by Hall, and later in 1807 by Jan Marmanus van Deyl, increased the capabilities of microscope systems. Microscopes developed by Carl Zeiss, Ernst Abbe and Hugh Powell in the late 1800's were built with high numerical aperture immersion lenses capable of diffraction limited resolution. By the beginning of the 20^{th} century, the light microscope had become a powerful scientific tool instrumental in the advancement of modern medicine and indeed, our understanding of the environment, both internal and external.

2.1.2. Contrast Based Modern Microscopy

Modern light microscopes are advanced tools with the ability to study samples with sub-diffraction limited resolution. In the typical commercial microscope, light generated by a lamp is focused for illumination onto the sample by a condenser. An objective lens collects the light from the focal plane, collimating it and then reflecting it to the eyepiece. An example of a modern light microscope is shown below in figure 2.4.

Figure 2.4 - Modern upright light microscope (Zeiss)(Zeiss).

When used for imaging, the objects in the focal plane of a microscope appear dark against a bright background generated from the illumination source. In this process, the contrast is based on two phenomena: scattering and absorption. Scattering, arising from Mie scattering processes, redirects photons away from their initial angle of propagation. The Mie algorithm models all of the "traditional" scattering processes caused by a spherical drop of water, such as external reflection, multiple internal reflections, transmission and surface waves. As such, a scattering object will decrease in apparent brightness appearing increasingly dark in the observed field. Absorption of the light by the sample also leads to reduced subject brightness. In a reflection configuration, image contrast is dominated by absorption and scattering, with absorption decreasing object brightness. Scattering - in particular the reflection

of illumination photons - will lead to positive contrast as an object will appear brighter.

It is possible to take advantage of scattering to improve image contrast. In dark field microscopy, scattering of illumination photons serves as the main source of contrast, with scattering objects appearing bright against a dark background. This is achieved by excluding the unscattered beam from the image. As a result, the field surrounding the specimen (i.e. where there is no specimen to scatter the beam) is generally dark.

Scattering and absorption alone, however, are not useful for when imaging thin, clear objects such as cells. While it is possible to see such objects when viewing them out of focus, such specimens will lose nearly all contrast when imaged directly in the focal plane. These samples can be visualized by taking advantage of a different kind of contrast: phase shifts. Zernike (Zernike 1942), in the early 1930s, developed phase microscopy which takes advantage of phase shifts that occur due to differential sample propagation length. While many photons pass through a sample without alteration, he noted that they may also diffract off certain objects in a specimen. Travelling at different angles than the incident light, these deviated photons will and therefore take longer to propagate through the medium. The typical phase delay through a thin sample due to diffraction is on the order of a quarter of the wavelength ($\lambda/4$). The human eye, however, cannot perceive phase changes of this magnitude. To visualize this phenomenon, Zernike made use of phase rings placed in the back of the objective converting phase to intensity. By placing a $\lambda/4$ phase retardation ring in the focal plane the photons can be delayed. When the zeroth order photons are then

combined with the delayed photons, interference can occur, revealing phase objects in the focal plane and allowing visualisation.

A related phase technique, called differential interference contrast (DIC), also generates contrast based on relative phase delays. DIC transforms the phase shift of the photons into detectable amplitude differences. An advantage of interference-derived contrast is that an object will appear bright against a dark background but without the diffraction halo associated with phase contrast. This technique, developed by Nomarski in the 1970s (Normarski 1955), makes use of polarised light and a special optic called a Wollaston Prism. A Wollaston prism has the ability to split an incoming beam of light into two beams propagating in different directions as illustrated below in Figure 2.5. The prism splits the incoming light into two beams that travel along through the sample in very closely spaced paths, which after the objective, are recombined by another Wollaston prism allows beam interference. If the two beams travelled through materials with different refractory indices, a relative phase delay between the beams will occur that results in interference. For this reason, DIC is sensitive to edges in specimens previously obscured by diffraction halos.

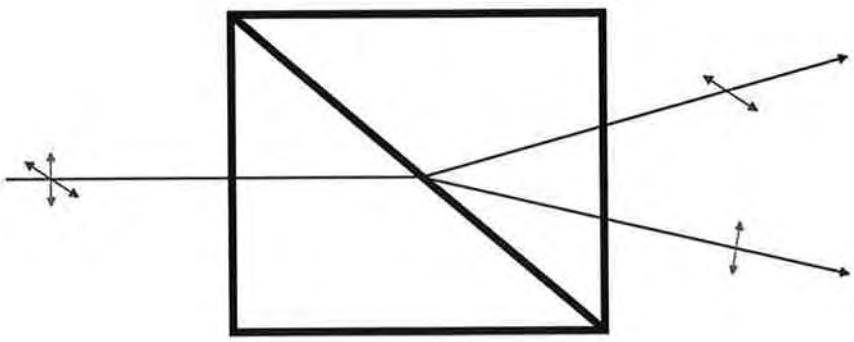

Figure 2.5 - Illustration of a Wollaston prism splitting an incoming beam of light into two beams propagating in different directions

It is also possible to make use of the polarisation of light for image contrast. Polarisation is the property of waves that describes the orientation of their oscillations. A common feature of optical microscopes is a pair of crossed polarising filters. Between the crossed polarisers, a birefringent sample will appear bright against a dark (isotropic) background. While isotropic materials have a single index of refraction, certain anisotropic crystals can have two different indices of refraction. In such birefringent materials, the indices of refraction have different values. A photon that encounters such a crystal will have its polarisation vector split into two components. As in DIC, the two components will experience different propagation times through the material, resulting in a phase difference. Upon recombination on an analyzer, this phase difference gives rise to images with striking contrast.

Each of these techniques give complementary information about a specimen through different sources of contrast and this remains the basis of several advanced microscopy techniques, such as Optical Coherence Tomography (de Boer, Cense et

al. 2003; Fujimoto 2003) and confocal reflectance microscopy (Rajadhyaksha, Grossman et al. 1995). As such, these microscopes are both restricted in their application but conversely are suitable and sensitive methods for imaging within the scope of their physical properties and in doing so avoid the need for extrinsic contrast media or labels. Optical Coherence Tomography as an imaging modality is further discussed below in Chapter 2.3.

2.1.3. Chemically and Molecular Selective Modern Microscopy

Fluorescence microscopy uses a molecule's electronic structure to provide chemically specific contrast. In a manner similar to histological staining methods, dyes are applied that can be engineered to specifically target a chemical of interest. Fluorescence microscopy is an extremely powerful technique that has been developed extensively. The contrast obtained is based primarily on the wavelength of light emitted when a molecule undergoes a process known as fluorescence. Fluorescence can be observed when a molecule absorbs a photon and becomes promoted to its excited state. As the excited state has a fixed lifetime, it eventually undergoes intramolecular vibrational relaxation, losing energy while emitting a photon and returning to the ground state.

The major drawback to fluorescence microscopy can be the act of labelling itself. Fluorescent labels can often distort the system of interest, causing unwanted artefacts (English, Min et al. 2006). Many labelling protocols require fixation thus preventing real-time imaging of a sample with chemical contrast. This issue has largely been overcome by means of exploiting the vibrational spectrum of biological samples that

can be used to identify the chemical components of a specimen. The vibrational modes of molecules oscillate with characteristic frequencies determined by the number and mass of the atoms in motion and the strength of the bonds involved. As such, every molecule has a unique vibrational signature that can be used as a fingerprint for chemical identification.

A more advanced vibrational imaging technique is Raman microscopy. In Raman scattering (Raman and Krishnan 1928), interaction of light with molecular vibrations creates new frequencies of light with energy spacings equal to the vibrational energy gap (Raman effect). The Raman effect occurs when light impinges upon a molecule and interacts with the electron cloud of the bonds of that molecule. The incident photon excites one of the electrons into a virtual state. For the spontaneous Raman effect, the molecule will be excited from the ground state to a virtual energy state, and relax into a vibrational excited state, which generates Stokes Raman scattering, as shown in Figure 2.6.

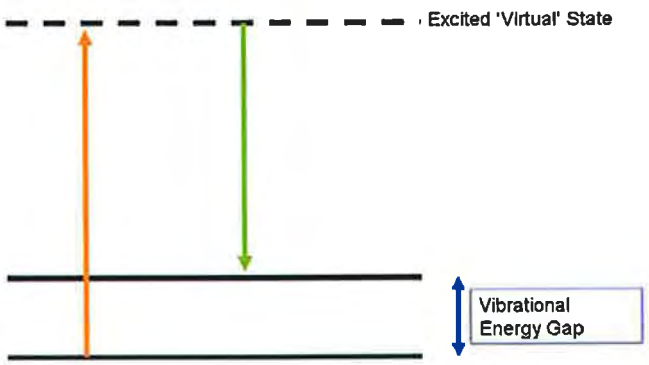

Figure 2.6 - Production of the Vibrational Energy Gap (Raman Effect) following excitation (orange) of a photon into a virtual state and relaxation (green) into a vibrational excited state.

If the molecule was already in an elevated vibrational energy state, the Raman scattering is then called anti-Stokes Raman scattering. As Raman scattering occurs for all wavelengths of light, it is possible to carry out high resolution, chemically-selective microscopy using Raman contrast. The main limitation of this technique is the extremely weak Raman effect and as such, Raman image acquisition times are long and require very high power laser sources. This combination limits its use in biological, living samples.

These limitations can be overcome with Coherent Anti-Stokes Raman Scattering (CARS) microscopy where stronger vibrational signals can be obtained using moderately powered laser sources suited for biological imaging.

2.2. Coherent Anti-Stokes Raman Scattering (CARS) Microscopy

2.2.1. CARS Microscopy

Coherent Anti-Stokes Raman Scattering (CARS) microscopy is a highly sensitive imaging modality. It differs from other molecule specific microscopes given that it functions without the need for extrinsic cell and tissue labelling and that a moderately powered laser source is used to produce high quality images with a resolution of up to 5μm in a non destructive fashion (Evans, Potma et al. 2005). Based on the principles and theory of Raman Microscopy and utilising the Anti Stokes effect it has developed into a sensitive tool capable of extremely high resolution, real time, non destructive imaging of biological samples and in particular shows a high affinity for lipid structures as shown below in Figure 2.7.

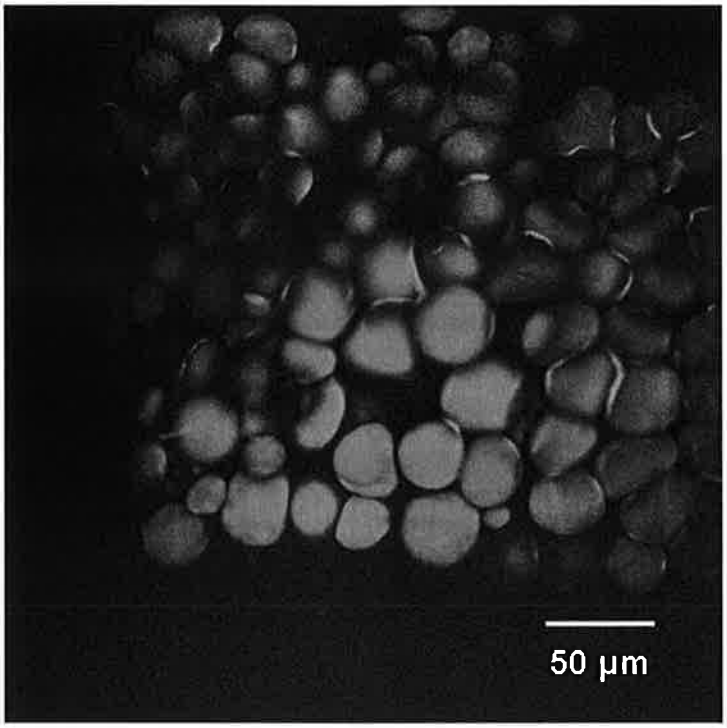

Figure 2.7- Adipocytes imaged with CARS Microscopy. These cells depict the bright contrasted results achieved when imaging lipid compounds as a result of the strong affinity of CARS Microscopy for Lipid rich structures.

While the detailed theory behind the CARS Microscope remains beyond the scope of this thesis a basic overview of its functional components and structure may be found in Chapter 3 and below in Chapter 2.2.2.. In brief CARS microscopy offers the following advantages that make it an ideal imaging technique for use in the field of neural diagnostics (Evans, Potma et al. 2005):

1) CARS microscopy provides contrast based on the intrinsic molecular vibrations of a specimen, circumventing the need for extrinsic labels.

2) CARS microscopy is more sensitive than spontaneous Raman microscopy, permitting video-rate vibrational imaging at moderate average excitation powers (i.e. up to 10 mW).

3) CARS microscopy has a 3D sectioning capability, which is useful for imaging thick tissues or cellular structures allowing for a slice by slice analysis of the tissue.

4) Using near infrared excitation wavelengths, CARS microscopy has a relatively large penetration depth of more than 0.4 mm into a sample, allowing imaging in thick tissues.

5) By using picosecond duration near-infrared light, it is possible to image a sample for hours with CARS Microscopy without inducing thermal damage.

2.2.2. History of CARS Microscopy

Coherent anti-Stokes Raman scattering was first reported by Maker and Terhune at the Ford Motor Company in 1965 (Maker and Terhune 1965). Ironically, the effect was not named CARS until almost ten years later (Begley, Harvey et al. 1974). Maker and Terhune used a pulsed ruby laser to investigate the third order response of materials in use in their industry. They first passed a ruby beam through a Raman shifter to create a second beam, and then directed the two beams simultaneously onto the sample. When the pulses from both beams overlapped in space and time, the Ford researchers observed a CARS signal. They also demonstrated that when the

difference frequency between the incident beams matches a Raman frequency of the sample, the signal increases significantly. Maker and Terhune described their technique as simply 'three wave mixing experiments'. The name coherent anti-Stokes Raman spectroscopy was assigned by Begley (Begley, Harvey et al. 1974) at Stanford University in 1974. Since then, this vibrationally sensitive nonlinear optical technique has been commonly known as CARS Microscopy.

The Reintjes group at the Naval Research Laboratory was the first to use the CARS effect in the field of microscopy as a contrast mechanism (Duncan, J et al. 1982). However, their work had many limitations, and the excitation with visible light rather than current near infrared laser techniques created an overwhelming non-resonant background due to two-photon electronic absorption resonances at the excitation frequencies. Because of the extreme technical difficulties, there were no further developments until 1999, when CARS microscopy was revived by the work of Sunney Xie and his lab at Harvard University. In this group, Zumbusch et al. (Zumbusch, Holtom et al. 1999) used near infrared laser pulses that led to a significant reduction of the two-photon enhanced non-resonant background. More importantly, they used highly focused collinear-propagating pump and Stokes beams that relaxed the so-called phase matching condition. CARS images were acquired by scanning the sample with respect to the small laser focal volume, resulting in high-resolution three-dimensional images. This innovation has led to a revival of CARS Microscopy. While advances to the technique remain slow, the avenues of investigation and applications of the microscope are evolving over time including its use as reported in this thesis regarding peripheral nerve imaging following injury.

2.2.3. Applications of CARS Microscopy

As an imaging technique, CARS is an ideal tool for chemically-selective imaging of molecules and tissues. In 2004, the first demonstration of a video-rate CARS microscope was used to visualize mouse skin *in vivo* (Evans, Potma et al. 2005). All of the properties that make CARS microscopy desirable were demonstrated in tissue: chemical specificity, high time-resolution, high spatial resolution and 3D sectioning capability.

CARS Microscopy has also been used with success in metabolite imaging where applications include studies of lipid metabolism, organelle transport in vivo, and viral disease. More recently experiments have used deuterium isotope substitution as a spectroscopic contrast agent to study the effects of Omega-3 fatty acids on liver cell lipid metabolism (Xie, Yu et al. 2006). Previous successful demonstrations of CARS microscopy have been reported in living cells at the phosphate stretch vibration (DNA), amide I vibration – protein (Cheng, Jia et al. 2002), OH stretching vibration – water (Potma, de Boeij et al. 2001), and CH group of stretching vibrations – lipids (Nan, Cheng et al. 2003; Nan, Potma et al. 2006).

The ability to image living tissue makes CARS microscopy a powerful biomedical modality in the study of the natural architecture of tissues and in the imaging of drug distribution in particular with reference to their interactions with the lipid bilayer in membrane chemistry. Utilising it's exquisite sensitivity to lipids, studies using CARS microscopy have successful seen not only single lipid bilayers, but also observed lipid phase segregation in a label-free manner (Potma and Xie 2005).

Its application to the field of neural imaging is again supported by the high lipid content of myelin, which structurally comprises 70% of the molecule (Morell and Quarles 1999). Identification of the myelin sheath in both the normal and remyelinating nerve, as well as noting absence of signal in the demyelinated nerve can therefore be used as a reliable means of assessing the neural microenvironment *in vivo*. This structural analysis can be used following injury to assess the regeneration of the nerve repeatedly over time, analogous to non invasive histology and has been preceded by work involving CARS microscopy of the central nervous system. This application revealed CARS as a valuable and promising modality in imaging brain tumour margins with subcellular spatial resolution in fresh, unstained tissue allowing for virtual histological margins to be assessed (Evans, Xu et al. 2007).

2.3. Optical Coherence Tomography

2.3.1. Introduction to Optical Coherence Tomography

Optical Coherence Tomography is an imaging technique used to obtain sub-surface images of tissue or material at a resolution equivalent to a low-power microscope (Huang, Swanson et al. 1991). Systems typically have an axial resolution between 5-10 microns with a lateral resolution between 10-20 microns (Schuman, Puliafito et al. 2006). It can be thought of as 'optical ultrasound', where the time delay of light reflected from within tissue is used in a method analogous to the formation of cross-sectional ultrasound images based on the timing and intensity of reflecting sound waves. OCT is particularly useful in biological applications given its ability to

achieve live sub-surface images at near-microscopic resolution, allowing for direct imaging of tissue morphology without the need for specialised contrast media, labelling agents, or the use of ionizing radiation.

In OCT, an optical beam is directed at the tissue and the small portion of the light that reflects from sub-surface features is collected. Most of the light incident on the tissue is not reflected but scattered and does not contribute to forming an image. This scatter contributes to glare and results in a material appearing opaque. Using the OCT technique, scattered light can be filtered out, completely removing the glare and thus concentrating on the refractory properties of the material alone. Even when the proportion of reflected light that is not scattered is minimal, it can still be detected and used to form an OCT image.

The principle allowing this filtering of scattered light is called optical coherence (Born, Wolf et al. 1999). Only the reflected (non-scattered) portion of light that maintains coherence (i.e., can be used to form spatially or temporally stationary interference) with respect to a reference beam is used. In the OCT instrument, a lens is used in such a manner as to detect all the light reflected back from the sample. This light is combined with a reference beam to form interference patterns. Light that has scattered randomly will not form interference fringes, thus, by limiting examination to only the interference pattern, the scattered light is stripped off from the reflected light in order to generate an image. During this process, depth and intensity of the light reflected from a sub-surface feature is obtained. A three-dimensional image can then be built up by scanning, as in a sonar or radar system.

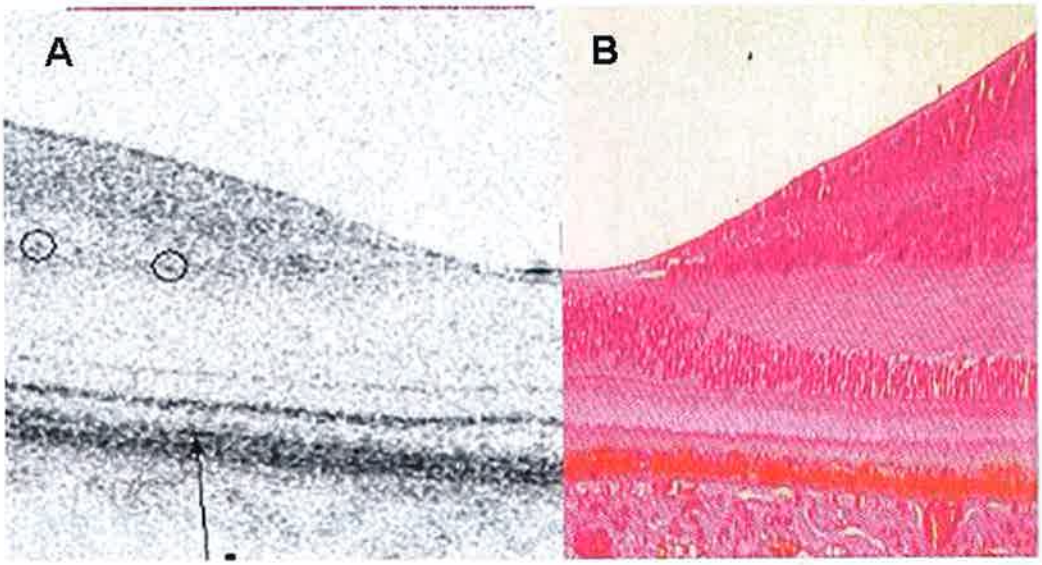

Figure 2.8 - Matched OCT (A) and histology (B) images acquired from a human retina. (Histology courtesy of Dr. Ralph C. Eagle, Jr., M.D. Director, Department of Pathology, Wills Eye Hospital Philadelphia, Image courtesy of B.H. Park)

OCT has created much interest among the medical and surgical communities (Schuman, Puliafito et al. 2006) due to its ability to provide images of tissue morphology at much higher resolution (< 10 μm) than other traditional imaging modalities such as MRI or ultrasound. Its continuing development, discussed below has resulted in many ongoing clinical investigations and its translation across to clinical practice as seen above in matched OCT and Histological assessment of the retina (Figure 2.8).

2.3.2. Evolution of Optical Coherence Tomography

Optical coherence tomography (O.C.T.) has found great utility for in vivo studies in a number of clinical fields (Huang, Swanson et al. 1991). With its conception as white-light interferometry for *in vivo* ocular eye measurements, O.C.T was born from the perseverance of multiple investigators worldwide pursuing a photo-based diagnostic tool in the field of ophthalmology. While first devised in 1990 by Naohiro Tannoo of Yamagata University, and closely followed in 1991 by Huang et al (Massachusetts Institute of Technology) (Huang, Swanson et al. 1991), optical coherence tomography (OCT) has become one the more prominent biomedical tissue-imaging techniques to date. From its basic form as a relatively simple 'white light interferometer,' it has evolved in less than 20 years to become a sophisticated diagnostic tool with wide clinical applications.

Traditional, or time-domain (TD) OCT systems detect the time delay of light back-reflected from within a sample in an analogous manner to detection of the time delays experienced by sound waves in ultrasound. However, the difference in propagation speed between sound and light necessitates interferometric detection as a reference arm length is scanned in order to detect the extremely short temporal delays for light back-reflected from different depths within a sample.

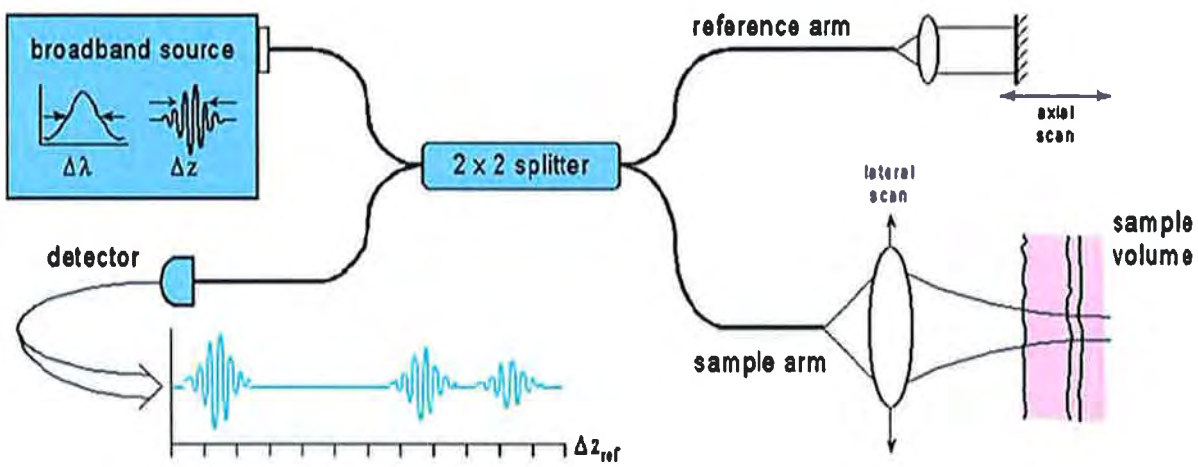

Figure 2.9 - Schematic of interferometric detection in OCT. (Courtesy of B.H.Park)

Over time functional extensions to OCT have augmented its clinical potential by providing more information on tissue properties than standard OCT imaging alone. Optical Doppler tomography (ODT), for example, is capable of depth-resolved imaging of flow (Wang, Milner et al. 1995; Chen, Milner et al. 1997; Chen, Milner et al. 1997; Izatt, Kulkami et al. 1997). Using this technique, sensitivity to flow can be achieved by measuring the shift in carrier frequency of the interference fringe pattern due to backscattering of light from moving particles (Doppler effect), or by observing differences in the phase of the interference patterns between successive depth scans. The recent advent of Fourier-domain OCT, in both swept-source and spectrometer-based varieties, has vastly improved the clinical utility of all OCT technology. In the spectrometer-based technique, otherwise known as spectral-domain optical coherence tomography (SD-OCT) (Fercher, Hitzenberger et al. 1995; Hausler and Lindner 1998; Wojtkowski, Kowalczyk et al. 2002; Wojtkowski, Leitgeb et al. 2002), the interference pattern for light returning from the sample and a

fixed reference arm is spatially dispersed using a custom-built high-resolution spectrometer. A schematic of interferometric detection in OCT is shown in figure 2.9. Mathematical transformation of the resulting signal allows for determination of all points in a particular depth profile simultaneously. Fixing the reference arm length improves the phase stability of the system, and spectral detection of the inteferogram has been shown to allow for much greater acquisition sensitivity at a particular optical power (Andretzky, Lindner et al. 1998; Mitsui 1999; Choma, Sarunic et al. 2003; de Boer, Cense et al. 2003; Leitgeb, Hitzenberger et al. 2003). This sensitivity improvement can be translated into an order of magnitude increase in imaging speed. Thus, SD-OCT provides for detailed scanning of a large volume of tissue, removing the sampling error associated with acquisition of particular two-dimensional images in time-domain OCT. Functional extensions of OCT can yield information not readily visible otherwise, much in the same way various stains can enhance histological processing.

2.3.3. Polarisation Sensitive Optical Coherence Tomography

Initially, the emphasis in OCT was the reconstruction of two-dimensional maps of tissue reflectivity while neglecting the polarisation state of light. Hee *et al.* then presented an OCT system capable of measuring the changes in the polarisation state of light reflected from a sample (Hee, Huang et al. 1992). Using an incoherent detection technique, they demonstrated birefringence-sensitive ranging in a wave plate, an electro-optic modulator, and calf coronary artery. In 1997, the first two-dimensional images of birefringence were presented using a similar system, and the effect of laser induced thermal damage on tissue birefringence in bovine tendon was

demonstrated (deBoer, Milner et al. 1997). This was followed in 1998 by a demonstration of the birefringence in porcine myocardium (de Boer, Srinivas et al. 1998). In 1999, phase sensitive detection was implemented to determine the phase relation between the interference fringes in orthogonal polarisation channels, which allowed for calculation of the Stokes parameters of the reflected light with a single measurement (de Boer, Milner et al. 1999). Hitzenberger *et al.* then used the phase relation in 2001 to determine the optic axis orientation of a birefringent sample (Hitzenberger, Gotzinger et al. 2001).

Polarisation-sensitive optical coherence tomography (PS-OCT) uses not only the amplitude, but also changes in the polarisation state of light returning from within a sample, allowing for access to light polarisation changing properties such as birefringence. A number of biological samples exhibit birefringence, the amount of which can be attributed to a combination of the density and organisation of fibrous structures. Birefringence is an optical property caused by the decomposition of light into two pathways when it passes through certain types of material, such as calcite crystals or boron nitride, and is dependent on the polarisation of the light (Born, Wolf et al. 1999). This effect can occur only if the structure of the material is anisotrophic (directionally dependent).

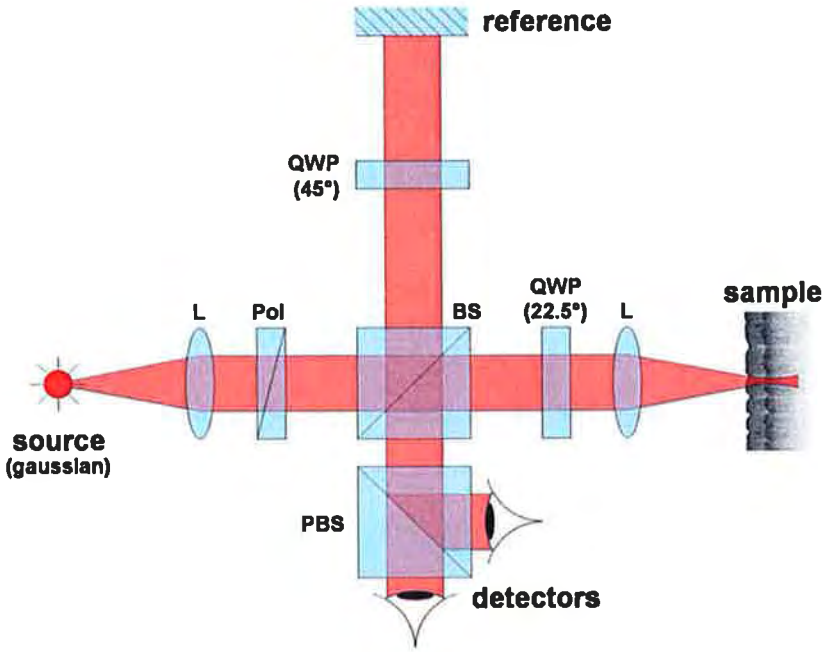

Figure 2.10 - Schematic of an early PS-OCT system implemented with bulk optics. (Courtesy of B.H.Park)

PS-OCT images identify birefringent regions in the tissue sample by measuring the polarisation state of light reflected throughout all depths of the sample. The polarisation state of incident light is determined at each location on the tissue surface and represented by a black-coloured pixel. Phase retardation is a cumulative measure of the difference in light propagation speed for different polarization states with depth. It is therefore affected by the depth travelled, and the magnitude of the speed difference. The intensity-weighted mean of the accumulated phase retardation angles experienced by the two incident polarisation states of light is displayed on a gray scale from black (0°) to white (180°), and to black (0°) again for complete wave retardation (360°). These angles are determined using a Poincaré sphere mathematical model, a construct used to display all possible polarisation states of light (Saxer, de Boer et al. 2000; Park, Saxer et al. 2001). This model allows

expression of birefringence by plotting the phase retardation angle over depth into the sample. On propagation through non-birefringent tissue, the polarisation state of light will not change as no phase retardation is incurred, and therefore the colour of the image remains unchanged with increasing depth. The rate at which the polarisation state changes with depth is proportional to the magnitude of tissue birefringence, which may be visualised by the frequency of black-to-white transitions in the images.

Collagenous structures such as dermis, muscle and nerve display birefringence and therefore have become suitable avenues of investigation for PS-OCT imaging. A schematic of an early PS-OCT system is shown in figure 2.10.

2.3.4. Applications of Optical Coherence Tomography

Ophthalmological applications of OCT have arguably driven a great deal of its development, and probably represent the most researched clinical application of the technology to date. The applications of OCT in its multiple forms are widespread across all disciplines of medicine and surgery (Schuman, Puliafito et al. 2006), for the most part in experimental phases of evaluation. However, clinical imaging systems are in use today in the clinical assessment of disorders such as glaucoma (Cense, Chen et al. 2002), The main areas of investigation and application regarding all forms of OCT remain the fields of Ophthalmology (Puliafito, Hee et al. 1996) and Dermatology (Pierce, Strasswimmer et al. 2004).

More basic OCT applications such as TD- and SD-ODT have allowed for imaging blood flow patterns in port-wine stains (Nelson, Kelly et al. 2001) and studying the dynamics of retinal blood flow *in vivo* (Leitgeb, Schmetter et al. 2003; White, Pierce et al. 2003) as well as complete anatomical mapping of the retina with histological correlation (example shown in Figure 2.8 above).

PS-OCT has also been applied to a wide variety of clinical problems, including the aforementioned as well as *in vivo* examination of the retinal nerve fibre layer (Ducros, de Boer et al. 1999; Ducros, Marsack et al. 2001; Cense, Chen et al. 2002; Cense, Chen et al. 2004; Cense, Chen et al. 2004; Pircher, Gotzinger et al. 2004; Gotzinger, Pircher et al. 2005; Naoun, Dorr et al. 2005; Rylander, Kemp et al. 2005; Zangwill and Bowd 2006), and examination of articular cartilage, specifically for the detection of osteoarthritis (Herrmann, Pitris et al. 1999; Drexler, Stamper et al. 2001; Han, Chu et al. 2003; Pan, Li et al. 2003; Chu, Lin et al. 2004; Li, Martin et al. 2005; Patel, Zoeller et al. 2005; Youn, Vargas et al. 2005), The additional contrast provided with polarisation sensitivity has shown promise for detecting changes in collagen birefringence due to thermal damage (de Boer, Srinivas et al. 1998; Park, Saxer et al. 2001; Cense, Chen et al. 2004) and in normal dermal collagen (Pierce, Strasswimmer et al. 2004) leading to the assessment of burn depth in human tissue (Pierce, Sheridan et al. 2004), identification and optical delineation of basal cell carcinoma margins (Strasswimmer, Pierce et al. 2004), and dermal photo-aging (Kuwahara, Strasswimmer et al. 2005). PS-OCT has also been used for potential early detection of glaucoma, the world's second leading cause of blindness. Ophthalmic studies can be performed using systems similar to that used by Cense et al. (Cense, Chen et al. 2002), in which a slit lamp has been adapted for use with PS-

OCT allowing ease of translation across to clinical use. Figure 2.11 shows examples of Histology, PS-OCT and OCT imaging of normal and burned skin highlighting the subtle differences in images acquired with the techniques.

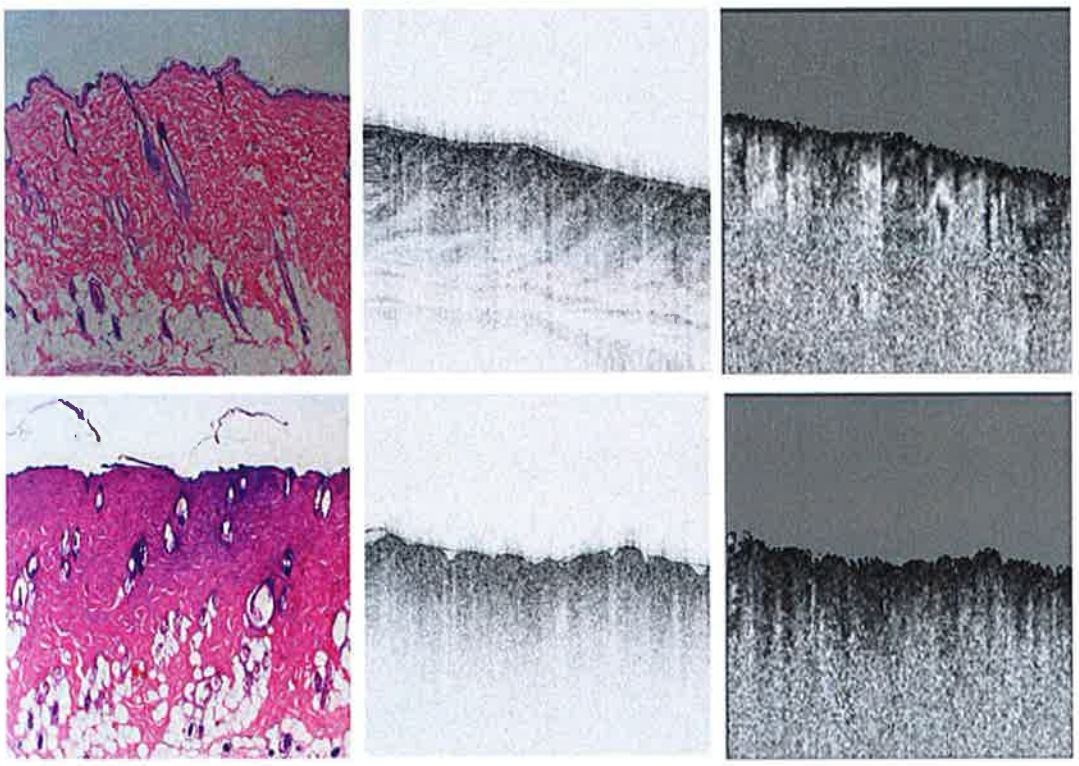

Figure 2.11 - Normal rat skin (top) and rat skin after thermal injury (below) (a) histology (b) OCT image and (c) PS-OCT Image. The dimensions of the histological images and phase maps are 3.2 mm by 2 mm. Adopted and reprinted with permission from the Society for Photonics in Engineering (B.H. Park, et al (Park, Saxer et al. 2001)).

In this thesis, the ability of PS-OCT to assess the microenvironment of the normal and regenerating peripheral nerve with subsequent development of a scale that may be used to predict nerve injury and regeneration by means of quantifying axonal

myelination in an in vivo non-destructive manner is evaluated. OCT has been previously used to identify nerve in tissue such as the prostate gland (Boppart, Herrmann et al. 2002; Fried, Rais-Bahrami et al. 2007), but was unable to assess the nerve microenvironment in a quantitative manner. The additional contrast provided with polarisation sensitivity lends itself toward use in this manner. Myelin is one such structure that exhibits birefringence, and to a much greater extent than anything else in the peripheral nerve. Therefore the hypothesis remains that the degree of myelination of the peripheral nerve can be quantifiably assessed through determination of its birefringence, and any subsequent change in this microenvironment following injury will be reflected in a change of birefringence.

2.4. Optical Microscopy & Diagnostics of the Peripheral Nerve - Aim

The aim of this section is to evaluate the ability of these optical microscopes in assessing the microenvironment of the normal and regenerating peripheral nerve in both a structural and quantitative manner.

To this end, video rate Coherent Anti-Stokes Raman Scattering (CARS) microscopy is assessed as a method of imaging the remyelinating peripheral nerve in a real time, *in vivo* and non-destructive manner, observing structural changes following a demyelinating injury.

PS-OCT is used to quantitatively assess the microenvironment of the normal and injured peripheral nerve with subsequent development of a scale that may be used to predict nerve injury and regeneration.

3. Materials and Methods – Optical Microscopy & Diagnostics

3.1. Coherent Anti Stokes Ramon Scattering (CARS) Microscopy

3.1.1. Animal Model & Surgical Procedures

The institutional Subcommittee on Research Animal Care (SRAC) at Massachusetts General Hospital approved all procedures described. The sciatic nerve of the Sprague Dawley rat (Charles River Laboratories, Wilmington, MA) was used as a model for this study. Animals were anaesthetised with an intraperitoneal injection of pentobarbital sodium (50mg/kg, Abbott Laboratories Chicago, Il).

A standardised demyelinating crush injury (Bridge, Ball et al. 1994) was reproduced by a single surgeon in the right sciatic nerve of the animals. Surgical exposure was undertaken via a right dorso-lateral muscle splitting incision following which the crush injury was achieved by holding a #5 jewellers forceps closed across the nerve for 30 seconds, 1cm distal from the exit of the nerve from the pelvis. This procedure is show in Figure 3.1 below. Following crush injury the site was then marked with a single 10.0 non-absorbable nylon suture (Ethicon, Somerville, NJ) placed under microscopic guidance into the epineurium of the nerve.

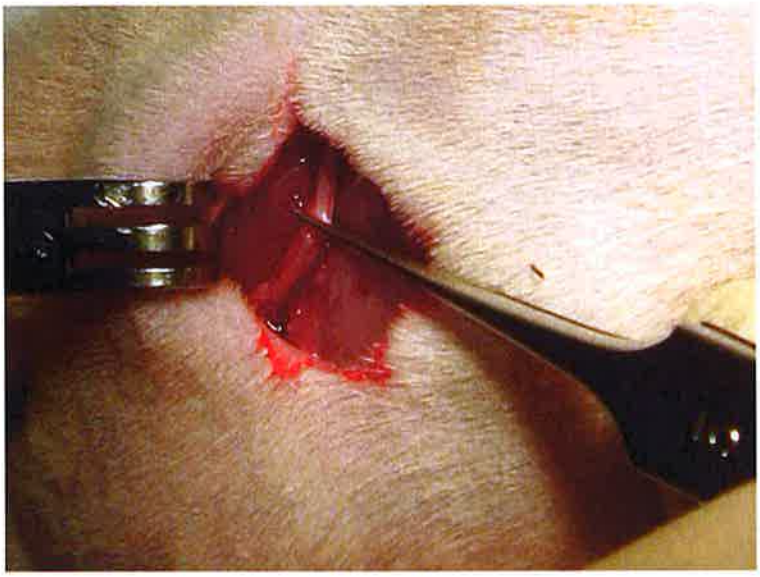

Figure 3.1 – Sciatic nerve Crush injury of the Sprague Dawley Rat using a # 5 Jewellers forceps.

Following the crush injury procedure the wounds were closed using 4-0 absorbable polyglactin sutures (Ethicon, Somerville, NJ). Postoperatively, animals were housed in the Massachusetts General Hospital animal facility with unlimited access to water and rat chow. Elizabethan collars were used to prevent wound mutilation in the immediate post operative period (4 Days) following which animals were permitted to mobilize without restraints

3.1.2. Experimental Design

Animals were randomised into groups and both imaging with CARS microscopy and functional analysis using walking track analysis was undertaken at day one and weeks one, two, three and four following injury. The uninjured nerve from the

contralateral limb was used as a control. In total 12 animals underwent imaging with sacrifice following imaging at each timepoint as shown below in table 3.1.

Table 3.1 – Experimental Groups (CARS Microscopy). Total n=12 with sacrifice following imaging at each time point.

Group	Week of Imaging	Number (n=)
1	Day 1	n=2
2	Week 1	n=2
3	Week 2	n=2
4	Week 3	n=2
5	Week 4	n=4

3.1.3. Functional Analysis

Walking track analysis was performed following injury in order to calculate a sciatic function index as described by Bain and Mackinnon (Bain, Mackinnon et al. 1989). This functional analysis was undertaken to confirm regeneration over time following sciatic nerve crush injury and is based on the morphological changes observed in the pawprint of the animal following sciatic nerve injury. These measurements are show in Figure 3.2 with an example of both the injured and normal pawprint of the Sprague Dawley Rat.

Figure 3.2 – Normal pawprint of the Sprague Dawley Rat shown on the Left with Print Length, Intermediary Toe Spread (Superior transverse line) and Full Toe spread (Inferior transverse line) show in Red. On the right is an example of a pawprint following sciatic nerve injury. A noted increase in print length along with a shortening of intermediary and full toe spread can be appreciated.

To achieve these measurements, the animal's hind paws were dipped in a dilute India ink solution before the alert animal was placed into a 10 x 40 cm corridor and allowed to walk into a darkened box. Removable paper lining the corridor recorded each individual print. Three separate measurements of print length, toe-spread (distance between first and fifth toes), and intermediary toe-spread (distance between second and fourth toes) were taken from both left and right paws, using a digital callipers, with the non-operative left paw print used as a control (normal). The sciatic function index was calculated, with a value of zero representing normal function and more negative values up to -100, representing sciatic or functional impairment. To achieve this, a factor was generated from the mean of the measurements obtained

from the walking track as described above. This factor was calculated by subtracting the normal (N) from the experimental (Injured) value (E) and dividing the difference from the normal measurement as shown below.

$$\text{Print Length factor (PLF)} = \text{EPL - NPL / NPL}$$

$$\text{Toe Spread Factor (TSF)} = \text{ETS - NTS / NTS}$$

$$\text{Intermediary Toe Spread Factor (ITF)} = \text{EIT - NIT / NIT}$$

These values were used to calculate a sciatic function index using the formula as described by Bain and MacKinnon (Bain, Mackinnon et al. 1989) and shown below.

$$SFI = -38.3\,(PLF) + 109.5\,(TSF) + 13.3\,(ITF) - 8.8$$

This standardised assessment was used in a longitudinal manner to correlate injury and subsequent regeneration with both histology and CARS imaging.

3.1.4. Coherent Anti-stokes Raman Scattering (CARS) Microscopy

CARS microscopy is based on contrast obtained from a four wave mixing process that can be loosely viewed as an enhanced Raman effect. The Raman effect occurs when light impinges upon a molecule and interacts with the electron cloud of the bonds of that molecule. The incident photon excites one of the electrons into a virtual state. For the spontaneous Raman effect, the molecule will be excited from the ground state to a virtual energy state, and relax into a vibrational excited state, which generates Stokes Raman scattering. If the molecule was already in an elevated

vibrational energy state, the Raman scattering is then called anti-Stokes Raman scattering. CARS Microscopy employs multiple photons to address the molecular vibrations, and produces a signal in which the emitted waves are coherent with one another. As a result, CARS is orders of magnitude stronger than spontaneous Raman emission.

CARS Microscopy requires three source photons (one Stokes photon, two pump photons) produced from two distinct laser beams. A Nd:Vanadate pulsed laser (7ps, picoTRAIN, High Q Laser, Austria) that produces 10 Watts of power at a repetition rate of 80 MHz and a wavelength of 1064 nm is split into two separate beams. A small fraction of the power (5%) is used for the Stokes beam, while the remaining power is used to synchronously pump an optical parametric oscillator (Levante, APE) that generates approximately 400mW at a wavelength of 817nm for the pump beam. When the frequency difference between the pump and stokes pulses matches the vibration frequency of a Raman active molecule, the resonant oscillators are coherently driven and generate an anti-Stokes photon (i.e., a signal photon at a shorter wavelength) that is detected to create the image. The enhanced contrast obtained with coherent anti-Stokes microscopy arises because this frequency difference between the pump and Stokes beams is selected to resonantly excite the vibrational resonance of CH2 stretch mode ($2845cm^{-1}$) predominantly localized in lipids. Since CARS has a nonlinear dependence on intensity, like two-photon excited fluorescence, the signal is generated only at the laser focus which allows for a point by point analysis of the tissue analogous to a true optical biopsy of the sample (Cheng, Volkmer et al. 2002).

The CARS system used for this study has been modified to include a confocal reflectance channel. Confocal reflectance is a separate and distinct contrast mechanism which produces images based on refractive index differences in the tissue (Rajadhyaksha, Grossman et al. 1995). It is non-specific and does not provide enhanced contrast data unlike CARS microscopy. Imaging with confocal reflectance (detecting only the 817nm beam) and with CARS is performed concurrently, with the reflectance data used to guide the user. Myelin, as a lipid rich molecule (Morell and Quarles 1999), accounts for the majority of the CARS signal in this case, while the confocal reflectance signal originates mainly from axonal tissue.

Imaging with CARS microscopy was undertaken on day one and weeks one, two, three and four following injury. Figure 3.3 shows the exposed sciatic nerve of the animal being imaged under the lens of the CARS Microscope.

Figure 3.3 – The exposed sciatic nerve of the Sprague Dawley Rat undergoing Imaging with CARS Microscopy.

All images were obtained with a real time video system allowing for immediate acquisition of data in both longitudinal and cross-sectional orientations. Imaging was achieved by mounting the anaesthetised animal on a custom-built stage under the lens objective. Multiple images are averaged for improved image quality (typically 30 images acquired in one second). Prior to averaging, a custom real-time correction algorithm is applied to correct the images for animal movement due to breathing and heartbeat.

Following anaesthesia the sciatic nerve was exposed via the surgical approach described above. Animals were euthanised following imaging (IP Pentobarbital

200mg/kg) and both sciatic nerves were harvested for histological processing as described below.

3.1.5. Histology & Histomorphometry

Following imaging, animals were sacrificed with an intraperitoneal injection of pentobarbital (200mg/kg). The right and left sciatic nerves were harvested and fixed in a 2% / 2% gluteraldehyde / paraformaldehyde solution at 4^0C for forty eight hours. Specimens were post fixed in 1% osmium tetroxide, dehydrated in ethanol and embedded in epon. Cross sections 1μm in thickness were made at 5mm proximal and distal to the crush site using a microtome (Leica, Germany). Sections were stained with 0.5% (w/v) Toluidine blue for light microscopy.

Nerve architecture was examined at 400X magnification. Histology was used to verify injury and remyelination in the nerve. Five 400X images were taken of evenly distributed areas within the nerve sample. Ten fibres were randomly selected in each image (total of 50 fibres per nerve sample). The fibre width and axon diameter were measured using Image J™ (National Institutes of Health) (Abramoff 2004) and the myelin thickness was derived from the difference between the fibre and axon diameter. Fibre diameter and axon diameter measurements are shown below in figure 3.4.

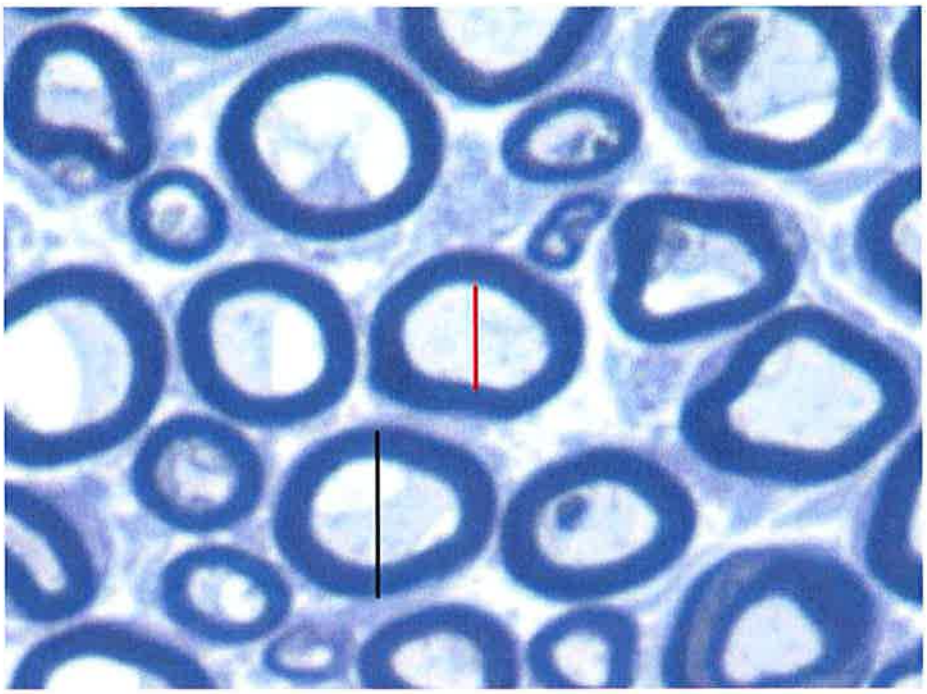

Figure 3.4 – Representative sample of nerve histology, stained with Toluidine blue at 400X magnification showing mature myelinated axons. The black line indicates the total fibre diameter and the red line indicates the Axon diameter as measured with Image J™ Software (Abramoff 2004).

3.1.6. Statistical Analysis

Histological values are expressed in terms of means with standard deviations. Statistical analysis of the data was performed using Microcal Origin 6.0 ™. Analysis of Variance (Two Way ANOVA) was used to evaluate the differences in histological regeneration at various time points following injury. Statistical significance was set at p-value <0.05.

3.2. Polarisation Sensitive Optical Coherence Tomography

3.2.1. Animal Model

The Massachusetts General Hospital Institutional Subcommittee on Research Animal Care (SRAC) approved all procedures described. The sciatic nerve of the Sprague Dawley rat (Charles River Laboratories, Wilmington, MA) as a model for this study. This robust model allows for manipulation of a nerve of similar calibre and size to the human digital nerve and has been described in the previous experiment as well as being a recognised standard model for this purpose.

3.2.2. Surgical Procedures & Experimental Design

To achieve a wide spectrum of injury and regeneration of the sciatic nerve two separate procedures were employed. A single crush injury, observed at various time points during recovery and a complete nerve transection to mirror findings consistent with a non regenerating nerve.

Nerve Crush Injury (Groups 1 – 4)

Animals were randomised into four groups (n = 8 per group) and anaesthesia was achieved with an intraperitoneal injection of pentobarbital sodium (50mg/kg, Abbott Laboratories Chicago, Il). This was followed by surgical exposure of the right sciatic nerve via a dorso-lateral muscle splitting incision. A standardised demyelinating crush injury was reproduced by a single surgeon in the right sciatic nerve of the animals (Bridge, Ball et al. 1994). The crush injury was produced as described

previously and the site was then marked with a single 10.0 non-absorbable nylon suture (Ethicon, Somerville, NJ) placed under microscopic guidance. Surgical wound closure was performed using 4-0 absorbable polyglactin sutures (Ethicon, Somerville, NJ). Functional analysis of walking track data was undertaken at week's one, two, three and four following injury. Surgical exposure followed by PS-OCT imaging was undertaken on week one, two, three and four following injury, at which point the animals were euthanised and imaged regions were harvested for histological processing. The uninjured nerve from the contralateral limb was used as a control and imaged concurrently with the experimental nerve.

Nerve Transection (Group 5)

An additional control group (n = 4) underwent nerve exposure as defined above. This was followed by sharp transaction of the nerve at a point 1 cm distal to the exit of the nerve from the pelvis. The distal stump of the nerve was buried in the surrounding muscle to prevent neural regeneration. Surgical closure followed the procedure as described above. These animals underwent PS-OCT imaging two weeks following their surgical procedure.

The experimental groups are summarized below in Table 3.2.

Table 3.2 – Experimental Groups (PS-OCT Imaging)

Group	Week of Imaging	Number (n=)	Procedure
1	Week 1	8	Nerve Crush
2	Week 2	8	Nerve Crush
3	Week 3	8	Nerve Crush
4	Week 4	8	Nerve Crush
5	Week 2	4	Nerve Transection

Throughout the study period, animals were housed in the Massachusetts General Hospital animal facility with unlimited access to water and rat chow. They were permitted to mobilize without restraints with Elizabethan collars used in the immediate post operative period to avoid wound mutilation by the animal. Buprenorphine 0.1-0.5 mg/kg SC every 8-12 hours was administered for three days following each surgical procedure to alleviate any pain and discomfort.

3.2.3. Functional Analysis

Walking track analysis was performed following injury in order to calculate a sciatic function index as described by Bain and Mackinnon (Bain, Mackinnon et al. 1989) and discussed previously.

Each animal underwent weekly functional analysis prior to imaging with PS-OCT and sacrifice.

3.2.4. Polarisation Sensitive-Optical Coherence Tomography (PS-OCT)

To achieve real time imaging of the injured and normal sciatic nerve, a high-speed multi-functional spectral-domain Optical Coherence Tomography (OCT) system was used (Park, Pierce et al. 2005). This system uses a broadband light source centered at 1.3μm and two InGaAs line scan cameras, allowing individual axial scans (in 24.4μs) to be acquired at a rate of 18,500 per second. The multi-functional properties of the system used allows for simultaneous intensity and PS-OCT imaging by passing the light from both arms through a fibre splitter and circulator and then directing it towards a polarisation-sensitive spectrometer. In the spectrometer, the light is split with a polarising beam splitter cube and projected onto two 512-element InGaAs line scan cameras (Sensors Inc., SU 512LX).

Data was acquired and visualised in real time using a custom multi-threaded software scheme running on a dual processor computer. Four separate displays allow for continuous real time updates of spectrum, intensity, flow and polarisation properties of the sample. Each image was calculated from a 3D data set measuring a 5mm x 5mm x 1.2 mm deep volume, which requires only 5 seconds to be acquired. The system used is shown below in Figure 3.5.

Figure 3.5 – Multifunctional Optical Coherence Tomography System showing separate displays allowing for continuous real time updates of spectrum, intensity, flow and polarisation properties of the sample being imaged.

Complete mathematical analysis of each data set was performed (Park, Saxer et al. 2001; Park, Pierce et al. 2003) and a mean of each birefringence value within the nerves was calculated to provide a single unit of depth-resolved birefringence per volume scanned.

Birefringent tissue regions are detected in PS-OCT by depth-dependent changes in the cumulative phase retardation experienced by different polarisation states of the reflected light. With an increase in tissue birefringence, more rapid changes in both phase retardation and polarisation state will be detected. Quantification of the depth-resolved rate of change in phase retardation is proportional to the birefringence of the tissue. The cumulative phase retardation can be expressed as an angle on a grey scale from black (0^{o}) to white (180^{o}). These angles are determined using a Poincaré sphere mathematical model, a construct used to display all possible polarisation states of light as previously described above in Chapter 2. This model allows expression of birefringence by plotting the phase retardation angle over depth into the sample and has been described in detail in the literature (Park, Pierce et al. 2003). Using the slope coefficient of the graphs generated from imaging, a numerical expression of birefringence can be generated to compare directly to that of known histomorphological measurements. As described in the previous experiment, imaging was achieved by mounting the anaesthetized animal on a custom-built stage under a mobile, hand held lens objective as shown in figure 3.6 below.

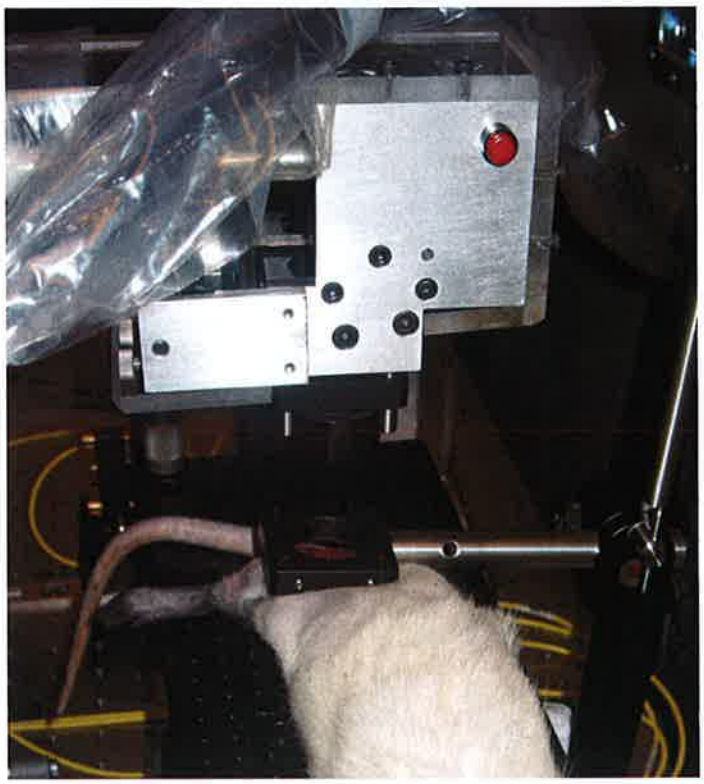

Figure 3.6 – Imaging the exposed sciatic nerve of the Sprague Dawley rat under the Mobile, hand-held lens objective of the Multi Functional Optical Coherence Tomography system.

3.2.5. Histology & Histomorphometry

Histological Preparation

Following PS-OCT imaging, animals were sacrificed with an intraperitoneal injection of pentobarbital (200mg/kg). Both experimental and uninjured sciatic nerves were harvested and fixed in a 2% / 2% glutaraldehyde / paraformaldehyde

solution at 4^0C for forty-eight hours. Specimens underwent post fixation in 1% osmium tetroxide. This was followed by dehydration in ethanol and embedding in epon. Cross sections (1μm) were made at the site of the nerve crush injury using a microtome (Leica Biosystems, Germany). The control nerve (uninjured and Group 5) underwent sectioning at a point 1 cm distal to the exit of the nerve from the pelvis and at the transection site of the nerve, respectively. All samples were stained with 0.5% (w/v) Toluidine blue in preparation for light microscopy.

Histomorphometric Analysis

Nerve architecture was examined at 400X magnification. Five 400X images were taken of evenly distributed areas of each segment within each nerve sample. Ten fibres were randomly selected in each image (total of 50 fibres per nerve sample). The fibre width and axon diameter were measured using Image J™ Software (Abramoff 2004). Myelin thickness was derived from the difference between the fibre and axon diameters. In additionally, the g-ratio of each fibre was calculated as a ratio of the axon diameter to the fibre diameter.

3.2.6. Statistical Analysis

Repeated-measures analysis of variance (ANOVA) was applied to compare the relationship between PS-OCT slope as a predictor of g-ratio and myelin thickness between the control (uninjured) nerve and at the crush site. To model the repeated measures, a compound symmetry structure was used and produced good fits to the data as judged using the Akaike information criterion (AIC). This strategy was used since each animal was evaluated for all conditions (Vittinghoff, Glidden et al. 2005).

Eight animals were evaluated at each time point (7, 14, 21, and 28 days) and each animal was measured using PS-OCT for each of the conditions. Linear regression analysis was performed to evaluate the fitted models in predicting g-ratio and myelin thickness for selected values of PS-OCT. At the crush site, significant relationships were observed between PS-OCT slope and g-ratio and myelin thickness. Regression analysis was applied to all time points pooled together, with a 95% confidence interval (CI) (Chatterjee and Hadi 2006). Power analysis indicated that the sample sizes provided 80% power to detect a significant Pearson correlation (r) between PS-OCT slope and the two dependent variables (g-ratio and myelin thickness) (version 7.0, nQuery Advisor, Statistical Solutions, Saugus, MA). Statistical analysis was performed using the SPSS software package (version 16.0, SPSS Inc., Chicago, IL). Two-tailed values of $P < 0.05$ were considered statistically significant.

4. Results & Discussion - Optical Microscopy & Diagnostics

4.1. Coherent Anti Stokes Ramon Scattering (CARS) Microscopy.

4.1.1. Functional Recovery

Serial walking track analysis as described previously allowed for analysis of functional impairment which was documented in all animals with a mean sciatic function index (SFI) of -88.5 +/- 10.5 at one week following injury. Week two following injury revealed a mean SFI of -76 +/- 15.8, representing minimal recovery / remyelination in the sciatic nerve at this time. Greater functional recovery was evident at weeks three and four with a mean SFI recorded of -35.7 +/- 19.5 and -16.4 +/- 14.8 respectively. This more rapid recovery can be appreciated in graphical form as shown in figure 4.1 below.

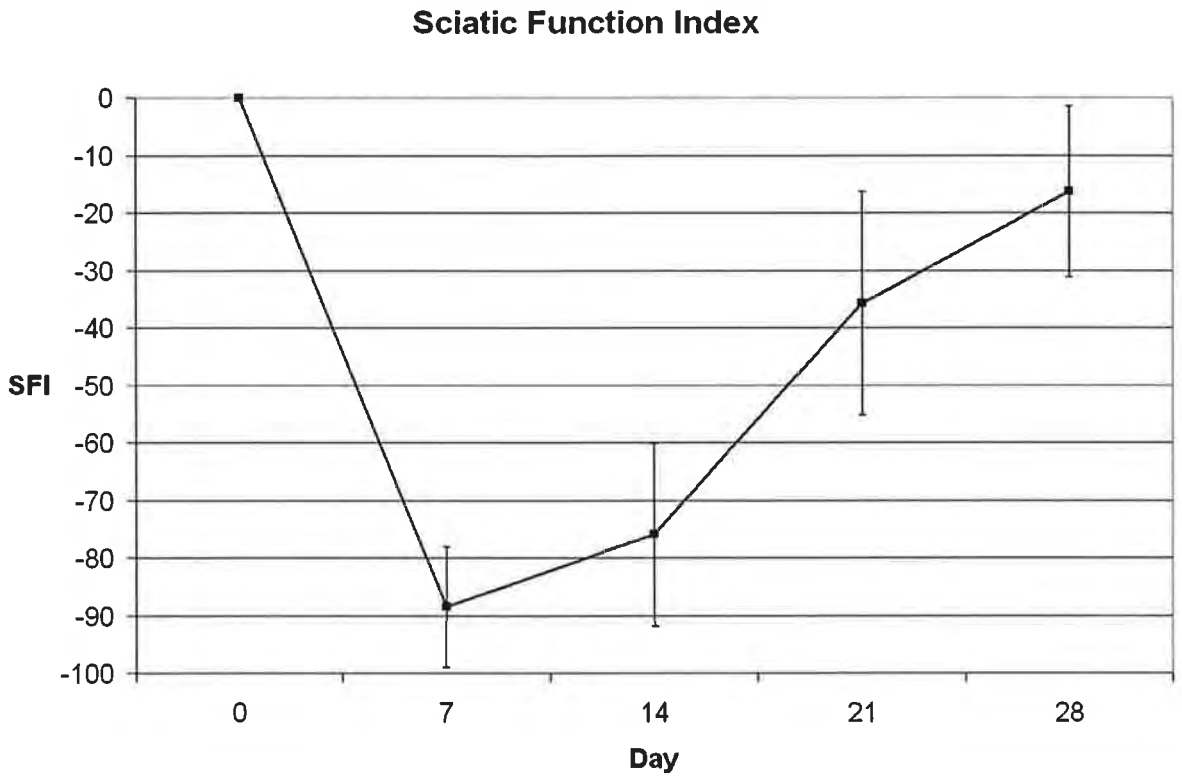

Figure 4.1 - Sciatic Function Index (SFI) over time following crush injury. Data is expressed in means with standard deviations showing time point day 7 (n=10), Day 14 (n=8,) Day 21 (n=6) and Day 28 (n=4).

4.1.2. Coherent Anti Stokes Ramon Scattering (CARS) Microscopy Results

Using confocal reflectance to guide the CARS microscopy images of the normal, *in vivo* nerve were achieved with a resolution of up to 5μm. Figure 4.2 represents both imaging modalities alone along with a combined colour enhanced image in longitudinal section. The combined central image (B) shows the axons (confocal image) in red with the myelin in green (CARS signal). A and C show both CARS and confocal imaging alone, the highly contrasted nature of CARS microscopy is evident with clear definition of the myelin tubules against a dark background.

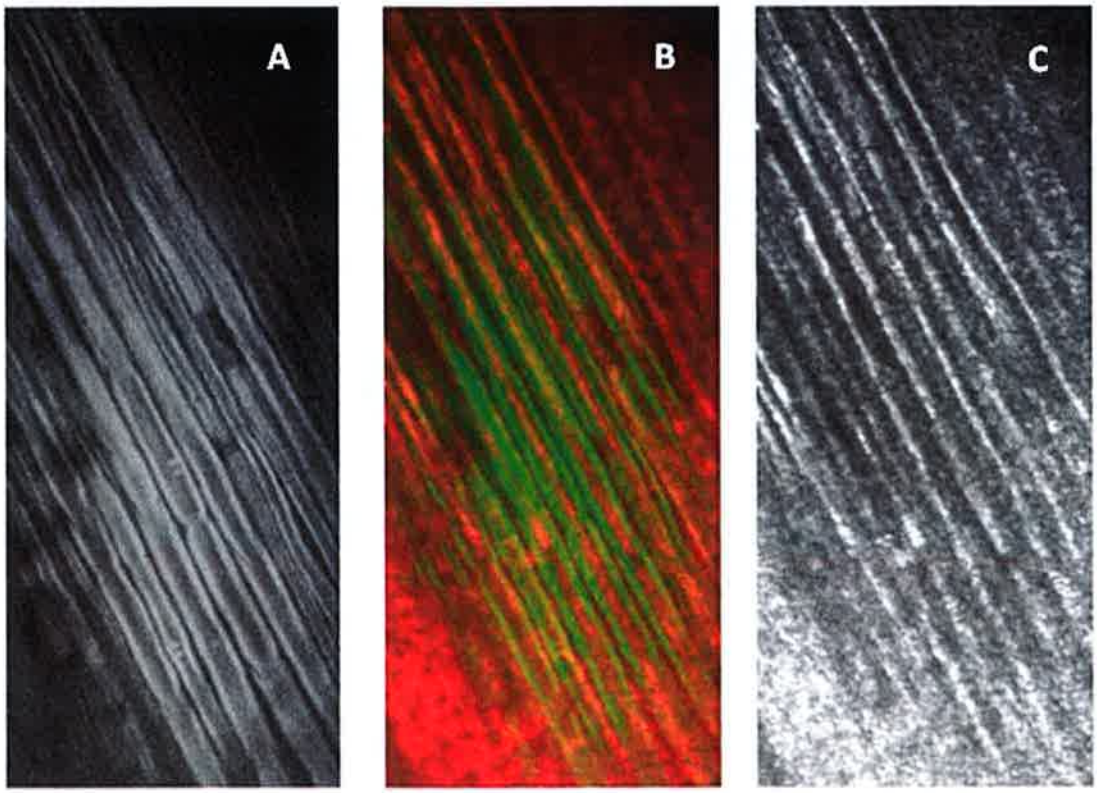

Figure 4.2 - Segment of an uninjured in vivo rat sciatic nerve as imaged with CARS Microscopy alone (Myelin – A), Confocal reflectance alone (Axons – C) and a central combined image (B) using both modalities with myelin in green and axons in red.

This enhanced intrinsic contrast of CARS microscopy revealed structured myelin tubules in longitudinal section and the resolution achieved allowed for identification of a single node of Ranvier easily identifiable in the centre of the myelinated fibres. These images allow for cross sectional analysis analogous to histological preparation of the nerve as viewed under high magnification, stained with toluidine blue (figure 4.3 below).

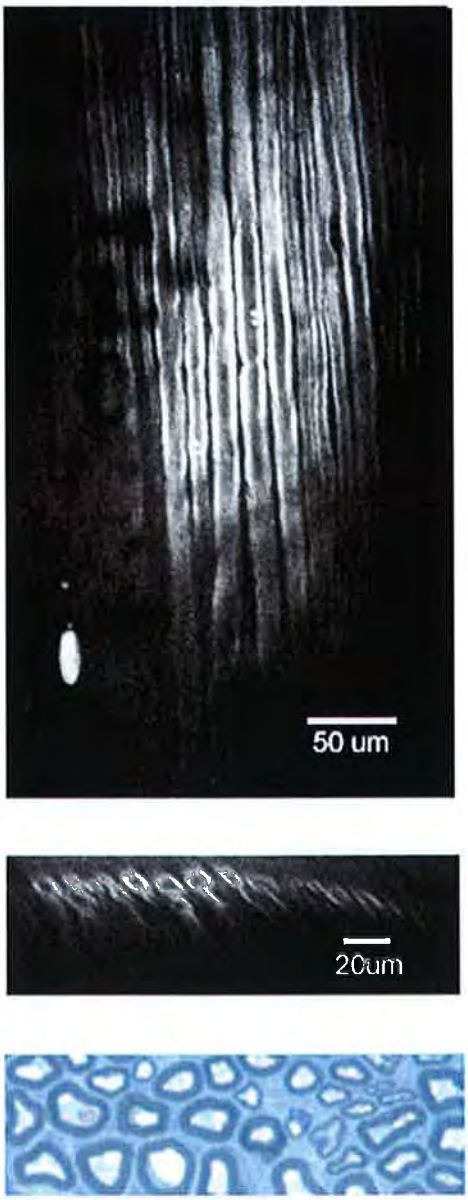

Figure 4.3 - CARS Microscopy showing longitudinal section (top) and cross section (middle) alongside histological preparation (Bottom- 400X Toluidine blue staining) of the normal in vivo rat sciatic nerve. The structured myelin sheaths are obvious in both imaging and histological preparation along with the easily identifiable node of Ranvier in the centre of the longitudinal image.

Following axonal demyelination, no CARS signal was evident in the initial phase following injury. At two weeks following injury a change in signal was noted in microscopy as demonstrated by the images achieved 5mm above the site of injury along with the signal achieved 5mm below the crush site (figure 4.4). Scattered demyelination with a marked loss of myelin sheath organization is evident above while a noted absence of myelin sheath structure is seen below the injury site. There is evidence of high lipid content molecules that are likely to be that of the Schwann cell population. However histological processing in epon precluded immunohistochemical techniques to confirm this. These findings at two weeks following injury are reflected in cross sectional analysis and histological processing of the nerve as shown in figure 4.4 below.

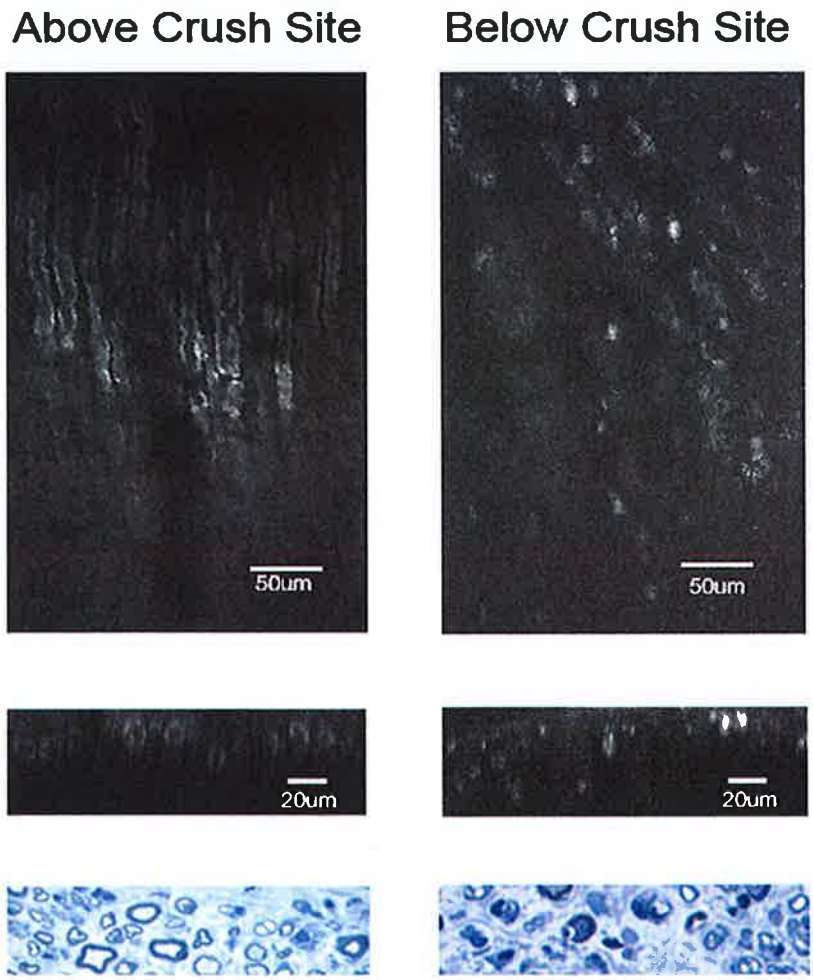

Figure 4.4 - CARS Microscopy with corresponding histology (400X, Toluidine blue) taken two weeks following crush injury of the in vivo rat sciatic nerve. Data shown from above the crush site reveals loss of structural organization of the myelin sheaths in both longitudinal and cross sectional images as well as a decrease in myelinated fibres on histological preparation. Data from below the crush site demonstrates a complete lack of myelin sheath organization in longitudinal section with cross section and histology showing minimal evidence of myelinated fibres along with an increase in debris throughout the nerve field. The cellular pattern of the longitudinal signal is likely to be representative of the Schwann cell population in the regenerating nerve.

Mapping of the nerve injury site was undertaken at 2 weeks following injury. This involved imaging at a depth of 100 μm beneath the surface of the nerve in a uniform fashion above and below the site of injury. Each individual image (500 μm x 500 μm) was then recombined following analysis to give a complete map of the injury site. The results of this analysis are shown below in Figure 4.5 and serves to highlight the disruption in continuity of the myelin sheaths following injury and during regeneration.

A noted increase in structured myelination was obvious both proximal and distal to the injury site following imaging achieved at three weeks and beyond (figure 4.6). While not quite achieving the structure of the normal control (figure 4.3), this improvement in myelination is comparable to the improvement noted in both functional analysis and histological preparation of the nerve.


Above Crush Site
Crush Site
Below Crush Site
1mm

Figure 4.5 – Reconstructed map of the Sciatic nerve 2 weeks following injury. Recombined individual images (500μm x 500μm) were processed at a depth of 100μm below the epineurial surface and scanned from above, through and below the nerve crush site. Loss of continuity of the individual myelin tubules (seen in white) is clearly evident at and below the crush site (indicated with red text) when compared to the proximal portion of the nerve.

Figure 4.6 - Three weeks following injury of the rat sciatic nerve. Structured remyelination is seen throughout the nerve sample as shown in longitudinal, cross section and histology (400X, Toluidine blue)

4.1.3. Histology & Histomorphometry

Nerve regeneration was assessed distal to the crush site in all animals. Increasing remyelination was noted with regeneration of normal architecture across all time points. Histomorphometric analysis demonstrated statistically significant differences in all three parameters calculated (axon length, fibre length and myelin thickness) over time ($p < 0.01$). Significance was shown comparing recovery at week 4 to week 2 values. This was achieved across all three variables.

Myelin thickness was shown to increase from a mean of 1.84μm +/- 0.60μm at two weeks following injury to 4.87μm +/- 0.62μm at four weeks. Total fibre diameter also demonstrated significant recovery with means of 5.67μm +/- 1.09μm and 10.39μm +/- 1.85μm at two and four weeks respectively and with axon diameter increasing from 3.82μm +/- 0.89μm at two weeks to 5.51μm +/- 1.64μm at four weeks. Neural recovery as defined by histomorphometry is shown in figure 4.7 below.

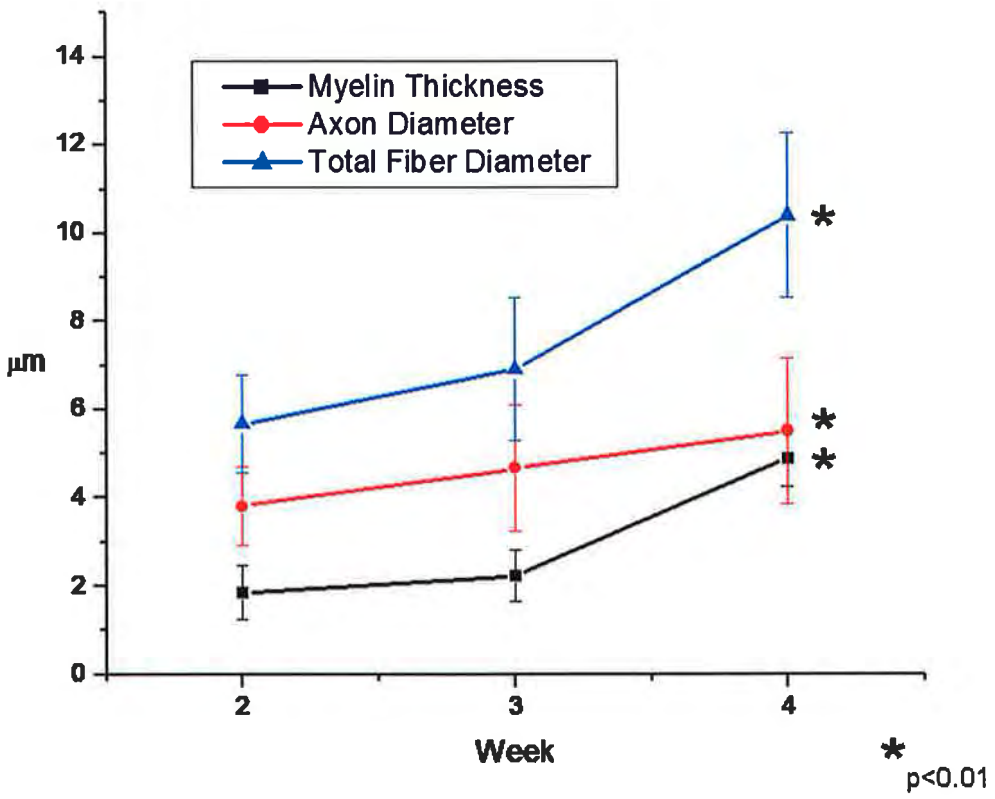

Figure 4.7 - Graphical representation of the mean myelin thickness, axon diameter and total fibre diameter (µm) over time (with standard deviations) demonstrating statistical significant ($p<0.01$) recovery from the two to four week time period. This time period corresponds to the time during which the greatest change in myelination was observed through imaging with CARS microscopy. Histological parameters were measured following sacrifice - week 2 (n=8,) week 3 (n=6) and week 4 (n=4). Significance was shown comparing recovery at week 4 to week 2 values. This was achieved across all three variables.

4.2. CARS Microscopy – Discussion of Findings

In this study CARS microscopy has been demonstrated to have the ability to image the microenvironment of a normal and regenerating peripheral nerve. In this trial of the technology it has been shown that with a demyelinating injury, followed by subsequent significant remyelination, images can be acquired that are in agreement with both functional recovery and histomorphometric analysis of the peripheral nerve. To date, there remains no comparable method of structurally assessing remyelination in a non-destructive manner such as this. This non-thermal, *in vivo* method can easily be used to achieve a method of assessing the structural environment of the nerve following injury over time.

Myelin as a lipid rich molecule (Morell and Quarles 1999) has subsequently been found to be a suitable medium for this unique imaging modality. The acquisition of images in the form of a true optical biopsy may lead to its use in the experimental setting to achieve a greater understanding regarding peripheral nerve regeneration in addition to its applications in clinical practice.

Achieving images with a resolution of up to 5μm and accurately assessing the internal architecture of the nerve has obvious advantages in clinical practice in both prognostic and diagnostic evaluation. Reducing the long periods of observation currently employed following nerve contusion would allow for an earlier determination for surgical intervention where necessary and hopefully an improved functional recovery (Mackinnon 1989). Diagnostically, the ability to accurately

assess myelination would be useful following both traumatic injury and that of chronic processes such as carpal tunnel disease and demyelinating neuropathies. Further avenues of investigation remain prior to this becoming an integral medical technology. The integration of this imaging modality into an endoscope (Legare, Evans et al. 2006) would alleviate the need to surgically expose the nerve and allow for a minimally invasive method of assessment. Further studies are also warranted across a variety of injury models to achieve a grade of injury and regeneration analogous to Sunderland's classification. This first step demonstrating CARS microscopy as a valuable resource in this field shows great promise for its continued use in this manner.

4.3. Polarisation Sensitive Optical Coherence Tomography (PS-OCT)

4.3.1 Functional Recovery

Initial loss of function followed by recovery over time was demonstrated in all animals on calculation of the sciatic function index (SFI). While initially a slow process following assessment at week one and two, the SFI is seen to rapidly approach normal at week three and four. Mean SFI, with corresponding standard deviations at week one and two following injury revealed a mean SFI of -84.07 (+/- 5.9) and -67.33 (+/- 7.53) respectively, representing minimal recovery / remyelination of the sciatic nerve. Greater functional recovery was represented at weeks three and four with a mean SFI recorded of -28.85 (+/- 6.03) and -13.03 (+/- 5.84) respectively. This data is represented in Figure 4.8 and serves to demonstrate

the functional loss and subsequent recovery of the nerve model used as seen previously in the CARS Microscopy investigation above.

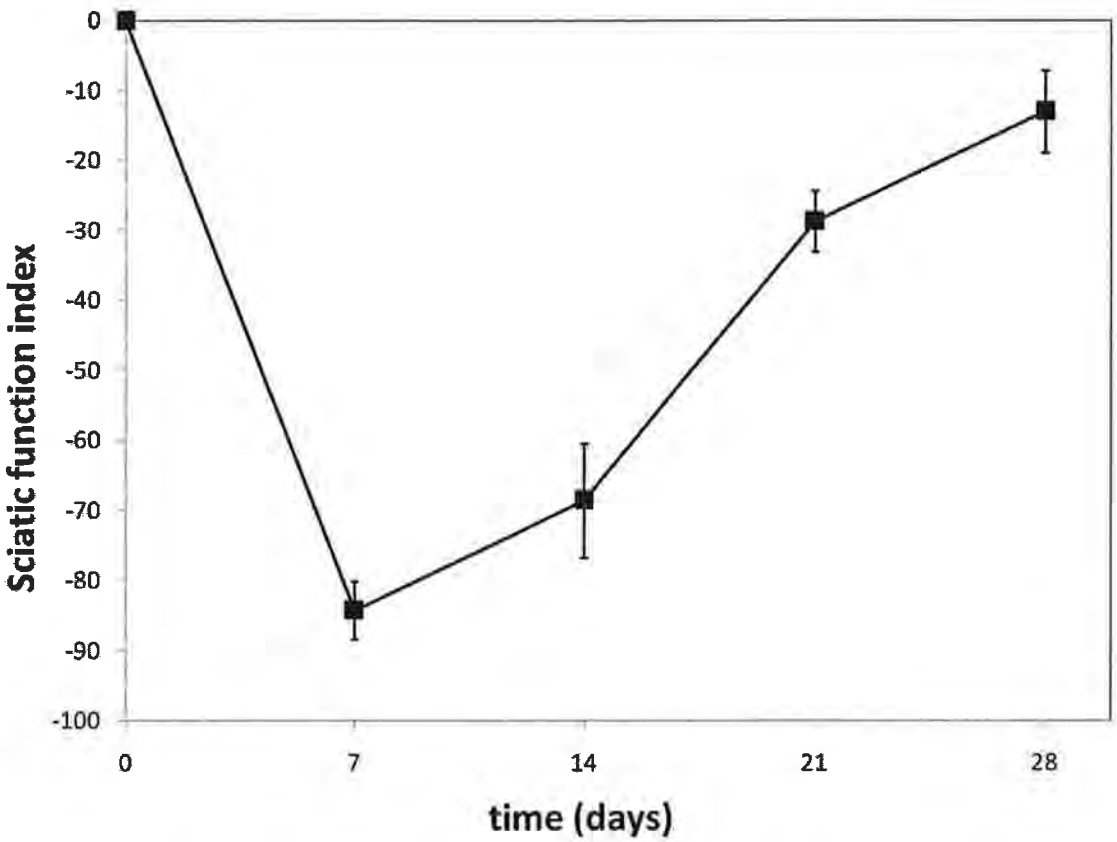

Figure 4.8 - Sciatic Function Index (SFI) over time following crush injury. Data is expressed in means with standard deviations showing time point day 7 (n=36), Day 14 (n=28,) Day 21 (n=16) and Day 28 (n=8). The larger animal number in this PS-OCT investigation allows for a smaller standard deviation to be achieved. Recovery over 4 weeks following the injury is clearly demonstrated by the SFI returning toward a baseline normal value of 0.

4.3.2. Histology & Histomorphometry

Histomorphometric analysis was undertaken of all nerve samples including controls following imaging and epon embedding. There was noted degeneration in the early groups with subsequent regeneration across all samples in the later groups. Samples were analysed and markers of axonal myelination were calculated as described previously. These included calculation of myelin thickness and g-ratio (axon diameter / fibre diameter). Histomorphometric parameters at the crush site for each group are outlined in Table 4.1 below. This shows the range of myelin thickness and G-ratio with Standard deviations from the transected nerves (1.21 μm ± 0.35 and 0.79 ± 0.062 respectively) to the regenerating nerve at week 4 (2.57 μm ± 1.08 and 0.63 ± 0.10 respectively) following injury. While considerable variation exists with the mean of each group, the data used to correlate with the nerve birefringence (as described previously) was taken on an individual animal basis rather than the collective mean of each group as shown below.

Table 4.1 - Histomorphometric parameters at the crush site for each group. Markers of axonal myelination (Myelin thickness and g-ratio) are demonstrated in means with standard deviations.

Group	Week of Imaging	Procedure	Myelin Thickness (μm)	G-Ratio
1	Week 1	Nerve Crush	2.57 (+/-1.07)	0.65 (+/-0.08)
2	Week 2	Nerve Crush	1.73 (+/-0.75)	0.70 (+/-0.08)
3	Week 3	Nerve Crush	2.17 (+/-0.94)	0.67 (+/-0.09)
4	Week 4	Nerve Crush	2.57 (+/-1.08)	0.63 (+/-0.10)
5	Week 2	Nerve Transection	1.21 (+/-0.35)	0.79 (+/-0.06)

4.3.3. Polarisation Sensitive Optical Coherence Tomography (PS-OCT)

Following exposure of the sciatic nerve the crush site was identified by locating the microsuture placed at the time of injury. A portable handpiece was mounted a fixed distance above the nerve, and an area of 5 mm x 5 mm was imaged across the crush site using PS-OCT. Figure 4.9 shows the results obtained from a normal nerve. Figure 4.9a displays the backreflected intensity of light on a logarithmic grey scale, and the position of the nerve with the surrounding muscle is evident. Figure 4.9b is an image of the cumulative phase retardation relative to the surface of the tissue.

This greyscale image characterised by rapid changes from white to black gives a strong birefringence signal which can be quantified and expressed as a depth-resolved graph of phase retardation graph as shown in Figure 4.9c. After allowing for the thickness of the epineurium in the first few microns, the initial slope of this graph (0.371°/micron) provides for a quantifiable measurement of birefringence. Figure 4.9d is an image of the corresponding histological section. The dark myelin sheaths surrounding individual axons are clearly evident.

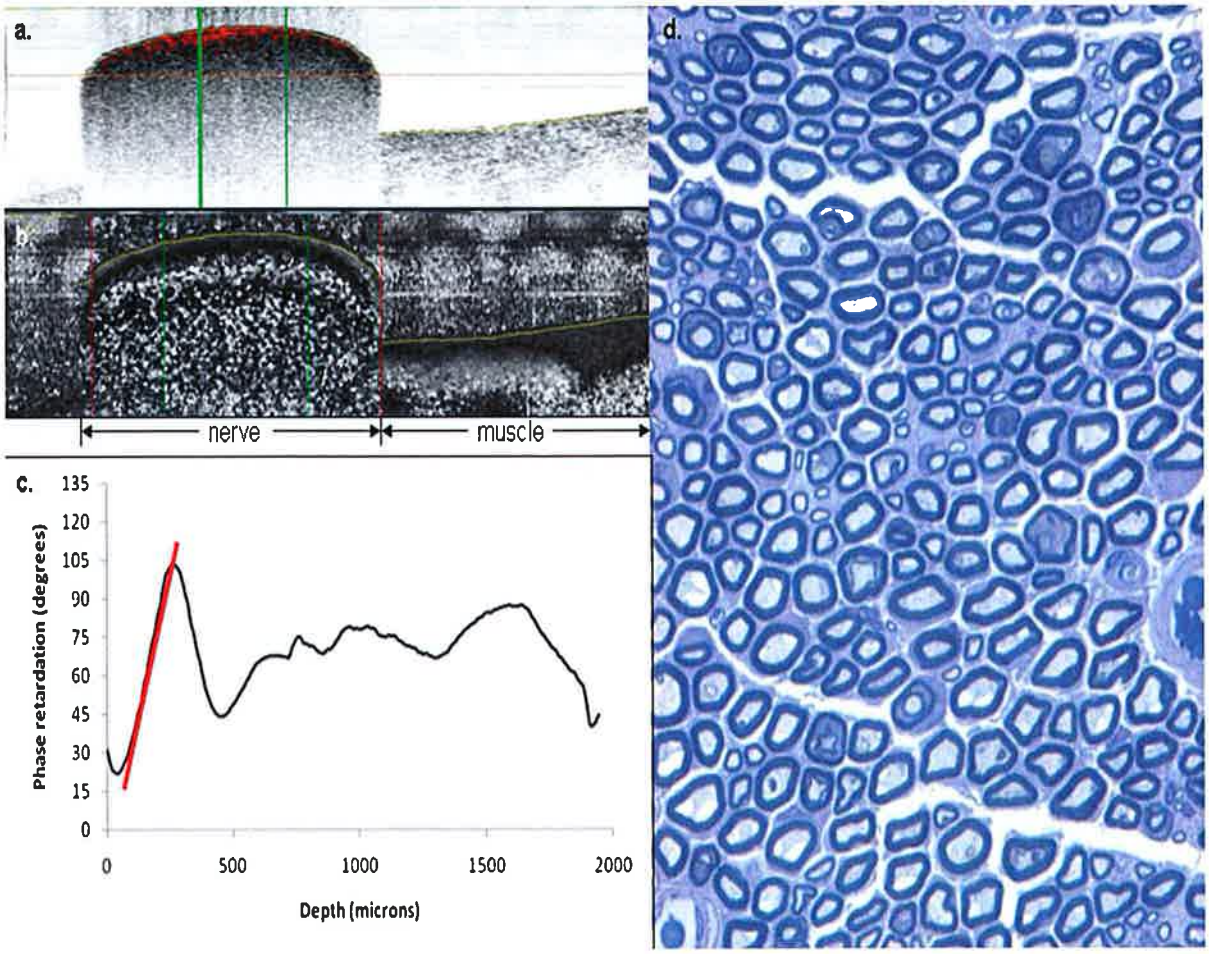

Figure 4.9 - Figure 4.9a represents the backreflected intensity of light as imaged with Spectral Domain Optical Coherence Tomography of the normal rat sciatic nerve, the position of the nerve with the surrounding muscle is clearly evident. Figure 4.9b is an image of the cumulative phase retardation relative to the surface of the tissue as imaged with Polarisation Sensitive Optical Coherence Tomography. This greyscale image characterized by rapid changes from white to black gives a strong birefringence signal which can be quantified and expressed as a depth-resolved graph of phase retardation graph as shown in Figure 4.9c. The initial slope of this graph, highlighted in red (0.371°/micron) provides for a quantifiable measurement of birefringence. Figure 4.9d is an image of the corresponding histological section of the normal nerve (toluidine blue 400X).

The effects of complete nerve transection (group 5) are shown below in Figure 4.10. Nerves in this group experienced complete or nearly complete loss of myelin, as can be observed in the histological image (Figure 4.10d). This is reflected in the optical measurement of birefringence, as determined by the slope of the initial portion of the depth-resolved plot of phase retardation (0.055°/micron) revealing complete loss of myelination and a decrease in birefringence with a resultant decrease in slope.

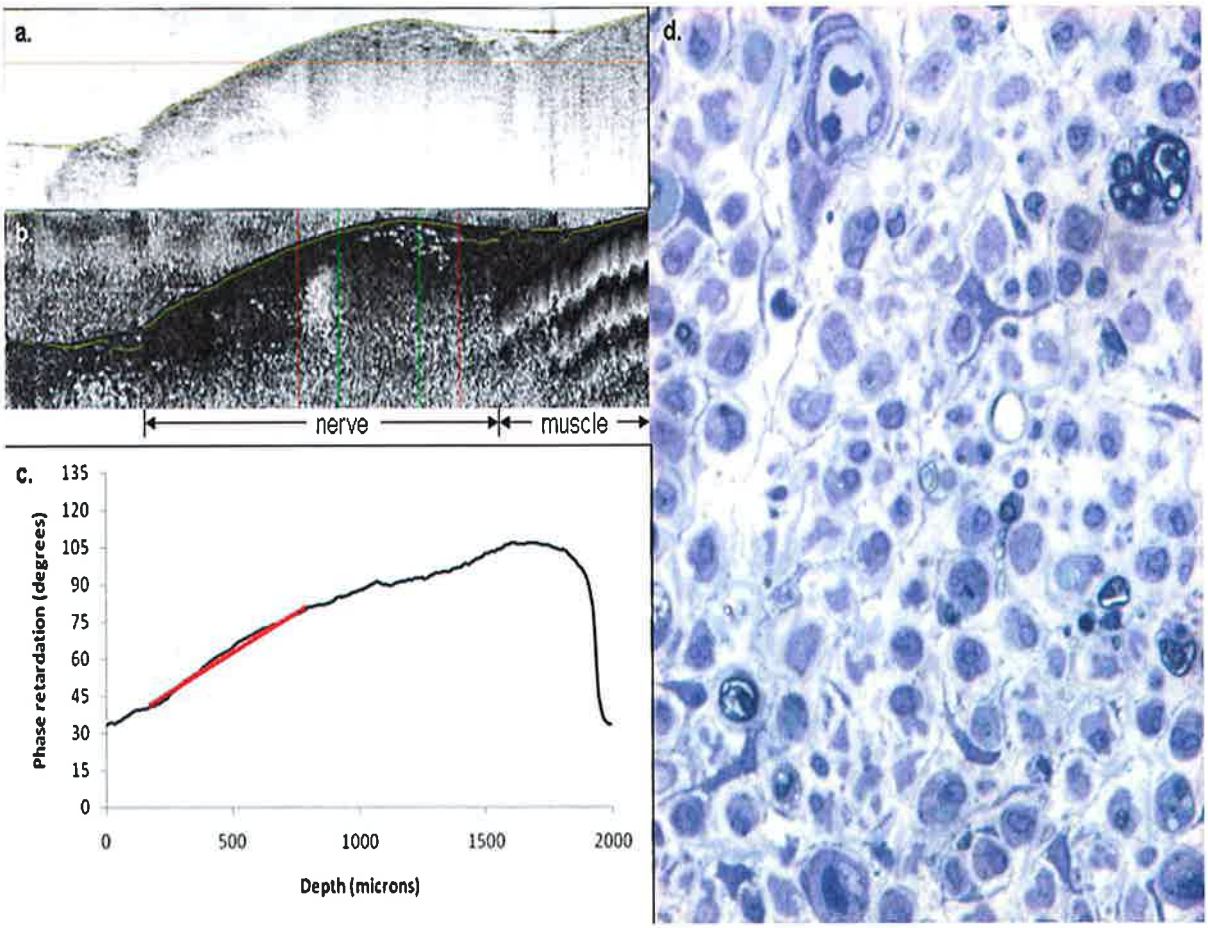

Figure 4.10 – Complete nerve transection resulting in a loss of birefringence as noted in figure 4.10b and a change in backreflected light intensity (figure 4.10a). This results in a decrease in slope of the phase retardation plot to 0.055°/micron shown in figure 4.10c. This can be verified with a noted lack of myelinated fibres in the histological sample (figure 4.10d).

Following crush injury as described previously the change in the morphometry of the imaged and histologically processed nerve is apparent. This time point also corresponds to that of a functionally impaired nerve as seen on calculation of the sciatic function index as shown above in figure 4.8. Figure 4.11 shows representative data of a nerve 2 weeks following injury. In this case, the nerve remains somewhat more embedded within the surrounding tissue and cannot be easily delineated from the intensity image (Figure 4.11a). However, the outer boundaries of the nerve can be observed in the corresponding phase retardation image (Figure 4.11b), as can a significant reduction in birefringence. This effect can be quantified by the initial slope (0.088°/micron) of the depth-resolved cumulative phase retardation plot shown in Figure 4.11c which can be seen to have decreased when compared to that of figure 4.9c (0.371°/micron) but an improvement over that of figure 4.10c (0.055°/micron). A reduction in myelination can also be appreciated in the histological section, as the thickness of the dark myelin bands surrounding the axons is visibly thinner due to Wallerian degeneration (figure 4.11d).

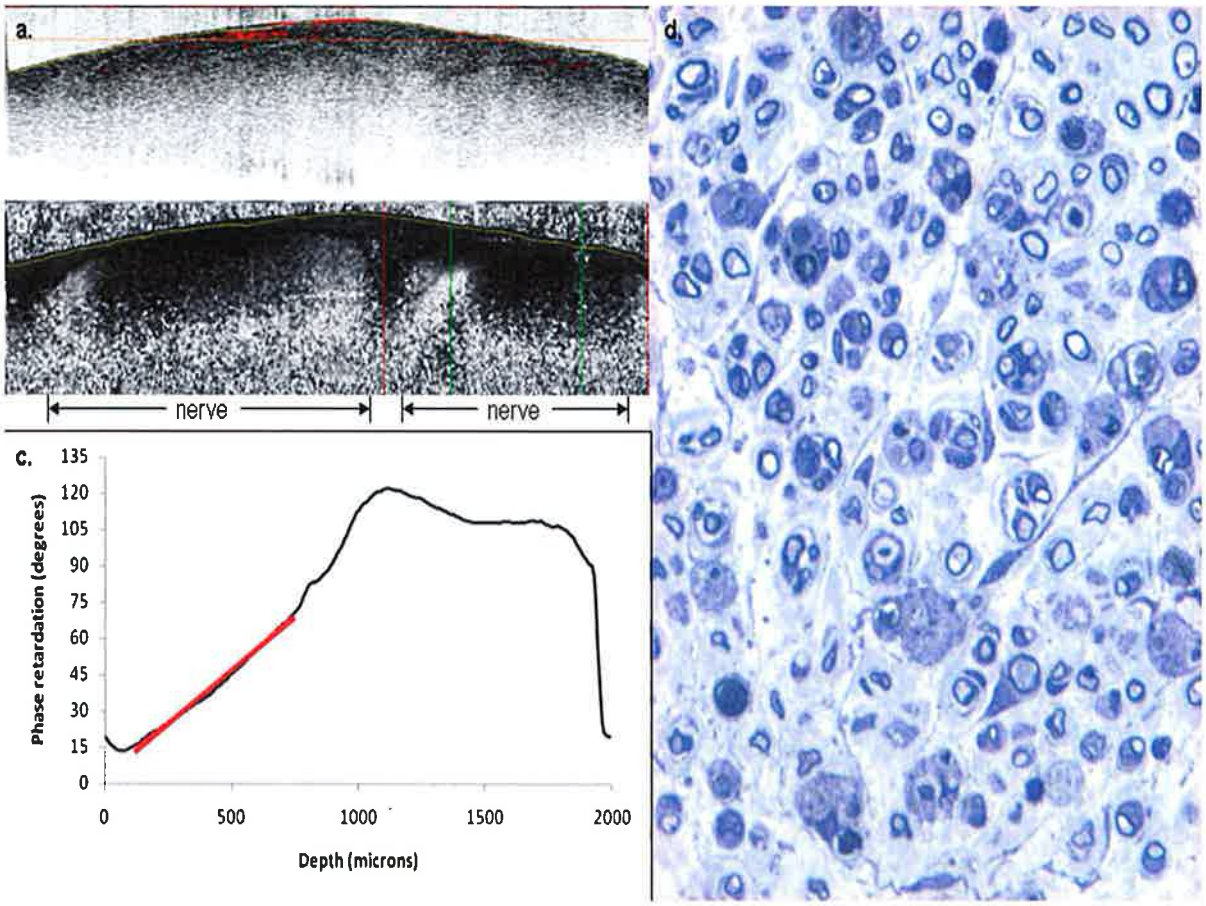

Figure 4.11 – SD-OCT with corresponding PS-OCT image of the nerve 2 weeks following crush injury (a & b respectively). The depth-resolved cumulative phase retardation plot shown in Figure 4.11c with an initial slope of 0.088°/micron corresponds to the degeneration of the nerve and verified with the histological sample in figure 4.11d.

The results of the previously described statistical analysis of relationships between the PS-OCT derived slope of each individual nerve, which is proportional to birefringence, and the histologically-determined g-ratio and myelin thickness are shown in Figures 4.12 and 4.13.

Repeated-measures ANOVA indicated a significant inverse relationship between the birefringence slope and g-ratio at the crush site of the experimental nerve ($P = 0.01$), and this linear relationship was significantly different when compared to control (uninjured) nerves ($p < 0.05$). Figure 4.12 below, displays a scatterplot of birefringence versus g-ratio for the control, transected, and injured nerves with the results of the regression fit overlaid. This clearly illustrates the modelled relationship between birefringence and g-ratio with data from days 7, 14, 21, and 28 pooled together. There was a positive correlation noted between the two variables (Pearson $r = -0.50$, $p = 0.015$). The relationship reveals some variation, however in general, lower values of birefringence are predictive, with statistical significance, of a higher g-ratio. It should also be noted that derived slopes for healthy nerves were typically above 0.03-0.04°/micron, whereas those of injured nerves were below that threshold.

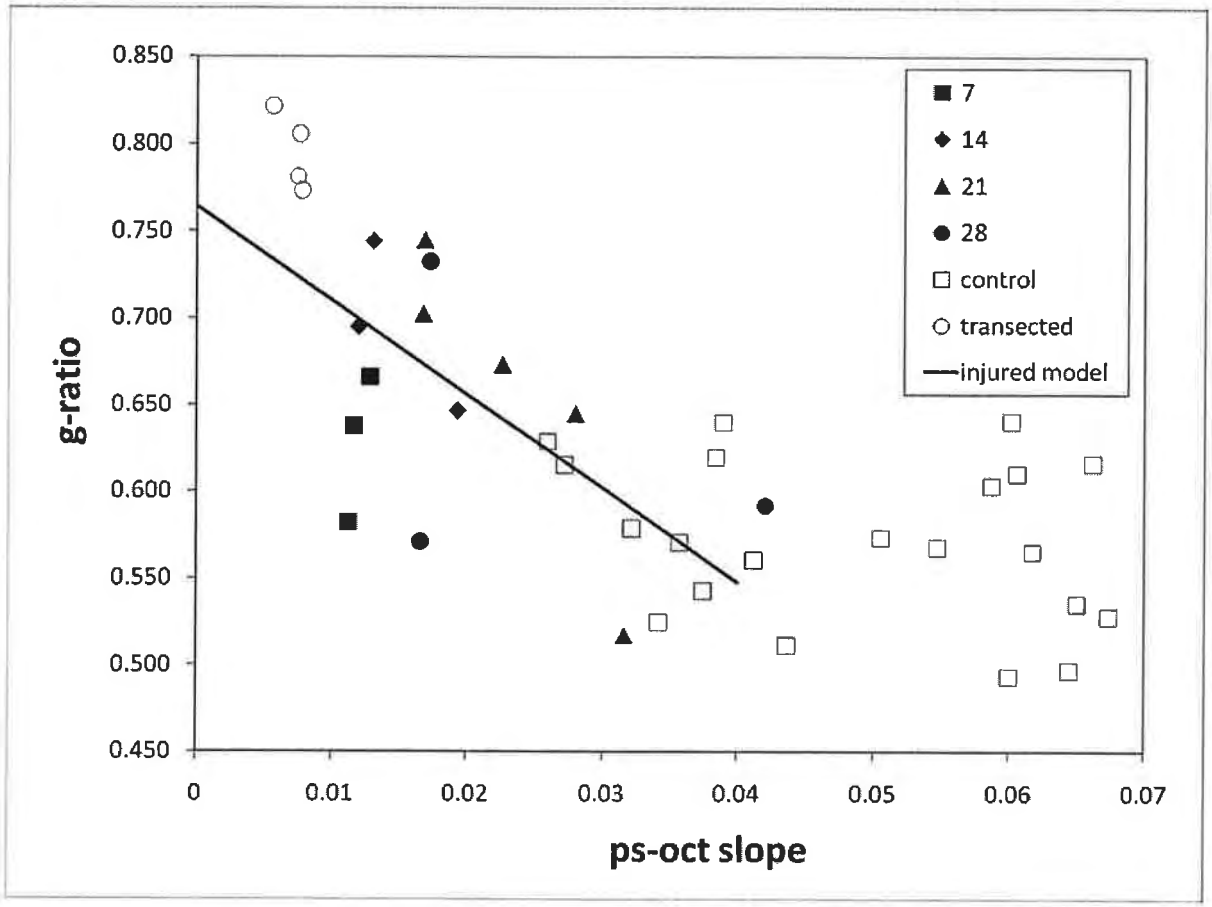

Figure 4.12 – A scatterplot of birefringence versus g-ratio (axon diameter / fibre diameter) for the control, transected, and injured nerves with the results of the regression fit overlaid. This clearly illustrates the modelled relationship between birefringence and g-ratio with data from days 7, 14, 21, and 28 pooled together. There was a positive correlation noted between the two variables (Pearson r = -0.50, p = 0.015), in general, lower values of birefringence are predictive, with statistical significance, of a higher g-ratio. It should also be noted that derived slopes for healthy nerves were typically above 0.03-0.04°/micron, whereas those of injured nerves were below that threshold.

For myelin thickness, the relationship with birefringence was positive and the strongest correlation was found at the nerve crush site compared to control ($P = 0.05$). Figure 4.13 below, illustrates the modelled relationship between PS-OCT and myelin thickness with data from days 7, 14, 21, and 28 pooled together. Regarding myelin thickness, the correlation in the scatterplot suggests a positive relationship with birefringence but also indicates some variability in the cloud of data points (Pearson $r = 0.38$, $P = 0.05$).

Using this graph, one can visually discern greater myelin thickness for larger values of the birefringence as evaluated at the nerve crush site.

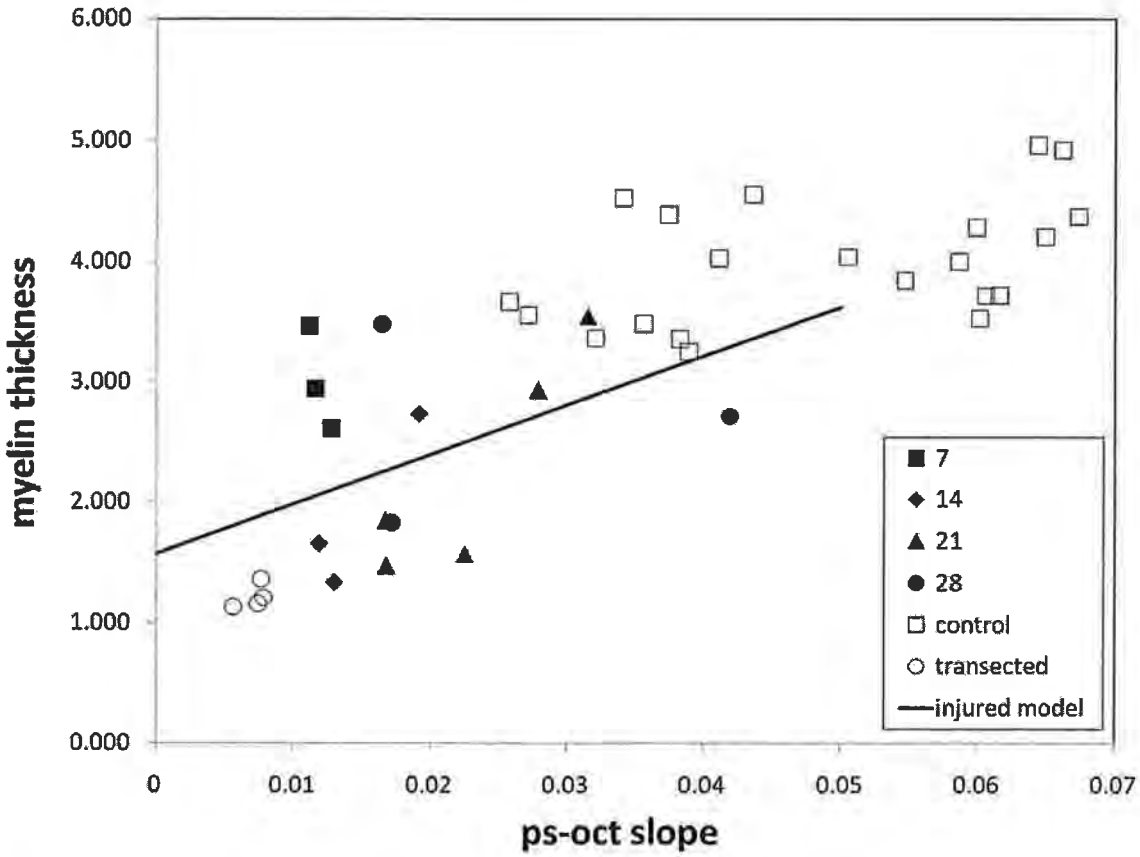

Figure 4.13 - Modelled relationship between PS-OCT and myelin thickness with data from days 7, 14, 21, and 28 pooled together. The correlation in the scatterplot suggests a positive relationship with birefringence but also indicates some variability in the cloud of data points (Pearson r = 0.38, p = 0.05). Using this graph, one can visually discern greater myelin thickness for larger values of the birefringence as evaluated at the nerve crush site.

Analysis of the data in this manner, with direct correlation of histological parameters with birefringence values obtained from PS-OCT images allows for a statistically significant, in vivo, non destructive method of quantifying axonal myelination in the normal and injured peripheral nerve.

Of the endpoints available in the field of neuroscience we chose to primarily examine axonal myelination as a true marker of neural health. Complete functional loss (with associated demyelination) of the nerve crush injury along with subsequent recovery and remyelination over time was also undertaken by means of standardised walking track analysis with calculation of a sciatic function index, as described previously with the results shown in figure 4.8 above. This allowed for a wide spectrum of functionally impaired nerves to be examined in this study. Figure 4.14 below depicts the averaged slopes compared to the average SFI for control, transected, and injured nerves at the 4 timepoints. This plot demonstrates a clear relationship between the non-contact optical measurement of neural myelination described in this manuscript and a functionally derived measure.

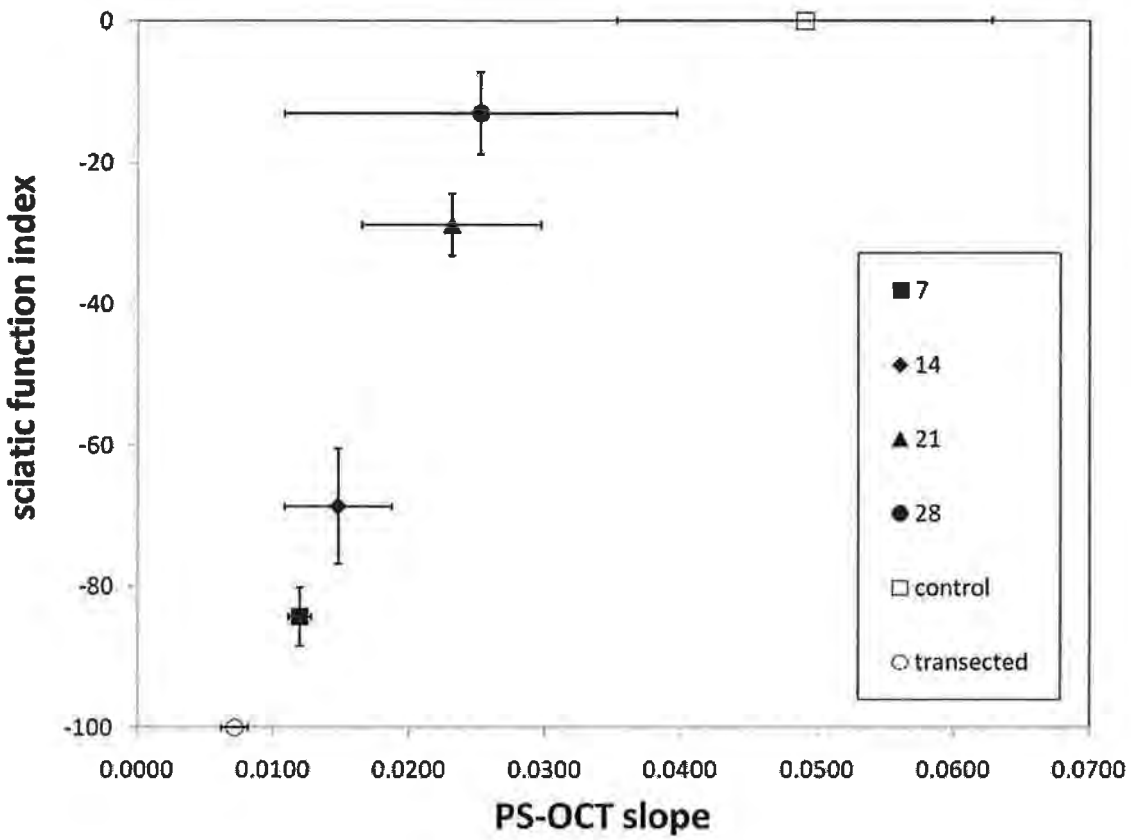

Figure 4.14 – Mean slopes of birefringence values per group compared to the average SFI for control, transected, and injured nerves at the 4 timepoints. This plot demonstrates a clear relationship between the non-contact optical measurement of neural myelination described in this manuscript and a functionally derived measure.

4.4. PS-OCT Imaging - Discussion of Findings

Achieving quantitative analysis and accurately assessing axonal myelination has obvious advantages in clinical practice for both prognostic and diagnostic evaluation of the nerve. Reducing often long periods of observation currently in practice following nerve contusion would allow for an earlier re-assessment of the need for

surgical intervention if necessary and ultimately an improved functional recovery (Mackinnon 1989). Diagnostically, the ability to quantify axonal myelination would be useful clinically following both traumatic injury and that of chronic processes such as carpal tunnel disease and demyelinating neuropathies.

Despite years of advancement in optical technologies and clinical imaging there remains no reliable method of assessing the microenvironment of the nerve. Current technology is either limited in the early phase of nerve injury, reliant on fluorescent labelling that is not practical clinically, or of a non specific nature. Indeed, the ability of PS-OCT to image without extrinsic labelling has been one of the reasons for its increasingly widespread application in both experimental and clinical settings.

Myelin as a structured molecule has been found to be a suitable medium for PS-OCT imaging and birefringence assessment. While birefringence is often exhibited by fibrous biological structures, not all such structures exhibit an appreciable amount of birefringence. Non-myelinated axons possess very little birefringence, as demonstrated by the optical measurements of the transected nerve (group 5). Form birefringence in fibrous structures is a combination of the density of the fibres with their overall degree of organisation. In dermatological applications, this can lead to some degree of variability as a loss in birefringence can be attributed to either a decrease in the density of dermal collagen or an increase in the disorganisation of existing fibrils (Pierce, Sheridan et al. 2004; Pierce, Strasswimmer et al. 2004). However, since the overall orientation of the myelin sheaths is dictated by that of the axons, a decrease in the birefringence of the sciatic nerve can only occur due to a decrease in the amount of myelin as there is little possibility for an increase in the

disorganisation of the nerve fibres. Additionally, since histological measures were obtained by sampling a few randomly chosen and discrete locations, it can be subject to a large degree of variability. However, PS-OCT measures the overall birefringence of a particular region, and is thus less sensitive to local sampling errors.

In this study polarisation-sensitive optical coherence tomography (PS-OCT) is demonstrated as a reliable in vivo, non-destructive method of assessing of axonal myelination. Preservation of the neural microenvironment while achieving a quantitative analysis of myelin shows promise for the translation of this imaging modality across to clinical practice and indeed for further expansion in the field of experimental neuroscience. For the purpose of this investigation, we chose to access the sciatic nerve of the Sprague Dawley via a muscle splitting incision. While this may be appropriate in cases of perioperative neuronal assessment, a more minimally invasive method of assessment would be more suitable prior to clinical trial, particularly if used as a diagnostic tool without operative intervention. OCT as an imaging modality has been used previously with success in conjunction with fibre optic technology and delivered via an endoscope (Vakoc, Shishko et al. 2007) or in the case of intravascular studies, through a vascular catheter (Yun, Tearney et al. 2006), thus allowing for translation across to endoscopic neural assessment with ease.

Further evaluation of function as an endpoint would include correlation of neurophysiological studies with our PS-OCT imaging. In this study we chose to correlate PS-OCT with standard histomorphometry and in particular, markers of

axonal myelination. Functional correlation of the PS-OCT images remains an avenue that warrants further exploration. Our preliminary evaluation of PS-OCT against sciatic function index does show promise however as a standalone measurement neither sciatic function index or standard neurophysiology are as reliable a means of assessing myelination as direct histomorphometric assessment in an animal model. Further clinical studies remain integral to establish a conclusive functional relationship.

These results demonstrate, by means of direct histological correlation, the ability of PS-OCT to assess and quantify markers of axonal myelination in a non-destructive, in vivo manner. Exploring the realm of optical microscopy in this manner has several advantages over previous techniques in print. Both MRI (Bendszus and Stoll 2003; Bendszus and Stoll 2005; Bendszus, Wessig et al. 2005; Kobayashi, Meir et al. 2005; Wessig, Bendszus et al. 2007; Wessig, Jestaedt et al. 2007; West, Davies et al. 2007) and Ultrasound (Prinz, Nakamura-Pereira et al. 2003; Stuart, Koh et al. 2004) lack the resolution or specificity of PS-OCT and while providing structural imaging they lack the quantitative capabilities shown here. PS-OCT remains a promising tool in this field and provides and insight into the in vivo neural microenvironment previously unseen.

5. Optical Therapeutics in Peripheral Nerve Surgery

5.1. Peripheral Neurorrhaphy

5.1.1. Peripheral Neurorrhaphy, a Historical Perspective

The Peripheral Nerve has long been a subject of interest amongst those who have defined the course of modern medicine. While the origins and practice of surgical technique remain vague at best, several noteworthy innovators over the centuries have contributed significantly to the body of knowledge available today. Initially documented in the basic anatomical investigations of pioneers such as Aristotle, Herophilos and Hippocrates (Belen, Aciduman et al. 2008), it was in 200AD when the possibility of nerve regeneration was first discussed and ultimately dismissed by Galen (Little, Zomorodi et al. 2004). While his work encompassed many medical specialities (figure 5.1), it was in the field of neuroscience mainly concerning the function of the brain and spinal cord following injury, where he distinguished nerves from tendon and his observations of the inability of a live pig to squeal following transection of the laryngeal nerve lead to the communicating branch of the internal laryngeal with the recurrent laryngeal nerve bearing his name.

Over 400 years later the basic concept of peripheral nerve repair or neurorrhaphy was described in the 7th century by Paul von Aegina (Gurunluoglu and Gurunluoglu 2001; Gurunluoglu and Gurunluoglu 2003). Best known for composing the medical encyclopaedia 'Medical Compendium in Seven Books', this Byzantine Greek physician described the technique of nerve repair in the context of traumatic wound

closure in the sixth of the seven volumes published. For many years in the Byzantine Empire, his work contained the sum of all Western medical knowledge and was unrivalled in its accuracy and completeness.

Figure 5.1 - Clinic Scene; This illustration accompanying Galen's work shows the surgical procedures described by Galen, on the head, eye, leg, mouth, bladder and genitals (Galen).

Despite the reverence these encyclopaedias held at the time, it was almost 1000 years later that the practice of these teachings was first performed in an animal by the Italian surgeon Gabriele Ferrara in 1543 (Artico, Cervoni et al. 1996). Ferrara, a pioneer in early peripheral nervous system surgery, sutured with a special needle that had been soaked in a decoction of rosemary, red wine, and roses. He described applying gentle traction on the retracted nerve stumps, achieving continuity with sutures and finally, insulating the sutured segment with a mixture of oils.

Interest waned over the centuries given the popular and widespread belief at the time that nerves did not support regeneration. Henceforth, contributions to the topic were rarely useful and thus progress remained slow until Waller's work in the 1850's led to the rediscovery of the nature of peripheral nerve degeneration and subsequent regeneration and gave rise to the pathological process termed Wallarian degeneration (Stoll, Jander et al. 2002).

Shortly afterwards, in 1864, two French surgeons (Laugier and Nélaton) independently performed the first nerve sutures in humans. Their observations, reported within one week of each other, detailed immediate functional recovery of the appropriate muscles following suturing and ignited controversy and a renewed interest in the repair of the peripheral nerve amongst the scientific community. Specifically, Nélaton reported removing a neuroma of the median nerve and reapproximating the cut nerve ends with two silver wires. However, on Day 7 postoperatively he described how the patient could move all of her fingers and oppose her thumb. This report led surgeons of the time to believe that the median nerve recovered its function in only 7 days (Kennedy 1898). While not completely accurate, the basic technique demonstrated by Laugier and Nélaton was adopted and further refined by Heuter in 1873 (Millesi 1979). He described what is now the clinical standard; a simple end-to-end epineurial repair. A potentially more accurate and more practical technique relative to epineurial repair was proposed by Langley and Hashimoto in 1917 (Langley and Hashimoto 1917). This perineurial or fascicular nerve repair involves suturing the corresponding fascicles to gain optimal alignment, theoretically allowing for optimal regeneration of axons along their predetermined paths. Both techniques are demonstrated in figure 5.2.

Over the next 60 years advancements in the field of neurorrhaphy centered on the concept of graft repair. Recognising that a tension free nerve repair site was optimal Foerster described the cutaneous nerve as a donor nerve in 1915 (Zulch 1968). In 1947 the cable graft as a management tool for partial transections and repair of the nerve gap in large nerves was described by Seddon (Seddon 1947) as well as the vascularised nerve graft by Strange (Strange 1950). Remarkably the observations made by these early investigators remain true to this day despite major advancements in the understanding of the neurosciences. Through his body of work Seddon reported sensory recovery in 53% of patients following epineurial repair of the ulnar nerve at the wrist with 78.5% demonstrating motor recovery at two to three years following epineurial repair. Nerve repairs in other regions showed recovery rates of between 30 and 70 % (Nicholson and Seddon 1957), a functional achievement that has yet to be surpassed.

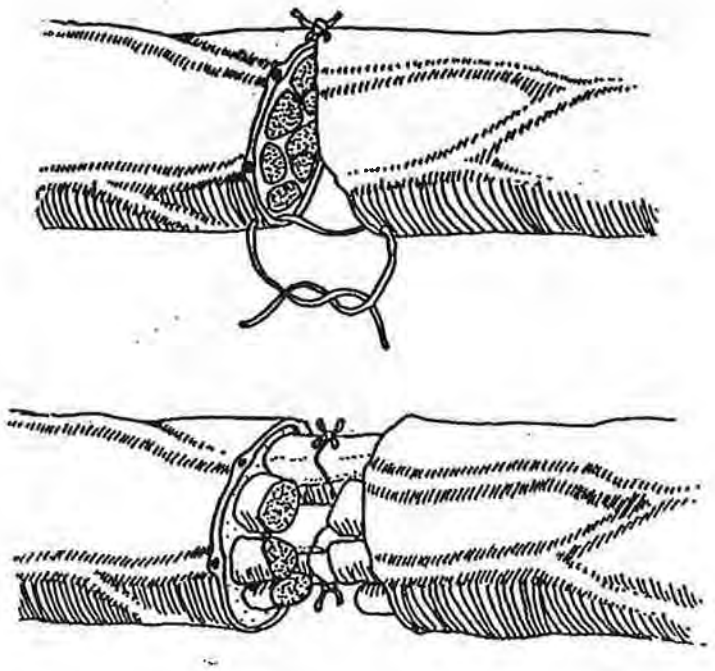

Figure 5.2 – Standard epineurial nerve repair (top) with fascicular nerve repair shown below. Adapted from Winograd et al, Mathes (Winograd and MacKinnon 2006).

The advent of microsurgery and its application to peripheral nerve surgery was preceded by key observations regarding the effects of repair on the nerve structure. Edshap and Goto reported that, although after epineurial repair the external appearance might appear satisfactory, histological examination revealed telescoping effects of the fascicles and this morphological effect due to suture technique affects the regeneration of the nerve (Chang, Leung et al. 1986). This was followed by Smith in 1964, he reported that by introducing the operative microscope as an operative aid, the surface vessels and external appearance of the peripheral nerve could be identified and placed in alignment more accurately and as a result, an epineurial anastomosis under magnification was obviously better than operation

under just plain vision (Smith 1964). The advantages of microsurgical technique have since been well established and lead to a more anatomical approach to nerve continuity being adopted. One further refinement of the technique since was reported in 1972 when Millesi et al (Millesi, Meissl et al. 1972) introduced the concept of the interfascicular nerve repair. Interfascicular repair involves direct apposition of the fascicles by means of suture placement in the interfascicular epineurium. While seemingly more accurate and practical approaches to achieving continuity, the application of fascicular and interfascicular repair over that of epineurial repair still causes some controversy. Pre-clinical studies have touted the superiority of one technique over the other (Levinthal, Brown et al. 1977), however no randomised controlled clinical trails exist to prove these theories. Brushart (Brushart, Tarlov et al. 1983) demonstrated through retrograde labelling, with horseradish peroxidise, of nerve fibres in the rat sciatic nerve, that postoperative anatomical segregation of motor fibres were better preserved in nerves repaired with fascicular neurorrhaphy, however, evaluation of this in a primate model was inconclusive (Grabb, Bement et al. 1970). While a higher degree of integrity can be obtained with more detailed apposition of the fibres, in practice alignment can be difficult due to haemorrhage and swelling of the nerve as well as the effects of the greater manipulation and dissection required to achieve individual fascicular alignment over the more straight forward epineurial repair. Thus the consensus remains that although alternate anatomical alignment techniques offer a theoretical advantage, epineurial repair as described in 1873 remains the clinical gold standard today.

5.1.2. Recent developments in Peripheral Neurorrhaphy

While the concept of direct microsurgical repair and its application in clinical practice has remained standard over the past 40 years, the field of neuroscience and in particular our understanding of the molecular basis of regeneration has expanded. From a more surgical perspective, advancements continue in the area of secondary repair of nerve defects through grafting techniques. Evolution of such disciplines as tissue engineering of conduits as well as engineering of non biological materials continue to add substantially to the field since the first description of a non-neural tube to bridge a deficit by Gluck in 1880 (Gluck 1880). To date however the efficacy of the autologous nerve graft as initially described by Albert (Valnicek and Wilflingseder 1982) in 1876 and Foerster (Zulch 1968) in 1915 has yet to be surpassed and it remains the clinical gold standard when appropriate donor nerves are available. Biological sources of nerve conduits besides autologous nerve, most commonly include the use of a vein graft (Rice and Berstein 1984; Chiu, Lovelace et al. 1988) or acellular muscle grafts (Glasby, Gschmeissner et al. 1986; Glasby, Gschmeissner et al. 1986; Glasby, Gschmeissner et al. 1986; Hall 1997) at which each end of the nerve is secured and regeneration across the gap is guided. These however, have limited success when compared to autologous nerve and are frequently overlooked given their limitations. The frequent collapse and fibrosis of vein grafts (Doolabh, Hertl et al. 1996) and the relatively slow regeneration of the nerve though the muscle graft (Glasby, Gschmeissner et al. 1986) remain unattractive attributes when selecting a suitable material. Properties by which a material can facilitate and maintain communication between the proximal and distal ends of the nerve defect, provide a physical guidance for axonal regrowth and block

external inhibitory factors remain the main criteria in investigating possible alternate sources.

To date the most investigated synthetic nerve graft has been that of the silicon tube, illustrated in figure 5.3. While providing the greatest degree of isolation from extrinsic factors in the wound their use has been more lauded in experimental models than in clinical trials. Lundborg et al (Lundborg, Dahlin et al. 1991) demonstrated equivocal results when comparing their use against primary repair in patients, however, they had to be removed in a second procedure given the inflammatory reaction evoked by their prolonged presence, a concept not isolated to this study (Merle, Dellon et al. 1989). Similar issues have been presented in the use of other synthetic non-absorbable nerve conduits such as Gore-Tex (Pitta, Wolford et al. 2001) and has led investigators to pursue absorbable synthetic grafts as an alternate.

In 1999, FDA approval was obtained for a polyglycolic acid nerve conduit – NeuroGen®. Polyglycolic acid is a bioabsorbable substance in use extensively as a suture material and is reabsorbed in approximately 90 days (Herrmann, Kelly et al. 1970). Its use as a conduit was investigated in a prospective clinical trial by Weber et al in 136 nerve repairs of the hand. In this investigation 2 populations were studied; 1) standard neurorrhaphy with either end-to-end anastomosis or nerve graft and 2) nerve repair using a polyglycolic acid conduit. There were no statistical differences between the 2 groups overall. However, 2-point discrimination was found to be better in the polyglycolic acid conduit group than in the control as well as the benefits of eliminating donor-site morbidity (Weber, Breidenbach et al. 2000).

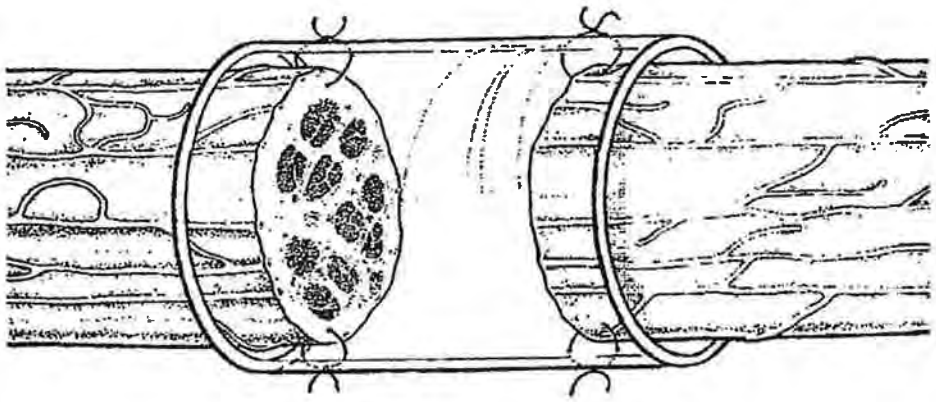

Figure 5.3 – Illustration of a Silicon Nerve conduit bridging a nerve defect, Adapted from Lundborg (Lundborg 2000).

Alternate therapies investigated in the field of nerve grafting include the nerve allograft and the concept of nerve transfer. The nerve allograft, while gathering momentum as a management option, has been limited clinically by the need for long term immunosuppression. This idea has been further promoted given the experimental evidence of enhanced neural regeneration with the immunosuppressant FK506 (Lee, Doolabh et al. 2000; Pan, Misgeld et al. 2003; Sobol, Lowe et al. 2003; Snyder, Fox et al. 2006). While clinical use has been documented its indication has been limited to severe, lengthy nerve injuries (Mackinnon 1996) and it's promise for the future hinges on more refined immunosuppressant techniques evolving to justify its use. Nerve transfers provide an alternate to repair and grafting, based on the technique of moving an uninjured nerve to innervate distal to the injury site, bypassing the defect. Commonly used in root avulsion injuries of the brachial plexus its clinical use has been expanding in more recent years as clinical outcomes often surpass that of nerve grafting injuries with extensive defects (Mackinnon and Novak 1999; Mackinnon and Colbert 2008).

The potential for manipulation of the nerve microenvironment following repair deserves mention as the neurosciences evolve into this century. While beyond the scope of this thesis the interests in its application have stemmed from the surge in knowledge surrounding the molecular response of the nerve to injury. The use of neurotrophic factors following nerve repair has been investigated as a means to both reduce neuronal death following injury as well as to improve initial axonal outgrowth. While no supportive clinical evidence exists to date regarding their use following neurorrhaphy, numerous experimental pre clinical studies have highlighted their potential. Nerve Growth Factor (NGF) has been shown to decrease the death of dorsal root ganglion cells following repair in animal models (Rich, Luszczynski et al. 1987), improve regeneration when supplied via a conduit (Rich, Alexander et al. 1989; Da-Silva, Lima et al. 1990) and has also been shown to have a role in supporting nerve cell viability in the management of both Parkinson's and Alzheimer's Disease (Olson, Backman et al. 1994). Exogenous Insulin-like Growth Factor (Kanje, Skottner et al. 1989; Sjoberg and Kanje 1989), Ciliary Neurotrophic Factor (Newman, Verity et al. 1996) and Fibroblast Growth Factor (Walter, Kurouglu et al. 1993; Fujimoto, Mizoguchi et al. 1997) have also been show in animal studies to promote nerve regeneration following repair. Non growth factor manipulations have also been trialled in experimental models with some success. These have included FK506 (Lee, Doolabh et al. 2000; Pan, Misgeld et al. 2003; Sobol, Lowe et al. 2003; Snyder, Fox et al. 2006) as mentioned previously, a hyperbaric oxygen environment following repair (Eguiluz-Ordonez, Sanchez et al. 2006), Leukemia Inhibitory Factor (Tham, Dowsing et al. 1997) and Chondroitin Sulfate Proteoglycan degradation (Zuo, Neubauer et al. 2002) to name but a few. Alternate molecular approaches to improving regenerative outcomes following nerve

repair by reducing extraneural scar formation using ADCON-T/N, a carbohydrate polymer gel, have also shown promise in rodent studies (Petersen, Russell et al. 1996). Ultimately, administration route and toxicity remain key concerns in the translation of these findings across to clinical practice and with this in mind much emphasis has been placed on local administration via a synthetic / bioabsorbable conduit or tissue engineered scaffold, allowing for a slow controlled release with ultimate exhaustion of the local supply.

5.1.3. Sutureless Peripheral Neurorrhaphy

While the advent of microsurgery has lead to more exact nerve approximation with epineurial, fascicular and interfascicular repairs now commonplace, the ideal of approximating each individual axon to its appropriate distal counterpart utilising these methods, is far from obtainable. The ultimate neurorrhaphy aims for a repair with accurate alignment along with minimal inflammation and trauma to the tissues. The microsurgical placement of sutures, regardless of filament size, still leaves gaps in these tubular structures that allows for scar tissue infiltration and migration of axonal sprouts during the regenerative process. Failure to circumferentially contain the axons within the epineurium permits axonal escape at the repair site and further reduces the number of axons reaching the target organ. Furthermore, non-absorbable sutures remain as permanent foreign bodies at the repair site. This initiates a fibroblastic proliferation resulting in granuloma or scar formation that in turn prevents the advancement of regenerating axons into the distal nerve segment. While the standard approach to surgical repair of tissue, sutures, whether natural or synthetic, contribute negatively to the overall inflammatory effect of the tissues

following repair. This cellular response when combined with the traumatic nature of suture placement highlights the fact that the current standard in neurorrhaphy is a less than ideal solution. Numerous studies have been performed regarding the reaction of tissue to sutures, including suture neurorrhaphy (Guttman 1943; Sunderland and Smith 1950; Mukherjee and Douglas 1951; DeLee, Smith et al. 1977). These studies have established two distinct host responses to the foreign material. Firstly, a cellular response aimed at removing the material from the tissue that involves recruitment of additional polymorphonucleocytes, lymphocytes, giant cells and histiocytes to the neurorrhaphy site. This initially intense reaction subsides following isolation of the suture by the second, fibroblastic response. While evidence has suggested that regenerating fibres are not adversely affected initially, the resultant scar formation during the fibroblastic response may result in a mechanical block to regenerating axons. This cellular response to suture, coupled with the additional trauma of suture placement has encouraged investigators to pursue a means by which neurorrhaphy may be undertaken either in a sutureless fashion or a technique allowing for minimal suture placement.

To date, emphasis has been placed on either a tissue adhesive or laser assisted approach to neurorrhaphy. While other methodologies exist, they remain as preclinical trials without offering significant improvement over standard nerve repair. These include the use of titanium clips and couplers. Both these mechanical devices have been thoroughly evaluated in the field of vascular surgery, however their application to neurorrhaphy has been limited by the lack of any clear advantage associated with their use over sutures. Titanium clips, while a rapid method of anastomosis does leave a significant amount of foreign material in the repair site and

this in turn increases the risk of external compression and fibrosis of the nerve repair site over time (Park, Lee et al. 2002; Payne, Hunt et al. 2002). Couplers, generally consisting of paired polyethylene rings fitted with pins everting the epineurium, also lend toward a speedy repair but fail to supersede the clinical standard and have been suggested to increase fibrous invasion at the repair site (Prevel, Eppley et al. 1994; Lutz and Lidman 2005). These properties are likely to impede adaption of the technique over to clinical use in this manner.

Adhesive Based Neurorrhaphy

The use of glue as a tissue adhesive has been studied extensively in neurorrhaphy, firstly as a primary repair tool and more recently as both a repair and a means to introduce exogenous growth factors into the microenvironment of the regenerating nerve (Jubran and Widenfalk 2003; Chunzheng, Shengzhong et al. 2008). While the emphasis remains on fibrin glues as an adhesive some synthetic glues (cyanoacrylate based) have also been trialled with mixed success (Wieken, Angioi-Duprez et al. 2003; Landegren, Risling et al. 2006). Fibrin glue is composed of two main ingredients, fibrinogen and thrombin, which, when mixed and placed in tissue mimic the final stages of the clotting cascade bypassing the extrinsic and intrinsic pathways of coagulation. Its initial licensing as a sealant and method of achieving haemostasis (Spotnitz, Dalton et al. 1987; Gibble and Ness 1990; Ochsner 1998) has been expanded in experimental and clinical models of tissue repair and anastomosis and although widespread clinical utilisation is not commonplace, a body of evidence exists supporting its role across a number of specialities (Thetter 1981; Sugiura, Nakatsuchi et al. 1985; Lilius 1987; McCarthy, Trastek et al. 1987; Schlag and Redl 1988).

The role of fibrin glues in the repair of the peripheral nerve was prompted by early innovators who described the use of concentrated coagulated blood as a means of anastomosis (Young and Medawar 1940). Using this plasma clot suture initially in dog and rabbit nerves they concluded that in the absence of undue tension, the substance was suitable as a means of opposing the nerves ends, was resorbed in a matter of weeks and ultimately not deleterious to nerve regeneration. Work continued in the area with several modifications including tubulisation of the fibrin clot and eventual progress to small clinical trials (Seddon and Medawar 1942; Singer 1945). Throughout this series of investigations it was noted however that the technique was flawed with difficult storage and preparation requirements and frequent separation of apposed nerve stumps. With the advent of refined microsurgery it was thought of as a primitive, early technique in comparison and attention dwindled from its development. The technique was revisited with the commercial availability of fibrin glue in the late 1970's and resulted in several clinical trials with promising results (Egloff and Narakas 1983; Narakas 1988; Sterkers, Becherel et al. 1989). Advocates of fibrin repair report superior approximation with more rapid regeneration (Ventura, Torri et al. 1980), greater isometric muscle contraction following regeneration (Faldini, Puntoni et al. 1984) and a decrease in inflammation and fibrosis of the repair site (Ornelas, Padilla et al. 2006) in numerous small and large animal studies. However, for each study promoting the technique several remain less enthusiastic with dehiscence rates utilising commercially available fibrin reported at 20% (Sames, Blahos et al. 1997; Temple, Ross et al. 2004), poorer electrophysiological outcomes and retrograde fluorescent imaging contradicting claims of superior axonal alignment (English

2005). Overall, the only consistent benefit found has been speed of technique with advantages of functional outcome still a source of debate with many inconclusive studies published.

Laser Based Neurorrhaphy

Laser assisted nerve repair offers significant theoretical advantages to overcoming the inherent problems associated with suture neurorrhaphy. Following the use of laser in fields such as vascular surgery and in particular microvascular anastomosis (Jain and Gorisch 1979; Jain and Gorisch 1979; Neblett, Morris et al. 1986), the transfer of the application to laser neurorrhaphy was inevitable. Laser anastomosis works by transfer of thermal energy to the tissue in question. While the complex sequence of events is largely unknown, this transfer results in thermal restructuring of the proteins by denaturation, which then, during the cooling period anneal together resulting in adhesion between both surfaces. While the technique when used correctly does not result in destruction of the regenerating fibres, a delicate balance remains between increasing power, subsequent thermal injury and a more robust tensile bonding of the anastomosis. High powers induce thermal injury to the fibres whereas low powers result in weak anastomosis with high rates of dehiscence. These limiting factors lead investigators to explore not only the use of the laser as a direct repair method but also as a soldering technique.

Several medical grade lasers have been used in an attempt to identify an optimal tool with the CO_2 laser being the most commonly investigated modality. The milliwatt CO_2 laser was reported as a successful technique in a two-part study by Fischer and Beggs (Fischer, Beggs et al. 1985; Beggs, Fischer et al. 1986). Using a pulsed spot

welding technique they described a 13% dehiscence rate in rat sciatic nerve repairs with no significant difference in histological parameters following regeneration compared to suture alone. The fibrotic response of the tissue to sutures was also reported in the control group and notably absent in the laser treated group. These findings have been reproduced with greater analysis of tensile strength, and a subsequent dehiscence rate of up to 40% using laser powers within reasonable limits (Huang, Blanks et al. 1992; Korff, Bent et al. 1992). With greater laser powers (1.0W) Korff et al (Korff, Bent et al. 1992) reported a 50% reduction in neural regeneration, highlighting the destructive potential of the technique. While dehiscence remains the most pertinent obstacle, carbonaceous deposits have also been described following Korff's repair with laser. While Korff described these as non significant in his study, in subsequent studies of nerves repaired with minimal tensile stress post procedure, both charring and a fibrotic reaction were noted on histology (Dort, Wolfensberger et al. 1994). This was a concurrent finding in a series which revealed no dehiscence following repair of the facial nerve model suggesting more deleterious effect than previously thought but also that laser repair may be more successful in areas not subject to positional tension.

Addition of a soldering technique to the field was hypothesised to increase bond strength while limiting the nerve exposure to thermal energy. While solders such as bovine serum albumin and autogenous blood droplets have reported success with a reduction in dehiscence and histological outcomes comparing favourably to suture alone, the concerns regarding thermal injury remain (Almquist, Nachemson et al. 1984; Lauto, Dawes et al. 1998; Lauto, Dawes et al. 1998). While a promising technique initially, these issues limit the transfer of the technique across to clinical

practice with the risk of thermal injury along with a high dehiscence rate confining laser repair studies to that of the animal model to date.

Other optical based repair models involved in nerve repair include that of light activated techniques. These primarily include the use of Photochemical tissue bonding as described below in chapter 5.2, but also includes a small pre clinical study investigating the use of a light activated tissue adhesive (Lauto, Foster et al. 2008). While a provisional study with a short follow up time the investigators remain optimistic regarding its application to the field of neurorrhaphy and propose that light activated techniques offer the significant advantages of a sutureless repair without the thermal injury associated with laser neurorrhaphy, and avoiding the low tensile strengths of both adhesive and laser repairs.

5.2. Photochemical Tissue Bonding

5.2.1. Introduction to Photochemical Tissue Bonding

Photochemical tissue bonding (PTB) is a sutureless tissue repair process that seals the repair site without trauma or foreign body reaction, thus allowing prompt restoration of the normal environment and healing. While the main avenues of investigation to date have centered on biological applications of PTB, non-biological applications have included the use of the PTB process as a crosslinking agent in the preparation of Collagen-based scaffolds in the field of tissue engineering (Chan and So 2005; Chan, Hui et al. 2007).

In PTB, a photoactive dye is applied to tissue surfaces that are then placed in contact and irradiated with green light. This technique utilises visible light (green laser light at 532 nm from a continuous wave Nd/YAG laser) at a power that does not thermally damage the tissue, unlike laser welding techniques, therefore preserving the nerve structure and surrounding tissues. The light activates the dye leading to immediate formation of covalent crosslink's between proteins on both surfaces, thereby forming a watertight seal. Crosslinking occurs following the formation of a reactive species (singlet oxygen), which interacts with potential electrons donors and acceptors such as the amino acids of proteins at both tissue interfaces (e.g. tryptophan, tyrosine and cysteine). These instantaneous 'nanosutures' contrast with laser welding where a thermal effect is employed to denature proteins and bonding occurs following intertwining of collagen molecules from the tissue edges as the proteins cool (DeCoste, Farinelli et al. 1992; Gayen, Katz et al. 2003). The dye commonly used in PTB is Rose Bengal (RB), a halogenated fluorescein derivative that is photochemically active when exposed to green light (Lambert, Stiel et al. 1996; Stiel, Teuchner et al. 1996). The Rose Bengal molecule is shown below in figure 5.4 along with the photoreactive pathway producing a reactive oxygen species.

Rose Bengal has been FDA-approved for use as a diagnostic agent in ophthalmology (Wilson 1976; Pavan-Langston 1985; Feenstra and Tseng 1992) and also described as a systemic diagnostic agent for hepatic function (Eyler, Schuman et al. 1965; Nordyke 1965). While phototoxic to cultured cells, Rose Bengal, in combination with PTB has been show to reduce inflammation, and in unpublished results from The Wellman Center for Photomedicine, work has shown enhanced fibroblast survival after PTB via induction of antioxidant production and activation of

signalling transduction pathways. A recent pre-clinical evaluation (Wachter, Dees et al. 2003) of the pharmacokinetics and safety of topical RB indicated that concentrations of RB <1% had negligible effects on normal skin either in the dark or after exposure to 532 nm green laser light using irradiances of ≤ 100 mW/cm^2. In this study a 10-fold lower RB concentration (0.1%) was used with our PTB technique and additionally, photoactivation of Rose Bengal with 532nm laser radiation has not induced an inflammatory reaction in any investigations to date.

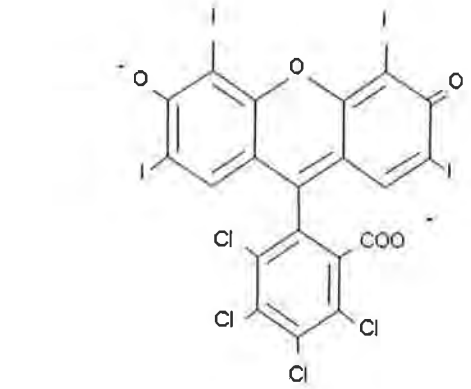

Figure 5.4 - Top; The Rose Bengal molecules at a neutral pH, Below; Photoreactive pathway following exposure of Rose Bengal (RB) to light resulting in a reactive oxygen species.

Tissue bonding with this technique is further strengthened by wound healing which proceeds uninterrupted following treatment. Through all investigations to date PTB has been demonstrated as a safe and reliable platform technology.

5.2.2. Previous applications of Photochemical Tissue Bonding

PTB has been previously demonstrated the efficacy in several tissues both ex vivo and in vivo. Corneal incisions in rabbit eyes treated with PTB healed without complications and the resultant seals produced resisted pressures at least 10-fold greater than the intraocular pressure (Proano, Mulroy et al. 2004). This application is currently under investigation in the use of PTB as a suture substitute in a corneal transplant model based on preliminary work where it was used to provide a water-tight seal with sutures for securing corneal transplants *in vivo* in rabbit eyes (Proano, Azar et al. 2004). An ex-vivo example of this application is shown below in figure 5.5. In addition, PTB enhanced the healing of severed tendons in a rat Achilles tendon model (Chan, Amann et al. 2005) and provided a sutureless microvascular anastomosis in a rat femoral artery model (O'Neill, Winograd et al. 2007). Enhancement of porcine skin grafts using this light activated process has also been demonstrated resulting in dermal-dermal bonding with no significant effect to skin cell viability (Chan, Kochevar et al. 2002).

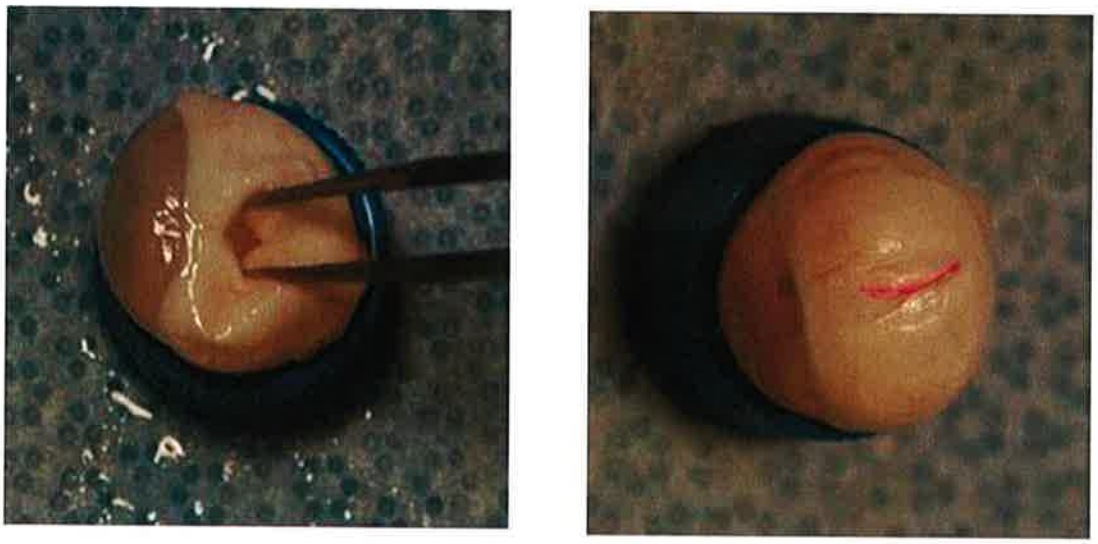

Figure 5.5 – The use of PTB in the repair of scleral lacerations and incisions of the eye. This rabbit ex vivo model shows the initial laceration on the left with the PTB sealed incision on the right. The pink staining is due to residual Rose Bengal over the wound following irradiation.

PTB as a technology has been evaluated to a greater degree in skin models of excision and incision closure. Indeed in this area, clinical trials are currently in progress where both cosmetic and functional benefits of simple wound closure with PTB are being evaluated. Previous studies compared PTB favourably with standard sutures and the cyanoacrylate compound tissue adhesive Dermabond® for closing incisions and excisions in pig skin (Kamegaya, Farinelli et al. 2005). The hypothesis tested was that PTB was equivalent to standard suture closure of incisions and excisions and was equivalent to Dermabond® for closure of incisions. Incisions and excisions (2-cm long) were created on the flanks of a Hanford mini-pig. All were managed initially with subcutaneous sutures. Eight incisions and eight excisions

were sutured with 3-0 monofilament, eight incisions and twelve excisions were treated with PTB, eight incisions were treated with Dermabond®, and eight incisions were treated with Dermabond®, followed by PTB. The incisions were treated with 100 J/cm^2 and excisions were treated with 75, 100 or 150 J/cm^2 532 nm radiation from a Nd:YAG laser. No acute or delayed adverse responses (e.g., erythema, inflammation) were observed at sites treated with PTB. All treated sites remained closed, suggesting that PTB produced bonds strong enough to resist opening despite the pig vigorously rubbing the cage walls. At 2, 4 and 6 weeks after the treatments, the sites were observed by three physicians who were blinded to the treatments. No significant differences were found in cosmetic appearance (scar colour, texture, contour, distortion and global appearance) between the treatment groups at any of the observation times. Measurements of the histological scar width using an ocular micrometer also indicated no differences between treatment groups. These results suggest that PTB is as effective as standard sutures or Dermabond® for closure of skin incisions and excisions and have encouraged both the progress to clinical trials and the use of this platform technology across a wide range of medical and surgical specialties.

5.2.3. Photochemical Tissue Bonding and Peripheral Nerve Repair

Photochemical Tissue bonding has been applied with success in two previous investigations regarding repair of the peripheral nerve in a rodent model. In a preliminary study (Johnson, O'Neill et al. 2007) PTB was used to restore the continuity of the severed nerve using an epineurial cuff technique as shown below in figure 5.6.

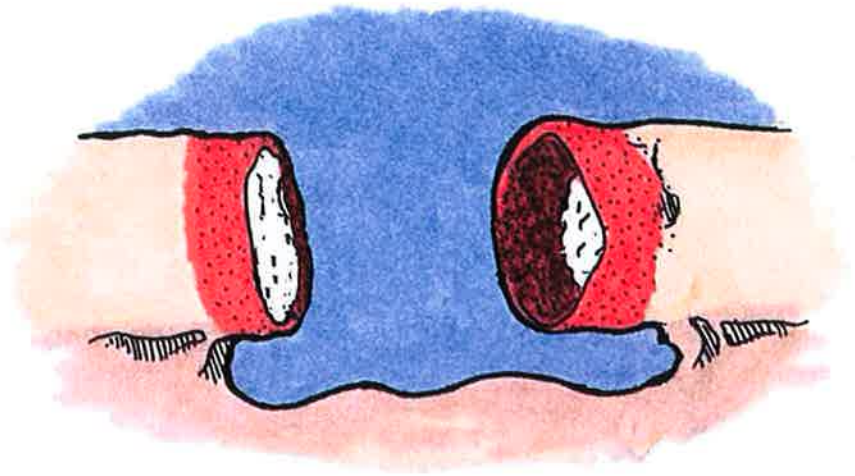

Figure 5.6 - Illustration of the epineurial cuff technique used in a preliminary study of nerve repair using PTB Technology (Courtesy of T. S. Johnson).

This study showed preservation of the neural micro-architecture and demonstrated the feasibility of PTB as a viable nerve repair technique. Functional recovery using sciatic function indices (Bain, Mackinnon et al. 1989) in the suture repair and epineurial cuff with PTB groups were not significantly different (–70.6 +/- 17.8 vs. – 76.9+/- 10.3) at ninety days post-repair and histology revealed good axonal regeneration with all repair techniques. While histomorphometric analysis found no significant difference between the repair groups, this study illustrated that peripheral nerves can be successfully repaired using a photochemical tissue bonding technique with preservation of the neural microenvironment following bonding and achieving results similar to the current gold standard of microsurgical repair.

In a second study (O'Neill, Bujold et al. 2008), photochemical tissue bonding was combined with a nerve wrapping technique to determine if this could reduce scar formation and improve outcome following primary peripheral nerve repair. Animals treated with amnion wraps sealed with PTB also showed an early improvement in functional recovery. All nerves received primary suture repair initially and in the PTB group, this procedure was followed by:

a) A 1 cm^2 piece of human amniotic membrane (HAM) was treated with RB and wrapped around the repair site

b) The site was then exposed to green light resulting in a sealed cuff around the repair, as shown in Figure 5.7 below.

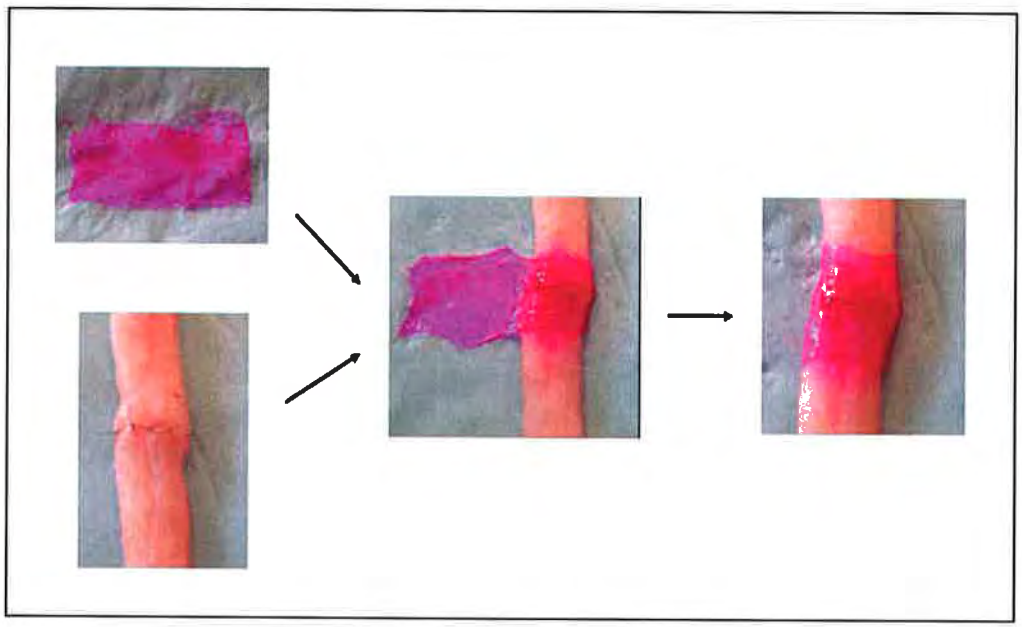

Figure 5.7 - Nerve wrapping procedure with human amniotic membrane (stained with Rose Bengal) in an ex vivo model of porcine nerve (Courtesy of A.C.O'Neill).

This combined treatment was evaluated against:

1) PTB sealing alone (no wrap),

2) Primary suture repair,

3) Amnion wrapping alone (no PTB treatment),

4) Autologous Vein wrap sealed with PTB,

5) Autologous vein wrap alone.

Sciatic function indices (a functional measure of nerve recovery)(Bain, Mackinnon et al. 1989) were significantly better in the Amnion / PTB sealed group compared to those receiving standard suture neurorrhaphy alone at 90 day following repair (Mean SFI -52.74 +/- 5.22 vs. -70.76 +/- 4.24). These findings were also supported by statistically significant histological findings of increased fibre and axon diameter as well as myelin thickness in nerve segments distal to the repair in the amnion / PTB animals. The use of PTB alone as a sealant with SN, without nerve wrapping, did offer significant improvement in functional recovery, however it failed to show significant improvement across any of the histological parameters measured.

This series of studies has shown PTB to be a viable nerve repair technique to improve functional outcome when combined with a HAM wrap and lead to the investigation discussed in this thesis where this technique is evaluated in a large animal model with electrophysiological endpoints.

5.2.4. Nerve Wrapping

There has been ongoing interest in nerve wrapping as a means to improve outcomes following peripheral neurorrhaphy. The broad aim of a wrap is to introduce a protective environment in which a nerve may regenerate across, or within. Nerve wraps have been used for two main purposes clinically. Firstly as an alternate or augmentation to suture repair. In this case the nerve is placed in a tube (tubulisation) or wrap and regeneration occurs in the protected environment. This has been theorised to reduce adhesion and scar formation in the postoperative period. Secondly, in the case of a nerve gap, when there is a nerve defect the tube allows guidance of regeneration across the gap and in to the distal portion of the nerve. The concept of a nerve wrap or in the latter case is to negate the need for allografting along with the associated donor morbidity; a nerve wrap in this case is generally referred to as a conduit. For the purpose of this investigation the role of the nerve wrap as an augmentation of regeneration in a repaired nerve is our primary concern rather than its role as a conduit across a nerve deficit.

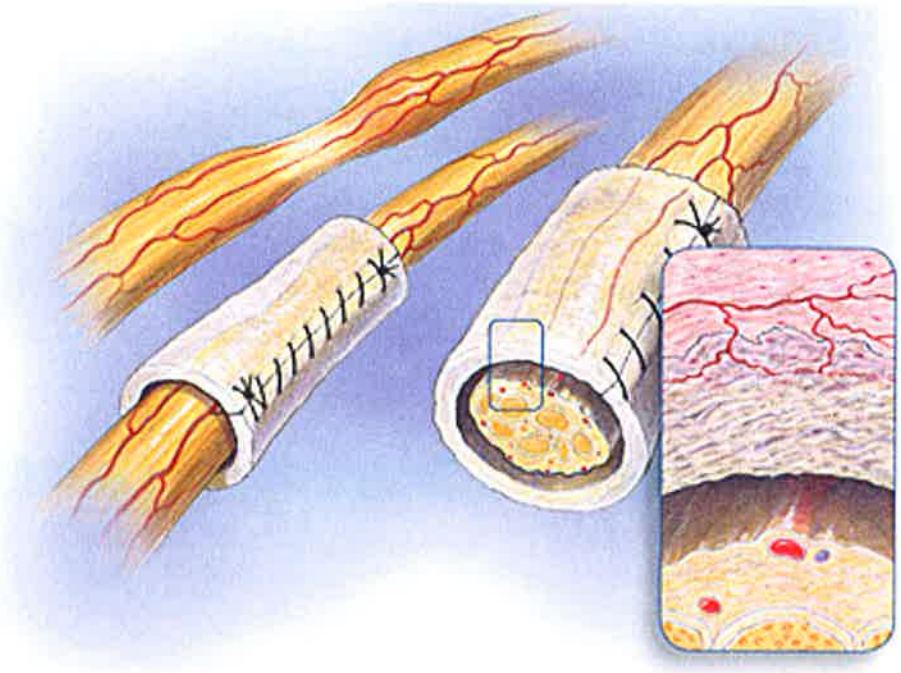

Figure 5.8 - The Neurogen® Nerve Wrap.(Neurogen 2008) A collagen based material for both tubulisation and use as a conduit.

Autologous vein is most commonly used as a wrap in clinical practice (Varitimidis, Riano et al. 2000; Varitimidis, Vardakas et al. 2001; Chou, Papadimitriou et al. 2003) but the use of human amniotic membrane (HAM) has also been reported (Ozgenel and Filiz 2004). While wrapping the nerve has been reported as a method for reducing scar formation (Ruch, Spinner et al. 1996), the vein wrap itself, has only been evaluated clinically in cases of severe recurrent scarring with associated nerve compression (Xu, Sotereanos et al. 1998; Xu, Varitimidis et al. 2000; Varitimidis, Vardakas et al. 2001) and generally used as a secondary procedure to loosely surround the site of injury without sealing

More recently attention has been given to the development of bioengineered materials for this purpose. Several animal studies have investigated the use of collagen (The Neurogen® Nerve Wrap as shown in figure 5.8*)* as a conduit and a wrap (Archibald, Krarup et al. 1991; Archibald, Shefner et al. 1995) as well as glass fibre wraps (Jeans, Healy et al. 2007; Jeans, Gilchrist et al. 2007). While the consensus remains that these materials are suitable for use in this manner, to date they have not been shown to be superior to standard microsurgical repair of the nerve. Tubulisation techniques with both silicone and the resorbable poly [(R)-3-hydroxybutyrate] (PHB) have also been described in clinical studies, in conjunction with and as an alternate to primary neurorrhaphy, and while results have been promising, they again fail to supersede standard neurorrhaphy in functional recovery (Lundborg, Rosen et al. 1997; Battiston, Geuna et al. 2005; Aberg, Ljungberg et al. 2008).

In this study, HAM is investigated as a suitable nerve wrap material, with the addition of PTB technology to seal the amnion over the repair site to isolate the regenerating nerve environment. The hypothesis remains that sealing the amnion nerve wrap with PTB technology would isolate the endoneurial environment from extrinsic inflammatory factors, and would maximize the intrinsic growth factors produced within the nerve repair site. A potential to minimize suture material should also result in a decreased foreign body reaction and subsequent scar formation (DeLee, Smith et al. 1977). Ultimately, with this unique combination of nerve wrapping with HAM, along with the sealing benefit of PTB, the hope is to improve on existing outcomes in this field and offer an alternate to both the existing nerve wrap as well as standard microsurgical repair.

5.2.3. Human Amniotic Membrane

The amniotic membrane is the innermost layer of the foetal membranes (demonstrated in figure 5.9). It is loosely joined to the chorion with a primitive mesenchyme and is in direct contact with the amniotic fluid. It is comprised of a collagen rich thick basement membrane and an avascular stroma and in the mature placenta, it functions as an epithelium and believed to have secretory activities as is evidenced by the numerous microvilli on its surface.

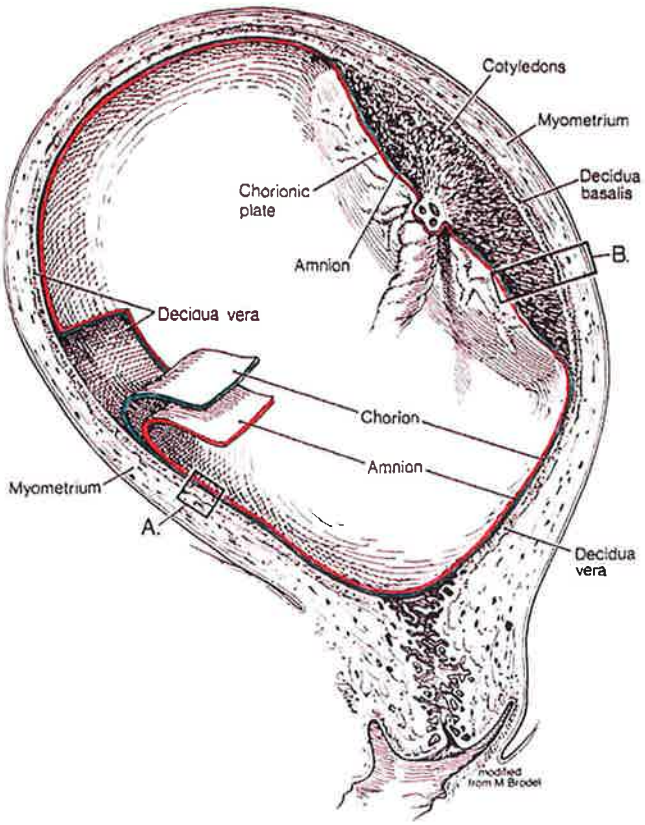

Figure 5.9 - The human placenta and its layers. The amniotic layer is the innermost layer, in contact with the amniotic fluid (Gray 2008).

It's first reported clinical use was in 1910 (Davis 1910) followed shortly after in 1913 when Stern reported it's use as a dressing on cutaneous wounds, both ulcerated and as result of burns (Stern 1913). They reported a lack of infection in the wounds, a decrease in pain and an increase in re-epithelisation of the wound surface. This interest waned for several years however it was reinvigorated in the 1940's when De Rotth used both amnion and chorion to repair corneal defects (de Rotth 1940). While only limited success was reported in this incidence, amnion was further investigated across several clinical specialities as source of tissue in the repair and epithelialisation of wounds, both traumatic and post operative. Clinically, it has been used as a wound dressing and found to increase re-epithelialisation rates (Sabella 1913; Stern 1913). In all cases granulation tissue as well as vascularity appeared within a few days of application (Faulk, Matthews et al. 1980). It has been subsequently described in a wide range of tissue repair models including vaginal, urethral and bladder reconstruction, adhesion prevention, and repair of the pericardium and splenic capsule (Gruss and Jirsch 1978; Fishman, Flores et al. 1987; Badawy, Baggish et al. 1989; Young, Cota et al. 1991; Erdener, Ulman et al. 1992; Brandt, Albuquerque et al. 2000; Ghanbari, Dahaghin et al. 2006). Of considerable benefit to its use in this manner it has been shown that human amniotic cells do not express HLA-A,B,C or DR antigens of β_2-microglobulin (Adinolfi 1982; Adinolfi, Akle et al. 1982) and the immunologic response to transplantation is negligible (Akle, Adinolfi et al. 1981). Indeed transplantation of amnion into human volunteers substantiate these facts given that none of the subjects (n=7) showed clinical signs of acute rejection, and amniotic epithelial cells were demonstrated by biopsy up to 7 weeks after implantation (Akle, Adinolfi et al. 1981). Regarding its use in animal models, a xenogenic response following treatment with Human Amniotic Membrane

has not been described despite several studies investigating its therapeutic effects. These include intraabdominal and pelvic adhesion prevention in both rodent (Badawy, Baggish et al. 1989) and rabbit (Young, Cota et al. 1991) models as well as investigations involving wound repair models of the cornea (Shimmura, Shimazaki et al. 2001) and evaluation of intraocular implantation in a rabbit model (Kubo, Sonoda et al. 2001).

Infiltration of neutrophils, lymphocytes and macrophages have been shown to be reduced in corneal perforations treated with amniotic membrane (Nobe, Moura et al. 1990), and it is in this area that amnion currently has its most common clinical use. Figure 5.10 below is an example of amnion being used as a corneal graft.

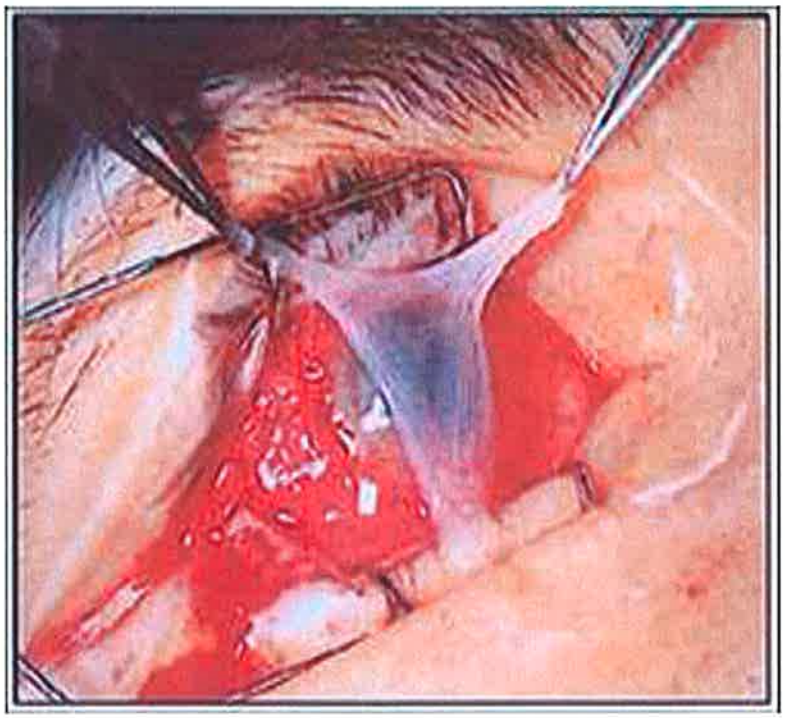

Figure 5.10 - Human amniotic membrane being used as a corneal graft (Nethradhama 2008).

Both anti-inflammatory and anti-angiogenic proteins have been identified along with increased apoptosis of polymorphonuclear neutrophils and CD20+ cells detected in wounds treated with amnion (Hao, Ma et al. 2000; Park and Tseng 2000; Shimmura, Shimazaki et al. 2001). Additional attributes that may be of particular importance in peripheral nerve repair include investigations that have shown Human amnion to contain a wide range of growth factors even after preservation (Koizumi, Inatomi et al. 2000). These include basic fibroblast growth factor (bFGF) and transforming growth factors (TGF-α, TGF-β1, TGF β2, TGF-β3), which have been implicated in the nerve repair process. Previous investigations using amnion in the field of neuroscience has involved in vitro work growing axons in an amnion based substratum and following on from this, using the amniotic membrane as a conduit to support nerve regeneration in both the central and peripheral nervous systems (Davis, Blaker et al. 1987). Indeed the use of amnion as a nerve conduit has been shown to be a viable alternative to autologous nerve grafting without the donor site morbidity associated with the clinical gold standard (Mohammad, Warnke et al. 2000; Mligiliche, Endo et al. 2002).

Human Amniotic Membrane (HAM) as a nerve wrap lends itself towards use with PTB given its thin (20 μm) translucent nature as well as its malleable handling properties. These attributes and properties, particularly concerning previous applications in the field of neuroscience, are favourable towards using HAM as a nerve wrap combined with PTB technology.

5.2.4. Optical Therapeutics in Peripheral Nerve Surgery – Aim

The broad aim of this study was to evaluate the efficacy of photochemical tissue bonding with an amnion nerve wrap in the repair of the peripheral nerve of a large animal model using neurophysiological assessments as a functional outcome along with histological analysis.

6. Materials and Methods - Optical Therapeutics

6.1. Animal Model

The Subcommittee on Research Animal Care at Massachusetts General Hospital approved all procedures in this study. The common peroneal nerve was chosen as a model for this study and is show in figure 6.1 below (ex vivo).

Figure 6.1 – Exposed sciatic nerve (left side) of the New Zealand White Rabbit (ex vivo). The Common Peroneal Nerve is evident proximally as the left branch of the nerve and distally, lying over the peroneal muscle complex.

Twenty-four female New Zealand White Rabbits (Charles River Laboratories, Wilmington, MA), weighing 2 - 2.5 kg were anaesthetised with isoflurane (2.5 – 3.5% by mask, Baxter Healthcare Corporation, Deerfield, IL.).

6.2. Human Amniotic Membrane Preparation

Human placenta was obtained with the approval of the Institutional Review Board (IRB) at Massachusetts General Hospital. All residual blood clots were removed from the placenta by washing the tissue several times with Earle's Balanced Salt Solution (EBBS). The amniotic membrane was peeled away from the chorion and placed on nitrocellulose paper (epithelial side down). The amnion was then cut into segments and stored at -80°C in medium consisting of a 1:1 solution of 100% glycerol and Dulbecco's modified Eagle's medium (Gibco, Grand Island, NY) with 1% penicillin-streptomycin (Gibco). Immediately prior to use, the amnion was defrosted and rinsed in PBS for 2 hours to remove all glycerol. The amnion was then further prepared by cutting into 1 x 1 cm pieces (figure 6.2) prior to use as described below.

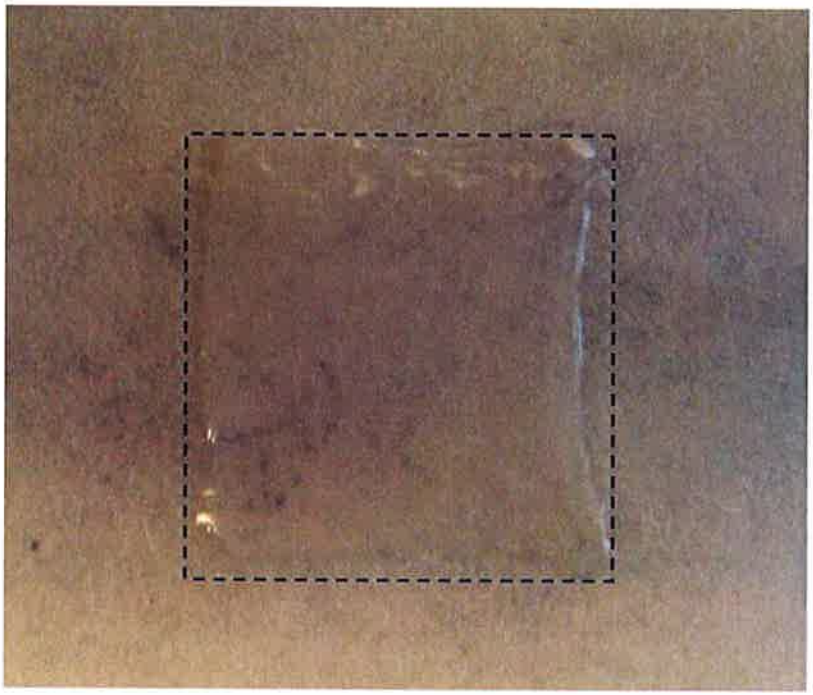

Figure 6.2 – Human amniotic membrane (1 x 1 cm – outlined in image) following cryopreservation and preparation for use as described above.

6.3. Surgical Procedures & Experimental Design

Following anaesthesia the right common peroneal nerve was exposed through a dorso-lateral muscle splitting incision as shown in figure 6.3 (intraoperative image).

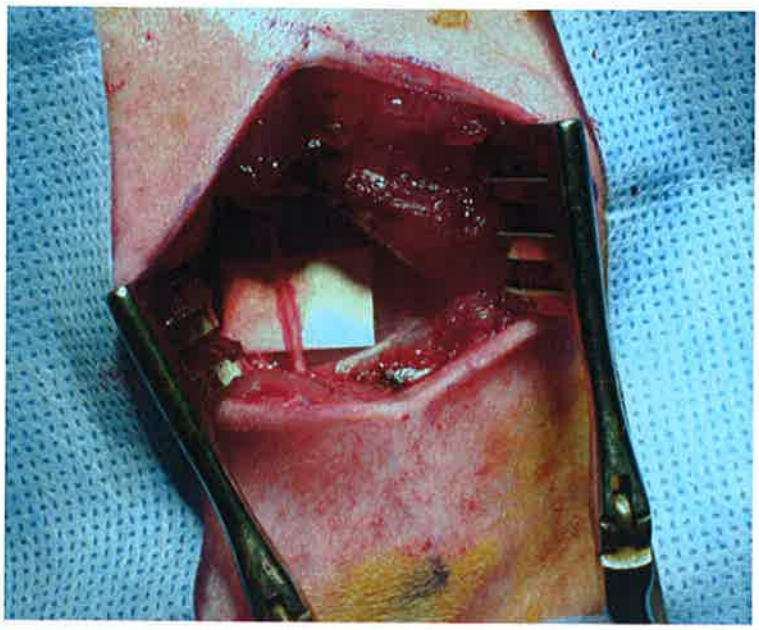

Figure 6.3 – Exposed Common peroneal Nerve of the New Zealand White Rabbit via a dorso-lateral muscle splitting incision.

Under microscopic guidance, the common peroneal nerve was isolated and sharply transected at a point 5 cm distal to the sciatic notch. The nerve was repaired immediately with three 10-0 nylon epineurial sutures (Ethicon, Somerville, NJ). Animals were then randomised to one of three experimental groups (n=8) as outlined below.

Standard Neurorrhaphy (SN) / Control Group (n=8)

These animals did not receive any further treatment following standard neurorrhaphy as described above. This served as the control group.

Standard Neurorrhaphy (SN) & HAM wrap (n=8)

The amniotic membrane was prepared as outlined previously. Following standard neurorrhaphy (described above), a 1 x 1 cm segment was wrapped around the repair site and secured to the epineurium using a single 10/0 nylon suture (Ethicon, Somerville, NJ) proximally and distally. No Rose Bengal was applied to the amnion.

Standard Neurorrhaphy (SN), HAM / PTB (n=8)

A 1 x 1 cm segment of amnion (stromal surface) was treated with 0.1% Rose Bengal. This pink dye was allowed to absorb for 1 minute, after which any excess was removed. Following standard neurorrhaphy, the segment was wrapped around the nerve, covering the epineurial repair site. This area was then exposed to green laser light at 532 nm from an Aura *i* continuous wave Nd/YAG laser (Laserscope, San Jose, CA), at an irradiance of ~ 0.5 W/cm^2 for 1 minute followed by 180° rotation and repeat irradiation on the opposite side. This procedure is outlined below in figure 6.4 with the following figure 6.5 showing the Nd/Yag laser used.

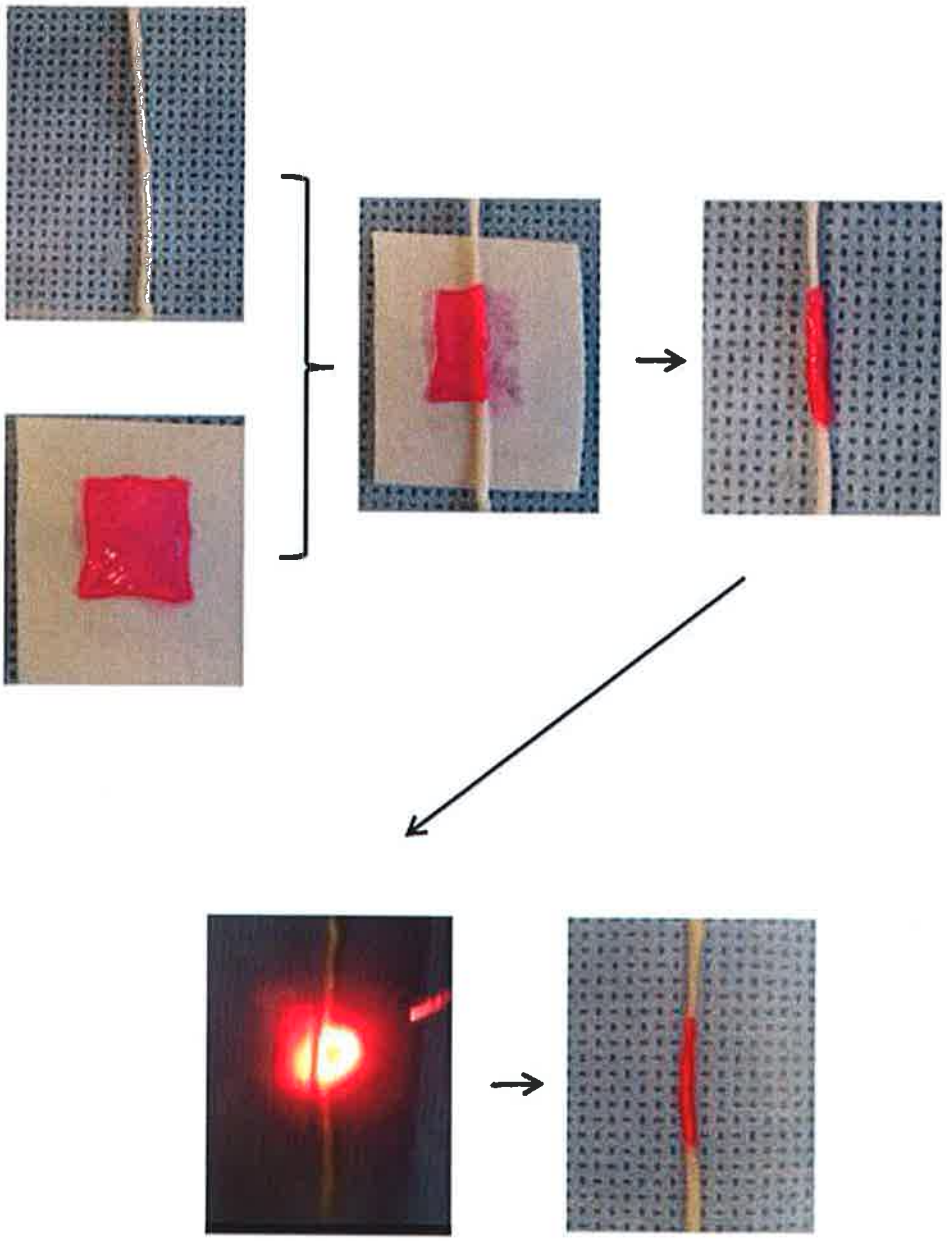

Figure 6.4 – Series depicting the placement of Rose Bengal saturated Human Amniotic Membrane around the peripheral neurorrhaphy site. This is then exposed to green laser light, via fibre optic delivery (pictured through a protective screen) and results in a photochemically bonded Amnion wrap around the repair site.

Figure 6.5 - Aura i continuous wave Nd/YAG laser, Laserscope, San Jose, CA, with fibreoptic delivery system

Following all repair procedures the wound was closed using 4/0 absorbable polyglactin sutures (Ethicon, Somerville, NJ). Postoperatively, animals were housed in the Massachusetts General Hospital animal facility and were permitted to mobilize freely with unlimited access to food and water. Experimental groups are summarized below in table 6.1.

Table 6.1 – Experimental Groups (Nerve Repair by Photochemical Tissue Bonding)

Group	Procedure	Number (n=)
1	Standard Neurorrhaphy (SN)	8
2	Standard Neurorrhaphy (SN) & HAM wrap	8
3	Standard Neurorrhaphy (SN), HAM / PTB Bonding	8

6.4. Electrophysiological Assessment

Electrophysiological measurements were performed prior to surgery, immediately post op and at 30, 60, 90 and 120 days following surgery. Measurements were taken using a Teca Synergy Multimedia EMG / EP (Oxford Instruments, Pleasantville, NY) from both experimental (right) and control (left) nerves at each time point. Nerve conduction studies were performed following anaesthesia with isoflurane (2.5 – 3.5% by mask, Baxter Healthcare Corporation, Deerfield, IL.).

Nerve Conduction Studies

Disposable self-adhesive gelled surface recording electrodes (Viasys Healthcare, Madison, WI) were placed over the tibialis anterior muscle in a belly-tendon montage. Subdermal needle electrode (0.70 x 30mm, 22G x 1 ¼ inch, Medtronic Sensory Needle Electrode, Medtronic A/S, Denmark) stimulation of the peroneal nerve was performed at the fibular head (below the site of nerve transection) and at the sciatic notch (above the site of transection). Using a stimulus duration of 0.02ms, stimulus intensity was increased gradually until a supramaximal compound muscle action potential (CMAP) was obtained. The CMAP amplitude was measured from baseline to peak and latencies were measured from stimulus to negative peak onset. The latency difference between the proximal and distal responses was divided into the distance between stimulation sites to generate a conduction velocity. Figure 6.6 shows the placement of both sensory and stimulating electrodes over the peroneal nerve distribution of the anaesthetized animal.

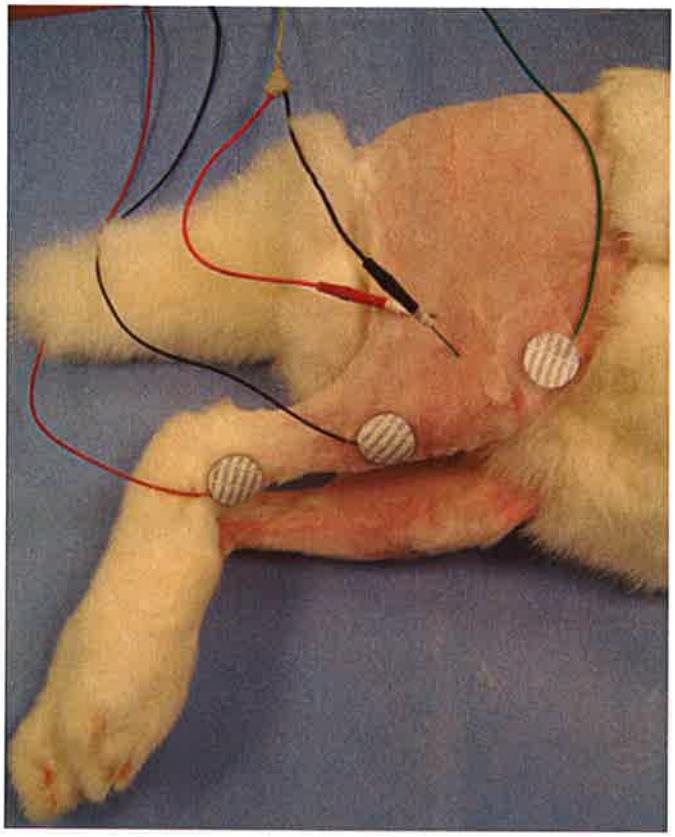

Figure 6.6 – Stimulating (subdermal) electrodes over the fibular head with recording gelled electrodes placed over the tibialis muscle complex. A third gelled electrode is also depicted (Green wire) and serves as an earthing pathway during neural stimulation.

6.5. Histology & Histomorphometry

At 120 days post surgical procedure animals were anaesthetized with isoflurane (2.5 – 3.5% by mask, Baxter Healthcare Corporation, Deerfield, IL) and following the final electrical assessment were sacrificed with an intracardiac injection of pentobarbital (Euthasol® 100-150 mg/kg, Virbac AH, Fort Worth, TX). The right

and left common peroneal nerves were harvested and fixed in a 2% / 2% glutaraldehyde / paraformaldehyde solution at 4°C for 48 hours. Specimens underwent post fixation in 1% osmium tetroxide, followed by dehydration in ethanol and embedding in epon. Cross sections (1 μm) were made 5 mm proximal and distal to the neurorrhaphy site using a microtome (Donsanto Corp, Natick, MA). All samples were stained with 0.5% (w/v) toluidine blue in preparation for light microscopy.

Histomorphometrical analysis was carried out on all nerves from each experimental group. Nerve architecture was examined at 400X magnification. Five 400X images were taken from each proximal and distal segment in the experimental nerves at sites evenly distributed within the cross section. Fifty fibres were randomly selected in each image (total of 250 fibres per nerve sample). Total fibre diameter and axon diameter were measured using Image J ™ Software (Abramoff 2004). The myelin thickness was derived from the difference between the fibre and axon diameter. In addition, the g-ratio of each fibre was calculated as a ratio of the axon diameter to the fibre diameter.

Using Microsoft Photo Editor Software ™, each 400X field was examined in detail. A manual count of endoneurial myelinated fibres was undertaken for each of the five 400X images (five above the repair site and five below the repair site). These counts were then averaged to produce a mean estimate of myelinated fibres per 400X field. To estimate the total number of fibres per nerve cross section the endoneurial area of each nerve using Metamorph Imaging Software v4.6 (Universal Imaging

Corporation™) was measured. Using this data, along with the count per 400X field, the total fibre counts were calculated.

Examination of the epineurium was also undertaken for the samples 5 mm below the repair site. Five 400X images were taken at sites evenly distributed throughout the epineurium and a manual count of nerve fibres was undertaken per 400X field. The mean count was taken per animal and using the area of the epineurium as measured using Microsoft Photo Editor Software™, an epineurial count of axon migration was achieved as described above for total fibre count estimation.

6.6. Statistical Analysis

Statistical significance was set at $p < 0.05$. Regarding histomorphometry and electrophysiological data, statistical significance was assessed per group at each time point using an unpaired student t-test. A linear regression model of overall percentage change in time (using the slope of the percent change in amplitude per 30 days as a variable) comparing each group was also analysed for the electrical data, thus allowing for an overall recovery rate to be expressed as a percentage and analysed for significance.

7. Results & Discussion - Optical Therapeutics

7.1. Photochemical Tissue Bonding - Results

7.1.1. Gross Findings & Surgical Complications

All nerves were in continuity at the time of harvest. There were no discernable differences noted between the groups regarding adhesion formation or macroscopic appearance of the nerve repair site. In the SN & HAM and SN & HAM / PTB groups, no residual evidence of the human amniotic membrane was found at 120 days post surgical procedure. Figure 7.1 shows examples of the nerve repair site following animal sacrifice and harvesting of the tissue, prior to histological processing.

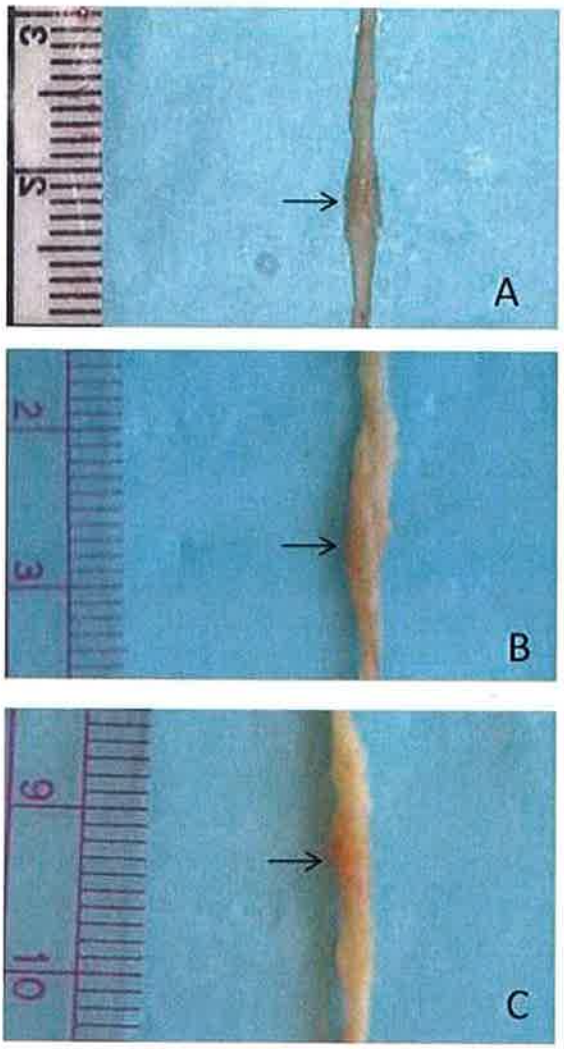

Figure 7.1 – Gross harvest samples of the Common Peroneal Nerve following sacrifice at 120 days post repair. The arrow indicated the repair site of each nerve. A – Group 1(Standard Neurorrhaphy), B – Group 2 (SN & HAM Wrap) and C – Group 3 (SN & HAM / PTB). No gross differences are evident on examination and there appears to be no evidence of residual amniotic membrane in either of Groups B or C.

There was a single mortality at day 60 post surgical procedure due to anaesthetic complications (SN & HAM group) and this animal was excluded from the data analysis. Mortality was a result of the general anaesthesia required at each timepoint (day 30, 60, 90 and 120) in order to perform nerve conduction studies. Anaesthesia with isoflurane (2.5 – 3.5% by mask, Baxter Healthcare Corporation, Deerfield, IL.) resulted in respiratory arrest during the electrical assessment of one animal at day 60 post surgical procedure. Electrical analysis of one animal in the SN & HAM / PTB group revealed a dispersed waveform following surgery and throughout the study period that resulted in an unreliable electrical endpoint. This may be explained by a chronic wound infection in the same animal requiring antibiotic administration and therefore this animal was excluded from the data analysis.

7.1.2. Electrophysiological Assessment

In order to assess technique reliability, the electrophysiological approach undertaken was verified by repeated measurements (four) at one time point on two separate specimens (one injured and one normal nerve). Both stimulating and recording electrodes were removed from the animal and replaced each time. The results of the electrophysiological assessment are shown below in Table 7.1 and serve to highlight the reliability of the electrical studies.

Table 7.1 – Repeated Electrophysiological Studies showing Latency, Amplitude and Conduction Velocity over 4 separate measurements on two distinct nerves (One Injured and One Normal). Standard Deviations remain within acceptable ranges allowing for confirmation of the reliability of the techniques used.

Test 1 (Normal Nerve)				Test 2 (Injured Nerve)			
	Latency	Amplitude	Velocity		Latency	Amplitude	Velocity
A	0.90	20.2	100.0	A	0.95	10.8	104.8
B	1.00	20.9	100.0	B	0.90	11.5	100.0
C	0.95	21.5	100.0	C	1.00	11.5	105.3
D	0.95	21.2	104.8	D	1.00	11.1	105.0
Mean	0.95	20.95	101.2		0.96	11.2	103.8
St.Dev.	0.041	0.56	2.40		0.047	0.34	2.52

Nerve Conduction Studies

No differences were noted in distal latency or conduction velocity among the groups. Regarding Amplitude, in order to avoid bias and negate inter-animal variability, results from each animal were examined individually and the change in distal amplitude (Δ) was expressed as a percentage of the total drop from the pre-op measurement to the Day 30 recording (maximal degeneration). This was calculated as follows:

$$\frac{\text{Amplitude Day X} - \text{Amplitude Day 30}}{\text{Amplitude Day 0} - \text{Amplitude Day 30}} \times 100 = \% \Delta \text{ at Day X}$$

This data is represented graphically in Figure 7.2 below. By 90 days post repair, an improvement in distal amplitude was noted in the SN & HAM / PTB group compared to the SN group (-52% ± 9.6% vs. -82.1% ± 5% respectively). This finding was statistically significant ($p<0.05$). No statistical difference was noted between the SN group and the SN & HAM group.

Furthermore, animals in the SN & HAM / PTB group showed an overall increased rate of recovery (as measured by percentage change over time with linear regression), which was 26.2% greater than that of the SN group. This difference was statistically significant ($p<0.05$). The SN & HAM group showed an overall rate of recovery that was 13.7% higher than the animals in the SN group, however this finding did not achieve statistical significance.

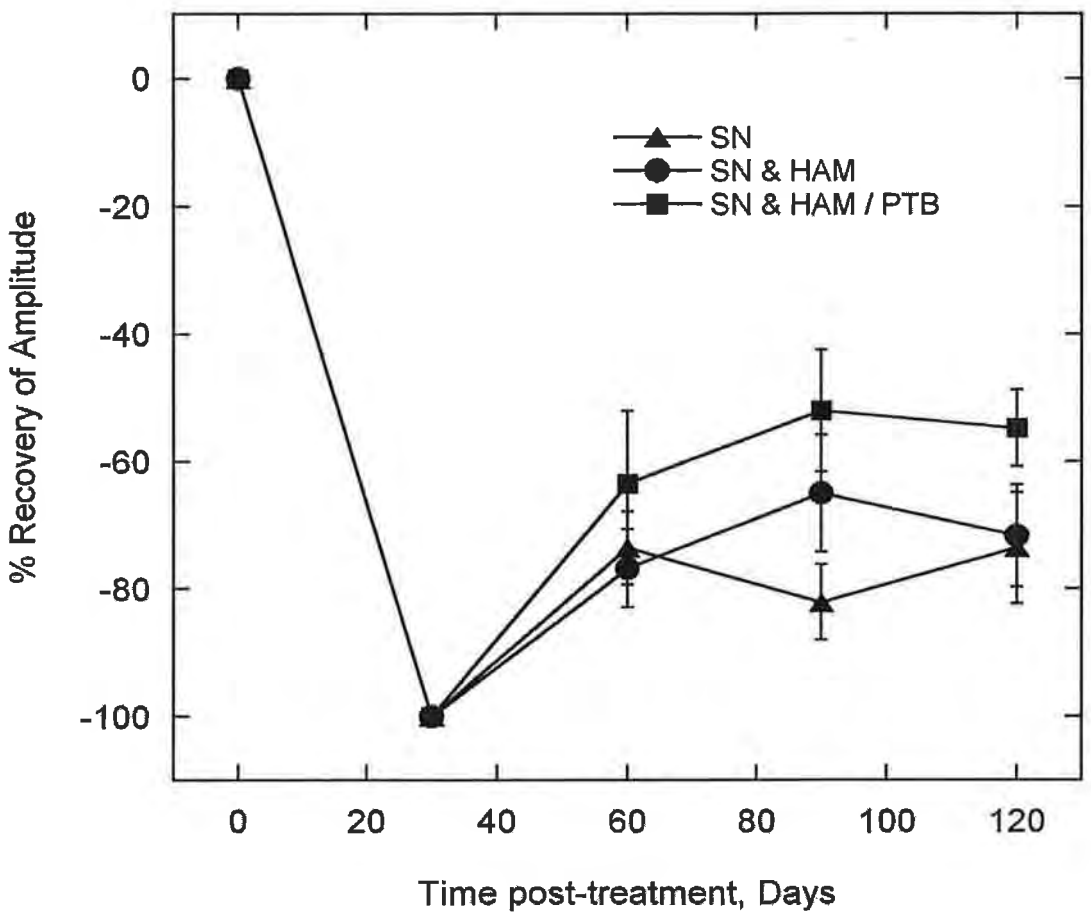

Figure 7.2 - Time course for recovery, as expressed by percentage change in distal amplitude over the total decrease in amplitude from the pre-op measurement to the Day 30 recording (maximal degeneration). Recovery over time revealed a statistically significant 26.2% improvement ($p<0.05$) in the SN & HAM / PTB Animals (■) over that of the SN & HAM wrap (●) and the SN alone groups (▲).

7.1.3. Histology and Histomorphometry

Regeneration of myelinated axons was seen in the proximal and distal segments of all experimental groups and normal neural architecture was restored. Examples of neural architecture are shown in Figure 7.3 below, both above and below the repair site for each group. The cross sections serve to demonstrate preservation of the normal architecture of the nerve following repair across all three modalities used and show little difference on macroscopic visualisation of the nerve fibres prior to detailed histomorphometry being undertaken.

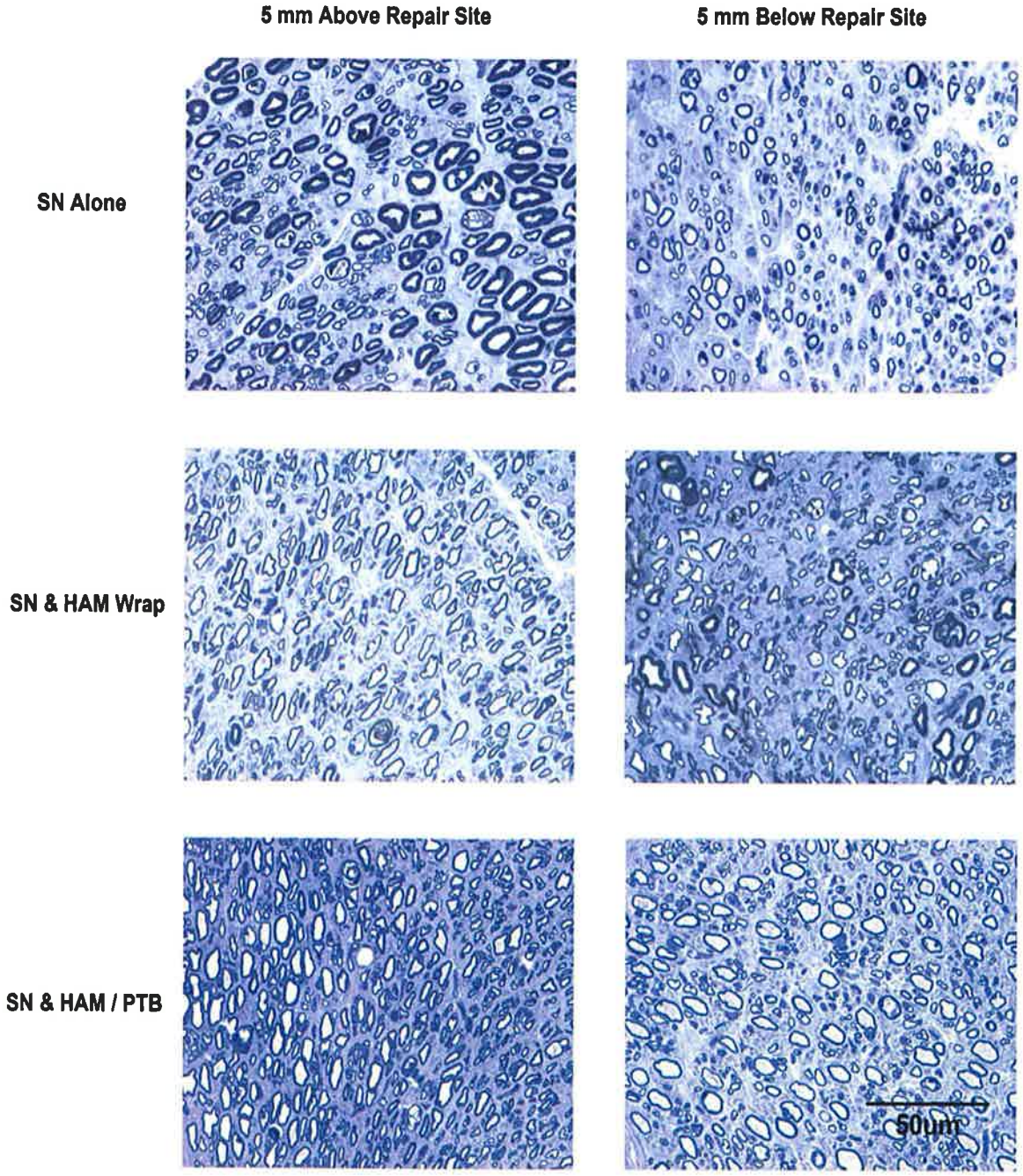

Figure 7.3 - Cross-sections 5 mm proximal and 5 mm distal to the repair site showing regeneration of myelinated axons of all experimental groups with preservation of normal neural architecture (toluidine blue 400X). The number below each panel indicates the experimental group. Scale (bottom right) indicates a 50 µm distance.

Above the repair site (5 mm) histomorphometric analysis demonstrated a statistically significant ($p<0.0001$) increase in myelin thickness in nerves treated with the SN & HAM / PTB group compared to SN alone and SN & HAM groups. G-Ratio was also significantly improved in this group ($p<0.0001$). There was no difference noted above the repair site in fibre or axon diameters. Below the repair site there was a statistically significant improvement across all four parameters in nerves treated with PTB sealed HAM wraps compared to the other groups ($p < 0.0001$ for Fibre Diameter, Myelin Thickness and G-Ratio, $p <0.05$ for Axon Diameter). Total fibre counts, while not statistically significant, showed an improved outcome in the SN & HAM / PTB group both above and below the repair site. Histomorphometric results for each experimental group ($N = 2000$) expressed in means and standard deviations are shown in Table 7.2 below.

Table 7.2 – Histomorphometric results across all parameters measures, expressed in means with standard deviations.

Group	Fibre Diameter (µm)	Axon Diameter (µm)	Myelin Thickness (µm)	G-Ratio	Total Fibre Count
5mm Above Repair site					
Group 1 (SN Alone)	8.49 (+/-2.39)	5.76 (+/-1.86)	2.73 (+/-1.02)	0.67 (+/-0.09)	3525 (+/-1311)
Group 2 (SN & Amnion Wrap)	6.85 (+/-1.6)	4.8 (+/-1.48)	2.05 (+/-0.72)	0.69 (+/-0.1)	4477 (+/-1741)
Group 3 (SN & Amnion / PTB)	8.62 (+/-1.78)	5.65 (+/-1.31)	*2.97 (+/-1.09)	*0.66 (+/-0.09)	4536 (+/-1143)
5mm Below Repair site					
Group 1 (SN Alone)	6.77 (+/-1.94)	4.98 (+/-1.81)	1.79 (+/-0.42)	0.72 (+/-0.09)	4316 (+/-1591)
Group 2 (SN & Amnion Wrap)	6.31 (+/-1.58)	4.52 (+/-1.44)	1.8 (+/-0.53)	0.7 (+/-0.087)	3560 (+/-1310)
Group 3 (SN & Amnion / PTB)	*7.47 (+/-1.37)	†5.08 (+/-1.06)	*2.39 (+/-0.7)	*0.68 (+/-0.071)	4489 (+/-1209)

*Denotes statistical significance $p < 0.0001$ compared to Standard Repair (SN) Alone

†Denotes statistical significance $p < 0.05$ compared to Standard Repair (SN) Alone

Axonal outgrowth through the epineurium was also noted as a feature associated in the SN and SN & HAM wrap groups. The SN & HAM / PTB group revealed a decrease in epineurial / extraneural axonal regeneration suggesting improved preservation of the neural microarchitecture using this repair technique. Axonal migration into and through the epineurium was also noted to be reduced in animals treated with SN & HAM / PTB when compared to that of the other groups. Figure 7.4 below is representative of 200X images of the epineurial outgrowth amongst the various groups.

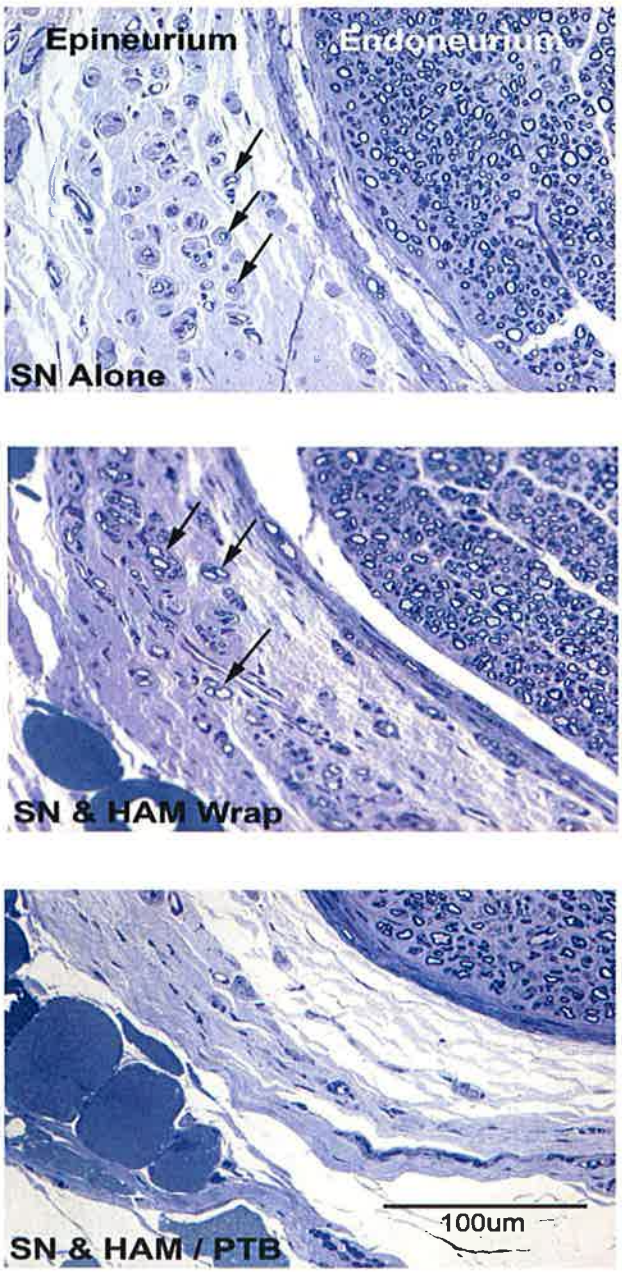

Figure 7.4 - Cross-sections 5 mm distal to the repair site showing axonal sprouting with regeneration into and through the epineurium in the SN & HAM wrap and the SN alone groups (examples highlighted by arrows). Sealing of the SN repair site with HAM / PTB was noted to reduce this phenomenon as shown above in the lower image (toluidine blue 200X).

This finding was quantified, and while not statistically significant, there was a trend toward preservation of endoneurial axonal regeneration using the SN & HAM / PTB technique when compared to the other groups, this achieved borderline statistical significance in a linear regression model with p=0.053 (Figure 7.5 below).

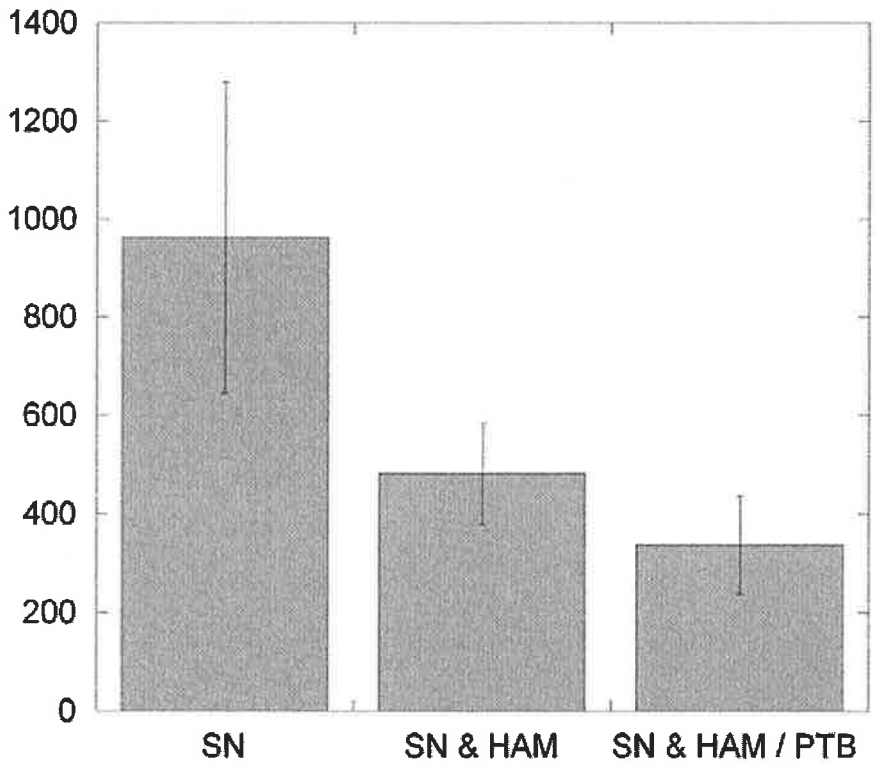

Figure 7.5 - Epineurial fibre count per group (denoting axonal migration outside the endoneurium). Data is shown in means with standard error. SN with PTB sealing of the HAM wrap (337.13 ± 98.7) clearly shows a trend towards preservation of normal axonal regeneration through the endoneurium over the SN alone and the SN & HAM wrap groups (961.9 ± 318 and 481.3 ± 103.4 respectively). In a Linear regression statistical model this data achieves borderline statistical significance with p = 0.053.

7.2. Photochemical Tissue Bonding – Discussion of Findings

This study has shown, using both neurophysiological and histological endpoints, that photochemical tissue bonding with a human amniotic membrane wrap significantly augments peripheral neurorrhaphy over that of the current gold standard. This large animal experiment highlights the reproducibility of the technique and confirms the benefits over conventional repair as seen in previous studies and discussed in Chapter 5.2.

These previous findings (Johnson, O'Neill et al. 2007; O'Neill, Bujold et al. 2008) led to this investigation in a larger animal model using neurophysiology as an endpoint. Utilising electrophysiological endpoints as a measurement of functional outcome in the current study adds valuable supportive evidence for this nerve repair technique. Standard electrophysiological amplitude measurements, as used in clinical practice, parallel the improvement in functional outcome seen in previous rodent studies (as measured by sciatic function index). The use of a larger animal also allows the technique to be evaluated in a robust nerve model over a longer regenerative distance than previously used in the sciatic nerve of the Sprague Dawley rat. Histomorphometry results also show an improvement in nerve maturity rather than simply improving regenerative capability. The use of Myelin thickness and G-Ratio denotes relative maturity of the fibres when compared to using fibre and axon diameter and fibre counts alone.

PTB creates an immediate watertight seal between tissue surfaces. In previous studies, photochemical crosslinking has been discussed in high collagen content tissues such as cornea (Proano, Azar et al. 2004; Chan, Amann et al. 2005). This methodology easy translates across to these neurorrhaphy techniques given the high collagen content of both the epineurium and amnion. Adopting PTB technology with the HAM nerve wrap has several advantages over standard repair, which may be a factor in the augmentation of both neurophysiological and histological outcomes. The presence of suture material has been associated with a foreign body reaction that further reduces functional outcome post op due to its association with endoneurial scar formation (DeLee, Smith et al. 1977). Isolation of the endoneurial environment by photochemically sealing the neurorrhaphy site may also allow for a reduction in extrinsic inflammatory infiltrate as well as maximising the potential of the intrinsic nerve growth factors. Recent advances in the field of neural regeneration have concentrated on the complex sequence of molecular and biological events which occur following neural injury (Jacobs and Fehlings 2003). The upregulation of growth factors and inflammatory mediators in both proximal and distal nerve stumps has been shown to both promote axonal regrowth and neural preservation. While exogenous factors introduced into this environment have shown some promise in the experimental stage (Newman, Verity et al. 1996; Tham, Dowsing et al. 1997; Zuo, Neubauer et al. 2002; Eguiluz-Ordonez, Sanchez et al. 2006), the hypothesis exists that the isolation of the neural microenvironment and resulting promotion of intrinsic upregulatory functions, as well as the reduction of extrinsic inflammatory infiltrate (by photochemically sealing the neurorrhaphy site) remains the key factor behind the success of this repair technique. This is supported by the performance of the SN &

HAM group, in which a sutured (unsealed) HAM wrap conferred no significant benefits above SN alone.

A further observation noted during this study involved a reduction in axonal outgrowth into the epineurium. Sealing of the peripheral neurorrhaphy site was seen to promote more efficient regeneration through the repair site rather than disorganised growth with extraneural axonal sprouting as seen in the SN and SN & HAM groups. Although not a feature or complication noted during the study, this may be relevant in the reduction of neuroma formation following peripheral nerve repair in the clinical scenario.

Ultimately, this investigation has shown that the photochemical technique along with a HAM wrap results in a strong reliable nerve repair that shows an improvement in both neurophysiological and histological outcomes over standard neurorrhaphy. This technique does not add significantly to operating time, does not require additional microsurgical training and would be implemented easily into clinical practice by microsurgeons.

8. Thesis Summary & Conclusion

8.1. Optical Microscopy

Despite years of advancement in microscopy and biomedical imaging there remains no reliable method of imaging the microenvironment of the nerve. Current technology used to assess nerve regeneration is faulted by both limitation in the early phase of injury and their non-specific nature. Furthermore, current imaging methods fail to achieve high resolution images which can be used to assess the nerve on a microscopic level. Both MRI (Bendszus and Stoll 2003; Bendszus and Stoll 2005; Bendszus, Wessig et al. 2005; Kobayashi, Meir et al. 2005; Wessig, Bendszus et al. 2007; Wessig, Jestaedt et al. 2007; West, Davies et al. 2007) and Ultrasound (Prinz, Nakamura-Pereira et al. 2003; Stuart, Koh et al. 2004) lack the resolution or specificity of optical microscopes and while providing some structural imaging they lack either the quantitative capabilities of PS-OCT or the high resolution structural imaging of CARS microscopy. Achieving neural resolution of up to 5μm and accurately assessing the internal architecture either quantitatively or structurally has obvious advantages in clinical practice in both prognostic and diagnostic evaluation. Reducing the long periods of observation currently employed following nerve injury would allow for an earlier determination for surgical intervention where necessary and ultimately an improved functional recovery. Diagnostically, the ability to accurately assess myelination in either a structural or quantitative manner would be useful following both traumatic injury (distinguishing between $2^{nd} - 4^{th}$ degree injuries) and that of chronic processes such as carpal tunnel disease and demyelinating neuropathies.

8.1.1. Coherent Anti-Stokes Raman Scattering (CARS) Microscopy

Through this investigation it is clear that CARS microscopy has the ability to image the normal peripheral nerve as well as following a demyelinating crush injury. This technology which permits *in vivo*, real time microscopy of nerves at a resolution of up to 5μm can provide invaluable diagnostic and prognostic information regarding intraneural preservation and recovery following injury. Given the relative infancy of the technology and in particular its slow evolution toward biomedical applications, there exists no precedent for its use in this manner.

The concept of using the lipid rich myelin molecule (Morell and Quarles 1999) as a medium for CARS was explored in imaging of the central nervous system in one previous study. In this study of *ex-vivo* spinal tissues Wang et al described detailed structural properties such as the node of Ranvier and were able to quantify the g-ratio of the spinal segment in question (Wang, Fu et al. 2005). Adopting this approach in the peripheral nervous system, while seemingly a logical progression, was in fact the first step into the realm of *in vivo* imaging using CARS microscopy. The ability of the CARS microscope to penetrate and image beyond the epineurium of the nerve had been previously untested and the aim to image the regenerating nerve was in order to assess the potential clinical application and benefit of CARS. In doing so, with success, many new avenues of investigations have opened which require further evaluation. The approach to the investigation as described in this thesis was that of a trial of technology on which a body of work may be based in the future. The high resolution images achieved warrant further evaluation in a subsequent study to assess direct histological correlation with the images. This was not practical in this

investigation as it would be better achieved using a large *ex vivo* trial rather than *in vivo* techniques and secondly would require a much larger number of animals. In choosing to deviate from the approach adopted by Wang et al in the central nervous system, the more valuable question of clinical relevance has been addressed.

To this end, work continues on adapting the microscope toward a more clinically applicable and mobile technology. Endoscopy remains a unachieved challenge, although much progress has been made in a recent publication by Legare et al (Legare, Evans et al. 2006). The relevance of this study lies in the description of a new potential clinical application and this trial of technology opens many avenues in which CARS microscopy may become a valuable tool in the field of neural research, regeneration and repair.

8.1.2. Polarisation Sensitive Optical Coherence Tomography

Following on from the preliminary structural analysis of the normal and regenerating peripheral nerve with CARS microscopy, the second part of this thesis discusses a more analytical approach to optical diagnostics. Utilising the unique birefringent properties of myelin, polarisation-sensitive optical coherence tomography (PS-OCT) is demonstrated as a reliable in vivo, non-destructive method of assessing of axonal myelination in a quantitative manner. Preservation of the neural microenvironment while achieving this quantitative analysis of myelin shows promise for the translation of this imaging modality across to clinical practice and indeed for further expansion in the field of experimental neuroscience.

In this study PS-OCT was found to be adept at analysing the peripheral nerve in an *in-vivo* manner as well as providing a reliable quantifiable marker of tissue birefringence. Histological correlation following optical analysis revealed a statistically significant relationship between that of the birefringence, as measured by PS-OCT and both myelin thickness and g-ratio of the nerve as measured histologically. Correlating PS-OCT technology with standard markers of axonal myelination in this manner was the first step in this investigation and resulted in a scale in graphical form in which the myelin thickness or g-ration of the nerve can be estimated in a statistically significant manner using the value obtained (Phase retardation slope) following imaging with PS-OCT. While a more established technology clinically, and with a background of successful translation across to clinical application in the field of Ophthalmology, PS-OCT has not been previously evaluated in investigating neural injury. Birefringence markers of dermal collagen following thermal injury had previously been evaluated (Pierce, Sheridan et al. 2004; Pierce, Strasswimmer et al. 2004) and had therefore established a precedent for correlation of this technology with birefringent tissues.

Using the animal model of the Sprague Dawley rat, functional analysis was achieved using the sciatic function index as described. While a useful modality in monitoring recovery of the nerve following injury it does not translate easily across to the clinical setting. While correlation of the imaging with this functional analysis did reveal a positive relationship, it did not achieve statistical significance. Further evaluation of function as an endpoint would include correlation of neurophysiological studies with PS-OCT imaging. This preliminary evaluation of PS-OCT against sciatic function index does show promise however, as a standalone

measurement neither sciatic function index or indeed standard neurophysiology are as reliable a means of assessing myelination as direct histomorphometric assessment in an animal model. Further clinical studies remain integral to establish a conclusive functional relationship that can assist in translation of this technology across to clinical practice.

These results demonstrate, by means of statistically significant direct histological correlation, the ability of PS-OCT to assess and quantify markers of axonal myelination in a non-destructive, *in vivo* manner. PS-OCT remains very promising tool in this field and provides an insight into the *in vivo* neural microenvironment previously unreported.

8.2. Optical Therapeutics – Photochemical Tissue Bonding

In this investigation photochemical tissue bonding with a human amniotic membrane wrap has been shown to significantly augment peripheral neurorrhaphy over that of the current gold standard. PTB & HAM was shown to provide a 26.2% improvement in electrical outcomes and a significant improvement across histomorphometric parameters following 5th degree injury to the peripheral nerve. This large animal investigation highlights the reproducibility of the technique and confirms the benefits over conventional repair as seen in previous studies (Johnson, O'Neill et al. 2007; O'Neill, Bujold et al. 2008). This, the third in a series of PTB neurorrhaphy investigations, has revealed PTB as a viable nerve repair technique improving functional (rodent), electrical (rabbit) and histological (rodent and rabbit) outcomes when combined with a HAM wrap.

A further observation noted during this study involved a reduction in axonal outgrowth into the epineurium. Sealing of the peripheral neurorrhaphy site was seen to promote more efficient regeneration through the repair site rather than disorganised growth with extraneural axonal sprouting as seen in the SN and SN & HAM groups. While not directly observed in any of the study groups, this observation may be relevant in the reduction of neuroma formation following peripheral nerve repair in the clinical scenario and ultimately more efficient regeneration of the axons across the neurorrhaphy site.

The use of a larger animal also allows the technique to be evaluated in a robust nerve model over a longer regenerative distance than previously used in the sciatic nerve of the Sprague Dawley rat. The histomorphometry results also show an improvement in nerve maturity rather than simply improving regenerative capability, i.e. the use of Myelin thickness and G-Ratio denotes relative maturity of the fibres when compared to using fibre and axon diameter and fibre counts alone. Utilising electrophysiological endpoints as a measurement of functional outcome in the current study adds valuable supportive evidence for this nerve repair technique. Standard electrophysiological amplitude measurements, as used in clinical practice, parallel the improvement in functional outcome seen in our previous rodent study (O'Neill, Bujold et al. 2008), however they do not provide a complete picture of functional recovery. For this a clinical trial with motor function outcomes would be necessary. The use of a non-primate model forgoes the use of a reliable and true assessment of functional motor recovery following nerve repair and this remains an avenue of investigation for the future.

HAM as a nerve wrap lends itself towards use with PTB given its thin (20 μm) translucent nature as well as its malleable handling properties. Clinically, it has been used as a wound dressing and found to increase re-epithelialisation rates and through its subsequent use in a wide range of tissue repair models its many benefits have been detailed (Gruss and Jirsch 1978; Faulk, Matthews et al. 1980; Hao, Ma et al. 2000; Koizumi, Inatomi et al. 2000; Shimmura, Shimazaki et al. 2001). These include a reduction in neutrophil, lymphocyte and macrophage infiltration as well as identification of both anti-inflammatory and anti-angiogenic proteins. The lack of expression of HLA-A,B,C or DR antigens of β_2-microglobulin result in a negligible immunologic response and further support its use as a nerve wrap combined with PTB technology (Akle, Adinolfi et al. 1981; Adinolfi 1982; Adinolfi, Akle et al. 1982). Adopting PTB technology with a HAM nerve wrap has several advantages over standard repair, which may be a factor in the augmentation of both neurophysiological and histological outcomes. The presence of suture material has been associated with a foreign body reaction that further reduces functional outcome due to its association with endoneurial scar formation (DeLee, Smith et al. 1977). Isolation of the endoneurial environment by photochemically sealing the neurorrhaphy site may also allow for a reduction in extrinsic inflammatory infiltrate as well as maximising the potential of the intrinsic nerve growth factors. While exogenous factors introduced into this environment have shown some promise in the experimental stage, we hypothesize that the isolation of the neural microenvironment and resulting promotion of intrinsic upregulatory functions, as well as the reduction of extrinsic inflammatory infiltrate (by photochemically sealing the neurorrhaphy site) remains the key factor behind the success of our repair technique. This

hypothesis is supported by the performance of our SN & HAM group, in which a sutured (unsealed) HAM wrap conferred no significant benefits above SN alone.

Ultimately, we have shown that our photochemical technique along with a HAM wrap results in a strong reliable nerve repair that shows an improvement in both neurophysiological and histological outcomes over standard neurorrhaphy. Again of note is that this technique does not add significantly to operating time, does not require additional microsurgical training and would be implemented easily into clinical practice by microsurgeons. These encouraging results warrant further investigation in a clinical trial, which is currently planned at the Massachusetts General Hospital, Boston, MA.

8.3. Conclusion

The classification of nerve injuries in use today remains that as described by Sunderland in 1951 and comprises of 5 degrees of nerve injury (Sunderland 1951). From a first-degree injury involving a temporary conduction block to a fifth-degree injury defined by complete transection of the nerve, the aim of operative diagnostics and intervention, if required, is to assess and restore neural continuity.

Despite the advances in clinical practice since 1951, Sunderland's grades remain a clinical measurement often aided by non specific diagnostic tools such as neurophysiological testing or indeed verified experimentally by destructive histological techniques. Furthermore regarding grade 5 injuries, microsurgical repair with sutures has remained the gold standard clinically despite a relatively poor outcome when the regenerative capability of the neural microenvironment is

considered. The objectives in this thesis were to apply novel optical technologies across the spectrum of nerve injuries as described above, including evaluation of two optical diagnostic microscopes as well as a light activated neurorrhaphy addressing a grade 5 injury.

The necessity for surgical intervention in peripheral nerve pathologies often depends on the severity of the injury as described above. For injured nerves in continuity that are contused, crushed, or stretched, assessment is very difficult due to the lack of a method to appraise the internal microarchitecture of the nerve. Direct clinical observation is inadequate when the nerve is not severed because it is impossible to determine the status of the axonal fibres, and electrical studies, while a useful diagnostic adjunct, cannot, in the early phase of injury distinguish between nerves with minor or severe disruption internally. A clinically useful, non-destructive method to evaluate the integrity of the nerve and the degree of myelination could provide valuable information on the extent of nerve injury and help shape treatment strategies for restoring neuromuscular function as quickly as possible.

This non destructive method would allow for an early grading of the level of injury, a more rapid and accurate determination of the prognosis, and an earlier, more informed decision about whether to continue observation or to proceed with nerve reconstruction. The latter turning a previous grade 3 or 4 injury into that of a grade 5 injury and necessitating microsurgical neurorrhaphy. Advances in this field of *in vivo* neural imaging will provide insight into the microenvironment of the regenerating nerve in a non destructive manner. Novel optical imaging modalities such as CARS Microscopy and OCT described in this thesis could easily translate across into

clinical practice and have an invaluable role in both prognostic and diagnostic assessment of neural injury.

Further studies are warranted across a variety of injury models to achieve an optical grade of injury analogous to Sunderland's classification. This first step demonstrating CARS microscopy and OCT as valuable resources in this field shows great promise for their continued use in this manner.
Indeed the future direction of these studies indicates validation of their use in a clinical trial of nerve contusion injuries such as a brachial plexus injury model. Early diagnostic evaluation, currently confined to clinical assessment, would allow for an earlier operative intervention if required in the form of nerve grafting, thus restoring neural stimulation to the muscle end organs and subsequently an improved functional outcome.

Peripheral neurorrhaphy remains the current gold standard in clinical practice whether in traumatic transection or in the event of elective nerve grafting as described above. Obvious deficiencies remain with this technique given that surgical repair of peripheral nerves does not result in complete functional recovery. While the environment of sensory and motor axons will support axonal regeneration, it is often compromised by intraneural scarring which occurs following microsurgical repair and serves as a mechanical barrier to regenerating axons. Furthermore, inflammatory cells from the surrounding tissues likely contribute to this scar formation. Improved recovery following peripheral neurorrhaphy would significantly influence the rehabilitation process, reducing the long-term care and disability associated with these injuries.

Photochemical tissue bonding (PTB) as a sutureless tissue repair process seals the repair site without trauma or foreign body reaction, thus allowing prompt restoration of the normal endoneural environment and healing. There has been ongoing interest in nerve wrapping as a means to improve outcomes following peripheral neurorrhaphy. While wrapping the nerve in a amnion sleeve has been reported as a method for reducing scar formation, it has only been evaluated in cases of severe recurrent scarring with associated nerve compression and generally used as a secondary procedure to loosely surround the site of injury without sealing. This thesis has described that sealing the amnion nerve wrap with PTB technology would isolate the endoneural environment from extrinsic inflammatory factors, and would maximize the intrinsic growth factors produced within the nerve repair site. A potential to minimize suture material should also result in a decreased foreign body reaction and subsequent scar formation.

This thesis has evaluated photochemical tissue bonding with a human amniotic membrane wrap and shown that it significantly augments peripheral neurorrhaphy over that of the current gold standard. Ultimately, this technique may be applied as a standard neurorrhaphy method and a valuable tool in the approach to grade 5 injuries. The future direction of this avenue of investigation lies in a clinical trial planned to assess its role in the management of digital nerve repair.

Management of the patient with peripheral nerve injury demands an understanding of all aspects of the disease process, from the transient conduction block to complete transection and loss of function. This understanding must be translated across from clinic to the lab and back again. While future clinical studies are required to

determine how to achieve optimal translation of these technologies the steps described in this thesis show great promise and encouragement. This integrated, optical approach to Sunderland's classification of nerve injuries will with momentum and continued work ultimately result in a progressive improvement in patient care.

Abbreviations

α	Alpha
β	Beta
Δ	Delta
μ	Micro
% (w/v)	Percentage weight per volume
3D	Three Dimensional
ATPase	Adenosine Triphosphate
ANOVA	Analysis of Variance
AIC	Akaike information criterion
BC	Before Christ
bFGF	basic Fibroblast Growth Factor
CI	Confidence Interval
CO_2	Carbon Dioxide
CARS	Coherent Anti-Stokes Raman Scattering
CMAP	Compound Muscle Action Potential
DIC	Differential Interference Contrast
DNA	Deoxyribonucleic Acid
EPL	Experimental Print Length factor
ETS	Experimental Toe Spread Factor
EMG	Electromyography
EIT	Experimental Intermediary Toe Spread Factor
FDA	Food and Drug Administration
HAM	Human Amniotic Membrane
HLA	Human Leukocyte Antigen
IRB	Institutional Review Board
IP	Intraperitoneal
ITF	Intermediary Toe Spread Factor
InGaAs	Indium Gallium Arsenide
MUP	Motor Unit Potentials
MRI	Magnetic Resonance Imaging
Nm	Nanometer

NTS	Normal Toe Spread Factor
NIT	Normal Intermediary Toe Spread Factor
NPL	Normal Print Length factor
NGF	Nerve Growth Factor
Nd/YAG laser	Neodymium-doped Yttrium Aluminium Garnet
NCAM	Neural Cell Adhesion Molecule
OCT	Optical Coherence Tomography
ODT	Optical Doppler tomography
PBS	Phosphate Buffered Saline
PHB	poly [(R)-3-hydroxybutyrate]
PLF	Print Length factor
PTB	Photochemical Tissue Bonding
PS-OCT	Polarisation-sensitive Optical Coherence Tomography
P	Probability coefficient
RNA	Ribonucleic Acid
r	Pearson correlation
RB	Rose Bengal
SN	Standard Neurorrhaphy
SC	Subcutaneous
SFI	Sciatic Function Index
SD-OCT	Spectral-domain Optical Coherence Tomography
SRAC	Subcommittee on Research Animal Care
SNAP	Sensory Nerve Action Potential
(TD) OCT	Time-domain Optical Coherence Tomography
TSF	Toe Spread Factor
TGF	Transforming Growth Factors

Figure and Table legend

sheaths are obvious in both imaging and histological preparation along with the easily identifiable node of Ranvier in the centre of the longitudinal image.

Figure 4.4 - CARS Microscopy with corresponding histology (400X, Toluidine blue) taken two weeks following crush injury of the in vivo rat sciatic nerve. Data shown from above the crush site reveals loss of structural organization of the myelin sheaths in both longitudinal and cross sectional images as well as a decrease in myelinated fibres on histological preparation. Data from below the crush site demonstrates a complete lack of myelin sheath organization in longitudinal section with cross section and histology showing minimal evidence of myelinated fibres along with an increase in debris throughout the nerve field. The cellular pattern of the longitudinal signal is likely to be representative of the Schwann cell population in the regenerating nerve.

Figure 4.5 – Reconstructed map of the Sciatic nerve 2 weeks following injury. Recombined individual images (500μm x 500μm) were processed at a depth of 100μm below the epineurial surface and scanned from above, through and below the nerve crush site. Loss of continuity of the individual myelin tubules (seen in white) is clearly evident at and below the crush site (indicated with red text) when compared to the proximal portion of the nerve.

Figure 4.6 - Three weeks following injury of the rat sciatic nerve. Structured remyelination is seen throughout the nerve sample as shown in longitudinal, cross section and histology (400X, Toluidine blue)

Figure 4.7 - Graphical representation of the mean myelin thickness, axon diameter and total fibre diameter (μm) over time (with standard deviations) demonstrating statistical significant ($p<0.01$) recovery from the two to four week time period. This time period corresponds to the time during which the

greatest change in myelination was observed through imaging with CARS microscopy. Histological parameters were measured following sacrifice - week 2 (n=8,) week 3 (n=6) and week 4 (n=4). Significance was shown comparing recovery at week 4 to week 2 values. This was achieved across all three variables.

Figure 4.8 - Sciatic Function Index (SFI) over time following crush injury. Data is expressed in means with standard deviations showing time point day 7 (n=36), Day 14 (n=28,) Day 21 (n=16) and Day 28 (n=8). The larger animal number in this PS-OCT investigation allows for a smaller standard deviation to be achieved. Recovery over 4 weeks following the injury is clearly demonstrated by the SFI returning toward a baseline normal value of 0.

Figure 4.9 - Figure 4.9a represents the backreflected intensity of light as imaged with Spectral Domain Optical Coherence Tomography of the normal rat sciatic nerve, the position of the nerve with the surrounding muscle is clearly evident. Figure 4.9b is an image of the cumulative phase retardation relative to the surface of the tissue as imaged with Polarisation Sensitive Optical Coherence Tomography. This greyscale image characterized by rapid changes from white to black gives a strong birefringence signal which can be quantified and expressed as a depth-resolved graph of phase retardation graph as shown in Figure 4.9c. The initial slope of this graph, highlighted in red (0.371°/micron) provides for a quantifiable measurement of birefringence. Figure 4.9d is an image of the corresponding histological section of the normal nerve (toluidine blue 400S).

Figure 4.10 – Complete nerve transection resulting in a loss of birefringence as noted in figure 4.10b and a change in backreflected light intensity (figure 4.10a).

This results in a decrease in slope of the phase retardation plot to 0.055°/micron shown in figure 4.10c. This can be verified with a noted lack of myelinated fibres in the histological sample (figure 4.10d).

Figure 4.11 – SD-OCT with corresponding PS-OCT image of the nerve 2 weeks following crush injury (a & b respectively). The depth-resolved cumulative phase retardation plot shown in Figure 4.11c with an initial slope of 0.088°/micron corresponds to the degeneration of the nerve and verified with the histological sample in figure 4.11d.

Figure 4.12 – A scatterplot of birefringence versus g-ratio (axon diameter / fibre diameter) for the control, transected, and injured nerves with the results of the regression fit overlaid. This clearly illustrates the modelled relationship between birefringence and g-ratio with data from days 7, 14, 21, and 28 pooled together. There was a positive correlation noted between the two variables (Pearson $r = -0.50$, $p = 0.015$, $n = 25$), in general, lower values of birefringence are predictive, with statistical significance, of a higher g-ratio. It should also be noted that derived slopes for healthy nerves were typically above 0.03-0.04°/micron, whereas those of injured nerves were below that threshold.

Figure 4.13 - Modelled relationship between PS-OCT and myelin thickness with data from days 7, 14, 21, and 28 pooled together. The correlation in the scatterplot suggests a positive relationship with birefringence but also indicates some variability in the cloud of data points (Pearson $r = 0.38$, $p = 0.05$, $n=25$). Using this graph, one can visually discern greater myelin thickness for larger values of the birefringence as evaluated at the nerve crush site.

sacrifice at 120 days post repair. The arrow indicated the repair site of each nerve. A – Group 1(Standard Neurorrhaphy), B – Group 2 (SN & HAM Wrap) and C – Group 3 (SN & HAM / PTB). No gross differences are evident on examination and there appears to be no evidence of residual amniotic membrane in either of Groups B or C.

Figure 7.2 - Time course for recovery, as expressed by percentage change in distal amplitude over the total decrease in amplitude from the pre-op measurement to the Day 30 recording (maximal degeneration). Recovery over time revealed a statistically significant 26.2% improvement ($p<0.05$) in the SN & HAM / PTB Animals (■) over that of the SN & HAM wrap (●) and the SN alone groups (▲).

Figure 7.3 - Cross-sections 5 mm proximal and 5 mm distal to the repair site showing regeneration of myelinated axons of all experimental groups with preservation of normal neural architecture (toluidine blue 400X). The number below each panel indicates the experimental group. Scale (bottom right) indicates a 50 μm distance.

Figure 7.4 - Cross-sections 5 mm distal to the repair site showing axonal sprouting with regeneration into and through the epineurium in the SN & HAM wrap and the SN alone groups (examples highlighted by arrows). Sealing of the SN repair site with HAM / PTB was noted to reduce this phenomenon as shown above in the lower image (toluidine blue 200X).

Figure 7.5 - Epineurial fibre count per group (denoting axonal migration outside the endoneurium). Data is shown in means with standard error. SN with PTB sealing of the HAM wrap (337.13 ± 98.7) clearly shows a trend towards

preservation of normal axonal regeneration through the endoneurium over the SN alone and the SN & HAM wrap groups (961.9 ± 318 and 481.3 ± 103.4 respectively). In a Linear regression statistical model this data achieves borderline statistical significance with $p = 0.053$.

References

Aberg, M., C. Ljungberg, et al. (2008). "Clinical evaluation of a resorbable wrap-around implant as an alternative to nerve repair: A prospective, assessor-blinded, randomised clinical study of sensory, motor and functional recovery after peripheral nerve repair." J Plast Reconstr Aesthet Surg.

Abramoff, M. D., Magelhaes, P.J., Ram, S.J. (2004). "Image Processing with ImageJ." Biophotonics International **11**(7): 36-42.

Adinolfi, M. (1982). "HLA typing of amniotic fluid cells." Prenat Diagn **2**(2): 147.

Adinolfi, M., C. A. Akle, et al. (1982). "Expression of HLA antigens, beta 2-microglobulin and enzymes by human amniotic epithelial cells." Nature **295**(5847): 325-7.

Aird, R. B. and H. C. Naffziger (1953). "The pathology of human striated muscle following denervation." J Neurosurg **10**(3): 216-27.

Akle, C. A., M. Adinolfi, et al. (1981). "Immunogenicity of human amniotic epithelial cells after transplantation into volunteers." Lancet **2**(8254): 1003-5.

Almquist, E. E., A. Nachemson, et al. (1984). "Evaluation of the use of the argon laser in repairing rat and primate nerves." J Hand Surg [Am] **9**(6): 792-9.

Amos, B. (2000). "Lessons from the history of light microscopy." Nat Cell Biol **2**(8): E151-2.

Andretzky, P., M. W. Lindner, et al. (1998). "Optical coherence tomography by spectral radar: dynamic range estimation and in vivo measurements of skin." Proc. SPIE **3567**: 78-87.

Archibald, S. J., C. Krarup, et al. (1991). "A collagen-based nerve guide conduit for peripheral nerve repair: an electrophysiological study of nerve regeneration in rodents and nonhuman primates." J Comp Neurol **306**(4): 685-96.

Archibald, S. J., J. Shefner, et al. (1995). "Monkey median nerve repaired by nerve graft or collagen nerve guide tube." J Neurosci **15**(5 Pt 2): 4109-23.

Artico, M., L. Cervoni, et al. (1996). "Birthday of peripheral nervous system surgery: the contribution of Gabriele Ferrara (1543-1627)." Neurosurgery **39**(2): 380-2; discussion 382-3.

Arvidsson, J., J. Ygge, et al. (1986). "Cell loss in lumbar dorsal root ganglia and transganglionic degeneration after sciatic nerve resection in the rat." Brain Res **373**(1-2): 15-21.

Badawy, S. Z., M. S. Baggish, et al. (1989). "Evaluation of tissue healing and adhesion formation after an intraabdominal amniotic membrane graft in the rat." J Reprod Med **34**(3): 198-202.

Bain, J. R., S. E. Mackinnon, et al. (1989). "Functional evaluation of complete sciatic, peroneal, and posterior tibial nerve lesions in the rat." Plast Reconstr Surg **83**(1): 129-38.

Bardell, D. "The Biologists' Forum: The invention of the microscope." BIOS **75**(2): 78-84.

Bardell, D. (1981). "Eyeglasses and the discovery of the microscope." The American Biology Teacher **43**: 157-159.

Bardell, D. (2005). "The Dawn of Microscopy." The American Biology Teacher **67**(7): 392-398.

Battiston, B., S. Geuna, et al. (2005). "Nerve repair by means of tubulization: literature review and personal clinical experience comparing biological and synthetic conduits for sensory nerve repair." Microsurgery **25**(4): 258-67.

Beggs, J. L., D. W. Fischer, et al. (1986). "Comparative study of rat sciatic nerve microepineurial anastomoses made with carbon dioxide laser and suture techniques: Part 2. A morphometric analysis of myelinated nerve fibers." Neurosurgery **18**(3): 266-9.

Begley, R., A. Harvey, et al. (1974). "Coherent anti-stokes raman scattering." Applied Physics Letters: P25.

Belen, D., A. Aciduman, et al. (2008). "History of peripheral nerve repair: may the procedure have been practiced in Hippocratic School?" Surg Neurol.

Bendszus, M. and G. Stoll (2003). "Caught in the act: in vivo mapping of macrophage infiltration in nerve injury by magnetic resonance imaging." J Neurosci **23**(34): 10892-6.

Bendszus, M. and G. Stoll (2005). "Technology insight: visualizing peripheral nerve injury using MRI." Nat Clin Pract Neurol **1**(1): 45-53.

Bendszus, M., C. Wessig, et al. (2005). "Assessment of nerve degeneration by gadofluorine M-enhanced magnetic resonance imaging." Ann Neurol **57**(3): 388-95.

Boppart, S. A., J. M. Herrmann, et al. (2002). "Real-time optical coherence tomography for minimally invasive imaging of prostate ablation." Journal of Urology **168**(1): 401-401.

Born, M., E. Wolf, et al. (1999). Principles of Optics: Electromagnetic Theory of Propagation, Interference and Diffraction of Light, Cambridge University Press.

Brandt, F. T., C. D. Albuquerque, et al. (2000). "Female urethral reconstruction with amnion grafts." Int J Surg Investig **1**(5): 409-14.

Breidenbach, W. C. and J. K. Terzis (1986). "The blood supply of vascularized nerve grafts." J Reconstr Microsurg **3**(1): 43-58.

Bridge, P. M., D. J. Ball, et al. (1994). "Nerve crush injuries--a model for axonotmesis." Exp Neurol **127**(2): 284-90.

Brushart, T. M. (1993). "Motor axons preferentially reinnervate motor pathways." J Neurosci **13**(6): 2730-8.

Brushart, T. M., E. C. Tarlov, et al. (1983). "Specificity of muscle reinnervation after epineurial and individual fascicular suture of the rat sciatic nerve." J Hand Surg [Am] **8**(3): 248-53.

Cajal, R. Y. (1928). Degeneration and Regeneration of the Nervous System. London, Oxford University Press.

Cense, B., H. C. Chen, et al. (2004). "In vivo birefringence and thickness measurements of the human retinal nerve fiber layer using polarization-sensitive optical coherence tomography." Journal of Biomedical Optics **9**(1): 121-125.

Cense, B., T. C. Chen, et al. (2002). "In vivo depth-resolved birefringence measurements of the human retinal nerve fiber layer by polarization-sensitive optical coherence tomography." Optics Letters **27**(18): 1610-1612.

Cense, B., T. C. Chen, et al. (2004). "Thickness and birefringence of healthy retinal nerve fiber layer tissue measured with polarization-sensitive optical coherence tomography." Investigative Ophthalmology & Visual Science **45**(8): 2606-2612.

Chan, B. P., C. Amann, et al. (2005). "Photochemical repair of Achilles tendon rupture in a rat model." J Surg Res **124**(2): 274-9.

Chan, B. P., T. Y. Hui, et al. (2007). "Photochemical cross-linking for collagen-based scaffolds: a study on optical properties, mechanical properties, stability, and hematocompatibility." Tissue Eng **13**(1): 73-85.

Chan, B. P., I. E. Kochevar, et al. (2002). "Enhancement of porcine skin graft adherence using a light-activated process." J Surg Res **108**(1): 77-84.

Chan, B. P. and K. F. So (2005). "Photochemical crosslinking improves the physicochemical properties of collagen scaffolds." J Biomed Mater Res A **75**(3): 689-701.

Chang, T. S., P. C. Leung, et al. (1986). Principles, Techniques and Applications in Microsurgery: Proceedings, World Scientific.

Chatterjee, S. and A. Hadi (2006). Regression analysis by example. New York, John Wiley & Sons.

Chen, Z. P., T. E. Milner, et al. (1997). "Optical Doppler tomographic imaging of fluid flow velocity in highly scattering media." Optics Letters **22**(1): 64-66.

Chen, Z. P., T. E. Milner, et al. (1997). "Noninvasive imaging of in vivo blood flow velocity using optical Doppler tomography." Optics Letters **22**(14): 1119-1121.

Cheng, J., A. Volkmer, et al. (2002). "Theoretical and experimental characterization of coherent anti-stokes Raman scattering microscopy." JOSA B **19**(6): 1363-1375.

Cheng, J. X., Y. K. Jia, et al. (2002). "Laser-scanning coherent anti-Stokes Raman scattering microscopy and applications to cell biology." Biophys J **83**(1): 502-9.

Chiu, D. T., R. E. Lovelace, et al. (1988). "Comparative electrophysiologic evaluation of nerve grafts and autogenous vein grafts as nerve conduits: an experimental study." J Reconstr Microsurg **4**(4): 303-9, 311-2.

Choma, M. A., M. V. Sarunic, et al. (2003). Sensitivity advantage of swept source and Fourier domain optical coherence tomography. Optics Express. **11:** 2183-2189.

Chou, K. H., N. G. Papadimitriou, et al. (2003). "Neovascularization and other histopathologic findings in an autogenous saphenous vein wrap used for recalcitrant carpal tunnel syndrome: a case report." J Hand Surg [Am] **28**(2): 262-6.

Chu, C. R., D. Lin, et al. (2004). "Arthroscopic microscopy of articular cartilage using optical coherence tomography." Am. J. Sports Med. **32**: 699-709.

Chunzheng, G., M. Shengzhong, et al. (2008). "Siatic nerve regeneration in rats stimulated by fibrin glue containing nerve growth factor: An experimental study." Injury.

Da-Silva, C. F., G. M. Lima, et al. (1990). "Local administration of interleukin-1 increases sensory neuron regeneration in vivo." Braz J Med Biol Res **23**(10): 981-4.

Darden, L. (1978). "Discoveries and the Emergence of New Fields in Science." PSA: Proceedings of the Biennial Meeting of the Philosophy of Science Association: 149-160.

Davis, G. E., S. N. Blaker, et al. (1987). "Human amnion membrane serves as a substratum for growing axons in vitro and in vivo." Science **236**(4805): 1106-9.

Davis, J. W. (1910). "Skin transplantation with a review of 550 cases at The Johns Hopkins Hospital." Johns Hopkins Med. J. **15**(307).

de Boer, J. F., B. Cense, et al. (2003). "Improved signal-to-noise ratio in spectral-domain compared with time-domain optical coherence tomography." Optics Letters **28**(21): 2067-2069.

de Boer, J. F., B. Cense, et al. (2003). "Improved signal-to-noise ratio in spectral-domain compared with time-domain optical coherence tomography." Opt Lett **28**(21): 2067-9.

de Boer, J. F., T. E. Milner, et al. (1999). "Determination of the depth-resolved Stokes parameters of light backscattered from turbid media by use of polarization-sensitive optical coherence tomography." Optics Letters **24**(5): 300-302.

de Boer, J. F., S. M. Srinivas, et al. (1998). "Imaging thermally damaged tissue by polarization sensitive optical coherence tomography." Opt. Express **3**: 212-8.

de Boer, J. F., S. M. Srinivas, et al. (1998). "Imaging thermally damaged tissue by polarization sensitive optical coherence tomography." Optics Express **3**(6): 212-218.

de Rotth, A. (1940). "Plastic repair of conjunctival defects with fetal membranes." Arch Ophthalmol **23**: 522-525.

deBoer, J. F., T. E. Milner, et al. (1997). "Two-dimensional birefringence imaging in biological tissue by polarization-sensitive optical coherence tomography." Optics Letters **22**(12): 934-936.

DeCoste, S. D., W. Farinelli, et al. (1992). "Dye-enhanced laser welding for skin closure." Lasers Surg Med **12**(1): 25-32.

Del Pinal, F. and G. I. Taylor (1990). "The venous drainage of nerves; anatomical study and clinical implications." Br J Plast Surg **43**(5): 511-20.

DeLee, J. C., M. T. Smith, et al. (1977). "The reaction of nerve tissue to various suture materials: a study in rabbits." J Hand Surg [Am] **2**(1): 38-43.

Doolabh, V. B., M. C. Hertl, et al. (1996). "The role of conduits in nerve repair: a review." Rev Neurosci **7**(1): 47-84.

Dort, J. C., M. Wolfensberger, et al. (1994). "CO2 laser repair of the facial nerve: an experimental study in the rat." J Laryngol Otol **108**(6): 466-9.

Dover, K. (1989). Aristophanes Clouds, Oxford.

Drexler, W., D. Stamper, et al. (2001). "Correlation of collagen organization with polarization sensitive imaging of in vitro cartilage: Implications for osteoarthritis." Journal of Rheumatology **28**(6): 1311-1318.

Droz, B. and C. P. Leblond (1963). "Axonal Migration of Proteins in the Central Nervous System and Peripheral Nerves as Shown by Radioautography." J Comp Neurol **121**: 325-46.

Droz, B., A. Rambourg, et al. (1975). "The smooth endoplasmic reticulum: structure and role in the renewal of axonal membrane and synaptic vesicles by fast axonal transport." Brain Res **93**(1): 1-13.

Ducker, T. B., L. G. Kempe, et al. (1969). "The metabolic background for peripheral nerve surgery." J Neurosurg **30**(3): 270-80.

Ducros, M. G., J. F. de Boer, et al. (1999). "Polarization sensitive optical coherence tomography of the rabbit eye." Ieee Journal of Selected Topics in Quantum Electronics **5**(4): 1159-1167.

Ducros, M. G., J. D. Marsack, et al. (2001). "Primate retina imaging with polarization-sensitive optical coherence tomography." Journal of the Optical Society of America a-Optics Image Science and Vision **18**(12): 2945-2956.

Duncan, M., R. J, et al. (1982). "Scanning coherent anti-Stokes Raman microscope." Optics Letters **7**(8): 350-352.

Egloff, D. V. and A. Narakas (1983). "Nerve anastomoses with human fibrin. Preliminary clinical report (56 cases)." Ann Chir Main **2**(2): 101-15.

Eguiluz-Ordonez, R., C. E. Sanchez, et al. (2006). "Effects of hyperbaric oxygen on peripheral nerves." Plast Reconstr Surg **118**(2): 350-7; discussion 358-9.

English, A. W. (2005). "Enhancing axon regeneration in peripheral nerves also increases functionally inappropriate reinnervation of targets." J Comp Neurol **490**(4): 427-41.

English, B. P., W. Min, et al. (2006). "Ever-fluctuating single enzyme molecules: Michaelis-Menten equation revisited." Nat Chem Biol **2**(2): 87-94.

Erdener, A., I. Ulman, et al. (1992). "Amniotic membrane wrapping: an alternative method to the splenorrhaphy in the injured spleen." Eur J Pediatr Surg **2**(1): 26-8.

Evans, C., X. Xu, et al. (2007). "Chemically-selective imaging of brain structures with CARS microscopy." Optics Express **15**(19): 12076.

Evans, C. L., E. O. Potma, et al. (2005). "Chemical imaging of tissue in vivo with video-rate coherent anti-Stokes Raman scattering microscopy." Proc Natl Acad Sci U S A **102**(46): 16807-12.

Evans, G. R. (2001). "Peripheral nerve injury: a review and approach to tissue engineered constructs." Anat Rec **263**(4): 396-404.

Eyler, W. R., B. M. Schuman, et al. (1965). "Rose bengal I-131 liver scan. An aid in the differential diagnosis of jaundice." Jama **194**(9): 990-2.

Faldini, A., P. Puntoni, et al. (1984). "Comparative neurophysiological assessments of nerve sutures performed by microsurgical methods and with fibrin glue: experimental study." Ital J Orthop Traumatol **10**(4): 527-32.

Faulk, W. P., R. Matthews, et al. (1980). "Human amnion as an adjunct in wound healing." Lancet **1**(8179): 1156-8.

Feenstra, R. P. and S. C. Tseng (1992). "What is actually stained by rose bengal?" Arch Ophthalmol **110**(7): 984-93.

Fercher, A. F., C. K. Hitzenberger, et al. (1995). "Measurement of Intraocular Distances by Backscattering Spectral Interferometry." Optics Communications **117**(1-2): 43-48.

Fischer, D. W., J. L. Beggs, et al. (1985). "Comparative study of microepineurial anastomoses with the use of CO2 laser and suture techniques in rat sciatic nerves: Part 1. Surgical technique, nerve action potentials, and morphological studies." Neurosurgery **17**(2): 300-8.

Fishman, I. J., F. N. Flores, et al. (1987). "Use of fresh placental membranes for bladder reconstruction." J Urol **138**(5): 1291-4.

Fried, N. M., S. Rais-Bahrami, et al. (2007). "Imaging the cavernous nerves in the rat prostate using optical coherence tomography." Lasers Surg Med **39**(1): 36-41.

Fu, S. Y. and T. Gordon (1997). "The cellular and molecular basis of peripheral nerve regeneration." Mol Neurobiol **14**(1-2): 67-116.

Fujimoto, E., A. Mizoguchi, et al. (1997). "Basic fibroblast growth factor promotes extension of regenerating axons of peripheral nerve. In vivo experiments using a Schwann cell basal lamina tube model." J Neurocytol **26**(8): 511-28.

Fujimoto, J. G. (2003). "Optical coherence tomography for ultrahigh resolution in vivo imaging." Nat Biotechnol **21**(11): 1361-7.

Galen. "Woodcut illustration from a Venetian edition of Galen's works, 1550." from http://www.hsl.virginia.edu/historical/artifacts/antiqua/galen.cfm.

Gayen, T. K., A. Katz, et al. (2003). "Aorta and skin tissues welded by near-infrared Cr4+:YAG laser." J Clin Laser Med Surg **21**(5): 259-69.

Ghanbari, Z., M. Dahaghin, et al. (2006). "Long-term outcomes of vaginal reconstruction with and without amnion grafts." Int J Gynaecol Obstet **92**(2): 163-4.

Gibble, J. W. and P. M. Ness (1990). "Fibrin glue: the perfect operative sealant?" Transfusion **30**(8): 741-7.

Glasby, M. A., S. Gschmeissner, et al. (1986). "Regeneration of the sciatic nerve in rats. The effect of muscle basement membrane." J Bone Joint Surg Br **68**(5): 829-33.

Glasby, M. A., S. E. Gschmeissner, et al. (1986). "Degenerated muscle grafts used for peripheral nerve repair in primates." J Hand Surg [Br] **11**(3): 347-51.

Glasby, M. A., S. G. Gschmeissner, et al. (1986). "The dependence of nerve regeneration through muscle grafts in the rat on the availability and orientation of basement membrane." J Neurocytol **15**(4): 497-510.

Gluck, T. (1880). "Uber Neuroplastic auf dem Wege der Transplantation." Arch Klin Chir **25**: 606.

Gorio, A., M. G. Nunzi, et al. (1982). "Synapse reformation and repression in muscle reinnervation: an evaluation of endogenous and exogenous influences on nerve regeneration." Prog Clin Biol Res **91**: 299-309.

Gottschal, J., W. Harder, et al. (1991). "Principles of enrichment, isolation, cultivation, and

preservation of bacteria." The Prokaryotes: 149-196.

Gotzinger, E., M. Pircher, et al. (2005). "High speed spectral domain polarization sensitive optical coherence tomography of the human retina." Optics Express **13**(25): 10217-10229.

Grabb, W. C., S. L. Bement, et al. (1970). "Comparison of methods of peripheral nerve suturing in monkeys." Plast Reconstr Surg **46**(1): 31-8.

Gray, L. D. (2008). from http://www.asm.org/Division/c/photo/1membra.jpg.

Gruss, J. S. and D. W. Jirsch (1978). "Human amniotic membrane: a versatile wound dressing." Can Med Assoc J **118**(10): 1237-46.

Gurunluoglu, R. and A. Gurunluoglu (2001). "Paulus Aegineta, a seventh century encyclopedist and surgeon: his role in the history of plastic surgery." Plast Reconstr Surg **108**(7): 2072-9.

Gurunluoglu, R. and A. Gurunluoglu (2003). "Paul of Aegina: landmark in surgical progress." World J Surg **27**(1): 18-25.

Guttman, L. (1943). "Experimental study on nerve suture with various suture materials." Br. J. Surg **30**: 370.

Hall, S. (1997). "Axonal regeneration through acellular muscle grafts." J Anat **190 (Pt 1)**: 57-71.

Han, C. W., C. R. Chu, et al. (2003). "Analysis of rabbit articular cartilage repair after chondroctye implantation using optical coherence tomography." Osteoarthritis Cartilage **11**: 111-21.

Hao, Y., D. H. Ma, et al. (2000). "Identification of antiangiogenic and antiinflammatory proteins in human amniotic membrane." Cornea **19**(3): 348-52.

Hausler, G. and M. W. Lindner (1998). ""Coherence Radar" and "Spectral Radar" - New Tools for Dermatological Diagnosis." Journal of Biomedical Optics **3**(1): 21-31.

Hee, M. R., D. Huang, et al. (1992). "Polarization-Sensitive Low-Coherence Reflectometer for Birefringence Characterization and Ranging." Journal of the Optical Society of America B-Optical Physics **9**(6): 903-908.

Herrmann, J. B., R. J. Kelly, et al. (1970). "Polyglycolic acid sutures. Laboratory and clinical evaluation of a new absorbable suture material." Arch Surg **100**(4): 486-90.

Herrmann, J. M., C. Pitris, et al. (1999). "High resolution imaging of normal and osteoarthritic cartilage with optical coherence tomography." Journal of Rheumatology **26**(3): 627-635.

Highmore, N. (1965). The History of Generation, J. Martin. London.

Hitzenberger, C. K., E. Gotzinger, et al. (2001). "Measurement and imaging of birefringence and optic axis orientation by phase resolved polarization sensitive optical coherence tomography." Optics Express **9**(13): 780-790.

Hooke, R. (1665). Micrographia: Or some physiological descriptions of minute bodies made by magnifying glasses with observations and inquiries thereupon, Royal Society, London.

Huang, D., E. A. Swanson, et al. (1991). "Optical Coherence Tomography." Science **254**(5035): 1178-1181.

Huang, T. C., R. H. Blanks, et al. (1992). "Laser vs. suture nerve anastomosis." Otolaryngol Head Neck Surg **107**(1): 14-20.

Hunter, M., Callahan (2002). Rehabilitation of the Hand and Upper Extremity, Elsevier Health Sciences.

Izatt, J. A., M. D. Kulkami, et al. (1997). "In vivo bidirectional color Doppler flow imaging of picoliter blood volumes using optical coherence tomograghy." Optics Letters **22**(18): 1439-1441.

Jacobs, W. B. and M. G. Fehlings (2003). "The molecular basis of neural regeneration." Neurosurgery **53**(4): 943-48; discussion 948-50.

Jain, K. K. and W. Gorisch (1979). "Microvascular repair with neodymium-YAG laser." Acta Neurochir Suppl (Wien) **28**(1): 260-2.

Jain, K. K. and W. Gorisch (1979). "Repair of small blood vessels with the neodymium-YAG laser: a preliminary report." Surgery **85**(6): 684-8.

Jeans, L., D. Healy, et al. (2007). "An evaluation using techniques to assess muscle and nerve regeneration of a flexible glass wrap in the repair of peripheral nerves." Acta Neurochir Suppl **100**: 25-8.

Jeans, L. A., T. Gilchrist, et al. (2007). "Peripheral nerve repair by means of a flexible biodegradable glass fibre wrap: a comparison with microsurgical epineurial repair." J Plast Reconstr Aesthet Surg **60**(12): 1302-8.

Johnson, T. S., A. C. O'Neill, et al. (2007). "Photochemical tissue bonding: a promising technique for peripheral nerve repair." J Surg Res **143**(2): 224-9.

Jubran, M. and J. Widenfalk (2003). "Repair of peripheral nerve transections with fibrin sealant containing neurotrophic factors." Exp Neurol **181**(2): 204-12.

Kamegaya, Y., W. A. Farinelli, et al. (2005). "Evaluation of photochemical tissue bonding for closure of skin incisions and excisions." Lasers Surg Med **37**(4): 264-70.

Kanje, M., A. Skottner, et al. (1989). "Insulin-like growth factor I (IGF-I) stimulates regeneration of the rat sciatic nerve." Brain Res **486**(2): 396-8.

Kennedy, R. (1898). "Nerve degeneration and regeneration." Phil Soc Glasgow **29**: 193-229.

Key, A. and G. Retzius (1876). Studien in der Anatomie des Nervensystems und des Bindegewebes. Stockholm, Samson & Wallin.

Kiefer, R., D. Lindholm, et al. (1993). "Interleukin-6 and transforming growth factor-beta 1 mRNAs are induced in rat facial nucleus following motoneuron axotomy." Eur J Neurosci **5**(7): 775-81.

Kobayashi, S., A. Meir, et al. (2005). "Imaging of intraneural edema by using gadolinium-enhanced MR imaging: experimental compression injury." AJNR Am J Neuroradiol **26**(4): 973-80.

Koizumi, N. J., T. J. Inatomi, et al. (2000). "Growth factor mRNA and protein in preserved human amniotic membrane." Curr Eye Res **20**(3): 173-7.

Korff, M., S. W. Bent, et al. (1992). "An investigation of the potential for laser nerve welding." Otolaryngol Head Neck Surg **106**(4): 345-50.

Kreutzberg, G. W. (1995). Reaction of the neuronal cell body to axon damage. New York, Oxford University Press.

Krishnamurti, A., R. Kanagasuntheram, et al. (1973). "Failure of reinnervation of Pacinian corpuscle after nerve crush. An electron microscopic study." Acta Neuropathol **23**(4): 338-41.

Kubo, M., Y. Sonoda, et al. (2001). "Immunogenicity of human amniotic membrane in experimental xenotransplantation." Invest Ophthalmol Vis Sci **42**(7): 1539-46.

Kuwahara, T., J. Strasswimmer, et al. (2005). "Noninvasive measurements of the photodamaged human skin in vivo by polarization-sensitive optical coherence tomography." Journal of the American Academy of Dermatology **52**(3): P163-P163.

Lambert, C. R., H. Stiel, et al. (1996). "Intensity-dependent enzyme photosensitization using 532 nm nanosecond laser pulses." Photochem Photobiol **63**(2): 154-60.

Landegren, T., M. Risling, et al. (2006). "Long-term results of peripheral nerve repair: a comparison of nerve anastomosis with ethyl-cyanoacrylate and epineural sutures." Scand J Plast Reconstr Surg Hand Surg **40**(2): 65-72.

Langley, J. N. and M. Hashimoto (1917). " On the suture of separate nerve bundles in a nerve trunk and on internal nerve plexuses." Physiol (London) **51**: 318-346.

Larson, D. L., A. E. Rodin, et al. (1966). "Perineural lymphatics: myth or fact." Am J Surg **112**(4): 488-92.

Lasek, J. R., M. L. Shelanski, et al. (1981). "Cytoskeletons and the architecture of nervous systems." Neuroscience Res Program Bull **19**: 1 - 153.

Lauto, A., J. M. Dawes, et al. (1998). "Laser nerve repair by solid protein band technique. I: identification of optimal laser dose, power, and solder surface area." Microsurgery **18**(1): 55-9.

Lauto, A., J. M. Dawes, et al. (1998). "Laser nerve repair by solid protein band technique. II: assessment of long-term nerve regeneration." Microsurgery **18**(1): 60-4.

Lauto, A., L. J. Foster, et al. (2008). "Sutureless nerve repair with laser-activated chitosan adhesive: a pilot in vivo study." Photomed Laser Surg **26**(3): 227-34.

Lee, M., V. B. Doolabh, et al. (2000). "FK506 promotes functional recovery in crushed rat sciatic nerve." Muscle Nerve **23**(4): 633-40.

Legare, F., C. Evans, et al. (2006). "Towards CARS Endoscopy." Optics Express **14**(10): 4427.

Leitgeb, R., C. K. Hitzenberger, et al. (2003). Performance of fourier domain vs. time domain optical coherence tomography. Optics Express. **11:** 889-894.

Leitgeb, R., L. Schmetter, et al. (2003). "Real-time assessment of retinal blood flow with ultrafast acquisition by color Doppler Fourier domain optical coherence tomography." Optics Express **11**(23): 3116-3121.

Levinthal, R., W. J. Brown, et al. (1977). "Comparison of fascicular, interfascicular and epineural suture techniques in the repair of simple nerve lacerations." J Neurosurg **47**(5): 744-50.

Li, X. D., S. Martin, et al. (2005). "High-resolution optical coherence tomographic imaging of osteoarthritic cartilage during open knee surgery." Arthritis Research & Therapy **7**(2): R318-R323.

Liang, J. and D. R. Williams (1997). "Aberrations and retinal image quality of the normal human eye." J Opt Soc Am A Opt Image Sci Vis **14**(11): 2873-83.

Lilius, P. (1987). "Fibrin adhesive: its use in selected skin grafting. Practical note." Scand J Plast Reconstr Surg Hand Surg **21**(3): 245-8.

Little, K. M., A. R. Zomorodi, et al. (2004). "An eclectic history of peripheral nerve surgery." Neurosurg Clin N Am **15**(2): 109-23.

Lubinska, L. and S. Niemierko (1971). "Velocity and intensity of bidirectional migration of acetylcholinesterase in transected nerves." Brain Res **27**(2): 329-42.

Lundborg, G. (1979). "The intrinsic vascularization of human peripheral nerves: structural and functional aspects." J Hand Surg [Am] **4**(1): 34-41.

Lundborg, G. (2000). "A 25-year perspective of peripheral nerve surgery: evolving neuroscientific concepts and clinical significance." J Hand Surg [Am] **25**(3): 391-414.

Lundborg, G., L. B. Dahlin, et al. (1991). "Ulnar nerve repair by the silicone chamber technique. Case report." Scand J Plast Reconstr Surg Hand Surg **25**(1): 79-82.

Lundborg, G., L. B. Dahlin, et al. (1986). "Tissue specificity in nerve regeneration." Scand J Plast Reconstr Surg **20**(3): 279-83.

Lundborg, G., B. Rosen, et al. (1997). "Tubular versus conventional repair of median and ulnar nerves in the human forearm: early results from a prospective, randomized, clinical study." J Hand Surg [Am] **22**(1): 99-106.

Lutz, B. S. and D. Lidman (2005). "Morphological and functional evaluation of leg-muscle reinnervation after coupler coaptation of the divided rat sciatic nerve." Microsurgery **25**(3): 235-40.

Mackel, R., E. Kunesch, et al. (1983). "Reinnervation of mechanoreceptors in the human glabrous skin following peripheral nerve repair." Brain Res **268**(1): 49-65.

Mackinnon, S. E. (1989). Current Therapy in Plastic Surgery. Philadelphia, BC Decker.

Mackinnon, S. E. (1989). "New directions in peripheral nerve surgery." Ann Plast Surg **22**(3): 257-73.

Mackinnon, S. E. (1996). "Nerve allotransplantation following severe tibial nerve injury. Case report." J Neurosurg **84**(4): 671-6.

Mackinnon, S. E. and S. H. Colbert (2008). "Nerve transfers in the hand and upper extremity surgery." Tech Hand Up Extrem Surg **12**(1): 20-33.

Mackinnon, S. E. and A. L. Dellon (1988). Surgery of the Peripheral Nerve. New York, Thieme.

Mackinnon, S. E., A. L. Dellon, et al. (1986). "A study of neurotrophism in a primate model." J Hand Surg [Am] **11**(6): 888-94.

Mackinnon, S. E., A. L. Dellon, et al. (1991). "Changes in nerve fiber numbers distal to a nerve repair in the rat sciatic nerve model." Muscle Nerve **14**(11): 1116-22.

Mackinnon, S. E. and C. B. Novak (1999). "Nerve transfers. New options for reconstruction following nerve injury." Hand Clin **15**(4): 643-66, ix.

MacKinnon, S. E. and C. B. Novak (2005). Compression Neuropathies. Philadelphia, Churchill Livingston.

Maker, P. and R. Terhune (1965). "Study of optical effects due to induced polarization third order in the electric field strenght." Physical Review **137**(A801).

McCarthy, P. M., V. F. Trastek, et al. (1987). "Esophagogastric anastomoses: the value of fibrin glue in preventing leakage." J Thorac Cardiovasc Surg **93**(2): 234-9.

Merle, M., A. L. Dellon, et al. (1989). "Complications from silicon-polymer intubulation of nerves." Microsurgery **10**(2): 130-3.

Millesi, H. (1979). "Microsurgery of peripheral nerves." World J Surg **3**(1): 67-79, 128-9.

Millesi, H., G. Meissl, et al. (1972). "The interfascicular nerve-grafting of the median and ulnar nerves." J Bone Joint Surg Am **54**(4): 727-50.

Mitsui, T. (1999). "Dynamic range of optical reflectometry with spectral interferometry." Japanese Journal of Applied Physics Part 1-Regular Papers Short Notes & Review Papers **38**(10): 6133-6137.

Mligiliche, N., K. Endo, et al. (2002). "Extracellular matrix of human amnion manufactured into tubes as conduits for peripheral nerve regeneration." J Biomed Mater Res **63**(5): 591-600.

Mohammad, J. A., P. H. Warnke, et al. (2000). "Increased axonal regeneration through a biodegradable amnionic tube nerve conduit: effect of local delivery and incorporation of nerve growth factor/hyaluronic acid media." Ann Plast Surg **44**(1): 59-64.

Morell, P. and R. Quarles (1999). Cellular Neurochemistry and Neuromembranes. Basic Neurochemistry; Molecular, Cellular and Medical Aspects, Lippincott, Williams & Wilkins.

Mukherjee, S. R. and D. M. Douglas (1951). "An investigation into the value of nylon and terylene as nerve sutures." Br J Surg **39**(155): 271-7.

Murphy, P. G., J. Grondin, et al. (1995). "Induction of interleukin-6 in axotomized sensory neurons." J Neurosci **15**(7 Pt 2): 5130-8.

Nan, X., J. X. Cheng, et al. (2003). "Vibrational imaging of lipid droplets in live fibroblast cells with coherent anti-Stokes Raman scattering microscopy." J Lipid Res **44**(11): 2202-8.

Nan, X., E. O. Potma, et al. (2006). "Nonperturbative chemical imaging of organelle transport in living cells with coherent anti-stokes Raman scattering microscopy." Biophys J **91**(2): 728-35.

Naoun, O. K., V. L. Dorr, et al. (2005). "Exploration of the retinal nerve fiber layer thickness by measurement of the linear dichroism." Applied Optics **44**(33): 7074-7082.

Narakas, A. (1988). "The use of fibrin glue in repair of peripheral nerves." Orthop Clin North Am **19**(1): 187-99.

Neblett, C. R., J. R. Morris, et al. (1986). "Laser-assisted microsurgical anastomosis." Neurosurgery **19**(6): 914-34.

Nelson, J. S., K. M. Kelly, et al. (2001). "Imaging Blood Flow in Human Port-wine Stain In Situ and in Real Time Using Optical Doppler Tomography." Archives of Dermatology **137**: 741-744.

Nethradhama. (2008). from http://www.nethradhama.org/amniotic_membrane_transplantation.html.

Neurogen. (2008). from http://www.integra-ls.com/products/?product=198.

Newman, J. P., A. N. Verity, et al. (1996). "Ciliary neurotrophic factors enhances peripheral nerve regeneration." Arch Otolaryngol Head Neck Surg **122**(4): 399-403.

Nicholson, O. R. and H. J. Seddon (1957). "Nerve repair in civil practice; results of treatment of median and ulnar nerve lesions." Br Med J **2**(5053): 1065-71.

Nissl, F. (1892). "Über die Veränderungen der Ganglienzellen am Faciali Kern des Kanichens nach Ausreissung der Nerven." Allg Psychiatric **48**: 197-198.

Nobe, J. R., B. T. Moura, et al. (1990). "Results of penetrating keratoplasty for the treatment of corneal perforations." Arch Ophthalmol **108**(7): 939-41.

Nordyke, R. A. (1965). "Surgical vs nonsurgical jaundice. Differentiation by a combination of rose bengal I-131 and standard liver-function tests." Jama **194**(9): 949-53.

Normarski, G. (1955). "Differential microinterferometer with polarized waves." J. Phys. Radium **16**(9).

O'Neill, A. C., K. E. Bujold, et al. (2008). "Photochemical Sealing Improves Outcome following Peripheral Neurorrhaphy." J Surg Res(Mar 5 (epub ahead of print)).

O'Neill, A. C., J. M. Winograd, et al. (2007). "Microvascular anastomosis using a photochemical tissue bonding technique." Lasers Surg Med **39**(9): 716-22.

Ochs, S. (1977). "Axoplasmic transport in peripheral nerve and hypothalamo-neurohypophyseal systems." Adv Exp Med Biol **87**: 13-40.

Ochs, S. (2004). A History of Nerve Functions: From Animal Spirits to Molecular Mechanisms. Cambridge, Cambridge University Press.

Ochsner, M. G. (1998). "Fibrin solutions to control hemorrhage in the trauma patient." J Long Term Eff Med Implants **8**(2): 161-73.

Olson, L., L. Backman, et al. (1994). "Role of growth factors in degeneration and regeneration in the central nervous system; clinical experiences with NGF in Parkinson's and Alzheimer's diseases." J Neurol **242**(1 Suppl 1): S12-5.

Olsson, Y. and T. S. Reese (1971). "Permeability of vasa nervorum and perineurium in mouse sciatic nerve studied by fluorescence and electron microscopy." J Neuropathol Exp Neurol **30**(1): 105-19.

Ornelas, L., L. Padilla, et al. (2006). "Fibrin glue: an alternative technique for nerve coaptation--Part II. Nerve regeneration and histomorphometric assessment." J Reconstr Microsurg **22**(2): 123-8.

Ozgenel, G. Y. and G. Filiz (2004). "Combined application of human amniotic membrane wrapping and hyaluronic acid injection in epineurectomized rat sciatic nerve." J Reconstr Microsurg **20**(2): 153-7.

Pan, Y. A., T. Misgeld, et al. (2003). "Effects of neurotoxic and neuroprotective agents on peripheral nerve regeneration assayed by time-lapse imaging in vivo." J Neurosci **23**(36): 11479-88.

Pan, Y. T., Z. G. Li, et al. (2003). "Hand-held arthroscopic optical coherence tomography for in vivo high-resolution imaging of articular cartilage." Journal of Biomedical Optics **8**(4): 648-654.

Park, B., M. Pierce, et al. (2003). "Real-time multi-functional optical coherence tomography." Optics Express **11**: 782-93.

Park, B. H., M. C. Pierce, et al. (2005). "Real-time fiber-based multi-functional spectral-domain optical coherence tomography at 1.3μm." Optics Express **13**(11): 3931-3944

Park, B. H., C. Saxer, et al. (2001). "In vivo burn depth determination by high-speed fiber-based polarization sensitive optical coherence tomography." Journal of Biomedical Optics **6**(4): 474-479.

Park, B. H., C. Saxer, et al. (2001). "In vivo burn depth determination by high-speed fiber-based polarization sensitive optical coherence tomography." J Biomed Opt **6**(4): 474-9.

Park, B. H., C. E. Saxer, et al. (2001). "*In vivo* burn depth determination by high-speed fiber-based polarization sensitive optical coherence tomography." J. Biomed. Opt. **6**(4): 474-9.

Park, J. W., K. S. Lee, et al. (2002). "Rapid neurorrhaphy with titanium clips." Microsurgery **22**(8): 386-90.

Park, W. C. and S. C. Tseng (2000). "Modulation of acute inflammation and keratocyte death by suturing, blood, and amniotic membrane in PRK." Invest Ophthalmol Vis Sci **41**(10): 2906-14.

Patel, N. A., J. Zoeller, et al. (2005). "Monitoring osteoarthritis in the rat model using optical coherence tomography." Ieee Transactions on Medical Imaging **24**(2): 155-159.

Pavan-Langston, D. (1985). Manual of ocular diagnosis and therapy. Boston, Little, Brown & Co.

Payne, C. E., S. P. Hunt, et al. (2002). "Primary sciatic nerve repair using titanium staples." Br J Plast Surg **55**(4): 330-4.

Petersen, J., L. Russell, et al. (1996). "Reduction of extraneural scarring by ADCON-T/N after surgical intervention." Neurosurgery **38**(5): 976-83; discussion 983-4.

Pierce, M. C., R. L. Sheridan, et al. (2004). "Collagen denaturation can be quantified in burned human skin using polarization-sensitive optical coherence tomography." Burns **30**(6): 511-7.

Pierce, M. C., R. L. Sheridan, et al. (2004). "Collagen denaturation can be quantified in burned human skin using polarization-sensitive optical coherence tomography." Burns **30**(6): 511-517.

Pierce, M. C., J. Strasswimmer, et al. (2004). "Birefringence measurements in human skin using polarization-sensitive optical coherence tomography." J Biomed Opt **9**(2): 287-91.

Pierce, M. C., J. Strasswimmer, et al. (2004). "Advances in optical coherence tomography imaging for dermatology." J Invest Dermatol **123**(3): 458-63.

Pierce, M. C., J. Strasswimmer, et al. (2004). "Advances in optical coherence tomography imaging for dermatology." Journal of Investigative Dermatology **123**(3): 458-463.

Pircher, M., E. Gotzinger, et al. (2004). "Imaging of polarization properties of human retina in vivo with phase resolved transversal PS-OCT." Optics Express **12**(24): 5940-5951.

Pitta, M. C., L. M. Wolford, et al. (2001). "Use of Gore-Tex tubing as a conduit for inferior alveolar and lingual nerve repair: experience with 6 cases." J Oral Maxillofac Surg **59**(5): 493-6; discussion 497.

Potma, E., W. P. de Boeij, et al. (2001). "Real-time visualization of intracellular hydrodynamics in single living cells." Proc Natl Acad Sci U S A **98**(4): 1577-82.

Potma, E. O. and X. S. Xie (2005). "Direct visualization of lipid phase segregation in single lipid bilayers with coherent anti-Stokes Raman scattering microscopy." Chemphyschem **6**(1): 77-9.

Potmesil, M. and I. Chakravarty (1981). "A lens and aperture camera model for synthetic image generation." Proceedings of the 8th annual conference on Computer graphics and interactive techniques: 295-305.

Prevel, C. D., B. L. Eppley, et al. (1994). "Mechanical anastomosis of nerves: a histological and functional comparison to conventional suturing." Ann Plast Surg **33**(6): 600-5.

Prinz, R. A., M. Nakamura-Pereira, et al. (2003). "Experimental chronic entrapment of the sciatic nerve in adult hamsters: an ultrastructural and morphometric study." Braz J Med Biol Res **36**(9): 1241-5.

Proano, C. E., D. T. Azar, et al. (2004). "Photochemical keratodesmos as an adjunct to sutures for bonding penetrating keratoplasty corneal incisions." J Cataract Refract Surg **30**(11): 2420-4.

Proano, C. E., L. Mulroy, et al. (2004). "Photochemical keratodesmos for bonding corneal incisions." Invest Ophthalmol Vis Sci **45**(7): 2177-81.

Puliafito, C. A., M. R. Hee, et al. (1996). Optical Coherence Tomography of Ocular Diseases, SLACK.

Rajadhyaksha, M., M. Grossman, et al. (1995). "In vivo confocal scanning laser microscopy of human skin: melanin provides strong contrast." J Invest Dermatol **104**(6): 946-52.

Raman, C. and K. Krishnan (1928). "A new type of secondary radiation." Nature **121**(3048): 501.

Ranvier, M. L. (1878). Leçons sur l'histologie du Système Nerveux. Paris, Librairie F. Savy.

Rashed, R. (1990). "A Pioneer in Anaclastics: Ibn Sahl on Burning Mirrors and Lenses." Isis **81**(3): 464-491.

Rawson, H. (1988). "Glass and its history of service." Science, Measurement and Technology, IEE Proceedings A **135**(6): 325-345.

Reichert, F., A. Saada, et al. (1994). "Peripheral nerve injury induces Schwann cells to express two macrophage phenotypes: phagocytosis and the galactose-specific lectin MAC-2." J Neurosci **14**(5 Pt 2): 3231-45.

Rice, D. H. and F. D. Berstein (1984). "The use of autogenous vein for nerve grafting." Otolaryngol Head Neck Surg **92**(4): 410-2.

Rich, K. M., T. D. Alexander, et al. (1989). "Nerve growth factor enhances regeneration through silicone chambers." Exp Neurol **105**(2): 162-70.

Rich, K. M., J. R. Luszczynski, et al. (1987). "Nerve growth factor protects adult sensory neurons from cell death and atrophy caused by nerve injury." J Neurocytol **16**(2): 261-8.

Ruch, D. S., R. M. Spinner, et al. (1996). "The histological effect of barrier vein wrapping of peripheral nerves." J Reconstr Microsurg **12**(5): 291-5.

Rylander, H. G., N. J. Kemp, et al. (2005). "Birefringence of the primate retinal nerve fiber layer." Experimental Eye Research **81**(1): 81-89.

Sabella, N. (1913). "Use of fetal membranes in skin grafting." Medical Records of New york **83**: 478.

Sames, M., J. Blahos, Jr., et al. (1997). "Comparison of microsurgical suture with fibrin glue connection of the sciatic nerve in rabbits." Physiol Res **46**(4): 303-6.

Saxer, C. E., J. F. de Boer, et al. (2000). "High-speed fiber-based polarization-sensitive optical coherence tomography of in vivo human skin." Optics Letters **25**(18): 1355-1357.

Schlag, G. and H. Redl (1988). "Fibrin sealant in orthopedic surgery." Clin Orthop Relat Res **227**: 269-85.

Schmalbruch, H. (1988). "The effect of peripheral nerve injury on immature motor and sensory neurons and on muscle fibres. Possible relation to the histogenesis of Werdnig-Hoffmann disease." Rev Neurol (Paris) **144**(11): 721-9.

Schmidt, O., K. Wilms, et al. (1999). "The visby lenses." Optom Vis Sci **76**(9): 464-491.

Schuman, J. S., C. A. Puliafito, et al. (2006). Everyday OCT: A Handbook for Clinicians and Technicians, SLACK.

Seddon, H. J. (1943). "Three Types of Nerve Injury." Brain **66**: 237.

Seddon, H. J. (1947). "The use of autogenous grafts for the repair of large gaps in peripheral nerves." Br J Surg **35**: 151-167.

Seddon, H. J. and P. B. Medawar (1942). "Fibrin suture of human nerves." Lancet **2**: 87.

Seddon, H. J., P. B. Medawar, et al. (1943). "Rate of regeneration of peripheral nerves in man." J Physiol **102**(2): 191-215.

Shanthaveerappa, T. R. and G. H. Bourne (1966). "Perineural epithelium: a new concept of its role in the integrity of the peripheral nervous system." Science **154**(755): 1464-7.

Shimmura, S., J. Shimazaki, et al. (2001). "Antiinflammatory effects of amniotic membrane transplantation in ocular surface disorders." Cornea **20**(4): 408-13.

Shinn, A. "Al Shinn's homemade Van Leeuwenhoek microscope." from www.mindspring.com/alshinn/.

Shinohara, H., H. Naora, et al. (1990). "Development of the innervation pattern in the upper limb of staged human embryos." Acta Anat (Basel) **138**(3): 265-9.

Singer, M. (1945). "The combined use of fibrin film and clot in end-to-end union of nerves: An experimental study." J Neurosurg **2**: 102.

Sjoberg, J. and M. Kanje (1989). "Insulin-like growth factor (IGF-1) as a stimulator of regeneration in the freeze-injured rat sciatic nerve." Brain Res **485**(1): 102-8.

Smith, B. H. and P. L. Kornblith (1982). "Axoplasmic transport and neurological surgery." Neurosurgery **10**(2): 268-76.

Smith, J. W. (1964). "Microsurgery of Peripheral Nerves." Plast Reconstr Surg **33**: 317-29.

Snyder, A. K., I. K. Fox, et al. (2006). "Neuroregenerative effects of preinjury FK-506 administration." Plast Reconstr Surg **118**(2): 360-7.

Sobol, J. B., I. J. Lowe, et al. (2003). "Effects of delaying FK506 administration on neuroregeneration in a rodent model." J Reconstr Microsurg **19**(2): 113-8.

Spotnitz, W. D., M. S. Dalton, et al. (1987). "Reduction of perioperative hemorrhage by anterior mediastinal spray application of fibrin glue during cardiac operations." Ann Thorac Surg **44**(5): 529-31.

Sterkers, O., P. Becherel, et al. (1989). "[Repair of the facial nerve exclusively by fibrin glue. 56 cases]." Ann Otolaryngol Chir Cervicofac **106**(3): 176-81.

Stern, M. (1913). "The grafting of preserved amniotic membrane to burned and ulcerated surfaces, substituting skin grafts." Journal of the American Medical Association **60**: 973.

Stiel, H., K. Teuchner, et al. (1996). "Quantitative comparison of excited state properties and intensity- dependent photosensitization by rose bengal." J Photochem Photobiol B **33**(3): 245-54.

Stockel, K., U. Paravicini, et al. (1974). "Specificity of the retrograde axonal transport of nerve growth factor." Brain Res **76**(3): 413-21.

Stoll, G., S. Jander, et al. (2002). "Degeneration and regeneration of the peripheral nervous system: from Augustus Waller's observations to neuroinflammation." J Peripher Nerv Syst **7**(1): 13-27.

Strange, F. G. (1950). "Case report on pedicled nerve-graft." Br J Surg **37**(147): 331-3.

Strasswimmer, J., M. C. Pierce, et al. (2004). "Polarization-sensitive optical coherence tomography of invasive basal cell carcinoma." Journal of Biomedical Optics **9**(2): 292-298.

Stuart, R. M., E. S. Koh, et al. (2004). "Sonography of peripheral nerve pathology." AJR Am J Roentgenol **182**(1): 123-9.

Sugiura, K., Y. Nakatsuchi, et al. (1985). "A new method for venous interposition grafts using fibrin glue." Microsurgery **6**(2): 125-8.

Sunderland, S. (1951). "A classification of peripheral nerve injuries producing loss of function." Brain **74**(4): 491-516.

Sunderland, S. (1978). Nerve and Nerve Injury. Edinburgh.

Sunderland, S. and L. J. Ray (1950). "Denervation changes in mammalian striated muscle." J Neurol Neurosurg Psychiatry **13**(3): 159-77.

Sunderland, S. and G. K. Smith (1950). "The relative merits of various suture materials for the repair of severed nerves." Aust N Z J Surg **20**(2): 85-113.

Taylor, C. A., D. Braza, et al. (2008). "The incidence of peripheral nerve injury in extremity trauma." Am J Phys Med Rehabil **87**(5): 381-5.

Temple, C. L., D. C. Ross, et al. (2004). "Resistance to disruption and gapping of peripheral nerve repairs: an in vitro biomechanical assessment of techniques." J Reconstr Microsurg **20**(8): 645-50.

Tham, S., B. Dowsing, et al. (1997). "Leukemia inhibitory factor enhances the regeneration of transected rat sciatic nerve and the function of reinnervated muscle." J Neurosci Res **47**(2): 208-15.

Thetter, O. (1981). "Fibrin adhesive and its application in thoracic surgery." Thorac Cardiovasc Surg **29**(5): 290-2.

Thoenen, H. and K. Stockel (1975). "Ortho- and retrograde axonal transport: importance for the function of adrenergic neurones." Clin Exp Pharmacol Physiol **Suppl 2**: 1-5.

Vakoc, B. J., M. Shishko, et al. (2007). "Comprehensive esophageal microscopy by using optical frequency-domain imaging (with video)." Gastrointest Endosc **65**(6): 898-905.

Valnicek, V. and P. Wilflingseder (1982). "Eduard Albert (1841 - 1900) and the First Nerve Graft." Chir Plastica **6**: 227-230.

Varitimidis, S. E., F. Riano, et al. (2000). "Recurrent compressive neuropathy of the median nerve at the wrist: treatment with autogenous saphenous vein wrapping." J Hand Surg [Br] **25**(3): 271-5.

Varitimidis, S. E., D. G. Vardakas, et al. (2001). "Treatment of recurrent compressive neuropathy of peripheral nerves in the upper extremity with an autologous vein insulator." J Hand Surg [Am] **26**(2): 296-302.

Ventura, R., G. Torri, et al. (1980). "Experimental suture of the peripheral nerves with "fibrin glue"." Ital J Orthop Traumatol **6**(3): 407-14.

Vittinghoff, E., D. Glidden, et al. (2005). Regression methods in biostatistics: Linear, logistic, survival, and repeated measures models. New York, Springer.

Wachter, E., C. Dees, et al. (2003). "Topical rose bengal: pre-clinical evaluation of pharmacokinetics and safety." Lasers Surg Med **32**(2): 101-10.

Waggoner, B. "Antony van Leeuwenhoek (1632-1723)." from http://www.ucmp.berkeley.edu/history/leeuwenhoek.html.

Walter, M. A., R. Kurouglu, et al. (1993). "Enhanced peripheral nerve regeneration by acidic fibroblast growth factor." Lymphokine Cytokine Res **12**(3): 135-41.

Wang, H., Y. Fu, et al. (2005). "Coherent anti-stokes Raman scattering imaging of axonal myelin in live spinal tissues." Biophys J **89**(1): 581-91.

Wang, X. J., T. E. Milner, et al. (1995). "Characterization of Fluid-Flow Velocity by Optical Doppler Tomography." Optics Letters **20**(11): 1337-1339.

Watchmaker, G. and S. E. Mackinnon (1996). Nerve Injury and Repair. New York, McGraw-Hill.

Weber, R. A., W. C. Breidenbach, et al. (2000). "A randomized prospective study of polyglycolic acid conduits for digital nerve reconstruction in humans." Plast Reconstr Surg **106**(5): 1036-45; discussion 1046-8.

Weiss, P. (1944). "Damming of axoplasm in constrictive nerve. A sign of perpetual nerve growth in the nerve fibers

" Anat Rec **88 (suppl)**(48).

Wessig, C., M. Bendszus, et al. (2007). "In vivo visualization of focal demyelination in peripheral nerves by gadofluorine M-enhanced magnetic resonance imaging." Exp Neurol **204**(1): 14-9.

Wessig, C., L. Jestaedt, et al. (2007). "Gadofluorine M-enhanced magnetic resonance nerve imaging: Comparison between acute inflammatory and chronic degenerative demyelination in rats." Exp Neurol.

West, C. A., K. A. Davies, et al. (2007). "Volumetric magnetic resonance imaging of dorsal root ganglia for the objective quantitative assessment of neuron death after peripheral nerve injury." Exp Neurol **203**(1): 22-33.

White, B. R., M. C. Pierce, et al. (2003). "In vivo dynamic human retinal blood flow imaging using ultra high-speed spectral domain optical Doppler tomography." Optics Express **11**(25): 3490-3497.

Wieken, K., K. Angioi-Duprez, et al. (2003). "Nerve anastomosis with glue: comparative histologic study of fibrin and cyanoacrylate glue." J Reconstr Microsurg **19**(1): 17-20.

Wilson, F. M., 2nd (1976). "Rose bengal staining of epibulbar squamous neoplasms." Ophthalmic Surg **7**(2): 21-3.

Winograd, J. M. and S. E. MacKinnon (2006). Peripheral Nerve Injuries: Repair and Reconstruction, Saunders Elsevier.

Wojtkowski, M., A. Kowalczyk, et al. (2002). "Fourier-domain optical coherence tomography: next step in optical imaging." Optica Applicata **32**(4): 569-580.

Wojtkowski, M., R. Leitgeb, et al. (2002). "In vivo human retinal imaging by Fourier domain optical coherence tomography." Journal of Biomedical Optics **7**(3): 457-463.

Xie, X. S., J. Yu, et al. (2006). "Living cells as test tubes." Science **312**(5771): 228-30.

Xu, J., D. G. Sotereanos, et al. (1998). "Nerve wrapping with vein grafts in a rat model: a safe technique for the treatment of recurrent chronic compressive neuropathy." J Reconstr Microsurg **14**(5): 323-8; discussion 329-30.

Xu, J., S. E. Varitimidis, et al. (2000). "The effect of wrapping scarred nerves with autogenous vein graft to treat recurrent chronic nerve compression." J Hand Surg [Am] **25**(1): 93-103.

Ygge, J. (1989). "Neuronal loss in lumbar dorsal root ganglia after proximal compared to distal sciatic nerve resection: a quantitative study in the rat." Brain Res **478**(1): 193-5.

Youn, J. I., G. Vargas, et al. (2005). "Depth-resolved phase retardation measurements for laser-assisted non-ablative cartilage reshaping." Physics in Medicine and Biology **50**(9): 1937-1950.

Young, J. Z. and P. B. Medawar (1940). "Fibrin suture of peripheral nerves." Lancet **2**: 126.

Young, R. L., J. Cota, et al. (1991). "The use of an amniotic membrane graft to prevent postoperative adhesions." Fertil Steril **55**(3): 624-8.

Yun, S. H., G. J. Tearney, et al. (2006). "Comprehensive volumetric optical microscopy in vivo." Nat Med **12**(12): 1429-33.

Zangwill, L. M. and C. Bowd (2006). "Retinal nerve fiber layer analysis in the diagnosis of glaucoma." Current Opinion in Ophthalmology **17**(2): 120-131.

Zeiss. "Zeiss." from http://www.zeiss.de/c12567be0045acf1/Contents-Frame/d02752b3607a3414c125697c00439fa1.

Zernike, F. (1942). "Phase contrast, a new method for the microscopic observation of transparent objects part II." Physica **9**(10): 974-986.

Zulch, K. J. (1968). "Otfrid Foerster, an appreciation (1873-1941)." J Neurol Sci **6**(2): 384-5.

Zumbusch, A., G. Holtom, et al. (1999). "Three-Dimensional Vibrational Imaging by Coherent Anti-Stokes Raman Scattering." Physical Review Letters **82**(20): 4142-4145.

Zuo, J., D. Neubauer, et al. (2002). "Regeneration of axons after nerve transection repair is enhanced by degradation of chondroitin sulfate proteoglycan." Exp Neurol **176**(1): 221-8.

Appendix 1

Improving electrophysiologic and histologic outcomes by photochemically sealing amnion to the peripheral nerve repair site.

Henry FP, Goyal NA, David WS, Wes D, Bujold KE, Randolph MA, Winograd JM, Kochevar IE, Redmond RW.

Surgery. 2009 Mar;145(3):313-21. Epub 2009 Jan 25. PMID: 19231584

Improving electrophysiologic and histologic outcomes by photochemically sealing amnion to the peripheral nerve repair site

Francis P. Henry, MD,[a,c] Namita A. Goyal, MD,[b] William S. David, MD, PhD,[b] David Wes, BA,[a] Kenneth E. Bujold, BS,[c] Mark A. Randolph, MAS,[a] Jonathan M. Winograd, MD,[a] Irene E. Kochevar, PhD,[c] *and* Robert W. Redmond, PhD,[c] *Boston, Mass*

Background. *The surgical approach used today in the repair of peripheral nerve injuries rarely achieves full functional recovery. This study determines whether isolation of the nerve repair site using photochemical tissue bonding (PTB) in combination with human amniotic membrane can improve both functional and histologic recovery.*

Methods. *New Zealand white rabbits (n = 24) underwent transection of the right common peroneal nerve. Epineural nerve repair was performed using 10-0 nylon sutures. The repair site was then wrapped in a cuff of human amniotic membrane, which either was secured with sutures or sealed using PTB. Standard neurorrhaphy alone was assessed as a control group. Functional recovery was recorded at 30-day intervals postoperatively by electrophysiologic assessment. At 120 days, animals were killed humanely and nerves harvested for histomorphometry.*

Results. *Nerves treated with amnion wraps and sealed with PTB demonstrated a statistically significant improvement across both functional and histologic parameters. Functional recovery, as measured by repeated electrophysiologic studies over time, revealed a 26.2% improvement over standard neurorrhaphy alone ($P < .05$). Nerves treated with PTB-sealed amnion wraps had significantly greater ($P < .001$) axon ($5.08 \pm 1.06\ \mu m$) and fiber diameters ($7.46 \pm 1.37\ \mu m$), as well as myelin thickness ($2.39 \pm 0.7\ \mu m$) and the g ratio (axon diameter/fiber diameter ratio; 0.68 ± 0.07) distal to the repair site compared to standard neurorrhaphy alone ($4.98 \pm 1.81\ \mu m$, $6.77 \pm 1.94\ \mu m$, $1.79 \pm 0.42\ \mu m$, and 0.71 ± 0.09, respectively).*

Conclusion. *Isolation of the repair site using a photochemically sealed amnion wrap improves electrophysiologic and histologic recovery compared to standard suture neurorrhaphy. (Surgery 2009;145:313-21.)*

From the Plastic Surgery Research Laboratory,[a] Neuromuscular Diagnostics Center,[b] and the Wellman Center for Photomedicine,[c] Massachusetts General Hospital, Harvard Medical School, Boston, Mass

Peripheral Nerve Injury remains a significant clinical challenge in the field of reconstructive microsurgery. Several million people in the United States suffer serious, traumatic, peripheral nerve injuries each year[1] and, despite more than a century of intensive research, the outcome of peripheral nerve repair is often poor. Microsurgical suture repair remains the current gold standard in clinical practice,[2] but obvious deficiencies remain with this technique, given that surgical repair of peripheral nerves does not result in complete functional recovery. Although the environment of sensory and motor axons will support axonal regeneration, it is often compromised by intraneural scarring, which occurs after microsurgical repair and serves as a mechanical barrier to regenerating axons. Furthermore, inflammatory cells from the surrounding tissues likely contribute to this scar formation. Improved recovery after peripheral neurorrhaphy would significantly influence the rehabilitation process, possibly reducing the long-term care and disability associated with these injuries.

Supported in part by a grant from the Department of Defense, Medical Free Electron Laser Program (F4 9620-01-1-0014) and the Bullock-Wellman Fellowship, awarded to F.P.H. by the Wellman Center for Photomedicine.

Accepted for publication November 11, 2008.

Reprint requests: Robert W. Redmond, PhD, Wellman Center for Photomedicine, Harvard Medical School, Massachusetts General Hospital Thier-224, Boston, MA 02114. E-mail: Redmond@helix.mgh.harvard.edu.

0039-6060/$ - see front matter

doi:10.1016/j.surg.2008.11.005

Photochemical tissue bonding (PTB) is a sutureless tissue repair process that seals the repair site without trauma or foreign body reaction, thus allowing prompt restoration of the normal endoneural environment and healing. In PTB, a photoactive dye is applied to tissue surfaces that are then placed in contact and irradiated with green light. This technique uses visible light at a power that does not thermally damage the tissue, unlike laser welding techniques, and therefore preserves the nerve structure and surrounding tissues. The light activates the dye, leading to immediate formation of covalent cross-links between proteins on both surfaces and thereby forming a water tight seal. The dye commonly used in PTB is rose bengal (RB), a halogenated fluorescein derivative that is photochemically active when exposed to green light.[3,4] Rose bengal has been FDA-approved for use as a diagnostic agent in ophthalmology[5-7] and described as a systemic diagnostic agent for hepatic function.[8,9] A recent preclinical evaluation[10] of the pharmacokinetics and safety of topical RB indicated that concentrations of RB <1% had negligible effects on normal skin either in the dark or after exposure to 532-nm green laser light using irradiances of ≤100 mW/cm^2. We used a 10-fold lower RB concentration (0.1%) with our PTB technique; in addition, photoactivation of RB with 532 nm laser radiation has not induced an inflammatory reaction in any of our previous investigations.

We have demonstrated previously the efficacy of PTB in several tissues both ex vivo and in vivo. For example, corneal incisions in rabbit eyes treated with PTB healed without complications, and the resultant seals produced resisted pressures >10-fold greater than the intraocular pressure.[11] PTB was also used to provide a watertight seal with sutures for securing corneal transplants in vivo in rabbit eyes.[12] In addition, PTB enhanced the healing of severed tendons[13] and provided a sutureless method of microvascular anastomosis in a rat femoral artery model.[14] Our studies also have demonstrated that PTB is a viable technology for sutureless skin closure for incisions in porcine skin,[15] and clinical trials are currently in progress in this area.

There has been ongoing interest in nerve wrapping as a means to improve outcomes after peripheral neurorrhaphy. Autologous vein is most commonly used as a wrap in clinical practice, but the use of human amniotic membrane (HAM) also has been discussed.[16] Although wrapping the nerve in a HAM sleeve has been reported as a method for reducing scar formation,[17] it has only been evaluated in cases of severe recurrent scarring with associated nerve compression[18-20] and generally used as a secondary procedure to loosely surround the site of injury without sealing. In this study, we have investigated HAM as a suitable nerve wrap material, with the addition of PTB technology to seal the amnion over the repair site to isolate the regenerating nerve environment. We hypothesized that sealing the amnion nerve wrap with PTB technology would isolate the endoneural environment from extrinsic inflammatory factors and maximize the intrinsic growth factors produced within the nerve repair site. A potential to minimize suture material should also result in a decreased foreign body reaction and subsequent scar formation.[21] Tubulization techniques also have been described clinically in conjunction with primary neurorrhaphy; although results have been promising, they have failed to supersede standard neurorrhaphy (SN) in functional recovery.[22,23] PTB with sealing of HAM wrap may improve outcomes over these approaches.

The broad aim of this study was to evaluate the efficacy of photochemical tissue bonding with an amnion nerve wrap in the repair of the peripheral nerve of a large animal model, using neurophysiologic assessments as a functional outcome in combination with histologic analysis.

METHODS

Surgical procedures. The Subcommittee on Research Animal Care at Massachusetts General Hospital approved all procedures in this study. A total of 24 female New Zealand white rabbits (Charles River Laboratories, Wilmington, Mass), weighing 2–2.5 kg, were anesthetized with isoflurane (2.5–3.5% by mask; Baxter Healthcare, Deerfield, Ill). The right common peroneal nerve was then exposed through a dorsolateral muscle-splitting incision. Under microscopic guidance, the common peroneal nerve was isolated and sharply transected at a point 5 cm distal to the sciatic notch. The nerve was repaired immediately with three 10-0 nylon epineural sutures (Ethicon, Somerville, NJ). Animals then were randomized to 1 of 3 experimental groups ($n = 8$).

Human amniotic membrane preparation. Human placenta was obtained with the approval of the Institutional Review Board at Massachusetts General Hospital. All residual blood clots were removed from the placenta by washing the tissue several times with Earle's balanced salt solution. The amniotic membrane was peeled away from the chorion and placed on nitrocellulose paper (epithelial side down). The amnion was cut into segments and

stored at –80°C in medium consisting of a 1:1 solution of 100% glycerol/Dulbecco's modified Eagle's medium (Gibco, Grand Island, NY) with 1% penicillin-streptomycin (Gibco). Immediately before use, the amnion was defrosted and rinsed in phosphate-buffered saline for 2 hours to remove all glycerol.

Experimental groups. *SN/Control group* (n = 8). These animals did not receive any further treatment after standard neurorrhaphy, as described above. This group served as the control.

SN & HAM wrap (n = 8). The amniotic membrane was prepared as outlined above. After standard neurorrhaphy (also described above), a 1 × 1-cm segment was wrapped around the repair site and secured to the epineurium using a single 10-0 nylon suture (Ethicon) proximally and distally. No RB was applied to the amnion.

SN, HAM/PTB (n = 8). A 1 × 1-cm segment of amnion (stromal surface) was treated with 0.1% RB. The dye was allowed to absorb for 1 minute, after which any excess was removed. After standard neurorrhaphy, the segment was wrapped around the nerve, covering the epineural repair site. This area was then exposed to green laser light at 532 nm from a continuous-wave Nd/YAG laser (Aura *i*; Laserscope, San Jose, Calif) at an irradiance of ~0.5 W/cm^2 for 1 minute; this was followed by 180° rotation and repeat irradiation on the opposite side.

After all repair procedures, the wound was closed using 4-0 absorbable polyglactin sutures (Ethicon). Postoperatively, animals were housed in the Massachusetts General Hospital animal facility and were permitted to mobilize freely with unlimited access to food and water.

Electrophysiologic assessment. Electrophysiologic measurements were performed before surgery, immediately postoperatively, and at 30, 60, 90, and 120 days after surgery. Measurements were taken using a Teca Synergy Multimedia EMG/EP (Oxford Instruments Medical, Pleasantville, NY) from both experimental (right) and control (left) nerves at each time point.

Nerve conduction studies. Disposable, self-adhesive, gelled surface recording electrodes (Viasys Healthcare, Madison, Wis) were placed over the tibialis anterior muscle in a belly-tendon montage. Subdermal needle electrode (0.70 × 30-mm, 22 G × 1.25 in; Medtronic Sensory Needle Electrode; Medtronic, Copenhagen, Denmark) stimulation of the peroneal nerve was performed at the fibular head (below the site of nerve transection) and at the sciatic notch (above the site of transection). Using stimulus duration of 0.02 ms, stimulus intensity was increased gradually until a supramaximal compound muscle action potential (CMAP) was obtained. The CMAP amplitude was measured from baseline to peak, and latencies were measured from stimulus to negative peak onset. The latency difference between the proximal and distal responses was divided into the distance between stimulation sites to generate a conduction velocity.

Histology and histomorphometry. At 120 days postoperatively, animals were anesthetized with isoflurane (2.5–3.5% by mask; Baxter Healthcare). After the final electrical assessment, the animals were killed humanely with an intracardiac injection of 100–150 mg/kg pentobarbital (Euthasol; Virbac, Fort Worth, Tex). The right and left common peroneal nerves were harvested and fixed in a 2%/2% glutaraldehyde/paraformaldehyde solution at 4°C for 48 hours. Specimens were postfixed in 1% osmium tetroxide and then dehydrated in ethanol and epoxy embedding resin. Cross-sections (1 μm) were made 5 mm proximal and distal to the neurorrhaphy site using a microtome (Donsanto, Natick, Mass). All samples were stained with 0.5% (w/v) toluidine blue in preparation for light microscopy.

Histomorphometric analysis was carried out on all nerves from each experimental group. Nerve architecture was examined at × 400 magnification. Five × 400 images were taken from each proximal and distal segment in the experimental nerves at sites evenly distributed within the cross-section. A total of 50 fibers were randomly selected in each image (total of 250 fibers per nerve sample). Total fiber diameter and axon diameter were measured using ImageJ software.[24] The myelin thickness was derived from the difference between the fiber and axon diameter. In addition, the g ratio of each fiber was calculated as the axon diameter-fiber diameter ratio.

Using photo editing software (Microsoft Photo Editor; Microsoft Corp, Redmond, Wash), each × 400 field was examined in detail. A manual count of endoneural myelinated fibers was undertaken for each of the five × 400 images (five above the repair site and five below the repair site). These counts were then averaged to produce a mean estimate of myelinated fibers per × 400 field. To estimate the total number of fibers per nerve cross-section, we measured the endoneurial area of each nerve using image analysis software (Metamorph v4.6; Universal Imaging, Downingtown, Pa). Using these data, in combination with the count per × 400 field, the total fiber counts were calculated.

The epineurium for the samples 5 mm below the repair site also was examined. Five × 400

Table I. Repeated electrophysiological assessment

	Test 1 (normal nerve)				*Test 2 (injured nerve)*		
	Latency	*Amplitude*	*Velocity*		*Latency*	*Amplitude*	*Velocity*
A	0.90	20.2	100.0	A	0.95	10.8	104.8
B	1.00	20.9	100.0	B	0.90	11.5	100.0
C	0.95	21.5	100.0	C	1.00	11.5	105.3
D	0.95	21.2	104.8	D	1.00	11.1	105.0
Mean	0.95	20.95	101.2		0.96	11.2	103.8
St.Dev.	0.041	0.56	2.40		0.047	0.34	2.52

images were taken at sites evenly distributed throughout the epineurium, and a manual count of nerve fibers was undertaken per × 400 field. The mean count was taken per animal. Using the area of the epineurium as measured with Microsoft Photo Editor software, an epineurial count of axon migration was achieved as described above for total fiber count estimation.

Statistics. Statistical significance was set at $P < .05$. Regarding histomorphometry and electrophysiologic data, statistical significance was assessed per group at each time point using the unpaired Student *t* test. A linear regression model of overall percentage change in time (using the slope of the percent change in amplitude per 30 days as a variable) comparing each group was also analyzed for the electrical data. This process enabled an overall recovery rate to be expressed as a percentage and analyzed for significance.

RESULTS

Gross findings/surgical complications. All nerves were in continuity at the time of harvest. There were no discernable differences noted between the groups regarding adhesion formation or macroscopic appearance of the nerve repair site. In the SN & HAM and SN & HAM/PTB groups, no residual evidence of the human amniotic membrane was found at 120 days postoperatively.

There was a single mortality at postoperative day 60 due to anesthetic complications (SN & HAM group), and this animal was excluded from the data analysis. Electrical analysis of 1 animal in the SN & HAM/PTB group revealed a dispersed wave form after surgery and throughout the study period that resulted in an unreliable electrical endpoint. This occurrence may be explained by a chronic wound infection in the same animal requiring antibiotic administration, and so we excluded this animal from the data analysis.

Electrophysiologic assessment. Reliability of our technique was verified by 4 repeated measurements at 1 time point on 2 separate specimens (1 injured and 1 normal nerve). Both stimulating and recording electrodes were removed from the animal and replaced each time. The results of the electrophysiologic assessment are shown in Table I.

Nerve conduction studies. To avoid bias and negate interanimal variability, amplitude results from each animal were examined individually. The change in distal amplitude (Δ) was expressed as a percentage of the total drop from the preoperative measurement to the day 30 recording (maximum degeneration) and calculated as follows:

$$\frac{\text{Amplitude Day X} - \text{Amplitude Day 30}}{\text{Amplitude Day 0} - \text{Amplitude Day 30}} \times 100 = \%\Delta \text{ at Day X}$$

These data are represented graphically in Fig 1. By 90 days post repair, an improvement in distal amplitude was noted in the SN & HAM/PTB group compared to the SN group (–52% ± 9.6% vs –82.1% ± 5%, respectively). This finding was statistically significant ($P < .05$). No statistical difference was noted between the SN group and the SN & HAM group. No differences were noted in distal latency or conduction velocity among the groups.

Furthermore, animals in the SN & HAM/PTB group showed an overall increased rate of recovery (as measured by percentage change over time with linear regression), which was 26.2% greater than the SN group. This difference was statistically significant ($P < .05$). The SN & HAM group showed an overall rate of recovery that was 13.7% greater than the animals in the SN group; this finding, however, did not achieve statistical significance.

Histology and histomorphometry. Regeneration of myelinated axons was observed in the proximal and distal segments of all experimental groups, and normal neural architecture was restored. Examples of neural architecture are shown in Fig 2, both above and below the repair site for each group. Above the repair site (5 mm), histomorphometric analysis

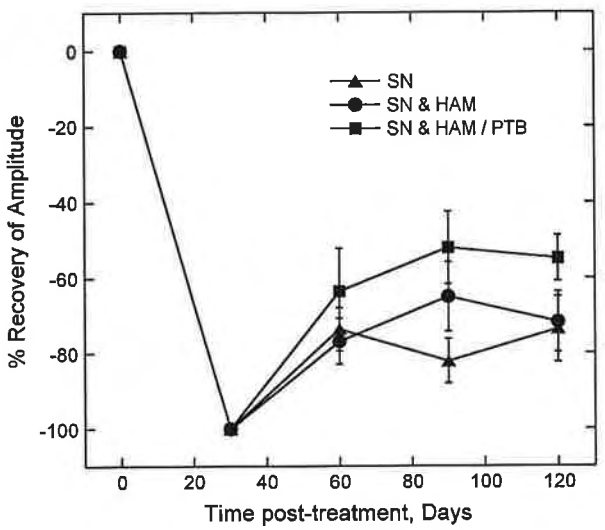

Fig 1. Time course for recovery, as expressed by percentage change in distal amplitude over the total decrease in amplitude from the preoperative measurement to the day 30 recording (maximum degeneration). Recovery over time revealed a statistically significant 26.2% improvement ($P < .05$) in the SN & HAM/PTB animals (*solid squares*) compared with the SN & HAM wrap (*solid circles*) and the SN alone groups (*solid triangles*).

demonstrated a statistically significant ($P < .0001$) in myelin thickness in nerves treated with the SN and HAM/PTB group compared to SN alone and SN & HAM groups. The g ratio was also significantly improved in this group ($P < .0001$). There was no difference noted above the repair site in fiber or axon diameters. Below the repair site, there was a statistically significant improvement across all 4 parameters in nerves treated with PTB-sealed HAM wraps compared to the other groups ($P < .0001$ for fiber diameter, myelin thickness, and g ratio; $P < .05$ for axon diameter). Total fiber counts, although not statistically significant, demonstrated an improved outcome in the SN & HAM/PTB group both above and below the repair site. Histomorphometric results for each experimental group (N = 2000) expressed in means and standard deviations are shown in Table II.

Axonal outgrowth through the epineurium was noted as a feature associated in the SN and SN & HAM wrap groups. The SN & HAM/PTB group revealed a decrease in epineurial/extraneural axonal regeneration, suggesting improved preservation of the neural microarchitecture using this repair technique. Axonal migration into and through the epineurium also was decreased in animals treated with SN & HAM/PTB compared to the other groups. Figure 3 is representative of × 200 images of the epineurial outgrowth among the various groups. This finding was quantified and, although not statistically significant, there was a trend toward preservation of endoneurial axonal regeneration using the SN & HAM/PTB technique (Fig 4).

DISCUSSION

In this study, we used both neurophysiologic and histologic endpoints to demonstrate that PTB with a human amniotic membrane wrap significantly augments peripheral neurorrhaphy compared to the current gold standard. This large animal study highlights the reproducibility of our technique and confirms its benefits compared to conventional repair as observed in our previous studies. In an initial study,[25] PTB was used to restore the continuity of the severed nerve using an epineurial cuff technique. That study showed preservation of the neural microarchitecture and demonstrated the feasibility of PTB as a viable nerve repair technique. These findings led to a second rodent study[26] in which we combined PTB with a nerve wrap. Rodents treated with HAM wraps sealed with PTB demonstrated an early improvement in functional recovery as measured by sciatic function index. This combined PTB/HAM wrap treatment was evaluated against the following: (1) SN, (2) SN with PTB sealing alone, (3) SN with HAM wrapping alone, (4) SN with autologous vein wrap sealed with PTB, and (5) SN with autologous vein wrap alone. The observed, significant functional improvement was also supported by histologic findings of increased fiber, axon diameter, and myelin thickness in nerve segments distal to the repair in the amnion/PTB animals. The use of PTB alone as a sealant with SN, without nerve wrapping, offered significant improvement in functional recovery; however, it failed to show significant improvement across any of the histologic parameters measured. This series of studies has shown PTB to be a viable nerve repair technique to improve functional outcome when combined with a HAM wrap.

The previous findings led to our investigation in a larger animal model using neurophysiology as an endpoint. Using electrophysiologic endpoints as a measurement of functional outcome in the current study adds valuable supportive evidence for this nerve repair technique. Standard electrophysiologic amplitude measurements, as used in clinical practice, parallel the improvement in functional outcome demonstrated in our previous rodent studies (as measured by sciatic function index). The use of a larger animal also allows the technique to be evaluated in a robust nerve model over a longer regenerative distance than previously used in

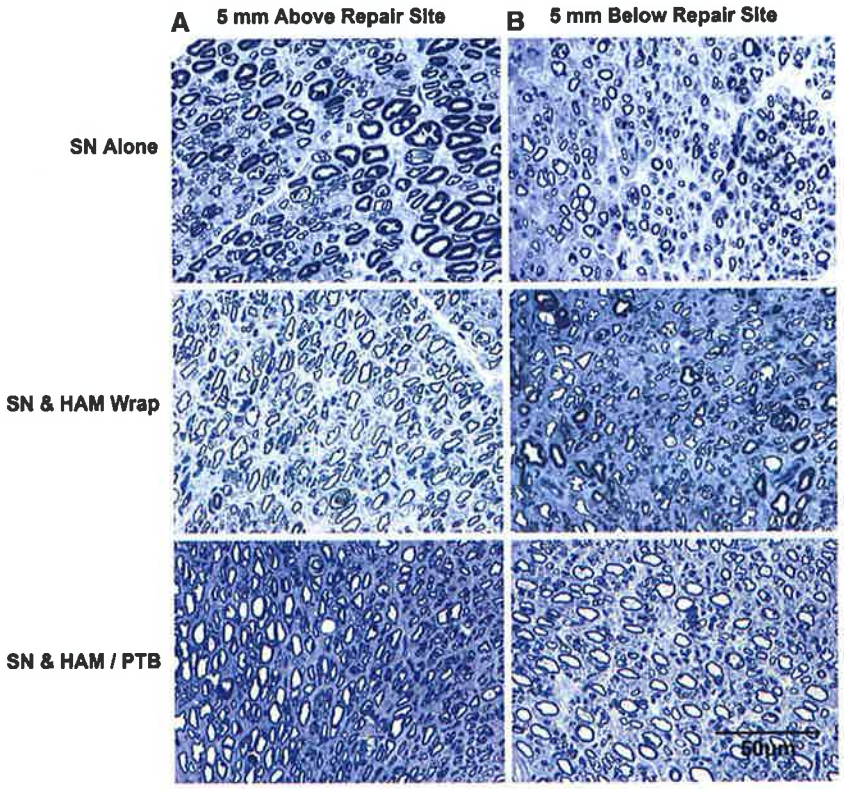

Fig 2. Cross-sections 5 mm proximal (*A*) and 5 mm distal (*B*) to the repair site showing regeneration of myelinated axons of all experimental groups with preservation of normal neural architecture (toluidine blue × 400). The number below each panel indicates the experimental group. Scale (*bottom right*) indicates a distance of 50 μm.

Table II. Histomorphometric parameters

Group	*Fiber diameter (μm)*	*Axon diameter (μm)*	*Myelin thickness (μm)*	*G ratio*	*Total fiber count*
		5 mm above repair site			
SN Alone	8.49 (+/–2.39)	5.76 (+/–1.86)	2.73 (+/–1.02)	0.67 (+/–0.09)	3,550 (+/–1,300)
SN & HAM Wrap	6.85 (+/–1.60)	4.8 (+/–1.48)	2.05 (+/–0.72)	0.69 (+/–0.10)	4,500 (+/–1,750)
SN & HAM/PTB	8.62 (+/–1.78)	5.65 (+/–1.31)	2.97 (+/–1.09)*	0.66 (+/–0.09)*	4,550 (+/–1,150)
		5 mm below repair site			
SN Alone	6.77 (+/–1.94)	4.98 (+/–1.81)	1.79 (+/–0.42)	0.72 (+/–0.09)	4,300 (+/–1,600)
SN & HAM Wrap	6.31 (+/–1.58)	4.52 (+/–1.44)	1.8 (+/–0.53)	0.7 (+/–0.09)	3,550 (+/–1,300)
SN & HAM/PTB	7.47 (+/–1.37)*	5.08 (+/–1.06)†	2.39 (+/–0.70)*	0.68 (+/–0.07)*	4,500 (+/–1,200)

*Denotes statistical significance $P < .0001$ compared to SN Alone.
†Denotes statistical significance $P < .05$ compared to SN Alone.

the sciatic nerve of the Sprague Dawley rat. Our histomorphometry results also show an improvement in nerve maturity rather than simply improving regenerative capability. The use of myelin thickness and g ratio denotes relative maturity of the fibers compared to using fiber and axon diameter and fiber counts alone.

HAM as a nerve wrap lends itself toward use with PTB given its thin (20 μm) translucent nature and its malleable handling properties. The amniotic membrane is the innermost layer of the fetal membranes, and it is composed of a thick basement membrane and an avascular stroma. Clinically, the amniotic membrane has been used as a wound dressing and found to increase reepithelialization rates.[27,28] It has been subsequently described in a wide range of tissue repair models including vaginal, urethral, and bladder reconstruction; adhesion prevention; and repair of the pericardium and splenic capsule.[29-35] Infiltration of neutrophils, lymphocytes, and macrophages have been shown to be reduced in corneal perforations treated with amniotic membrane,[36] and amnion currently is most commonly used in this clinical area. Both antiinflammatory

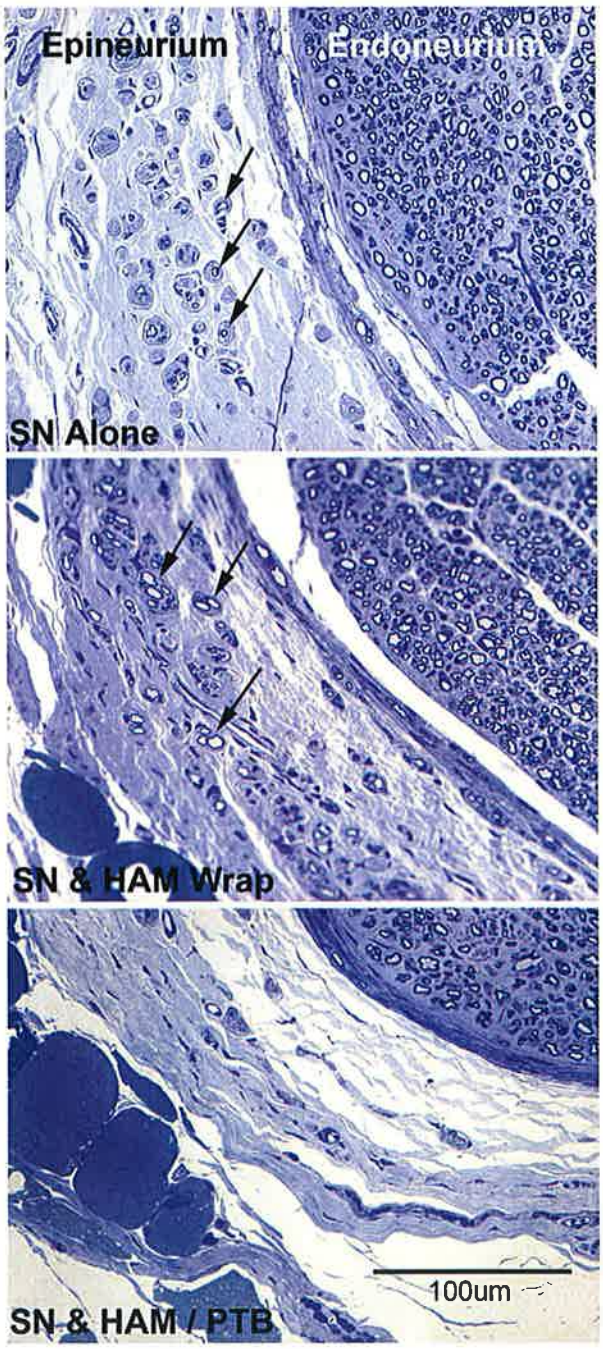

Fig 3. Cross-sections 5 mm distal to the repair site showing axonal sprouting with regeneration into and through the epineurium in the SN & HAM wrap and the SN alone groups (*arrows*). Sealing of the SN repair site with HAM/PTB was noted to reduce this phenomenon as shown above in the lower image (toluidine blue × 200).

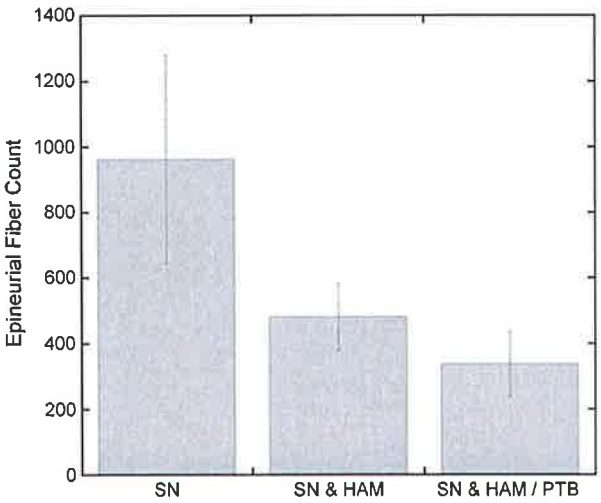

Fig 4. Epineurial fiber count per group (denoting axonal migration outside the endoneurium). Data are shown as standard errors of the mean. SN with PTB sealing of the HAM wrap (337.13 ± 98.7) clearly shows a trend toward preservation of normal axonal regeneration through the endoneurium over the SN alone and the SN & HAM wrap groups (961.9 ± 318 and 481.3 ± 103.4, respectively). In a linear regression statistical model, these data achieve borderline statistical significance ($P = .053$).

and antiangiogenic proteins[37] have been identified in wounds treated with amnion, as has increased apoptosis of polymorphonuclear neutrophils and CD20+ cells.[38,39] Human amniotic cells do not express HLA-A, B, C, or DR antigens of β_2-microglobulin,[40,41] and the immunologic response to transplantation is negligible.[42] Indeed, transplantation of amnion into human volunteers substantiate these facts; none of the subjects ($n = 7$) showed clinical signs of acute rejection, and amniotic epithelial cells were demonstrated by biopsy ≥7 weeks after implantation.[42] We believe these attributes to be favorable when using HAM as a nerve wrap combined with PTB technology.

Regarding its use in animal models, a xenogenic response after treatment with human amniotic membrane has not been described, despite several studies investigating its therapeutic effects. These studies include intraabdominal and pelvic adhesion prevention in both rodent[29] and rabbit models,[35] as well as investigations involving wound repair models of the cornea[39] and evaluation of intraocular implantation in a rabbit model.[43]

PTB creates an immediate watertight seal between tissue surfaces. In previous studies, we have discussed photochemical cross-linking in tissues, such as the cornea, with high collagen content.[11,12] This methodology easy translates to our neurorrhaphy techniques, given the high collagen content of both the epineurium and amnion. Adopting PTB technology with our HAM nerve wrap has several advantages over standard repair, which may be a factor

in the augmentation of both neurophysiologic and histologic outcomes. The presence of suture material has been associated with a foreign body reaction that further reduces functional outcome postoperatively due to its association with endoneurial scar formation.[21] Isolation of the endoneurial environment by photochemically sealing the neurorrhaphy site may also allow for a reduction in extrinsic inflammatory infiltrate and maximize the potential of the intrinsic nerve growth factors.

Recent advances in the field of neural regeneration have concentrated on the complex sequence of biologic events that occur after neural injury. The upregulation of growth factors and inflammatory mediators in proximal and distal nerve stumps have been shown to promote axonal regrowth and neural preservation. Whereas exogenous factors introduced into this environment have demonstrated some promise in the experimental stage, we hypothesize that the isolation of the neural microenvironment and resulting promotion of intrinsic upregulatory functions, as well as the reduction of extrinsic inflammatory infiltrate (by photochemically sealing the neurorrhaphy site), remain the key factors behind the success of our repair technique. This hypothesis is supported by the performance of our SN & HAM group, in which a sutured (unsealed) HAM wrap conferred no significant benefits greater than SN alone.

A further observation noted during our study involved a reduction in axonal outgrowth into the epineurium. Sealing of the peripheral neurorrhaphy site promoted more efficient regeneration through the repair site rather than the disorganized growth with extraneural axonal sprouting observed in the SN and SN & HAM groups. Although not a feature or complication noted during the study, this finding may be relevant in the reduction of neuroma formation after peripheral nerve repair in the clinical scenario.

Ultimately, we have demonstrated that our photochemical technique in combination with a HAM wrap results in a strong, reliable nerve repair with improved neurophysiologic and histologic outcomes compared to standard neurorrhaphy. This technique does not add significantly to operating time, does not require additional microsurgical training, and could be implemented easily into clinical practice by microsurgeons. These encouraging results warrant further investigation in a clinical trial, which is currently planned.

The authors thank Esther A. Z. Rust for assistance in the care of the animals, Ms Peggy Sherwood for excellent histologic processing, Laura Baldassari for her assistance with statistical analysis, and Anne C. O'Neill for valuable discussions.

REFERENCES

1. Dagum AB. Peripheral nerve regeneration, repair, and grafting. J Hand Ther 1998;11:111-7.
2. Lundborg G. A 25-year perspective of peripheral nerve surgery: evolving neuroscientific concepts and clinical significance. J Hand Surg (Am) 2000;25:391-414.
3. Lambert CR, Stiel H, Leupold D, Lynch MC, Kochevar IE. Intensity-dependent enzyme photosensitization using 532 nm nanosecond laser pulses. Photochem Photobiol 1996;63:154-60.
4. Stiel H, Teuchner K, Paul A, Leupold D, Kochevar IE. Quantitative comparison of excited state properties and intensity- dependent photosensitization by rose bengal. J Photochem Photobiol B 1996;33:245-54.
5. Feenstra RP, Tseng SC. What is actually stained by rose bengal? Arch Ophthalmol 1992;110:984-93.
6. Pavan-Langston D. Manual of ocular diagnosis and therapy. Little, Brown & Co., 1985.
7. Wilson FM, II. Rose bengal staining of epibulbar squamous neoplasms. Ophthalmic Surg 1976;7:21-3.
8. Eyler WR, Schuman BM, Du Sault LA, Hinson RA. Rose bengal I-131 liver scan. An aid in the differential diagnosis of jaundice. JAMA 1965;194:990-2.
9. Nordyke RA. Surgical vs nonsurgical jaundice. Differentiation by a combination of rose bengal I-131 and standard liver-function tests. JAMA 1965;194:949-53.
10. Wachter E, Dees C, Harkins J, Scott T, Petersen M, Rush RE, et al. Topical rose bengal: pre-clinical evaluation of pharmacokinetics and safety. Lasers Surg Med 2003;32: 101-10.
11. Proano CE, Mulroy L, Jones E, Azar DT, Redmond RW, Kochevar IE. Photochemical keratodesmos for bonding corneal incisions. Invest Ophthalmol Vis Sci 2004;45: 2177-81.
12. Proano CE, Azar DT, Mocan MC, Redmond RW, Kochevar IE. Photochemical keratodesmos as an adjunct to sutures for bonding penetrating keratoplasty corneal incisions. J Cataract Refract Surg 2004;30:2420-4.
13. Chan BP, Amann C, Yaroslavsky AN, Title C, Smink D, Zarins B, et al. Photochemical repair of Achilles tendon rupture in a rat model. J Surg Res 2005;124:274-9.
14. O'Neill AC, Winograd JM, Zeballos JL, Johnson TS, Randolph MA, Bujold KE, et al. Microvascular anastomosis using a photochemical tissue bonding technique. Lasers Surg Med 2007;39:716-22.
15. Kamegaya Y, Farinelli WA, Vila Echague AV, Akita H, Gallagher J, Flotte TJ, et al. Evaluation of photochemical tissue bonding for closure of skin incisions and excisions. Lasers Surg Med 2005;37:264-70.
16. Ozgenel GY, Filiz G. Combined application of human amniotic membrane wrapping and hyaluronic acid injection in epineurectomized rat sciatic nerve. J Reconstr Microsurg 2004;20:153-7.
17. Ruch DS, Spinner RM, Koman LA, Challa VR, O'Farrell D, Levin LS. The histologic effect of barrier vein wrapping of peripheral nerves. J Reconstr Microsurg 1996;12:291-5.
18. Varitimidis SE, Vardakas DG, Goebel F, Sotereanos DG. Treatment of recurrent compressive neuropathy of peripheral nerves in the upper extremity with an autologous vein insulator. J Hand Surg (Am) 2001;26:296-302.
19. Xu J, Sotereanos DG, Moller AR, Jacobsohn J, Tomaino MM, Fischer KJ, et al. Nerve wrapping with vein grafts in

a rat model: a safe technique for the treatment of recurrent chronic compressive neuropathy. J Reconstr Microsurg 1998;14:323-8; discussion 329-30.
20. Xu J, Varitimidis SE, Fisher KJ, Tomaino MM, Sotereanos DG. The effect of wrapping scarred nerves with autogenous vein graft to treat recurrent chronic nerve compression. J Hand Surg (Am) 2000;25:93-103.
21. DeLee JC, Smith MT, Green DP. The reaction of nerve tissue to various suture materials: a study in rabbits. J Hand Surg (Am) 1977;2:38-43.
22. Battiston B, Geuna S, Ferrero M, Tos P. Nerve repair by means of tubulization: literature review and personal clinical experience comparing biological and synthetic conduits for sensory nerve repair. Microsurgery 2005;25:258-67.
23. Lundborg G, Rosen B, Dahlin L, Danielsen N, Holmberg J. Tubular versus conventional repair of median and ulnar nerves in the human forearm: early results from a prospective, randomized, clinical study. J Hand Surg (Am) 1997;22:99-106.
24. Abramoff MD, Magelhaes PJ, Ram SJ. Image processing with Image. J. Biophoton Int 2004;11:36-42.
25. Johnson TS, O'Neill AC, Motarjem PM, Amann C, Nguyen T, Randolph MA, et al. Photochemical tissue bonding: a promising technique for peripheral nerve repair. J Surg Res 2007;143:224-9.
26. O'Neill AC, Randolph MA, Bujold KE, Kochevar IE, Redmond RW, Winograd JM. Photochemical sealing improves outcome following peripheral neurorrhaphy. J Surg Res 2009;151:33-9.
27. Sabella N. Use of fetal membranes in skin grafting. Med Records NY 1913;83:478.
28. Stern M. The grafting of preserved amniotic membrane to burned and ulcerated surfaces, substituting skin grafts. JAMA 1913;60:973.
29. Badawy SZ, Baggish MS, ElBakry MM, Baltoyannis P. Evaluation of tissue healing and adhesion formation after an intraabdominal amniotic membrane graft in the rat. J Reprod Med 1989;34:198-202.
30. Brandt FT, Albuquerque CD, Lorenzato FR. Female urethral reconstruction with amnion grafts. Int J Surg Investig 2000;1:409-14.
31. Erdener A, Ulman I, Ilhan H, Soydan S. Amniotic membrane wrapping: an alternative method to the splenorrhaphy in the injured spleen. Eur J Pediatr Surg 1992;2:26-8.
32. Fishman IJ, Flores FN, Scott FB, Spjut HJ, Morrow B. Use of fresh placental membranes for bladder reconstruction. J Urol 1987;138:1291-4.
33. Ghanbari Z, Dahaghin M, Borna S. Long-term outcomes of vaginal reconstruction with and without amnion grafts. Int J Gynaecol Obstet 2006;92:163-4.
34. Gruss JS, Jirsch DW. Human amniotic membrane: a versatile wound dressing. Can Med Assoc J 1978;118:1237-46.
35. Young RL, Cota J, Zund G, Mason BA, Wheeler JM. The use of an amniotic membrane graft to prevent postoperative adhesions. Fertil Steril 1991;55:624-8.
36. Nobe JR, Moura BT, Robin JB, Smith RE. Results of penetrating keratoplasty for the treatment of corneal perforations. Arch Ophthalmol 1990;108:939-41.
37. Hao Y, Ma DH, Hwang DG, Kim WS, Zhang F. Identification of antiangiogenic and antiinflammatory proteins in human amniotic membrane. Cornea 2000;19:348-52.
38. Park WC, Tseng SC. Modulation of acute inflammation and keratocyte death by suturing, blood, and amniotic membrane in PRK. Invest Ophthalmol Vis Sci 2000;41: 2906-14.
39. Shimmura S, Shimazaki J, Ohashi Y, Tsubota K. Antiinflammatory effects of amniotic membrane transplantation in ocular surface disorders. Cornea 2001;20:408-13.
40. Adinolfi M. HLA typing of amniotic fluid cells. Prenat Diagn 1982;2:147.
41. Adinolfi M, Akle CA, McColl I, Fensom AH, Tansley L, Connolly P, et al. Expression of HLA antigens, beta 2-microglobulin and enzymes by human amniotic epithelial cells. Nature 1982;295:325-7.
42. Akle CA, Adinolfi M, Welsh KI, Leibowitz S, McColl I. Immunogenicity of human amniotic epithelial cells after transplantation into volunteers. Lancet 1981;2:1003-5.
43. Kubo M, Sonoda Y, Muramatsu R, Usui M. Immunogenicity of human amniotic membrane in experimental xenotransplantation. Invest Ophthalmol Vis Sci 2001;42:1539-46.

Appendix 2

Real-time in vivo assessment of the nerve microenvironment with coherent anti-Stokes Raman scattering microscopy.

Henry FP, Côté D, Randolph MA, Rust EA, Redmond RW, Kochevar IE, Lin CP, Winograd JM

Plastic and Reconstructive Surgery. 2009 Feb;123(2 Suppl):123S-30S.

PMID: 19182671

Real-Time In Vivo Assessment of the Nerve Microenvironment with Coherent Anti–Stokes Raman Scattering Microscopy

Francis P. Henry, M.D.
Daniel Côté, Ph.D.
Mark A. Randolph, M.A.S.
Esther A. Z. Rust
Robert W. Redmond, Ph.D.
Irene E. Kochevar, Ph.D.
Charles P. Lin, Ph.D.
Jonathan M. Winograd, M.D.

Boston, Mass.

Background: Current analysis of nerve injury and repair relies largely on electrophysiologic and ex vivo histologic techniques. In vivo architectural assessment of a nerve without removal or destruction of the tissue would greatly assist in the grading of nerve injury and in the monitoring of nerve regeneration over time. Coherent anti–Stokes Raman scattering microscopy is an optical process with particular sensitivity for high-lipid-containing molecules such as myelin. This in vivo nonthermal technique offers high-resolution images that the authors aim to evaluate in both normal and injured nerves.

Methods: A demyelinating crush injury was reproduced in the sciatic nerves of Sprague-Dawley rats (n = 12). Animals were randomized into groups, and coherent anti–Stokes Raman scattering microscopy was undertaken at day 1 and weekly up to 4 weeks after injury. Functional analysis was undertaken weekly and histomorphometry was completed after imaging.

Results: All animals demonstrated loss of sciatic nerve function following injury. Recovery was documented, with functional data approaching normal at 3 and 4 weeks. Demyelination was confirmed in nerves up to 2 weeks after injury. Remyelination was observed in the 3-week group and beyond. Imaging of normal nerve revealed structured myelin bundles. These results were consistent with histologic findings that showed a statistically significant improvement in myelination over time.

Conclusions: The authors conclude that coherent anti–Stokes Raman scattering microscopy has the ability to image the peripheral nerve following demyelinating crush injury. This technology, which permits in vivo, real-time microscopy of nerves at a resolution of 5 μm, could provide invaluable diagnostic and prognostic information regarding intraneural preservation and recovery following injury. (*Plast. Reconstr. Surg.* 123 (Suppl.): 123S, 2009.)

In the field of peripheral nerve surgery, there remains no reliable, in vivo method of assessing the internal microenvironment of a normal or injured nerve. Surgical approaches to assess injured nerve rely on exposure of the nerve and, in the event of a complete nerve transection, primary microsurgical suture repair. However, in the case of neural abnormality resulting from contusion/blunt trauma, stretch injury, or chronic neurop-

From the Plastic Surgery Research Laboratory and the Wellman Center for Photomedicine, Massachusetts General Hospital, Harvard Medical School.
Received for publication December 6, 2007; accepted April 15, 2008.
Presented at the Annual Meeting of the New England Society of Plastic and Reconstructive Surgeons, in Newport, Rhode Island, June 1 through 3, 2007 (received the Joseph E. Murray, M.D., award for best scientific paper), and the 52nd Annual Meeting of the Plastic Surgery Research Council, in Stanford, California, June 20 through 23, 2007.

DOI: 10.1097/PRS.0b013e318191c5b8

Disclosure: *None of the authors has any commercial disclosures or financial conflicts of interest involved with this study.*

Supplemental digital content is available for this article. A direct URL citation appears in the printed text; simply type the URL address into any web browser to access this content. A clickable link to the material is provided in the HTML text and PDF of this article on the *Journal*'s Web site (www.PRSJournal.com).

athies, the ability to distinguish between mild and severe injury as defined by Sunderland[1] is limited at present to destructive histologic techniques not suitable in clinical practice. Electrical studies and serial clinical examination are the current standards by which the functional recovery of a nerve may be assessed. However, they do not provide early accurate prognostic information in a manner by which the need for surgical intervention can be evaluated. Furthermore, only after recovery has occurred over a period of months can such a determination be made empirically. This wait-and-see approach prolongs the period of muscle denervation distally and ultimately results in a poorer functional result should nerve reconstruction be required.[2]

A means by which in vivo longitudinal assessment of neural regeneration, or lack thereof, could be assessed would allow for development of more accurate diagnostic and prognostic indicators that would in turn allow for early surgical intervention if required. Continued development of optical microscopy has resulted in many novel diagnostic approaches in both experimental and clinical surgery. Translation into clinical practice is dependant on identifying both the unique properties of the optical microscope and that of the tissue in question. Coherent anti–Stokes Raman scattering microscopy is a highly lipid-sensitive imaging modality. It differs from other molecule-specific microscopes given that it functions without the need for extrinsic cell and tissue labeling and that a moderately powered laser source is used to produce high-quality images with a resolution of up to 5 μm in a nondestructive fashion.[3] Its application to the field of neural imaging is supported by the high lipid content of myelin, which structurally constitutes 70 percent of the molecule.[4] Identification of the myelin sheath in both the normal and remyelinating nerve, and noting absence of signal in the demyelinated nerve, can therefore be used as a reliable means of assessing the neural microenvironment in vivo. This structural analysis can be used following injury to assess the regeneration of the nerve repeatedly over time, analogous to noninvasive histology.

In this pilot study, we evaluated the ability of video rate-coherent anti–Stokes Raman scattering microscopy to image the remyelinating peripheral nerve in a real-time, in vivo, nondestructive manner. A trial of this technology could allow for further evaluation in both experimental and clinical settings.

MATERIALS AND METHODS

Animal Model

The Institutional Subcommittee on Research Animal Care at Massachusetts General Hospital approved all procedures described. The sciatic nerve of the Sprague-Dawley rat (Charles River Laboratories, Wilmington, Mass.) was used as a model for this study. Animals ($n = 12$) were anesthetized with an intraperitoneal injection of pentobarbital sodium (50 mg/kg; Abbott Laboratories, Chicago, Ill.).

A standardized demyelinating crush injury[5] was reproduced by a single surgeon in the right sciatic nerve of the animals. Surgical exposure was undertaken by means of a right dorsolateral muscle-splitting incision. Crush injury was achieved by holding a no. 5 jeweler's forceps closed across the nerve for 30 seconds, 1 cm distal from the exit of the nerve from the pelvis. After the above procedure, the wounds were closed using 4-0 absorbable polyglactin sutures (Ethicon, Inc., Somerville, N.J.). Postoperatively, animals were housed in the Massachusetts General Hospital animal facility with unlimited access to water and rat chow. Animals were permitted to mobilize without restraints.

Animals were randomized into groups ($n = 2$, with $n = 4$ in the final week-4 group) and both imaging with coherent anti–Stokes Raman scattering microscopy and functional analysis using walking track analysis were undertaken at day 1 and weeks 1, 2, 3, and 4 after injury. The uninjured nerve from the contralateral limb was used as a control.

Functional Analysis

Functional assessment of nerve regeneration was undertaken weekly following injury using walking track analysis.[6] To achieve this, the animal's hind prints were dipped in a dilute India ink solution and they were allowed to walk down a 10 × 40-cm corridor into a darkened box. The floor of the corridor was lined with removable paper. Measurements of print length, toe spread (distance between first and fifth toes), and intermediary toe spread (distance between second and fourth toes) were taken from three individual prints, with the nonoperative left paw print used as a control. The Sciatic Function Index was calculated using the formula as described by Bain et al.,[6] with a value of zero representing normal function and more negative values up to a maximum of –100 representing functional impairment. This standardized assessment was used in a longitudi-

nal manner to correlate injury and subsequent regeneration with both histology and coherent anti–Stokes Raman scattering imaging.

Coherent Anti–Stokes Raman Scattering Microscopy

Coherent anti–Stokes Raman scattering microscopy is based on contrast obtained from a four-wave mixing process that can be loosely viewed as an enhanced Raman mechanism. It requires three source photons (one Stokes photon and two pump photons) produced from two distinct laser beams. A neodymium:vanadate pulsed laser (7 ps, picoTRAIN; High Q Laser, Hohenems, Austria) produces 10 W of power at a repetition rate of 80 MHz and a wavelength of 1064 nm that is split into two separate beams. A small fraction of the power (5 percent) is used for the Stokes beam, whereas the remaining power is used to synchronously pump an optical parametric oscillator (Levante; APE GmbH, Berlin, Germany) that generates approximately 400 mW at a wavelength of 817 nm for the pump beam. When the frequency difference between the pump and Stokes pulses matches the vibration frequency of a Raman active molecule, the resonant oscillators are coherently driven and generate an anti-Stokes photon (i.e., a signal photon at a shorter wavelength) that is detected to create the image. The enhanced contrast obtained with coherent anti-Stokes microscopy arises because this frequency difference between the pump and Stokes beams is selected to resonantly excite the vibrational resonance of CH2 stretch mode (2845 cm^{-1}) predominantly localized in lipids. Because coherent anti–Stokes Raman scattering has a nonlinear dependence on intensity, like two-photon excited fluorescence, the signal is generated only at the laser focus, which allows for a point-by-point analysis of the tissue, analogous to a true optical biopsy of the sample.[7]

The coherent anti–Stokes Raman scattering system used for this study has been modified to include a confocal reflectance channel. Confocal reflectance is a separate and distinct contrast mechanism that produces images based on refractive index differences in the tissue.[8] It is nonspecific and does not provide enhanced contrast data, unlike coherent anti–Stokes Raman scattering microscopy. Imaging with confocal reflectance (detecting only the 817-nm beam) and with coherent anti–Stokes Raman scattering is performed concurrently, with the reflectance data used to guide the user. Myelin, as a lipid-rich molecule, accounts for the majority of the coherent anti–Stokes Raman scattering signal in this case, whereas the confocal reflectance signal originates mainly from axonal tissue.

Imaging with coherent anti–Stokes Raman scattering microscopy was undertaken on day 1 and weeks 1, 2, 3, and 4 after injury. All images were obtained with a real-time video system, allowing for immediate acquisition of data in both longitudinal and cross-sectional orientations. Imaging was achieved by mounting the anesthetized animal on a custom-built stage under the lens objective. Multiple images are averaged for improved image quality (typically, 30 images acquired in 1 second). Before averaging, a custom real-time correction algorithm is applied to correct the images for animal movement attributable to breathing and heartbeat.

After anesthesia, the sciatic nerve was exposed by means of the surgical approach described above. Animals were euthanized after imaging (pentobarbital, 200 mg/kg administered intraperitoneally) and both sciatic nerves were harvested for histologic processing as described below.

Histologic Evaluation

After imaging, animals were humanely killed with an intraperitoneal injection of pentobarbital (200 mg/kg). The right and left sciatic nerves were harvested and fixed in a 2%/2% glutaraldehyde/paraformaldehyde solution at 4°C for 48 hours. Specimens were postfixed in 1% osmium tetroxide, dehydrated in ethanol, and embedded in araldite. Cross-sections 1 μm thick were made 5 mm proximal and distal to the crush site using a microtome (Leica, Nussloch, Germany). Sections were stained with 0.5% (weight/volume) toluidine blue for light microscopy.

Nerve architecture was examined at 400× magnification. Histologic examination was used to verify injury and remyelination in the nerve. Five 400× images were taken of evenly distributed areas within the nerve sample. Ten fibers were selected randomly in each image (a total of 50 fibers per nerve sample). The fiber width and axon diameter were measured using ImageJ (National Institutes of Health, Bethesda, Md.). The myelin thickness was derived from the difference between the fiber and axon diameter.

Statistical Analysis

Values are expressed in terms of means with standard deviations. Statistical analysis of the data

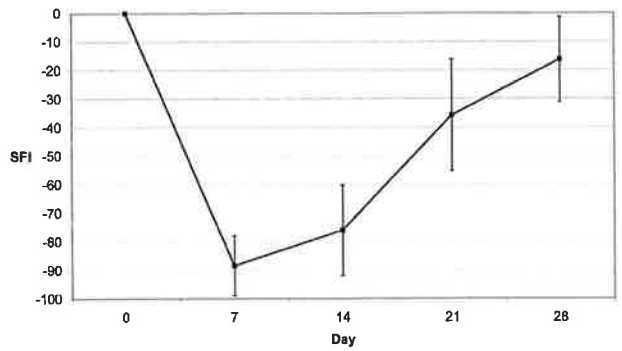

Fig. 1. Sciatic Function Index (*SFI*) over time after crush injury. Data are expressed as means with standard deviations.

was performed using Origin 6.0 (Microcal Software, Inc., Northampton, Mass.). Values of $p < 0.05$ were considered statistically significant. Two-way analysis of variance was used to evaluate the differences in regeneration at various time points after injury.

RESULTS

Functional Analysis

Functional impairment was documented in all animals following injury, with a mean Sciatic Function Index of -88.5 ± 10.5 at 1 week after injury. Week 2 after injury revealed a mean Sciatic Function Index of -76 ± 15.8, representing minimal recovery/remyelination in the sciatic nerve at this time. Greater functional recovery was evident at weeks 3 and 4, with a mean Sciatic Function Index recorded of -35.7 ± 19.5 and -16.4 ± 14.8, respectively. This more rapid recovery can be appreciated in graphic form as shown in Figure 1.

Coherent Anti–Stokes Raman Scattering Microscopy

Using confocal reflectance to guide coherent anti–Stokes Raman scattering microscopy, images of the normal, in vivo nerve were achieved with a resolution of up to 5 μm. Figure 2 represents both imaging modalities alone along with a combined color-enhanced image in longitudinal section. The combined central image (Fig. 2, *center*) shows the axons (confocal image) in red with the myelin in green (coherent anti–Stokes Raman scattering signal). Figure 2, *left* and *right* show both coherent anti–Stokes Raman scattering and confocal imaging alone; the highly contrasted nature of coherent anti–Stokes Raman scattering microscopy is evident with clear definition of the myelin tubules against a dark background. This enhanced intrinsic contrast of coherent anti–Stokes Raman scat-

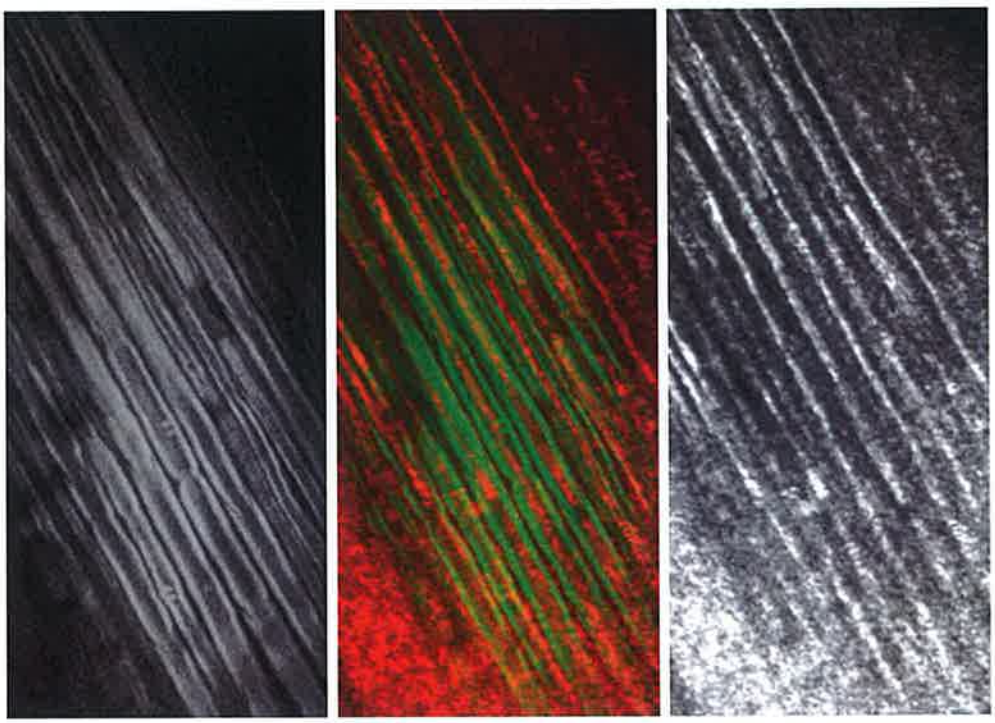

Fig. 2. Segment of in vivo rat sciatic nerve as imaged with coherent anti–Stokes Raman scattering microscopy alone (*left*, myelin), confocal reflectance alone (*right*, axons), and a combined image (*center*) using both modalities with myelin in *green* and axons in *red*.

tering microscopy revealed structured myelin tubules in longitudinal section, and the resolution achieved allowed for identification of a single node of Ranvier easily identifiable in the center of the myelinated fibers. These images allow for cross-sectional analysis analogous to histologic preparation of the nerve as viewed under high magnification, stained with toluidine blue (Fig. 3). Real-time video imaging of the normal nerve microenvironment is demonstrated in **Supplemental Digital Content 1,** which shows real-time in vivo video acquisition of images from the normal rat sciatic nerve using coherent anti–Stokes Raman scattering microscopy, ***http://links.lww.com/A662.*** This short video (500 × 500 μm), taken at a depth of 150 μm into the nerve, demonstrates the information that is available immediately to the microscope operator. The highly contrasted, structured, myelin tubules are clearly evident in longitudinal orientation.

After neural demyelination, no coherent anti–Stokes Raman scattering signal was evident in the initial phase after injury. At 2 weeks after injury, a change in signal was noted on microscopy as demonstrated by the signal achieved 5 mm above the site of injury along with the signal achieved 5 mm below the crush site (Fig. 4). Scattered demyelination with a marked loss of myelin sheath organization is evident above, and a noted absence of myelin sheath structure is seen below the injury site. There is evidence of high-lipid-content molecules that are likely to be that of the Schwann cell population. However, histologic processing in araldite precluded immunohistochemical techniques to confirm this. These findings at 2 weeks after injury are reflected in cross-sectional analysis and histologic processing of the nerve as shown in Figure 4.

A noted increase in structured myelination was obvious both proximal and distal to the injury site following imaging achieved at 3 weeks and beyond (Fig. 5). Although not quite achieving the structure of the normal control (Fig. 3), this improvement in myelination is comparable to the improvement noted in both functional analysis and histologic preparation of the nerve.

Histology

Nerve regeneration was assessed distal to the crush site in all animals. Increasing remyelination was noted with regeneration of normal architecture across all time points. Histomorphometric analysis demonstrated statistically significant differences in all three parameters calculated (axon length, fiber length, and myelin thickness) over time ($p < 0.01$).

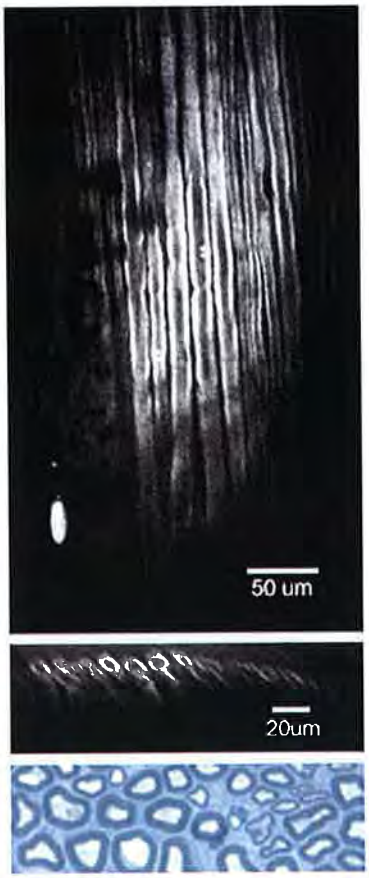

Fig. 3. Coherent anti–Stokes Raman scattering microscopy showing longitudinal section (*above*) and cross-section (*center*) alongside histologic preparation (*below*; toluidine blue staining; original magnification, × 400) of the normal in vivo rat sciatic nerve. The structured myelin sheaths are obvious in both imaging and histologic preparation along with the easily identifiable node of Ranvier on the longitudinal image.

Myelin thickness was shown to increase from a mean of 1.84 ± 0.60 μm at 2 weeks after injury to 4.87 ± 0.62 μm at 4 weeks. Total fiber diameter also demonstrated significant recovery, with means of 5.67 ± 1.09 μm and 10.39 ± 1.85 μm at 2 and 4 weeks, respectively, with axon diameter increasing from 3.82 ± 0.89 μm at 2 weeks to 5.51 ± 1.64 μm at 4 weeks. Neural recovery as defined by histomorphometry is shown in Figure 6.

DISCUSSION

In this study, we have demonstrated that coherent anti–Stokes Raman scattering microscopy has the ability to image the microenvironment of a normal and regenerating peripheral nerve. In this trial of the technology, we have shown that,

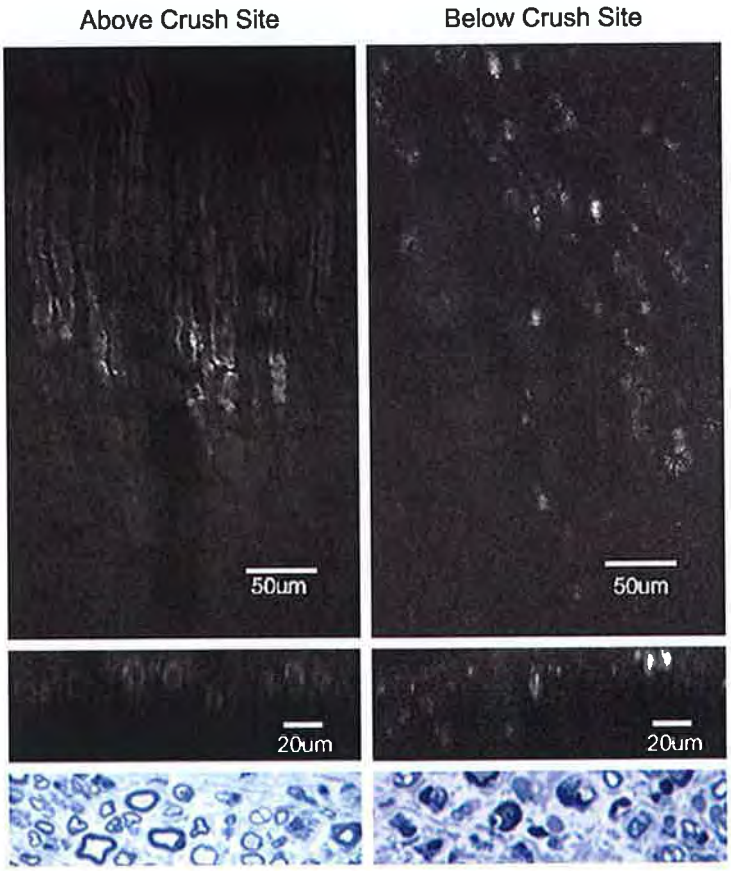

Fig. 4. Coherent anti–Stokes Raman scattering microscopy with appropriate histology (toluidine blue; original magnification, × 400) taken 2 weeks after crush injury of the in vivo rat sciatic nerve. Data shown from above the crush site reveal loss of structural organization of the myelin sheaths in both longitudinal and cross-sectional images and a decrease in myelinated fibers on histologic preparation. Data from below the crush site demonstrate a complete lack of sheath organization on longitudinal section, with cross-section and histology showing minimal evidence of myelinated fibers along with an increase in debris throughout the nerve field. The cellular pattern of the longitudinal signal is likely to be representative of the Schwann cell population in the regenerating nerve.

after a demyelinating injury followed by subsequent significant remyelination, images can be acquired that are in agreement with both functional recovery and histomorphometric analysis of the peripheral nerve. To date, there remains no comparable method of assessing remyelination in a nondestructive manner such as this. This nonthermal, in vivo method can easily be used to achieve a method of grading neural injury over time that has not been previously described in either the experimental or clinical setting.

Coherent anti–Stokes Raman scattering microscopy in its traditional form has been used in the past in the fields of cell biology[9] and membrane chemistry.[10] The ability to image without extrinsic labeling has been the focus of its widespread application in these fields. The development of a real-time video system for acquiring images[3] has led to its use for in vivo biological samples.[11]

Myelin as a lipid-rich molecule has subsequently been found to be a suitable medium for this unique imaging modality. The acquisition of images in the form of a true optical biopsy may lead to its use in the experimental setting to achieve a greater understanding regarding peripheral nerve regeneration. The ability to analyze a longitudinal model of nerve regeneration in a nondestructive manner could prove to be a valuable tool.

Fig. 5. Images 5 mm below the crush site obtained 3 weeks after injury of the rat sciatic nerve. Structured remyelination is seen throughout the nerve sample as shown on longitudinal cross-section and by histologic evaluation (toluidine blue; original magnification, × 400).

Despite years of advancement in microscopy, there remains no reliable method of imaging the microenvironment of the nerve. Current technology used to assess nerve regeneration is faulted by both its limitation in the early phase of injury and its nonspecific nature.[12] Achieving images with a resolution of up to 5 μm and accurately assessing the internal architecture of the nerve has obvious advantages in clinical practice in both prognostic and diagnostic evaluation. Reducing the long periods of observation currently used following nerve contusion would allow for an earlier determination for surgical intervention where necessary and possibly an improved functional recovery.[13] Diagnostically, the ability to accurately assess myelination would be useful following both traumatic injury and that of chronic processes such as carpal tunnel disease and demyelinating neuropathies.

Further avenues of investigation remain before this becomes an integral medical technology. The integration of this imaging modality into an endoscope[14] would alleviate the need to surgically expose the nerve and allow for a minimally invasive method of assessment. Further studies are also warranted across a variety of injury models to achieve a grade of injury analogous to Sunderland's classification. This first step demonstrating coherent anti–Stokes Raman scattering microscopy as a valuable resource in this field shows great promise for its continued use in this manner.

CONCLUSIONS

Coherent anti–Stokes Raman scattering microscopy has the ability to image the peripheral nerve following demyelinating crush injury. This technology that permits in vivo, real-time micros-

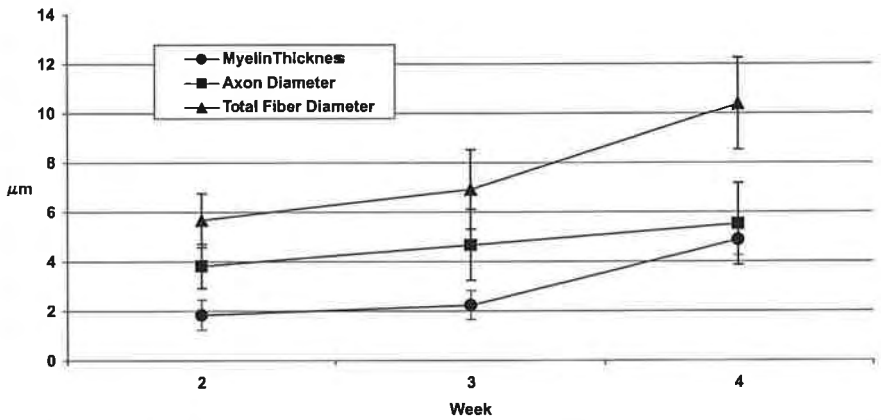

Fig. 6. Graphic representation of the mean myelin thickness, axon diameter, and total fiber diameter (in microns) over time (with standard deviations) demonstrating statistically significant ($p < 0.01$) recovery from the 2- to 4-week time period. This time period corresponds to the time during which the greatest change in myelination was observed through imaging with coherent anti–Stokes Raman scattering microscopy.

copy of nerves at a resolution of up to 5 μm could provide invaluable diagnostic and prognostic information regarding intraneural preservation and recovery following injury. This trial of technology opens many avenues through which coherent anti–Stokes Raman scattering microscopy may become a valuable tool in the field of neural research, regeneration, and repair.

Mark A. Randolph, M.A.S.
Division of Plastic Surgery, WAC 453
Massachusetts General Hospital
15 Parkman Street
Boston, Mass. 02114
marandolph@partners.org

ACKNOWLEDGMENTS

The authors gratefully acknowledge funding from the Plastic Surgery Educational Foundation, Basic Science Grant 2007, and the Bullock-Wellman Fellowship from the MGH Wellman Center for Photomedicine.

REFERENCES

1. Sunderland S. A classification of peripheral nerve injuries producing loss of function. *Brain* 1951;74:491–516.
2. Winograd JM, MacKinnon SE. Peripheral nerve injuries: Repair and reconstruction. In: Mathes SJ, ed. *Plastic Surgery.* Vol. 1. Philadelphia: Saunders Elsevier; 2006:471–514.
3. Evans CL, Potma EO, Pouris'haag M, Côté D, Lin CP, Xie XS. Chemical imaging of tissue in vivo with video-rate coherent anti stokes Raman scattering microscopy. *Proc Natl Acad Sci USA* 2005;102:16807–16812.
4. Morell P, Quarles RH. Myelin formation, structure and biochemistry. In: Siegel GJ, Agranoff BW, Fisher SK, Albers RW, Uhler MD, eds. *Basic Neurochemistry; Molecular, Cellular and Medical Aspects: Part 1. Cellular Neurochemistry and Neural Membranes.* 6th ed. Philadelphia: Lippincott-Raven Publishers; 1999:69–94.
5. Bridge PM, Ball DJ, MacKinnon SE, et al. Nerve crush injuries: A model for axonotmesis. *Exp Neurol.* 1994;127:284–290.
6. Bain J, Mackinnon S, Hunter D. Functional evaluation of complete sciatic, peroneal and posterior tibial nerve lesions in the rat. *Plast Reconstr Surg.* 1989;83:129–138.
7. Cheng JX, Volkmer A, Xie SE. Theoretical and experimental characterization of coherent anti-stokes Raman scattering microscopy. *J Opt Soc Am B* 2002;19:1363–1375.
8. Rajadhyaksha M, Gonzalez S, Zavislan J, Anderson RR, Webb RH. In vivo confocal scanning laser microscopy of human skin II: Advances in instrumentation and comparison with histology. *J Invest Dermatol.* 1999;113:293–303.
9. Cheng JX, Jia YJ, Zheng G, Xie XS. Laser-scanning coherent anti-Stokes Raman scattering microscopy and applications to cell biology. *Biophys J.* 2002;83:502–509.
10. Cheng JX, Pautot S, Weitz D, Xie XS. Ordering of water molecules between phospholipid bilayers visualized by coherent anti-Stokes Raman scattering microscopy. *Proc Natl Acad Sci USA.* 2003;100:9826–9830.
11. Wang H, Fu Yan Zickmund P, Shi R, Cheng JX. Coherent anti-Stokes Raman scattering imaging of axonal myelin in live spinal tissues. *Biophys J.* 2005;89:581–591.
12. Kline DG, Hudson AR. *Nerve Injuries: Operative Results for Major Nerve Injuries, Entrapments and Tumors.* Philadelphia: Sanders; 1995.
13. MacKinnon SE. Closed nerve injury. In: Marsh L, ed. *Current Therapy in Plastic and Reconstructive Surgery.* Philadelphia: Decker; 1989:22–23.
14. Legare F, Evans CL, Ganikhanov F, et al. Towards CARS endoscopy. *Opt Express* 2006;14:4427.